ACTA UNIVERSITATIS CAROLINAE

AUC **GEOGRAPHICA**

59
1/2024

CHARLES UNIVERSITY • KAROLINUM PRESS

ISSN 0300-5402 (Print)
ISSN 2336-1980 (Online)

The COVID-19 disaster in Mexico City: Exploring risk drivers at the local scale

Perla Lorena Romero-Gaeta[1,*], Irasema Alcántara-Ayala[2]

[1] Postgraduate Programme in Geography, National Autonomous University of Mexico (UNAM), Mexico
[2] Institute of Geography, National Autonomous University of Mexico (UNAM), Mexico
[*] Corresponding author: lorena.romerogaeta@gmail.com

ABSTRACT

The COVID-19 pandemic had a significant impact on the inhabitants of Mexico City. With over 9 million people living in 16 districts, infections and mortality rates varied greatly. In this article, demographic and socio-economic factors were analyzed to determine vulnerability and exposure to COVID-19 during the crisis from 27 February 2020 to 10 May 2021. The study revealed that mortality and infections were distributed differently across the districts of Mexico City. The districts with the most confirmed cases did not necessarily have the highest death rates. Many deaths were linked to age and comorbidities, such as hypertension, diabetes, and obesity. Poverty, overcrowding, the lack of space, and basic services contributed to vulnerability and exposure to the disease. Inequalities in the city's development over time resulted in varying degrees of vulnerability and exposure to COVID-19, leading to different patterns of infections and deaths across the districts. The prevalence of infections in the city´s southwestern districts can be attributed to the combination of marginalization, poverty, and inadequate services. Conversely, the northwest areas of the city, with a higher concentration of elderly residents, experienced a greater number of fatalities.

KEYWORDS

Covid-19; disaster; disaster risk drivers; Mexico City

Received: 20 June 2023
Accepted: 26 January 2024
Published online: 21 March 2024

Romero-Gaeta, P. L., Alcántara-Ayala, I. (2024): The COVID-19 disaster in Mexico City: Exploring risk drivers at the local scale. AUC Geographica 59(1), 3–19
https://doi.org/10.14712/23361980.2024.1

1. Introduction

Since its emergence in early 2020, the pandemic resulting from the transmission of the SARS-CoV-2 virus, which causes COVID-19, has had a profound social, economic, and health impact worldwide. It is a unique disaster in modern history that has transcended borders and disrupted societies at various scales, from individual, family, national and global levels (Lavell and Lavell 2020; Alcántara-Ayala 2021).

The impacts, beyond material damage, translate into human and economic losses worldwide, where, as of 10 March 2023, around 676,6 million confirmed cases and 6,881,955 deaths associated with the disease were counted (Johns Hopkins University 2023). In Mexico, infections and deaths exceed 7,483,444 and 333,188, respectively. Mexico City had the highest percentage of damage within the territory, accounting for 27% of positive cases and 15% of deaths of the national total (DGE 2021).

As with other types of disasters, those linked to COVID-19 highlight the repercussions derived from the intense and extensive intervention of human activities on nature, often related to incipient and ill-informed development that prioritizes unequal economic growth over social well-being and environmental care, and which, over time, contributes to the generation of risk conditions that have a differentiated impact on diverse populations (Alcántara-Ayala et al. 2021; Oliver-Smith et al. 2016).

The increase in zoonotic infectious diseases in humans, such as COVID-19, is due to various environmental and social factors (Morse 2004). On the one hand, due to climate change, pathogens have undergone genetic changes and adaptations that result in variations in their dispersal, infection, and lethality characteristics (Morens and Fauci 2013; Alcántara-Ayala 2021). On the other hand, increasing human interventionism in nature, together with the increase in mobility on a global scale and the concentration of the population in large cities, play an important role in the dispersion of pathogens and, therefore, in the generation of scenarios of high exposure to different diseases (Lavell and Lavell 2020; Alpuche-Aranda 2020).

In such circumstances, human groups face such diseases from a situation of inherent susceptibility due to the absence of an immunity to new infectious forms (Alpuche-Aranda 2020), as well as from a series of socioeconomic, political, and cultural characteristics, which are reflected among other things in the existence of marginalized social groups or those with some degree of poverty, which makes them more vulnerable to this type of hazard (Alcántara-Ayala et al. 2021).

This highlights the importance of approaching the COVID-19 disaster from an integral and disaster risk perspective, which allows the understanding, beyond the characteristics of the virus, of the social dimension in the construction of risk and the resulting disaster (Oliver-Smith et al. 2016; Alcántara-Ayala et al. 2021).

Mexico City, the capital of the country, is in the center of the national territory, between 19°03′ and 19°36′ north latitude and 98°57′ and 99°22′ west longitude. It is politically and administratively divided into 16 districts with 9,209,944 inhabitants, making it Mexico's second most populated entity (INEGI 2020).

On the other hand, in terms of health, Mexico is one of the countries with the largest population over 20 years of age suffering from obesity (36.1%) and overweight (39.1%). According to data collected in the National Health and Nutrition Survey, Mexico City is home to around one million people with diabetes and just over three million with hypertension, representing 12.7% and 20.2% of the national total, respectively (INEGI and INSP 2018).

Although this area in Mexico had the highest infection rate among its inhabitants (7,138 infections per 100,000 people) and the highest mortality rate in the country (383 deaths per 100,000 inhabitants), the impact of COVID-19 was not evenly distributed throughout the region (DGE 2021). Therefore, it is crucial to study and comprehend the epidemic in Mexico City to identify the underlying reasons behind the varying effects of the virus. Accordingly, this study aims to analyze the driving factors of disaster risk of COVID-19 in Mexico City, focusing on the varying levels of vulnerability and exposure among the population.

2. Theoretical framework

2.1 COVID-19, a global disaster: understanding disaster risk associated with biological hazards

The study and understanding of disasters have undergone several epistemological transformations in recent decades. Research increasingly shows a series of complex socio-natural relationships articulated in the configuration of disasters, refuting the physicalist conception that disasters are the product of nature (Blaikie et al. 1994; Wisner et al. 2004; Oliver-Smith et al. 2016; 2017).

Disasters have become a critical issue in contemporary society. A disaster is a severe disruption of the functioning of a community or society resulting from diverse types of hazards that interact with conditions of exposure, vulnerability, and capacity. The aftermath of such an event can lead to a range of losses and impacts, including those that are human, material, economic, and environmental. The effects of a disaster can be immediate and confined to a specific area, or they can be far-reaching and long-lasting, surpassing the ability of a community or society to manage the situation with its resources. External resources, such as neighboring jurisdictions, national agencies,

or international organizations, may be called upon to aid (UN General Assembly 2016).

In recent decades, disasters caused by geological, geophysical, and hydrometeorological hazards have been extensively studied and discussed. However, since 2020, the world has witnessed the enormous impact of biological hazards. A hazard is any process, phenomenon, or human activity that can cause harm to human life, health, property, or the environment or disrupt social and economic stability. Hazards can be natural or human-induced and may occur individually, combined, or in a cascade, with their classification based on specific attributes. Each hazard is characterized by location, intensity or magnitude, frequency, and probability. Organic sources or biological agents can give rise to biological hazards. Such hazards encompass pathogenic microorganisms, toxins, other bioactive substances, venomous wildlife and insects, poisonous plants, and mosquitoes that can carry disease-causing agents. These hazards are distinguished by their infectiousness, toxicity, and other pathogen-related qualities (UN General Assembly 2016).

Disasters were once seen as unpredictable events caused by nature or fate, but since the 1980s, they have been recognized as socially constructed processes often linked to misguided development policies (Blaikie et al. 1994; Lavell and Maskrey 2014). Economic growth often takes priority over social and environmental considerations, creating diverse conditions of vulnerability and exposure, and thus, disaster risk and ultimately leading to the occurrence of disasters (Blaikie et al. 1994; Oliver-Smith et al. 2016; Alcántara-Ayala et al. 2021; 2023). The pandemic is an example of a disaster arising from underlying risk conditions and systemic environmental hazards (Lavell et al. 2020; Alcántara-Ayala et al. 2021).

The COVID-19 virus becomes a biological hazard for exposed and vulnerable populations, and global economic structures heavily influence its spread. Although it does not cause physical destruction like disasters associated with other hazards, for instance, earthquakes or floods, the pandemic has significantly impacted the world, leading it to be classified as a global disaster. Its effects have disrupted societies and caused negative consequences in various domains, including social, economic, cultural, political, and institutional. This is mainly due to the challenges of the virus's high susceptibility and rapid spread, combined with pre-existing societal vulnerabilities and exposure conditions. The global economy played a significant role in shaping exposure to COVID-19, mainly through economic integration and social inequalities. Factors such as international travel, displacement, and urbanization increased the risk of exposure (Lavell et al. 2020; Alcántara-Ayala 2021; Alcántara-Ayala et al. 2021).

The expansion of urban areas, including suburbanization, post-suburbanization, and peri-urbanization, can have negative consequences on public health by increasing the transmission of infectious diseases. Factors such as demographic changes, infrastructure, and governance play a significant role in determining the susceptibility of peri-urban and suburban regions to such diseases. The socio-ecological changes that occur on the outskirts of cities may further exacerbate the risk of infection. As urbanization continues to extend, the conditions for the spread of infectious diseases are amplified (Connolly et al. 2021).

The COVID-19 pandemic has profoundly impacted countries worldwide, resulting in widespread illness, loss of life, and societal upheaval. The pandemic has overwhelmed healthcare systems and exposed global public health infrastructure fragilities (Jovanović et al. 2020). Like other disasters, its humanitarian impact has affected millions directly or indirectly. The pandemic has also triggered economic downturns, job losses, and business disruptions on a global scale, further exacerbating existing inequalities (Maital and Barzani 2020). Measures such as lockdowns, social distancing, and quarantine protocols disrupted daily life, with significant consequences for mental health, education, and social well-being (Nurunnabi et al. 2020). These effects are typical of disasters, often resulting in social dislocation and community-level impacts. As with disasters triggered by geo-hazards or climate-related hazards, the COVID-19 pandemic will have long-term consequences beyond the immediate crisis, necessitating ongoing efforts to recover and rebuild (Fakhruddin et al. 2020). The global response to the pandemic has required collaboration between governments, international organizations, and non-governmental entities, reflecting the characteristics of disaster response (Pawar 2020).

A growing body of literature has examined diverse spheres of the COVID-19 pandemic from a disaster risk perspective. The pandemic was recognized as a disaster in several countries from the early stages of its outbreak. In Indonesia, for example, the significance of disaster risk communication emerged as a major concern due to the exacerbation of communication breakdowns, which impeded both government and public efforts to curb the spread of the virus (Rudianto and Hendra 2021).

Mostafanezhad (2020) affirms that the pandemic reframed as a disaster creates new debates at the intersection of tourism geographies and political ecologies of hope, which can provide a better understanding of the impact of the pandemic on society and the environment. Cvetković et al. (2020) conducted an online survey in Serbia to assess citizens' readiness for the COVID-19 disaster. Their study revealed differences in risk perception, suggesting the need for targeted strategies to improve decision-making and preparedness.

As disaster management systems continue to evolve, they now encompass human-induced hazards and emerging crises associated with biological hazards like epidemics and pandemics. Kim and Ashihara

(2020) pointed out that individuals look to their governments for guidance and assistance during times of crisis. Therefore, the recent outbreak of COVID-19 in South Korea underscored the need for a more proactive and organized national approach to disaster management.

A full discussion of analyzing the COVID-19 pandemic as a disaster lies beyond the scope of this study. However, it is important to acknowledge its profound impact on a global scale and the uncertainty surrounding the direction of disaster risk reduction policymaking at both the national and local levels. This involves understanding the vulnerability and exposure of individuals to biological hazards and implementing measures to reduce disaster risk and improve disaster risk governance.

Consequently, to understand the pattern of damage resulting from the pandemic in Mexico City, it is necessary to analyze it from the paradigm of the social construction of risk in order to identify the disaster risk drivers that are linked to the vulnerability and exposure of the city's population (Oliver-Smith et al. 2016; Alcántara-Ayala et al. 2021). Against this background, disaster risk refers to the possibility of adverse impacts in economic, social, environmental, material, or human losses triggered by one or more hazards under specific conditions of vulnerability and exposure in communities, livelihoods, and environmental systems (UN General Assembly 2016).

COVID-19 is a socio-biological hazard since it is a natural element – the SARS-coV-2 virus (of zoonotic origin) – whose transmission derives from human interventionism in natural spaces, which responds to current economic processes (Morens and Fauci 2013; Karesh et al. 2004; Alcántara-Ayala 2021; Li et al. 2020). In addition, this virus is positioned as a hazard as conditions of exposure and vulnerability favor the spread of this virus in society (Alcántara-Ayala 2021; Lavell et al. 2020).

According to Oliver-Smith et al. (2016), exposure plays a crucial role in determining the level of risk. Exposure refers to the physical presence of people, infrastructure, housing, production capacities, and other human assets in areas susceptible to hazards, as defined by the UN General Assembly (2016).

Transmission of COVID-19 occurs from person to person or through direct contact with a surface on which the virus is present and subsequent contact with the mucous membranes of the face (Li et al. 2020; Lavell and Lavell 2020). In general terms, human exposure to the virus is directly linked to the global economic structure, which conditions the mobility patterns of individuals, the integration of societies in densely populated cities, and the organization of territory and urban space (Lavell et al. 2020; Alcántara-Ayala et al. 2021).

The COVID-19 pandemic posed significant challenges for informal and poor residential settlements in the Global South, including Mexico City. These communities face a shortage of essential resources, including water, sanitation facilities, secure housing, and waste management systems, making them ill-equipped to deal with the crisis. Additionally, the dense population, lack of space, and prevalence of violence make it difficult for residents to practice physical distancing or self-isolation, exacerbating the risk of COVID-19 transmission (Corburn et al. 2020).

Various situations, ranging from utilizing mass public transportation in urban regions to residing in densely populated areas or overcrowded living quarters, can heighten an individual's exposure to biological hazards, such as COVID-19. Moreover, specific professions, such as informal labor or occupations that necessitate direct interaction with others, can also increase the likelihood of contracting diseases (Lavell et al. 2020; Alcántara-Ayala et al. 2021).

In the context of the pandemic, all of humanity is vulnerable to the virus – since, until vaccination, the necessary antibodies to combat it were unavailable (Alpuche-Aranda 2020). However, the form and degree of susceptibility of individuals are marked by intrinsic or endogenous factors, such as genetics, age or the existence of or susceptibility to chronic degenerative diseases and can be enhanced by conditions of poverty or malnutrition that are linked to processes of inequality, corruption and lack of access to basic education and health services (Lavell and Lavell 2020; Alcántara-Ayala 2021; Alcántara-Ayala et al. 2021).

In other words, once an individual is exposed to the virus and therefore infected, the harm they present – in terms of health and/or livelihoods – will be directly related to intrinsic susceptibility and vulnerability (Lavell and Lavell 2020).

Among the population considered most susceptible to acute symptomatology or death worldwide are adults over 60 years of age and/or with pre-existing chronic degenerative or autoimmune diseases, such as hypertension, diabetes, asthma, chronic obstructive pulmonary disease (COPD) or cardiovascular problems and obesity (Porcel-Gálvez et al. 2020; Luna-Nemecio 2020; Martínez-Martínez et al. 2020; Villerías and Juárez 2020). This results in higher levels of vulnerability in those countries or cities where the population is older than in societies with younger populations, even with the same degree of hazard and exposure (Lavell et al. 2020).

Studies have revealed a connection between the density of urban areas and the number of COVID-19 cases in Latin America. Urban areas have reported more cases and deaths compared to their rural counterparts. The reasons for this include factors such as cramped living conditions, poor sanitation, high population density, and inadequate public services. These factors increase the risk of getting infected and developing complications from the disease (Luna-Nemecio 2020; Ortega et al. 2020).

Different individuals and societies may not be affected similarly when exposed to a hazard. This is

because their susceptibility or vulnerability to the hazard will play a significant role. In this context, vulnerability arises from various dynamic processes and underlying causes (Oliver-Smith et al. 2016). Such underlying causes often result from physical, social, economic, and environmental factors or processes, which increase the vulnerability of an individual, community, assets, or systems to the effects of hazards (UN General Assembly 2016).

The susceptibility of a population to a virus like SARS-CoV-2 is not solely determined by intrinsic factors such as age and gender. Socio-economic factors, such as access to healthcare and public services, insecure employment, inadequate housing leading to overcrowding, and marginalization and discrimination of specific social groups, also play a crucial role. Therefore, the degree of exposure varies according to each population's mobility structures, territorial organization, and cultural practices, resulting in different impacts on infections and deaths across countries or regions (Lavell et al. 2020).

The Latin American region is facing high vulnerability due to marginalization, poverty, social inequality, labor informality, and weak health systems, which have caused various social groups to be vulnerable to COVID-19 disease. ECLAC (2020) reports that the most vulnerable groups include indigenous and Afro-descendant populations, with limited access to social protection and communication and labor market difficulties. In Mexico, COVID-19 has affected the indigenous population with a higher lethality rate (18.8%) compared to the general population (11%), which could be attributed to delayed prevention measures and a lack of culturally and linguistically appropriate information on COVID-19 (Cortéz-Gómez et al. 2020).

3. Mexico City in the Context of the COVID-19 Pandemic

3.1 Mexico City's socio-demographic characteristics: Shaping vulnerability and exposure

Internally, the socioeconomic and demographic characteristics of Mexico City (Fig. 1) maintain a heterogeneous distribution in space based on a center-periphery model in which there are clear differences

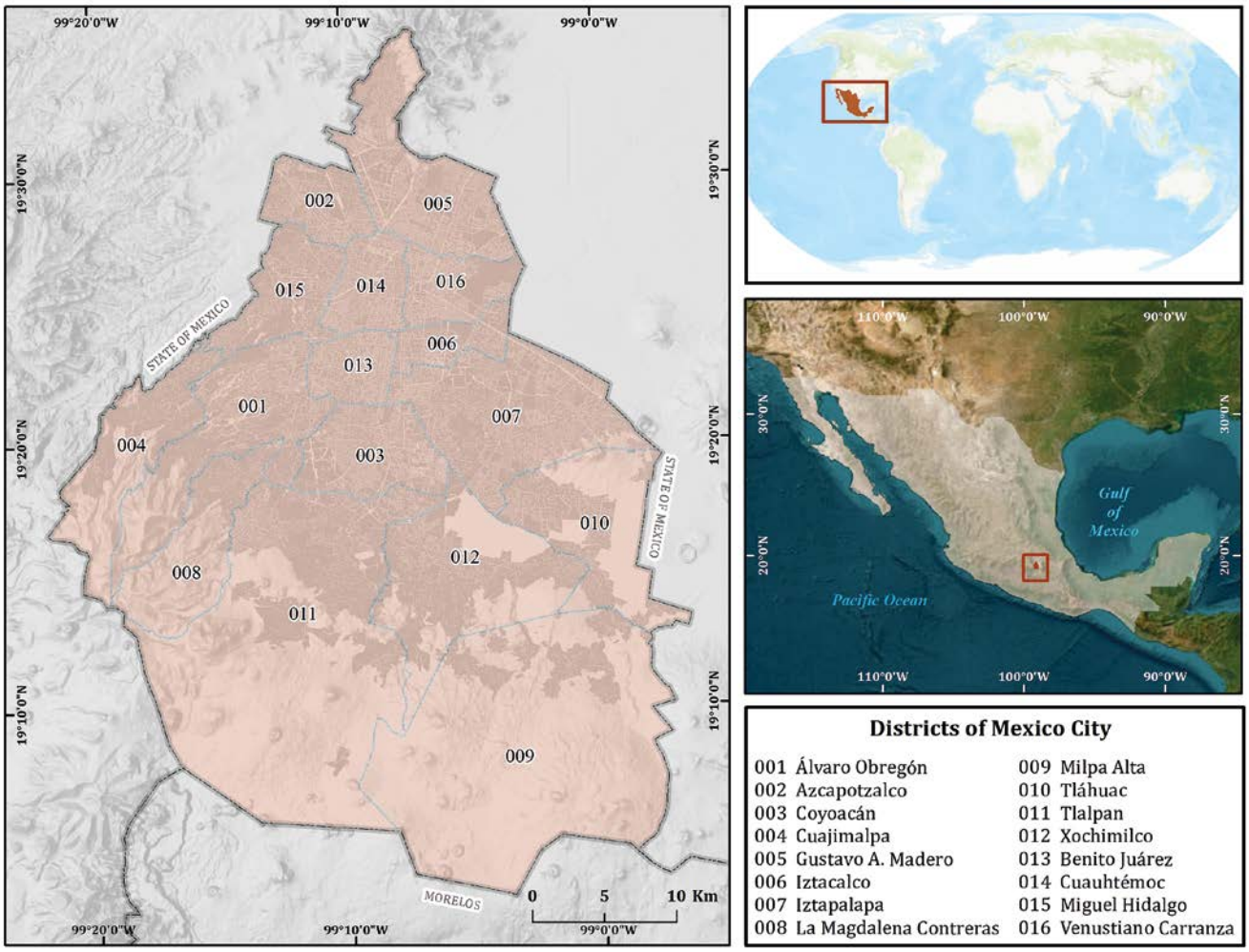

Fig. 1 Location of Mexico City and its districts.

between the central and northern districts and those in the south.

In the first group, the districts of Benito Juárez, Miguel Hidalgo, Azcapotzalco, Coyoacán, Álvaro Obregón, Venustiano Carranza, and Cuauhtémoc have the highest population density in the city (more than 8,000 inhabitants/km^2), the highest percentages of the population over 60 years of age (between 17% and 20.3%), the highest median ages (between 36 and 39 years) as well as the highest levels of schooling (more than ten years of formal education). In contrast, these districts had the lowest percentages in terms of illiteracy, poverty, overcrowding, lack of quality of housing spaces and services, lack of health services, and lack of basic housing services in this region (INEGI 2020; CONAPO 2020; CONEVAL 2020).

They are also the districts with the lowest percentage of indigenous population (less than 1.15%, except for Coyoacán with 1.29%) and, at the same time, the highest concentration of Afro-descendant population (between 2% and 2.8%, except for Coyoacán with 1.8%) (INEGI 2020). In other words, in the central and north-central districts, there is a high population density associated with inhabitants over 37 years of age, with significant percentages of older adults, high levels of schooling, adequate access to services and quality of housing spaces, and health services.

Despite their location, Iztapalapa, Iztacalco, and Gustavo A. Madero do not share the same particularities as the rest of the central-northern districts; on the contrary, the former, despite having a high population density (16,219 inhabitants/km^2), also presents high levels of poverty (43.8%), marginalization (59.5%), and lack of health services (31.8%), and, in contrast, low levels of schooling (10.4 years of formal education) and a percentage of the population over 60 years of age (14.2%) (INEGI 2020; CONAPO 2020; CONEVAL 2020) (Tab. 1).

In the case of Iztacalco and Gustavo A. Madero, the population density is high (17,522 inhabitants/km^2 and 13,347 inhabitants/km^2), as is the level of schooling (11.5 and 11.1 years of formal education), and the degree of marginalization (60.4% and 60.1%). However, they present intermediate levels in the percentage of the population aged 60 and over (17.5% and 17.3%, respectively), illiteracy (1.16% and 1.53%,

Tab. 1 Demographic and socioeconomic characteristics by district.

District	Álvaro Obregón	Azcapotzalco	Benito Juárez	Coyoacán	Cuajimalpa	Cuauhtémoc	Gustavo A. Madero	Iztacalco	Iztapalapa	La Magdalena C.	Miguel Hidalgo	Milpa Alta	Tláhuac	Tlalpan	Venustiano Carranza	Xochimilco
PD	7916	12892	16259	11395	3059	16783	13347	17533	16219	3904	8927	512	4569	2225	13102	3874
AA	35	37	39	38	32	36	36	36	33	34	37	30	31	34	36	33
P. >60 years (%)	16.13	18.72	20.12	20.60	11.85	17.18	17.34	17.52	14.28	15.37	17.40	10.76	11.77	15.59	17.81	13.79
IP	9.24	7.53	9.37	8.88	9.65	8.64	6.57	6.84	7.87	9.75	5.01	20.32	14.63	11.85	5.86	12.39
AP	2.10	2.05	2.84	1.80	1.40	2.70	1.85	1.72	1.81	2.20	2.72	1.46	1.86	1.75	2.36	2.22
SGL	11.30	11.90	14.50	12.50	11.40	12.40	11.10	11.50	10.40	10.80	13.10	10.00	10.50	11.50	11.50	10.80
I	1.57	1.02	0.35	1.10	1.50	0.95	1.53	1.16	1.84	1.87	0.75	2.77	1.67	1.61	1.09	1.96
P	37.70	24.20	7.90	27.10	32.50	20.90	33.80	25.20	43.90	42.50	13.50	54.70	42.40	39.70	30.00	48.20
Marg.	60.48	60.63	62.39	60.87	60.44	61.33	60.10	60.44	59.54	59.68	61.22	57.28	59.32	59.56	60.38	58.57
LSQH	5.30	3.50	0.90	3.00	5.80	3.60	3.90	3.40	6.30	6.30	2.20	11.60	6.20	6.70	3.40	10.50
Oc.	0.80	0.80	0.60	0.70	0.80	0.70	0.80	0.80	0.90	0.90	0.70	1.00	0.90	0.80	0.80	0.90
LBHS	3.50	1.00	0.10	1.50	3.10	0.40	1.00	0.30	0.60	8.90	0.40	23.30	4.10	9.10	0.40	13.00
EAP	64.70	63.40	70.40	62.60	65.80	70.20	61.30	64.10	63.50	62.90	68.10	67.00	63.20	64.20	64.80	63.20
PPEPS	0.23	0.05	0.08	0.06	0.30	0.11	0.13	0.18	0.17	0.27	0.09	8.68	1.49	0.89	0.09	2.93
PPESS	14.69	17.40	9.60	11.74	17.82	8.93	17.35	13.72	18.00	14.09	11.62	19.80	18.76	14.62	11.44	15.18
PPES	65.30	59.00	73.90	67.70	63.20	64.40	58.20	62.00	55.10	65.30	68.60	49.30	55.80	65.50	59.70	58.10
PPET	16.11	20.99	14.00	16.19	14.71	23.07	22.30	21.29	24.51	16.03	15.03	21.18	22.11	15.89	25.68	20.03

Population density (PD), Average age (AA), Population over 60 years of age (P. >60 years), Indigenous population (IP), Afro-descendant population (AP), School grade level, (SGL), Illiteracy (I), Poverty (P), Marginalization Index (Marg), Lack of Space and Quality in Housing (LSQH), Overcrowding (Oc), Lack of basic housing service (LBHS), Economically Active Population (EAP), Percentage of the population employed in the primary sector (PPEPS), Percentage of the population employed in the secondary sector (PPESS), Percentage of the population employed in service (PPES), Percentage of the population employed in trade (PPET), Lack of access to basic health service (LABHS).

respectively), overcrowding (13.5% and 16.4%), poverty (25% and 33%) and lack of quality of services and housing spaces (3.4%) (INEGI 2020; CONAPO 2020; CONEVAL 2020) (Tab. 1).

The dissimilarities among these districts can be attributed to unique geo-historical formation processes distinct from those observed in neighboring districts.

The southern districts, on the other hand, corresponding to Milpa Alta, Tláhuac, La Magdalena Contreras, Cuajimalpa, and Xochimilco, have the lowest population densities (less than 4,570 inhabitants/km^2), average ages between 30 and 34, and the lowest percentages of the population aged 60 and over (between 15.3% and 10.7%) (INEGI 2020). Furthermore, this region has the lowest levels of schooling (between 10 and 10.8 years of formal education received), apart from Cuajimalpa and Tlalpan (with 11.4 and 11.5 years of education, respectively) (Tab. 1).

In contrast, poverty (between 32.4% and 54.7%), illiteracy (between 1.5% and 2.8%), overcrowding (ranging from 17.85% to 25.9%), lack of quality of housing spaces and services (between 6.3% and 11.6%), lack of health services (between 21.9% and 34.6%) and lack of basic housing services (between 3.1% and 23.3%) have the highest levels in the city. At the same time, the south of the city has the highest percentage of the indigenous population, especially in the districts of Milpa Alta (with 20.32% of the state total), Tláhuac (with 14.63%), and Xochimilco (with 12.40%) (Tab. 1) (INEGI 2020). Thus, the population of these districts is characterized by a primarily young population (between 30 and 34 years old), with low levels of schooling and high percentages of problems associated with the quality of housing and the distribution of spaces, including a high level of overcrowding.

3.2 The impacts of COVID-19 in Mexico City

The first active case of COVID-19 was confirmed in Mexico City on 27 February 2020 (Suárez et al. 2020).

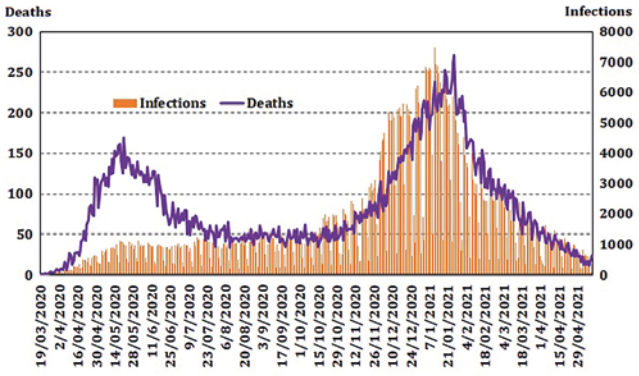

Fig. 2 Total number of infections and deaths in Mexico City from March 2020 to May 2021.

Since then, two waves of the virus have affected the population, significantly increasing infections and fatalities (Fig. 2). The first wave occurred between April and August 2020, at the start of the health crisis. The second wave, which saw the highest incidence of cases in January, occurred between November 2020 and May 2021, with up to 250 deaths per day (DGE 2021). These are the findings of a study conducted until May 10 2021.

For the dates mentioned, the damage in terms of infections and deaths amounted to 648,479 and 33,027, respectively, representing 27% and 15% of the national total. The districts with the highest rates of confirmed cases were Álvaro Obregón, Tlalpan, and Tláhuac, with 11,000, 9,323, and 8,804 cases per 100,000 inhabitants, while the lowest rates were in Benito Juárez (5,198), Miguel Hidalgo (5,672) and Iztapalapa (5,743) (DGE 2021), as shown in Fig. 3.

On the other hand, the highest death rates were in Azcapotzalco, Iztacalco, and Gustavo A. Madero, with 565, 561, and 469, respectively, in contrast to Milpa Alta, Cuajimalpa, and Tláhuac, which have rates of less than 250 deaths per 100,000 inhabitants (Fig. 3) (DGE 2021).

Demographic and socio-economic characteristics constitute some factors that induce the vulnerability and exposure of Mexico City's population to COVID-19.

4. Methodology

The study period covers sixty-three weeks, from the beginning of the pandemic in Mexico – 27 February 2020 – until 10 May 2021, the estimated date of the end of the second wave. In the time after this period, there was a drastic decrease in the lethality of the virus in the population of the capital (DGE 2021), which could be explained by the effects of the National Vaccination Campaign COVID-19 that began at the end of December 2020 and was applied in the first instance to health personnel and older adults (Secretaría de Salud 2020).

The methodological route was based on the search for and processing of information on the impacts in terms of health and mortality at the district level in Mexico City, considering the data issued from the official website of the Ministry of Health, from the National Council of Humanities, Sciences and Technologies CONAHCyT (DGE 2021). With regard to mortality, the portal's statistical record provides a detailed breakdown that correlates the percentage of patients with different comorbidities to COVID-19-related deaths. Furthermore, it also highlights the age range of those who have been infected, which can aid in the analysis of the correlation between these factors and COVID-19 fatalities.

At the same time, a bibliographic analysis was carried out to determine those elements linked to

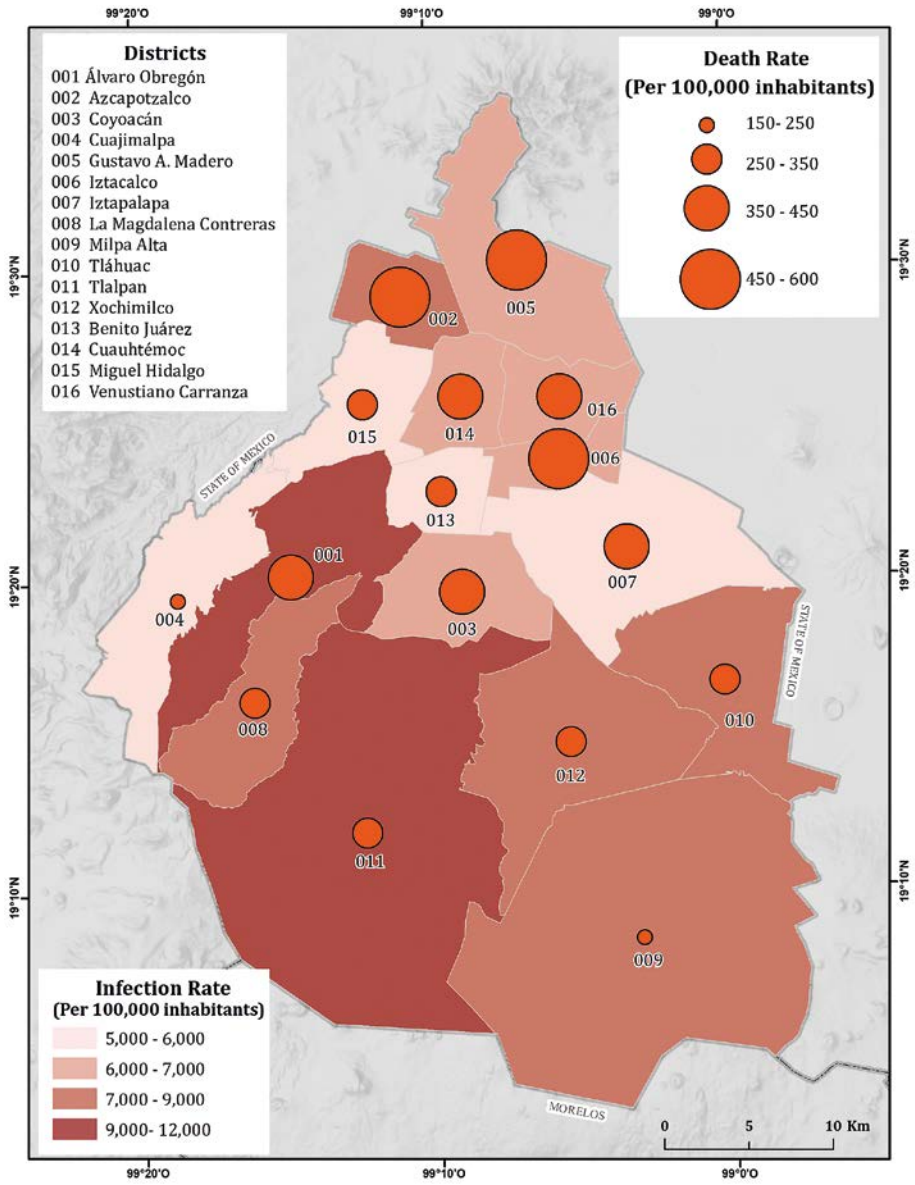

Fig. 3 Infection and death rates by districts, Mexico City (Source: Own elaboration with data from DGE 2021; INEGI 2020; CONAPO 2020; CONEVAL 2020).

greater vulnerability and exposure of the population to COVID-19, which acted as disaster risk drivers (Fig. 4).

Thus, seventeen demographic and socio-economic indicators were determined and obtained through the pages of the Population and Housing Census of the National Institute of Statistics and Geography (INEGI 2020), the marginalization indices by district generated by the National Population Council (CONAPO 2020), as well as the poverty indicators for each district of the National Council for the Evaluation of Social Development Policy (CONEVAL 2020) (Tab. 2).

The demographic dimension variables are mainly related to the characteristics of the population, such as age or the presence of certain comorbidities. The socio-economic indicators, urban marginalization and poverty indices were considered in the first instance, as both express some of the fundamental deprivations of the population numerically.

In addition, some indicators associated with the social dimensions that make up both variables were analyzed to determine their direct influence on the construction of vulnerability and exposure of the population. Finally, other indicators linked to the presence of indigenous or Afro-descendant groups, the level of education, and the economically active population by sector of occupation were included.

4.1 Statistical analysis

Using R Studio software version 4.2.1, 34 statistical tests of Pearson's Correlation Coefficient (r) were carried out between pairs of continuous variables, which made it possible to establish in numerical form the linear relationship and intensity between the two (Vargas 1995). For this paper, the infections and deaths per 100,000 inhabitants at the district level in

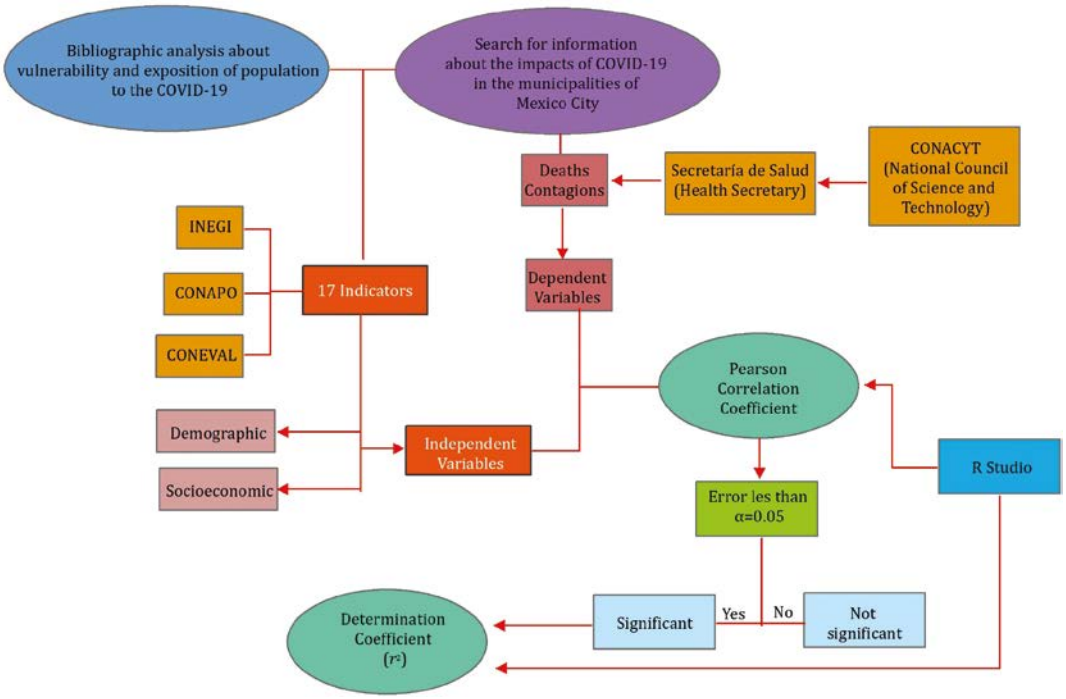

Fig. 4 Scheme of the procedure from literature search to correlation analysis.
INEGI: National Institute of Statistics and Geography. CONAPO: National Population Council. CONEVAL: National Council for Evaluation of Social Development Policy. CONACHyT: National Council of Humanities, Sciences, and Technologies.

Mexico City were considered dependent variables. In contrast, demographic and socio-economic indicators were considered as independent variables.

The conventional confidence level of $\alpha = 0.05$ was used for the statistical tests, i.e., with a probability of error of less than 5%. The values obtained reflect the magnitude and direction of the correlation and can range from −1 to +1, where positive results refer to directly proportional linear correlations and vice versa. For Social Sciences, a magnitude greater than ±0.30 is considered high.

Additionally, Pearson's Coefficient of Determination (r^2) was calculated with significant tests to determine the strength of association between the variables. This made it possible to establish, as a proportion, the variation of the dependent element that its association with the independent variable explains.

Upon obtaining the results of the correlations, the interpretation was made to identify the factors driving disaster risk. These factors are manifested in specific socio-economic and demographic characteristics that give rise to conditions of vulnerability and exposure among the population.

5. Results

The data collected from the official website of the General Directorate of Epidemiology (DGE 2021) showed a differentiated distribution regarding mortality and infections in the different districts that constitute Mexico City. The districts with the highest rates of confirmed cases did not reflect a similar trend in the pattern of deaths in the entity.

In terms of mortality, the data obtained from the interpretation of the statistics provided on the CONACHyT portal revealed that a high percentage of deaths were linked to the presence of comorbidities in the population, including hypertension (39.7%), diabetes (33.2%), and obesity (20%).

The findings of the study are showcased using scatter graphs (Fig. 5) that adeptly depict the relationships between pairs of variables that had a considerable correlation with the number of deaths or infections. Furthermore, a radial graph (Fig. 6) facilitates a comparison of the strength of relationships between the variables. The scatter graphs reveal the direct or inverse linear relationships that exist between the independent variables (demographic and socioeconomic indicators) and the dependent variables (the disease's behavior in terms of deaths and infections).

The radial graph shows the 17 indicators that were selected for the study and the extent to which they are associated with deaths and infections. The data presented in the figure highlights the correlation between infections in Mexico City and socioeconomic variables and the association between deaths and demographic variables of the population.

The results of the study indicate a significant correlation between the age variable and the progression of the disease (Fig. 5). It was observed that the

Tab. 2 Demographic and socio-economic indicators used in the analysis.

Dimension	Indicator	Definition	Source
Demographic	Mean age	The mean age of the population per district.	INEGI 2020
	Population over 60 years of age	Percentage of population over 60 years of age by district.	INEGI 2020
Socioeconomic	Indigenous population	Percentage of the population aged five years and over who speak an indigenous language.	INEGI 2020
	Afro-descendant population	Percentage of the population that considers itself Afro-descendant.	INEGI 2020
	School grade level	Number of years that, on average, persons aged 15 and over passed in the National Education System.	INEGI 2020
	Illiteracy	Percentage of persons aged 15 and over who cannot read and write.	CONAPO 2020
	Poverty	Percentage of the population living in poverty, i.e., when exercising at least one of their rights for social development is not guaranteed, and their income is insufficient to acquire the goods and services they require to satisfy their needs.	CONEVAL 2020
	Marginalization	Marginalization Index. A summary measure identifies the level of deprivation in a population due to lack of access to education, basic services, quality housing, and insufficient income. In this index, a larger number shows a lower degree of marginalization. That is, a larger number implies a smaller lack of the factors that make up the index.	CONAPO 2020
	Lack of space and quality in housing	Percentage of population living in dwellings with at least one of the following characteristics: – material of earthen floors, – roofs of sheeting, cardboard, or waste, – material of mud, bark, reed, bamboo or palm, cardboard, metal, or asbestos sheeting, – having greater than 2.5.	CONEVAL 2020
	Overcrowding	The average number of inhabitants per room in the home. It is considered an index of overcrowding by the National Institute of Geography and Statistics.	INEGI 2020
	Lack of basic housing services	The percentage of the population living in dwellings with the following characteristics: – The water is obtained from a well, river, lake, stream, pipe, or piped water by carrying it from another dwelling or the public tap or hydrant. – They do not have sewerage service or the drainage is connected to a pipe that leads to a river, lake, sea, ravine, or crevice. – No electricity is available. – The fuel used for cooking or heating food is wood or charcoal without a chimney.	CONEVAL 2020
	Economically Active Population	Percentage of economically active population by district.	INEGI 2020
	Percentage of the population employed in the primary sector	Percentage of persons engaged in economic activities in agriculture, animal husbandry, forestry, beekeeping, aquaculture, logging, hunting, and fishing.	INEGI 2017
	Percentage of the population employed in the secondary sector	Percentage of persons engaged in economic activities in mining, oil and gas extraction, manufacturing, electricity generation and distribution, water distribution, and construction.	INEGI 2017
	Percentage of the population employed in trade	The proportion of persons engaged in economic activities in communications, transport, finance, tourism, hotels and catering, leisure, culture, entertainment, public administration, and so-called public services.	INEGI 2017
	Percentage of the population employed in services		INEGI 2017
	Lack of access to basic health services	The percentage of the population without affiliation or entitlement to medical services from any institution providing medical services, including Seguro Popular, public social security institutions (IMSS, federal or state ISSSTE, PEMEX, Army or Navy), or private medical services.	CONEVAL 2020

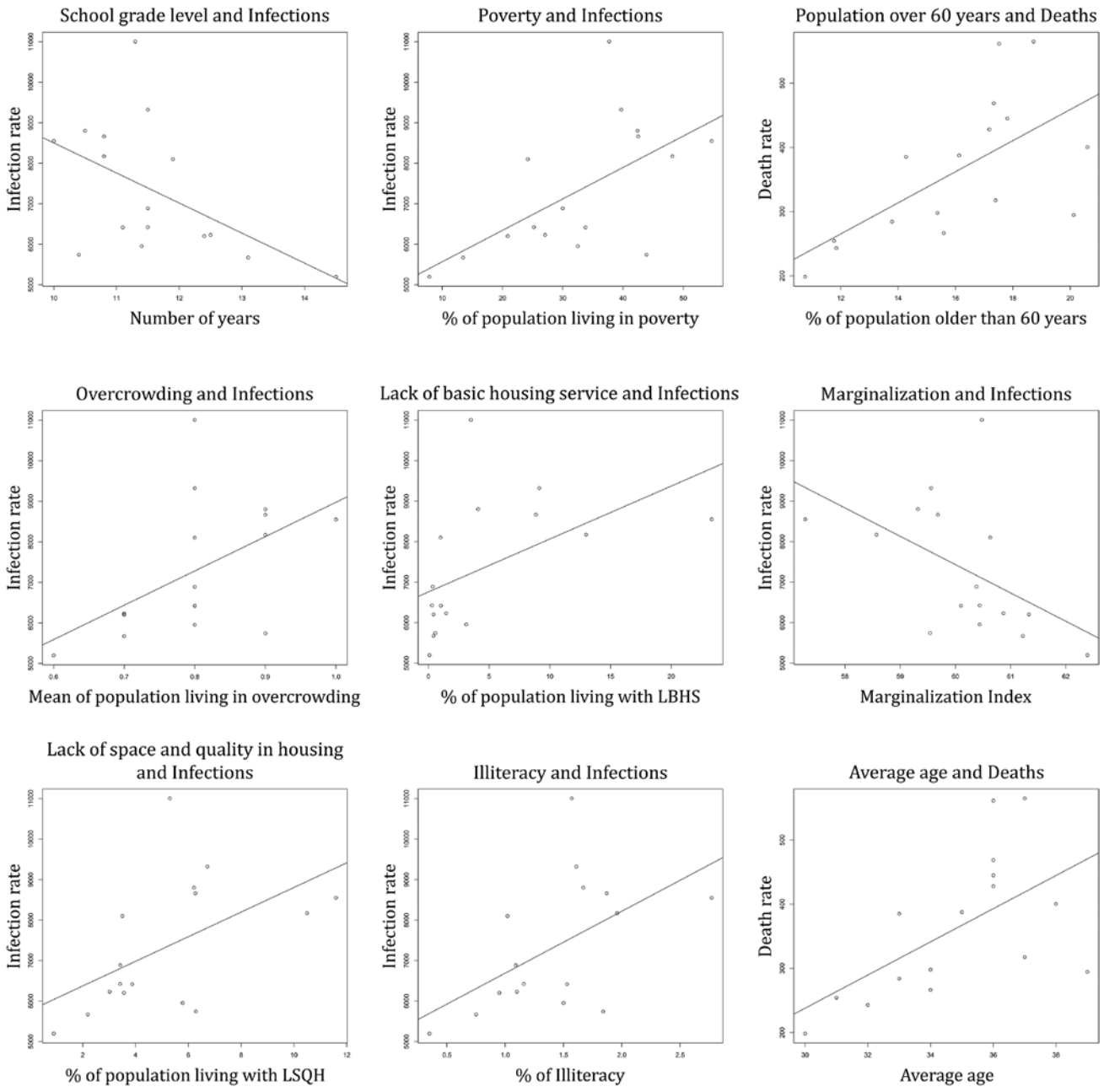

Fig. 5 Scatter plots of the variables that show significant correlations with deaths and infections.

number of deaths increased considerably with the number of years of life of the individuals, as reported by DGE (2021).

Along this vein, the results showed that the average age of the population and the percentage of adults over 60 years of age maintained a positive association with the death rate at the district level with 0.35 and 0.40, respectively; in other words, as the average age and the presence of older adults in the population increased, the number of deaths per 100,000 inhabitants increased by 35% and 40%.

In contrast, as shown in Fig. 6, there is no apparent linear relationship between deaths and the presence of indigenous or Afro-descendant populations, nor with socio-economic aspects such as marginalization, poverty or educational level, the sector of economic activity of the employed population, or access to health and housing services.

On the other hand, of the seventeen Pearson Correlation tests performed to understand the spatial distribution of infections in Mexico City, only seven were significant (Fig. 5). The highest coefficient of determination was obtained when analyzing the poverty data, as this variable explains 36% of the positive cases in the entity. The marginalization index indicates that areas with the highest index are the least marginal. Therefore, the greater the depth of inequality, the higher the rate of infection.

Thus, both the marginalization index and the variables that explained the lack of space and quality in

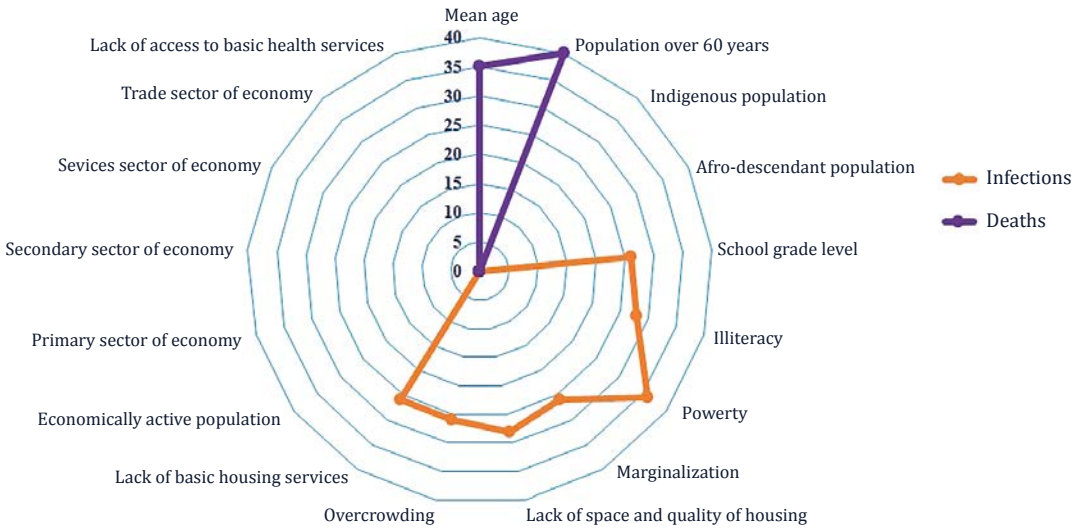

Fig. 6 Percentage of the strength of association between variables.

housing, overcrowding in the home, and the absence of basic services proved to be decisive factors in the construction of vulnerability and exposure of the population, with values ranging from 26% to 28% of the association. The lack of basic services, proper housing, and economic resources can explain 26% to 36% of COVID-19 cases in Mexico City. This is because these factors influence the spread of the virus and the effectiveness of hygiene measures to prevent infection.

Likewise, the level of education and the percentage of illiteracy by demarcation showed significant relationships with the number of infections (Fig. 5). According to the results obtained, the average number of years of schooling is inversely proportional to the infection rate per district; in other words, the lower the level of schooling in the population, the higher the number of positive cases by 26%. Similarly, as the percentage of the illiterate population increased, so did the number of confirmed cases at the district level.

The findings indicate a correlation between the education levels of a population and the range of occupations available. Typically, individuals with lower levels of education may pursue professions that require significant human interaction and are susceptible to job loss (industrial or commercial positions), resulting in greater exposure to potential risk factors.

Populations with a high proportion of illiterate individuals encounter notable obstacles in obtaining dependable information, particularly in written form. This dearth of knowledge can lead to a failure to comprehend key aspects of diseases and the critical steps required to curtail the spread of infections.

In that sense, for the infection, contrary to the behavior of deaths, neither the age of the individuals nor the presence of certain previous illnesses was determinant in the number of reported infections.

Finally, according to the results of the analyses, variables related to the economically active population and the sector of occupation did not play an important role in the population's exposure or vulnerability. Similarly, lack of access to public and private health services, as well as belonging to an indigenous or Afro-descendant group, showed no apparent linear relationship with the pandemic situation in the city.

6. Discussion

The results of the statistical analysis showed that the deaths are closely and exclusively related to factors linked to the intrinsic susceptibility of the populations, that is, to characteristics related to the internal conditions and processes of each individual – such as age or the presence of previous illnesses – that make them more sensitive to the effects of the virus on the body. Thus, the districts with the highest death rates correspond to those with statistically larger populations and some of the highest percentages of individuals aged 60 and over.

Research conducted on children in Mexico showed that 2.8% of confirmed COVID-19 cases were among those under 18, with a median age of 12 and a mortality rate of 1.3%. The study identified several risk factors for mortality, including pneumonia, ICU admission, obesity, hypertension, immunosuppression, diabetes, chronic lung disease, and renal disease (Wong-Chew et al. 2022). These findings are consistent with our analyses as they demonstrate that lethality in infants is significantly lower than that in older adults (over 60 years) and is closely linked to the presence of previous diseases.

Based on the research, it appears that there is a connection between comorbidities and the surge in COVID-19 mortality rates. Furthermore, the study highlights the significance of age, which is strongly linked to the rise in fatalities due to the weakening of the immune system.

On the other hand, infection rates reflect important correlations with factors related to extrinsic vulnerability, that is, with socio-economic aspects such as poverty and marginalization, particularly those related to lack of space and quality in housing, overcrowding, and lack of basic services in the home (piped drinking water, drainage, electricity, and gas cooker), which can be related to the impossibility of observing adequate hygiene and distance measures within the home. Consequently, access to basic services like water is crucial in determining how vulnerable communities are to various hazards, including socio-biological ones like Sars-Cov-2. The lack of these services in homes can create problems. During lockdowns, it made it even harder for vulnerable groups such as homeless individuals to access safe water, sanitation, and hygiene services. This highlights the challenges in applying a human rights approach to the water and sanitation sector, particularly in cases where local governments and service providers fail to operationalize human rights, such as in Mexico City (Liera et al. 2023).

Similar observations have been made in various parts of the world, including New York City. In this area, studies have revealed a positive correlation between several socioeconomic factors, including income, ethnicity, overcrowding, and the infection rate (Hamidi and Hamidi 2021). This highlights the direct impact that the structural characteristics of a population can have on disease transmission. Consequently, it is reasonable to expect that areas with greater inequality may experience more varied patterns of virus distribution.

Furthermore, according to the results, educational level and illiteracy are also important factors in the distribution of infections in the capital. This is primarily explained by the access to written information and the type of economic activity in which most of the population is employed, which prevented compliance with containment measures during the critical period of the pandemic.

The outcomes are ascribed to the societal disparities in the framework that individuals with diverse educational backgrounds encounter. These disparities incorporate the availability of information, mobility, and profession. As per Almagro and Orane-Hutchinson (2022), specific communities demarcated by their socioeconomic traits are more prevalent in various job categories. This aligns with the discoveries of Quinn and Rubb (2005), who contend that an individual's level of education corresponds to their professional undertakings, which may be more or less specialized.

Certain occupations carry a higher risk of contracting the virus, often due to the nature of the work and an individual's education level or specialization. Research by Almagro and Orane-Hutchinson in 2022 on New York City confirms this correlation, with a positive relationship between disease incidence rates and work activities. This can be classified as "occupational exposure".

According to Credit's 2020 study on COVID-19 infections in Chicago and New York, a positive correlation was discovered between the number of health sector professionals and infections in these cities. Almagro and Orane-Hutchinson's 2022 study on servers and workers in the public transportation system also observed the same result.

It is likely that in Mexico City, those with lower levels of education are at a higher risk of contracting the virus due to their participation in activities that require greater human interaction. As a result, any occupation that cannot be suspended due to its inherent nature is associated with an increased risk of exposure.

The displacement of marginalized communities is frequently linked to the widespread use of public transportation, which, when combined with high population densities, has been identified as a contributing factor to the rapid spread of the virus in numerous regions. This phenomenon has been observed in various countries, including England and Wales (Sá 2020), Brazil (Martíns-Filho 2021), and Poland (Ciupa and Suligowski 2021). In Mexico City, population density data at the municipal level may be skewed due to the presence of large geographical areas with small yet densely populated sectors.

Mexico was among the top 10 countries with the highest number of COVID-19 cases and the top 5 countries with the most pandemic-related deaths in 2020 and 2021 despite implementing the sentinel surveillance system (De La Cruz-Hernández and Álvarez-Contreras 2022). Under these circumstances, Knaul et al. (2023) recommended bolstering the Mexican healthcare system in the short term by enhancing accessibility for at-risk populations, expanding healthcare services, including telemedicine, forging public-private partnerships, implementing regulatory measures, and evaluating public health insurance initiatives.

The COVID-19 pandemic put the scientific and technical community in the spotlight of policy-making. In some countries, governments sought their expertise to make well-informed decisions about the best action. Nevertheless, this involved challenges when holding decision-makers responsible for their actions. While scientific and technical experts can offer valuable insights into the virus's spread and the potential impact of various policies, government officials are ultimately responsible for formulating and executing those policies (Weible et al. 2020).

Older adults face multiple risks during the COVID-19 pandemic, including ageism, sexism, susceptibility to illness, and limited access to essential services. These risks threaten their health and well-being and will likely continue to impact them even after the pandemic ends. As such, it would be necessary to implement interventions to meet the unique needs of older adults. These include streamlining care, delivering necessities to their doorstep,

prioritizing older adults among repatriated migrants and refugees, and providing social security measures. It is important to note that older adults with cognitive impairment and those in long-term care facilities are particularly vulnerable to COVID-19 (D'cruz and Banerjee 2020). These measures should be integrated into existing services to reduce resource burden, particularly in lower- and middle-income countries like Mexico.

According to a study by Hidayati and Situmorang (2023), it is essential to assist families and residential communities in aiding the elderly in managing the negative effects of COVID-19. These support systems have created effective coping mechanisms to help the elderly navigate the pandemic and maintain their well-being. To provide the best possible support, family members who are closest to the elderly should receive education on their physical and psychological needs. Furthermore, customized health insurance and social protection policies should be implemented to help the elderly cope with the pandemic's impact. Financial aid should also be available to purchase medication and nutritionally tailored foods for the elderly.

It is essential to take swift and unprecedented measures to protect the health and well-being of all individuals, especially the elderly, who are at a higher risk of serious illness or even death from the virus. From a pedagogical perspective, providing effective interventions and education is crucial to counter any misconceptions about COVID-19 or other viruses. To this end, Kakaşçı et al. (2022) recommend using accurate information alongside innovative methods, such as incorporating visual aids like *pecha kucha* in presentations, which have been shown to be more effective than traditional lectures in reducing anxiety among women aged 65 and older with chronic diseases. Cultural contexts should also be considered in shaping these particular approaches.

Shekhar et al. (2022) analyzed 20 global south cities, including Mexico City and concluded they have high exposure and low adaptive capacity. Accordingly, while some cities perform better in certain indicators of susceptibility, like poverty reduction and formal job provision, high population density and lack of open space remain major areas of concern. The role of urban management and governance is crucial in reducing disaster risks, and the community must be involved in risk preparation, especially vulnerable groups such as the elderly.

7. Conclusions

The disaster triggered by the COVID-19 pandemic has exposed pre-existing risk factors in societies worldwide, such as disproportionate resource use and environmental impact. The world economic system, international mobility, population concentrations, and inequality have created a scenario for new threats to emerge. Vulnerability and exposure are intertwined with socioeconomic factors, such as marginalization, poverty, and limited access to essential services. In Mexico City, several disaster risk drivers increase the risk of COVID-19, including individual traits and broader socioeconomic conditions. Marginalization, poverty, and limited access to services contribute to the spread of the virus. Additionally, uneven population distribution, living conditions, and public transportation use lead to unique transmission patterns. The development model in Mexico has resulted in rapid and disorganized urban growth, exacerbating the inequality gap and increasing vulnerability to hazards, including those of biological origin, such as COVID-19.

The COVID-19 pandemic brought to light apprehensions concerning Mexico's response. It has been observed that the country hasn't adequately catered to the specific requirements of older citizens and other vulnerable groups, who are at greater risk of contracting the virus and facing severe health implications. To overcome this challenge, it is fundamental to enhance the healthcare system, better the working conditions of healthcare workers, and grant broader access to medical services. Additionally, offering all-encompassing support to the elderly, such as financial aid and emotional assistance, can help them deal with the impacts of the pandemic.

Overall, effective disaster risk management is crucial to reduce the potential risks arising from different types of hazards. This approach should be science-informed, integrated and expeditious. It should consider the needs of vulnerable groups, such as the ageing population, and the unique complexities and realities of local contexts. Only by identifying and reducing the vulnerability and exposure of people to risks associated with known and emergent hazards can disasters be avoided.

Acknowledgments

Thanks to the National Council of Humanities, Sciences, and Technologies (CONAHCYT) who provided a student fellowship for Perla Lorena Romero-Gaeta.

References

Alcántara-Ayala, I. (2021): COVID-19, beyond the virus: An outlook to the anatomy of a syndemic pan-disaster. Investigaciones Geográficas 104, 1–15, https://doi.org/10.14350/rig.60218.

Alcántara-Ayala, I., Gomez, Ch., Chmutina, K., van Niekerk, D., Raju, E., Marchezini, V., Cadag, J. R., Gaillard, J. C. (2023): Disaster Risk. London: Taylor & Francis, https://doi.org/10.4324/9781315469614-3.

Alcántara-Ayala, I., Burton, I., Lavell, A., Mansilla, E., Maskrey, A., Oliver-Smith, A., Ramírez-Gómez, F. (2021):

Root causes and policy dilemmas of the COVID-19 pandemic global disaster. International Journal of Disaster Risk Reduction 52: 101892, https://doi.org/10.1016/j.ijdrr.2020.101892.

Almagro, M., Orane-Hutchinson, A. (2022): The determinants of the differential exposure to COVID-19 in New York city and their evolution over time. Journal of Urban Economics 127: 103293, https://doi.org/10.1016/j.jue.2020.103293.

Alpuche-Aranda, C. (2020): Infecciones emergentes, el gran reto de la salud global: Covid-19. Salud Pública de México 62(2), https://doi.org/10.21149/11284.

Blaikie, P., Cannon, T., Davis, I., Wisner, B. (1994): At Risk: Natural Hazards, People Vulnerability and Disasters. London: Routledge, https://doi.org/10.4324/9780203714775.

Ciupa, T., Suligowski, R. (2021): Green-Blue Spaces and Population Density versus COVID-19 Cases and Deaths in Poland. International Journal of Environmental Research and Public Health 18: 6636, https://doi.org/10.3390/ijerph18126636.

CONAPO (2020): Índices de marginación 2020. Publicaciones recientes. Available online: https://www.gob.mx/conapo/documentos/indices-de-marginacion-2020-284372 (accessed on 28 February 2023).

CONEVAL (2020): Indicadores de pobreza por municipio. Medición de la pobreza, Estados Unidos Mexicanos, 2010–2020. Anexo estadístico. Available online: https://www.coneval.org.mx/Medicion/Paginas/Pobreza-municipio-2010-2020.aspx (accessed on 7 March 2023).

Connolly, C., Keil, R., Harris Ali, S. (2021): Extended urbanisation and the spatialities of infectious disease: Demographic change, infrastructure and governance. Urban Studies 58(2), 245–263, https://doi.org/10.1177/0042098020910873.

Corburn, J., Vlahov, D., Mberu, B. et al. (2020): Slum health: arresting COVID-19 and improving well-being in urban informal settlements. Journal of Urban Health 97, 348–357, https://doi.org/10.1007/s11524-020-00438-6.

Cortez-Gómez, R., Muñoz-Martínez, R., Ponce-Jimenez, P. (2020): Vulnerabilidad estructural de los pueblos indígenas ante el COVID-19. Boletín sobre Covid-19, Salud Pública y Epidemiología (Structural vulnerability of indigenous peoples to COVID-19. Bulletin on Covid-19, Public Health and Epidemiology) 1 (7–8), 7–10. In Spanish. Available online: https://dsp.facmed.unam.mx/wp-content/uploads/2022/03/COVID-19-No.7-8-04-Vulnerabilidad-estructural-de-los-pueblos-indigenas.pdf (accessed on 22 March 2023).

Credit, K. (2020): Neighbourhood: Exploring the factors underlying racial and ethnic disparities in COVID-19 testing and infection rates using ZIP code data in Chicago and New York. Center for Spatial Data Science. Regional Science Policy and Practice 12 (6), 1249–1271, https://doi.org/10.1111/rsp3.12321.

Cvetković, V. M., Nikolić, N., Radovanović Nenadić, U., Öcal, A. K. Noji, E., Zečević, M. (2020): Preparedness and preventive behaviors for a pandemic disaster caused by COVID-19 in Serbia. International Journal of Environmental Research and Public Health 17(11): 4124, https://doi.org/10.3390/ijerph17114124.

D'cruz, M., Banerjee, D. (2020): An invisible human rights crisis': The marginalization of older adults during the COVID-19 pandemic – An advocacy review. Psychiatry Research 292: 113369, https://doi.org/10.1016/j.psychres.2020.113369.

De La Cruz-Hernández, S. I., Álvarez-Contreras, A. K. (2022): COVID-19 pandemic in Mexico: The Response and Reopening. Disaster Medicine and Public Health Preparedness 16(6), 2264–2266, https://doi.org/10.1017/dmp.2022.177.

Dirección General de Epidemiología (DGE) (2021): Información General (General Information). Secretaría de Salud. In Spanish. Available online: https://datos.covid-19.conacyt.mx (accessed on 23 January 2023).

ECLAC (2020): Salud y economía: una convergencia necesaria para enfrentar el COVID-19 y retomar la senda hacia el desarrollo sostenible en América Latina y el Caribe. Informe COVID-19 (Health and economy: a necessary convergence to face COVID-19 and resume the path towards sustainable development in Latin America and the Caribbean. COVID-19 report). In Spanish. Available online: https://repositorio.cepal.org/bitstream/handle/11362/45840/S2000462_es.pdf?sequence=4&isAllowed=y (accessed on 15 March 2023).

Fakhruddin, B., Blanchard, K., Ragupathy, D. (2020): Are we there yet? The transition from response to recovery for the COVID-19 pandemic. Progress in Disaster Science (7): 100102, https://doi.org/10.1016/j.pdisas.2020.100102.

Hidayati, D., Widayatun Situmorang, A. (2023): The Importance of Family and Community Approach in Reducing the Risk Faced by the Elderly During the COVID-19 Pandemic. Journal of Disaster Research 18(4), 415–423, https://doi.org/10.20965/jdr.2023.p0415.

Jovanović, A., Klimek, P., Renn, O., Schneider, R., Øien, K., Brown, J., DiGennaro, M., Liu, Y., Pfau, V., Jelic, M., Rosen, T., Caillard, B., Chakravarty, S., Chhantyal, P. (2020): Assessing resilience of healthcare infrastructure exposed to COVID-19: emerging risks, resilience indicators, interdependencies and international standards. Environment Systems and Decisions 40, 252–286, https://doi.org/10.1007/s10669-020-09779-8.

Kakaşçı, Ç. G., Bakır, N., Demir, C. (2022): The effect of pecha-kucha training on fear and belief in myths of COVID-19 in elderly women. International Journal of Disaster Risk Reduction 82: 103353, https://doi.org/10.1016/j.ijdrr.2022.103353.

Knaul, F. M., Arreola-Ornelas, H., Touchton, M., McDonald, T., Blofield, M., Avila Burgos, L., Gómez-Dantés, O., Kuri, P., Martínez-Valle, A., Méndez-Carniado, O., Nargund, R. S., Porteny, T., Sosa-Rubí, S. G., Serván-Mori, E., Symes, M., Vargas Enciso, V., Frenk, J. (2023): Setbacks in the quest for universal health coverage in Mexico: Polarised politics, policy upheaval, and pandemic disruption. The Lancet 402(10403), 731–746, https://doi.org/10.1016/S0140-6736(23)00777-8.

Hamidi, S., Hamidi, I. (2021): Subway Ridership, Crowding, or Population Density: Determinants of COVID-19 Infection Rates in New York City. American Journal of Preventive Medicine 60 (5), 614–620, https://doi.org/10.1016/j.amepre.2020.11.016.

INEGI (2020): Censo de Población y Vivienda 2020. Available online: https://censo2020.mx (accessed on 13 February 2023).

INEGI and INSP (2018): Encuesta Nacional de Salud y Nutrición. Instituto Nacional de Salud Pública, Presentación de resultados. Available online: https://

ensanut.insp.mx/encuestas/ensanut2018/doctos/informes/ensanut_2018_presentacion_resultados.pdf (accessed on 21 February 2023).

Johns Hopkins University (2023): COVID-19 Case Tracker. Coronavirus Resource Center. Available online: https://coronavirus.jhu.edu/map.html (accessed on 10 February 2023).

Karesh, W. B., Dobson, A., Lloyd-Smith, J. O., Lubroth, J., Dixon, M. A., Bennett, M., Aldrich, S., Harrington, T., Formenty, P., Loh, E. H., Machalaba, C. C., Mathew, J., Haymann, D. L. (2004): Ecology of zoonoses: natural and unnatural histories. The Lancet 380 (9857), 1936–1945, https://doi.org/10.1016/S0140-6736(12)61678-X.

Kim, J., Ashihara, K. (2020): National disaster management system: COVID-19 case in Korea. International journal of environmental research and public health 17(18):6691, https://doi.org/10.3390/ijerph17186691.

Lavell, A., Lavell, Ch. (2020): El COVID-19: Relaciones con el riesgo de desastres, su concepto y gestión. KNOW-Conocimiento en acción para la Igualdad Urbana. SG FLACSO y DPU-USL, Londres: 1–43. Available online: https://arise.mx/quiqueg/uploads/2020/03/Lavell_Covid-19_Covid_and_disasters_ESP.pdf (accessed on 3 April 2023).

Lavell, A., Maskrey, M. (2014): The future of disaster risk management. Environmental Hazards 13(4), 267–280, https://doi.org/10.1080/17477891.2014.935282.

Lavell, A., Mansilla, E., Maskrey, A., Ramirez, F. (2020): La construcción social de la pandemia COVID-19: desastre, acumulación de riesgos y políticas públicas. LA RED (Red de estudios sociales para la prevención de desastres en América Latina). Available online: https://www.desenredando.org/covid19/Construcci%C3%B3n-social-pandemia-Covid19-desastre-riesgo-politicas-publicas-RNI-LA-RED-23-04-2020.pdf (accessed on 27 March 2023).

Li, J.-Y., You, Z., Wang, Qi., Zhou, Z.-J., Qiu, Y., Luo, R., Ge, X.-Y. (2020): The epidemic of 2019-novel-coronavirus (2019-nCoV) pneumonia and insights for emerging infectious diseases in the future. Microbes and Infection 22(2), 80–85, https://doi.org/10.1016/j.micinf.2020.02.002.

Liera, C., Dickin, S., Rishworth, A., Bisung, E., Moreno, A., Elliott, S. J. (2023): Human rights, COVID-19, and barriers to safe water and sanitation among people experiencing homelessness in Mexico City. Frontiers in Water 5: 1054182, https://doi.org/10.3389/frwa.2023.1054182.

Luna-Nemecio, J. (2020): Determinaciones socioambientales del COVID-19 y vulnerabilidad económica, espacial y sanitario-institucional. Revista de Ciencias Sociales 26(2), 21–26, https://doi.org/10.31876/rcs.v26i2.32419.

Maital, S., Barzani, E. (2020): The global economic impact of COVID-19: A summary of research. Samuel Neaman Institute for National Policy Research, 1-12. Available online: https://www.neaman.org.il/EN/Files/Global%20Economic%20Impact%20of%20COVID19.pdf (accessed on 6 April 2023).

Martínez-Martínez, A. L., Clemente Soler, J. A., Rodríguez Guillén, D. (2020): La tercera edad como población vulnerable ante el Covid-19. Revista Kairós-Gerontologia 23, (Número Temático Especial 28, "COVID-19 e Envelhecimento"), 365–378. Available online: https://revistas.pucsp.br/index.php/kairos/article/view/51492/33647 (accessed on 10 March 2023).

Martins-Filho, P. R. (2021): Relationship between population density and COVID-19 incidence and mortality estimates: A county-level analysis. Journal of Infection and Public Health 14 (8), 1087–1088, https://doi.org/10.1016/j.jiph.2021.06.018.

Morens, D. M., Fauci, A. S. (2013): Emerging Infectious Diseases: Threats to Human Health and Global Stability. PLoS Pathogens 9(7): e1003467, https://doi.org/10.1371/journal.ppat.1003467.

Morse, S. S. (2004): Factors and determinants of disease emergence. Revue Scientifique et Technique 23(2), 443–451. http://dx.doi.org/10.20506/rst.23.2.1494.

Mostafanezhad, M. (2020): Covid-19 is an unnatural disaster: Hope in revelatory moments of crisis. Tourism Geographies 22(3): 639–645, https://doi.org/10.1080/14616688.2020.1763446.

Nurunnabi, M., Almusharraf, N., Aldeghaither, D. (2020): Mental health and well-being during the COVID-19 pandemic in higher education: Evidence from G20 countries. Journal of Public Health Research 9(1_suppl), https://doi.org/10.4081/jphr.2020.2010.

Oliver-Smith, A., Alcántara-Ayala, I., Burton, I., Lavell, A. (2016): Forensic Investigations of Disasters (FORIN): a conceptual framework and guide to research. México: Integrated Research on Disaster Risk, Instituto de Geografía, Universidad Nacional Autónoma de México. Available online: https://api.semanticscholar.org/CorpusID:134452702 (accessed on 4 February 2023).

Oliver-Smith, A., Alcántara-Ayala, I., Burton, I., Lavell, A. (2017): The social construction of disaster risk: Seeking root causes. International Journal of Disaster Risk Reduction 22, 469–474, https://doi.org/10.1016/j.ijdrr.2016.10.006.

Ortega, A., Armenta, C., García, H., García, J. (2020): Índice de vulnerabilidad en la infraestructura de la vivienda ante el COVID-19 en México. Notas de Población 111. CEPAL. Available online: https://repositorio.cepal.org/bitstream/handle/11362/46559/20-00528_LDN111_07_Diaz.pdf?sequence=1&isAllowed=y (accessed on 18 April 2023).

Pawar, M. (2020): The Global Impact of and Responses to the COVID-19 Pandemic. The International Journal of Community and Social Development 2(2), 111–120, https://doi.org/10.1177/251660262093.

Porcel-Gálvez, A. M., Badanta, B., Barrientos-Trigo, S., Lima-Serrano, M. (2020): Personas mayores, dependencia y vulnerabilidad en la pandemia por coronavirus: emergencia, integración social y sanitaria. Enfermería Clínica 31(1), 18–23, https://doi.org/10.1016/j.enfcli.2020.05.004.

Quinn, M. A., Rubb, S. (2005): The importance of education-occupation matching in migration decisions. Demography 42(1), 153–167, https://doi.org/10.1353/dem.2005.0008.

Rudianto, B., Hendra, Y. (2021): Communication of COVID-19 Pandemic Disaster in Indonesia. Utopía y Praxis Latinoamericana 26(1), 46–54. Available online: https://www.redalyc.org/journal/279/27966119005/27966119005.pdf (accessed on 8 January 2024).

Sá, F. (2020): Socioeconomic Determinants of COVID-19 Infections and Mortality: Evidence from England and

Wales. Policy paper series, IZA Policy Paper No. 159. Institute of Labor Economics. Available online: https://docs.iza.org/pp159.pdf (accessed on 11 January 2024).

Secretaría de Salud (2020): 266. Arranca vacunación contra COVID-19 en México. Available online: https://www.gob.mx/salud/prensa/266-arranca-vacunacion-contra-covid-19-en-mexico?idiom=es (accessed on February 8 2023).

Shekhar, H., Rautela, M., Maqsood, M., Paris, R., Flores de León, R.M., Romero-Aguirre, M. F., Balinos, M., Velázquez, M. E., Amri, G. S., Rahman, T., Asuah, A. Y., Hosni, J., Rahman, Md. S. (2022): Are leading urban centers predisposed to global risks-An analysis of the global south from COVID-19 perspective. Habitat International 121:102517, https://doi.org/10.1016/j.habitatint.2022.102517.

Suárez, V., Suarez Quezada, M., Oros Ruiz, S., Ronquillo De Jesús, E. (2020): Epidemiología de COVID-19 en México: del 27 de febrero al 30 de abril de 2020. Revista Clínica Española 220(8), 463–471, https://doi.org/10.1016/j.rce.2020.05.007.

UN General Assembly (2016): Report of the Open-ended Intergovernmental Expert Working Group on Indicators and Terminology Relating to Disaster Risk Reduction; United Nations General Assembly: 41p. New York. Available online: https://digitallibrary.un.org/record/852089#record-files-collapse-header (accessed on 10 January 2024).

Vargas Sabadías, A. (1995): Estadística descriptiva e inferencial. Murcia. Universidad de Castilla-La Mancha. Available online: https://books.google.cz/books?id=RbaC-wPWqjsC&printsec=frontcover&hl=cs#v=onepage&q&f=false.

Villerías, I., Juárez, M. (2020): México: las enfermedades crónico-degenerativas (diabetes melitus e hipertensión) y la vulnerabilidad ante el COVID-19. Posición. Revista Del Instituto De Investigaciones Geográficas 3, 1–15. Available online: https://posicion-inigeo.unlu.edu.ar/posicion/article/view/135 (accessed on 21 March 2023).

Weible, Ch. M., Nohrsted, D., Cairney, P., Carter, D. P., Crow, D. A., Durnová, A. P., Heikkila, T., Ingold, K., McConnell, A., Stone, D. (2020): COVID-19 and the policy sciences: initial reactions and perspectives. Policy Sciences 53, 225–241, https://doi.org/10.1007/s11077-020-09381-4.

Wisner, B., Blaikie, P., Cannon, T., Davis, I. (2004): At Risk: natural hazards, people's vulnerability and disasters. Psychology Press. Available online: https://www.preventionweb.net/files/670_72351.pdf (accessed on 17 January 2023).

Wong-Chew, R. M., Noyola, D. E., Villa, A. R. (2022): Clinical characteristics and mortality risk factors in patients aged less than 18 years with COVID-19 in Mexico and Mexico City. Anales de Pediatría (English Edition) 97(2), 119–128, https://doi.org/10.1016/j.anpede.2022.03.001.

The nature, dimensions, causes and implications of in and out migration in North-East India

Arundhuti Patangia[1,*], Bimal K. Kar[2]

[1] T.H.B. College, Department of Geography, India
[2] Gauhati University, Department of Geography, India
[*] Corresponding author: arundhutipatangia@gmail.com

ABSTRACT

This article analyses the patterns of inter-state migration (both inward and outward migration within the country) in India's north-east states of Arunachal Pradesh, Assam, Manipur, Meghalaya, Mizoram, Nagaland and Tripura. While most of the previous studies of population migration in India were related to international migration, this article focuses on the analysis of trends and spatial variation of inter-state inward and outward migration and associated rural-urban and male-female differentials in the region. The analysis is primarily based on the Census of India data for 2001 and 2011, because the 2021 Census has not been yet conducted in the country.

KEYWORDS

migration; inter-state migration; inward migration; outward migration; place of origin; place of destination; net migration rate; pull factors; push factors

Received: 8 September 2023
Accepted: 22 March 2024
Published online: 9 April 2024

Patangia, A., Kar, B. K. (2024): The nature, dimensions, causes and implications of in and out migration in North-East India. AUC Geographica 59(1), 20–34
https://doi.org/10.14712/23361980.2024.2

1. Introduction

The process of human migration, which is a universal phenomenon and a key feature of human history, can be considered as one of the most dynamic human activities (Sali and Astig 2015). In simple words, migration is the process of movement of people from one place to another involving change in the place of residence due to a variety of causes. It acts as a factor of redistribution of population over space and time. Sometimes it can be interpreted as a spontaneous effort to achieve a better balance between population and resources. In the words of Lee, migration is a process of change of residence either permanently or semi-permanently.

Indian Constitution provides basic freedom to move to any part of the country, right to reside and earn livelihood of their choices. That is why migrants are not needed to take permission or register at the place of origin as well as at the place of destination (Lusome and Bhagat 2010). India has a long history of internal migration. 2011 Census of India enumerated 450 million internal migrants in the country (based on place of last residence) constituting 37 per cent of its total population (Rajan and Bhagat 2021). The levels of internal migration which can be identified in the country as intra-district, inter-district and inter-state migration Inter-district migrants account for around 10% of the total population of the country as per 2011 Census. In 2001, inter-state migration stood at 4.1% of the total population of the country (Census of India 2001). It slightly increased to 4.6% in 2011. The process of internal migration in India is facilitated by the economic development (Malhotra and Devi 2016). According to Louis-Georges Arsenault, UNICEF India Representative, internal migration is an integral part of development and it should be recognized as such as an indicator of socio-economic progress (Singh 2016).

From the demographic point of view, North-East India, which is considered as a miniature India, is the home of almost all the ethno-linguistically and religiously major groups of people found in the country. There are eleven major streams and waves of migration which built up the present population of North-East India. Thus, migration played an important role in reshaping the population composition in North-East India. In the context of internal migration, intra-district movement is the dominant stream of migration in North-East India. The North-East India had experienced a large volume of influx from across the international border, as more than 99% of its total boundary is shared with foreign countries (Gogoi et al. 2009). Around 2.5% of the total migrants in North-East India have originated from foreign countries. Apart from the international migrants, North-East India has been the receiver of migrants coming from other states and union territories of the country. Most importantly, despite prevalence of almost similar trend of birth and death rates as in the country, the considerably high growth rates of population in the region have been contributed by significant volume of migration from within and outside the country as against considerably low mobility of its people to other parts of the country (Sharma and Kar 1997). Increasing regional inequalities and uneven economic development have led to interstate mobility of people within India. Of the total migrants of North-East India, around 3.5% have come to this region from other states of India (Lusome and Bhagat 2020).

The present work mainly focuses on the analysis of the changing pattern of movement of people between North-East India and the rest of the country in both the directions. The analysis of the causes of migration and male-female differential would provide further insight into the prevailing socio-economic condition of North-East India and its different parts. In view of this, the study bears demographic, socio-economic and political significance.

2. The study area

North-East India (the study area), commonly called the 'Land of Seven Sisters', is located between 20°N and 29°30′N latitudes and 89°46′E and 97°30′E longitudes. Although it has become a common practice to include the state of Sikkim, which is a member-state of North-Eastern Council, within North-East India, here this easternmost region of India consisting of Arunachal Pradesh, Assam, Manipur, Meghalaya, Mizoram, Nagaland and Tripura being contiguous to one another as a region is considered as north-eastern region of India or North-East India. It covers a total area of 255,036 km^2 representing about 7.3% of India's total geographical area. It is surrounded by the hills and mountains from three sides. Its northern and eastern boundaries are represented by the Himalayas and Patkai Hill ranges respectively. North-East India is surrounded by four foreign countries; viz. China, Myanmar, Bangladesh and Bhutan. Towards the west, this region is bordered by plains. To the north of the region lies the Himalayan Kingdom of Bhutan and Tibetan part of China. It is bounded by Myanmar on the east and West Bengal and Bangladesh on the west. The Arakan Yoma of Myanmar and Chittagong hills of Bangladesh, Tripura Hills and Surma plain of Bangladesh lie to the south and south-west of the region. This region is connected with mainland of India through a very narrow corridor of around 22 km width is called Siliguri corridor.

The total population of North-East India is 45,161,611 as per 2011 Census of India, which constitutes 3.7% of the total population of India. The population density of North-East India is 176 persons per km^2 as per 2011 Census data. Among the states of North-East India, Assam is the most densely populated with an average population density of

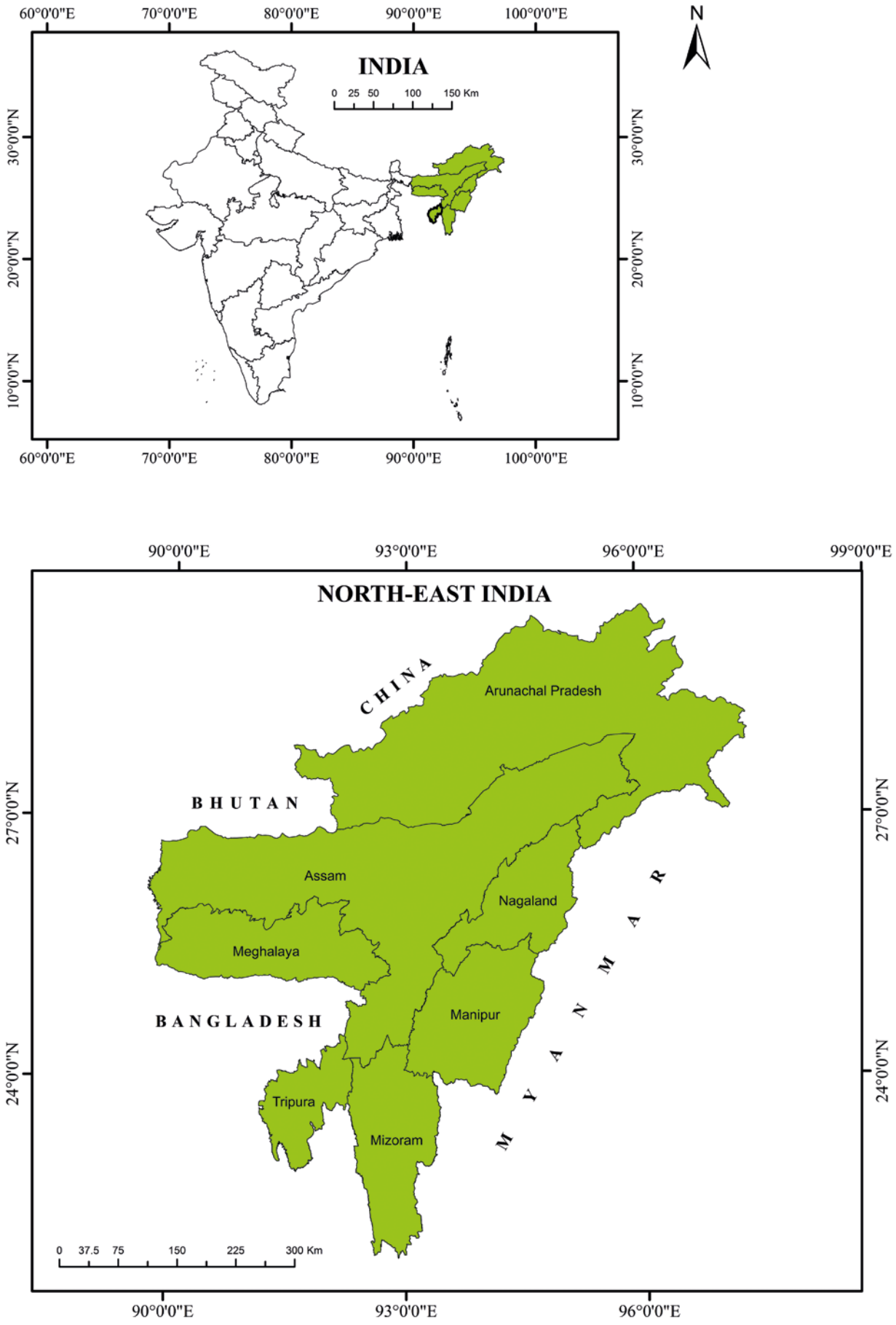

Fig. 1 Location map of the study area (North-East India).
Source: Prepared by the authors.

398 persons per km^2. With an average population density of 17 persons per km^2 Arunachal Pradesh is the most sparsely populated state in this region. The sex ratio of North-East India is 960, which is higher than that of the national average (943). Among the states in North-East India, Manipur has recorded the highest sex ratio (985), followed by Meghalaya (989) and Mizoram (976).

Agriculture is the backbone of the economy of N-E India. About 65% of the total working population is employed in the agricultural sector. This region accounts for a little over 2.5% of the country's GDP. This region (Fig. 1) is lagged behind in economic development due to rapid growth of population, general poverty, subsistence economic base, low level of resource utilization, recurrence of floods, unemployment, lack of technical and vocational education, lack of entrepreneurship, poor infrastructure, poor marketing facilities, insurgency, and illegal migration from neighboring countries (Taher and Ahmed 1998).

3. Data base and methodology

This study is primarily based on secondary sources of data. Data on migration of North-East India are collected from the Census of India which is considered as one of the most reliable sources of population data in the country. Moreover, unit level data of 64th round of National Sample Survey, 2008–2009 is also considered in this study wherever necessary. In this work, trend of inward and outward migration in North-East India is studied on the basis of migration data available as per place of birth. Reasons for migration are categorized as work, business, marriage, moved after birth, and moved with households. The pattern of male-female composition and rural-urban differentials in inward and outward migration of the study area is also analysed through the data available in Census of India. As 2021 Census has not yet been conducted in the country, the present study involves use of data for only 2001 and 2011. The data so obtained from different volumes of Census of India have been processed, analysed and mapped, as and when necessary, through simple quantitative and cartographic techniques. Spatial variation in net migration rate in North-East India is represented thorough choropleth map prepared in the GIS platform (Arc GIS). Here, Net Migration Rate (NMR) is calculated by using the following formula:

$$\text{Net Migration Rate} = \frac{\text{Total number of inward migrants} - \text{Total number of outward migrants}}{\text{Mid-year population}} \times 1000$$

The conclusions of the study are merely based on the results derived from data analysis and available relevant literature.

4. Results and discussion

4.1 Trend and spatial variation of inter-state inward and outward migration

The history of North-East India can be referred to as the history of migration. The states of North-East India have experienced a large influx of people both internally and internationally. In response to socio-economic changes, the spatial pattern of inward and outward migration in North-East India is witnessing changes over time.

According to 2011 Census, 590,939 people migrated to North-East India from the rest of the country as per record of birth. This number was 591,212 in 2001 (Tab. 1). So far the proportion of such in-migrants to total population of this north-east region is concerned; it witnessed a gradual decline from 1.82% in 1991 to 1.54% in 2001 and 1.31% in 2011. It thus reveals that the volume of in-migrants to the north-east region is on decline, although there has been a notion among the people of the north-east that a large number of people from different parts of the country are pouring into it (Lusome and Bhagat 2010). The implementation of Inner Line Permit (ILP) in some north-eastern states restricts the free flow of migrants to the region. Hence, the ILP is regarded by Mizoram, Nagaland, Arunachal Pradesh and Manipur as a constitutional tool to safeguard their native identities and cultures and to manage the population of their tribes and races within their own state by controlling the arrival of outsiders. The state of Meghalaya has also recently demanded the implementation of ILP in the state (Mahanta 2016). Moreover, the North-eastern people are racially, ethnically and culturally different from the people in the rest of the country. Prevailing cultural gaps, prolonged insurgency, ethnic conflicts may be the reasons behind the gradual decline of migrants to North-East India.

According to Kingsley Davis, the movement of people from one state to another within India is less because of the prevalence of the caste system, traditional values, joint family system, diversity of culture, etc. (Davis 1951). Zachariah also observed less mobility of people from one state to another in India as compared to western countries (Zachariah 1964). As regards the volume of out-migration from the North-East India to other states and union territories of India, it witnessed a decrease from 691,234 to 510,353 during 2001–2011 (Tab. 2). It is thus observed that although there has been decline in the volumes of both in-migrants and out-migrants of the region during 2001–2011, the volume of decline in out-migration has been remarkable (Tab. 1 and Tab. 2). Implementation of MNREGA in rural areas may be one of the reasons behind such a decline in the trend of out-migration from N-E India. Besides, gradual progress of infrastructure and consequent steady socio-economic growth in most parts of the region

has also been no less significant in checking out-migration in recent times. Moreover, in the metropolitan cities like Delhi, racism affects the migrants from North-East India at every stage of life, including house rentals, employment, and promotions (Jaiswal 2017). In the mainland India, people from the North-east are often treated "outsiders". The North-east region is poorly understood and frequently disregarded by the media, leaving the people of the main land in the dark regarding its customs and culture. According to a North-East Support Center and Helpline survey on North-East Migration and Challenges in National Cities, 86% of North-Easters claimed to have experienced racial discrimination in Indian metropolises based on this kind of cultural profiling in the years 2009–2010. It is not unusual for a North-east Indian to be asked, "Are you from China?" They disparagingly call North-Easterners "chinky" or make other offensive comments. Novel coronavirus reinforces xenophobia and intolerance against North-eastern people. They were subjected to racial profiling and derogatory stereotypes as the "face of coronavirus" during the Covid-19 outbreak in many mainland Indian cities (Haokip 2021). The experience of migrants in these cities is regrettably marred by racism, violence and prejudice that could be the cause of the sharp fall in the trend of out-migration from N-E India to rest of the country.

The prevailing gap between in-migration and out-migration of population in the region, which can be better understood through net migration rate per thousand population, is found to be low negative (−2.61) in 2001 and low positive (1.78) in 2011. Among the states in the region, Arunachal Pradesh recorded very high positive net migration rates in both 2001 and 2011 (49.63 and 31.85 respectively), Nagaland with very high negative in 2001 (−49.94) and medium positive in 2011 (12.93), and the remaining with low positive and low negative (Tab. 3). It is thus clear that the contribution of in-migrants to the overall growth of population in Arunachal Pradesh during 2001–2011 had been quite significant. On the other hand, very high negative net migration as witnessed in Nagaland in 2001 had been indicative of large scale outmigration probably due to the long continued insurgency. A marked alteration in the balance between inward and out-ward inter-state migration is noticed in Nagaland, Tripura and Assam between the year 2001 and 2011. Manipur is the only state of North-East India where inter-state out-migration exceeded the inter-state in-migration in both 2001 and 2011 (Fig. 2). However, some sort of a balance between in-migration and out-migration is somehow maintained in the region.

Variations can be observed with respect to volume of migration from different parts of the country to North-East India. For the purpose of comparison in this respect, India is divided into five zones, viz**. 1. Northern India zone** comprising Jammu and Kashmir, Himachal Pradesh, Punjab, Uttarakhand, Haryana, Rajasthan, Delhi and Chandigarh; **2. Western India** comprising Gujarat, Maharashtra, Goa, Daman and Diu, Dadra and Nagar Haveli and Lakshadweep;

Tab. 1 State-wise inward migration to North-East India from other states/UTs of India (excluding inter-state migration within N-E India) as per place of birth, 2001 and 2011.

State	Number of in-migrants	
	2001	2011
1. Arunachal Pradesh	65,463	56,400
2. Nagaland	37,554	38,595
3. Manipur	9,395	7,725
4. Mizoram	7,524	6,330
5. Tripura	16,982	36,916
6. Meghalaya	33,037	34,815
7. Assam	421,257	410,158
North-East India	**591,212**	**590,939**

Source: Migration Table D-1, India, Census of India, 2001 and 2011.

Tab. 2 State-wise outward migration from North-East India to other states/UTs of India (excluding inter-state migration within N-E India) as per place of birth, 2001 and 2011.

State	Number of out-migrants	
	2001	2011
1. Arunachal Pradesh	10,969	12,324
2. Nagaland	136,933	13,022
3. Manipur	22,824	29,777
4. Mizoram	5,055	4,343
5. Tripura	25,314	33,913
6. Meghalaya	18,196	19,104
7. Assam	471,943	397,870
North-East India	**691,234**	**510,353**

Source: Migration Table D-1, Census of India, India, 2001 and 2011.

Tab. 3 Net migration rate in North-East India at state level, 2001 and 2011.

State	Net migration rate (per thousand population)	
	2001	2011
1. Arunachal Pradesh	49.63	31.85
2. Nagaland	−49.94	12.93
3. Manipur	−6.20	−7.72
4. Mizoram	2.79	1.81
5. Tripura	−2.60	0.82
6. Meghalaya	6.40	5.30
7. Assam	−1.90	0.39
North-East India	**−2.61**	**1.78**

Source: Calculated based on Migration Table D-1, Census of India, India, 2001 and 2011.

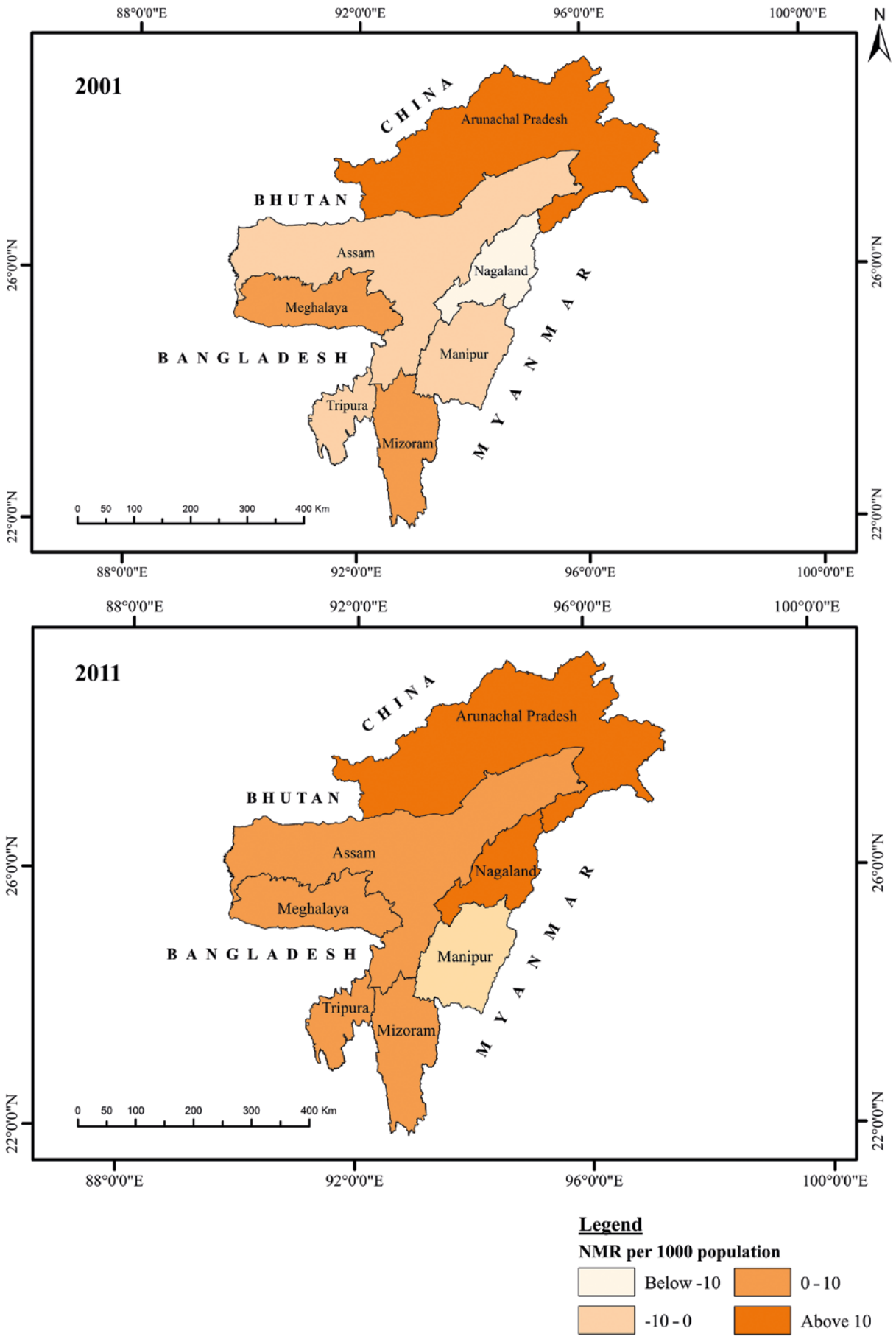

Fig. 2 Net migration rate of North-East India as per place of birth, 2001 and 2011.
Source: Prepared by the authors.

3. Central India comprising Chhattisgarh, Madhya Pradesh and Uttar Pradesh; **4. Southern India** comprising Andhra Pradesh, Telangana, Karnataka, Kerala, Tamil Nadu and Puducherry; and **5. Eastern India** comprising Bihar, Jharkhand, Odisha, Sikkim, West Bengal, and Andaman and Nicobar Islands.

So far volume of in-migration to the N-E India from different parts of India is concerned; it is found that the states of Eastern India are the major source of in-migrants to North-East India. Among the five regions of India, it contributes to around 68% to the total inter-state in-migrants (excluding inter-state migrants within N-E India) in the year 2001. It further increased to more than 73% in 2011 (Tab. 4). On the other hand, constituting merely 1% of total in-migrants, the volume of in-migration from Western India to the north-eastern region is the lowest.

It is further observed that among the north-eastern states, Assam is the major destination of migrants coming from different parts of India (other than N-E India), where more than 4.1 lakh in-migrants constituting 69.41% of total in-migrants settled in 2011. It is distantly followed by Arunachal Pradesh, which received 9.54% of the total migrants from other states and UTs of India (outside N-E India) in 2011. On the other hand, Mizoram with 6,330 migrants coming from other states/UTs of India (outside N-E India) records the lowest position (1.07 per cent) in this respect (Tab. 1).

Now, as regards volume of out-migrants from N-E India to different regions of India is concerned, Eastern India is the largest receiver of migrants originated from North-East India due to its proximity and emergence of Kolkata as one of the largest urban agglomerations in the country. The Eastern Indian states are the destination for about 60% of the inter-state out-migrants (excluding inter-state migrants within N-E India) originated from the North-eastern states of India as per 2001 Census data. This figure, however, declined to 47% in 2011 Census. On the other hand, Southern India received the lowest number of migrants originated from N-E India in 2001. It is found that out of the total inter-state out-migrants (outside North-East India), only 2.87% migrated to Southern India as per 2001 Census, which increased to 13.17% in 2011. With only around 8.83% of the total inter-state out-migrants (outside N-E India), Central India is the lowest receiver of migrants originated from North-East India as per 2011 Census data. It is further observed that unlike other parts of the country, the number of out-migrants from North-East India to Southern and Western India has increased significantly during 2001–2011 due to fast industrialization and prevailing higher wage as compared to other parts of the country, and as a consequence Southern India witnessed a growth of 238% and Western India 107% as against negative growth in the other regions of the country (Tab. 5). So far migration of North-easterners to Southern India is concerned; the state of Karnataka is the largest receiver of migrants. Around 54% of the total migrants to South India from North-East India settled in Karnataka in 2011. Bangalore, the Capital of Karnataka as well as the country's fifth-largest UA, has recorded more than one third of the North-eastern migrants to South India. Here, the majority of N-E migrants are male, i.e. 65% (Census of India 2011). Bangalore, "Silicon Valley of India", probably offers more options that are better suited for men. Due to distance factor, women are less likely to choose Karnataka as their destination. In Bangalore, most of the migrants from the North-East work in both organized and unorganized industries, including retail, hotel, and BPO (Reimeingam 2018). Furthermore, a greater proportion of the migrants arriving in Bangalore comes from urban areas, where people appear to be more informative, educated and affluent. In 2001, about 66 per cent of the migrants from the region to Bangalore originated from urban areas which are increased to 74% after a decade in 2011. Employment is the largest reason for migration with

Tab. 4 Spatial variation in inward migration to N-E India from other parts of India (excluding inter-state migrants within N-E India) as per place of birth, 2001 and 2011.

States of N-E India (place of destination)	Place of origin									
	North India		West India		Central India		South India		East India	
	2001	2011	2001	2011	2001	2011	2001	2011	2001	2011
1. Arunachal Pradesh	6,365	4,454	967	531	12,654	10,197	4,777	3,327	40,700	37,864
2. Nagaland	6,214	4,857	907	397	5,567	4,793	3,586	2,427	21,280	26,121
3. Manipur	2,180	1,500	341	210	1,409	1,028	1,047	365	4,418	4,622
4. Mizoram	869	740	177	105	701	671	832	623	4,945	4,191
5. Tripura	2,181	1,374	357	347	1,789	1,860	855	671	11,800	32,662
6. Meghalaya	5,926	5,460	582	778	3,797	3,775	2,262	2,109	20,470	22,693
7. Assam	47,686	48,140	4,193	3,587	55,575	45,495	14,670	9,451	299,133	303,485
Total	**71,421**	**66,525**	**7,524**	**5,955**	**81,492**	**67,819**	**28,029**	**18,973**	**402,746**	**431,638**

Source: Migration Table D-1, Census of India, India, 2001 and 2011.

Tab. 5 Spatial variation in outward migration from N-E India to other parts of India (excluding inter-state migration within N-E India) as per place of birth, 2001 and 2011.

States of N-E India (place of origin)	Place of destination									
	North India		West India		Central India		South India		East India	
	2001	2011	2001	2011	2001	2011	2001	2011	2001	2011
1. Arunachal Pradesh	3,005	3,828	685	971	799	1,013	2,566	3,209	3,914	3,303
2. Nagaland	24,010	3,727	707	1,426	8,119	1,001	1,034	2,650	103,063	4,218
3. Manipur	8,837	10,317	2,818	4,012	4,906	1,966	2,728	8,869	3,535	4,613
4. Mizoram	2,598	1,615	592	528	395	393	565	990	905	817
5. Tripura	3,674	4,410	1,552	2,381	2,094	1,387	895	2,738	17,099	22,997
6. Meghalaya	8,110	4,510	1,531	2,258	1,041	1,270	1,379	2,791	6,135	8,275
7. Assam	59,675	71,437	20,219	46,598	103,410	38,052	10,697	45,983	277,942	195,800
Total	**109,909**	**99,844**	**28,104**	**58,174**	**120,664**	**45,082**	**19,864**	**67,230**	**412,593**	**240,023**

Source: Migration Table D-1, Census of India, India, 2001 and 2011.

a share of about 46 per cent, followed by the education with 17 per cent, movement of family with 16 per cent and the rest for marriage, business and others. The number of persons migrating from North-East to Bangalore for work climbed by 26 percentage points between 2001 and 2011 that highlights the unemployment problem in the place of origin. Another popular destination for North-eastern migrants is Chennai, the fourth largest Urban Agglomeration in India. As per Census of India, 2011, the number of out-migrants from North-East India to Chennai is 4,817, and majority of which are coming due to movement of family.

When the source of out-migration from among the north-eastern states is looked at, although there has been overall decline during 2001–2011 (Tab. 5), the contribution of Assam to the total volume of out-migration to other parts of the country constitutes 78% as per 2011 Census data (Tab. 2).

4.2 Pattern of rural-urban differential in inward and outward migration

The prevalence of less employment opportunities, low wages, lack of basic amenities, lack of educational facilities, etc., acts as the push factors of out-migration from most of the rural areas. In view of this many people migrate from rural to urban areas in search of better employment opportunities, higher income, better wages and better facilities (Sali and Astig 2015). Since the initiation of economic reforms in 1991, India has been experiencing the rapid flow of migration from rural to urban areas (Bhati 2015). The majority of rural youths migrate to urban areas mainly for better education and livelihood (Deotti and Estrusch 2016). In the case of North-East India also, the movement of people from rural to urban areas constitutes the major stream of in-migrants from other parts of the country as per 2011 Census data. Out of the total inward migrants to North-East India from other parts of the country (outside N-E India), above 63% of migrants are urban-centric (Tab. 6 and Fig. 3). However, when compared between rural to urban and urban to urban in-migration to N-E India, the contribution of rural to urban is more (37.43%) than that of urban to urban (25.68%) with the exception of Mizoram (62.57%). As the tendency of the urban people to move to rural areas is extremely low, the proportion of urban to rural migrants from outside is found to be as low as 6.31 per cent in N-E India. Although the overall pattern of such rural-urban migration is almost the same in N-E India, excepting the state of Tripura, there exist some variations in this respect among the other states of the region. Due to lack of desired level of development of life and living in the urban areas as of Tripura, the urban centric migration in the state is found to be as low as 31%. Among other states, the contribution of urban-centric in-migration from outside N-E India is found to be very high in Nagaland (79%), Meghalaya (77%) and Mizoram (74%) due to fast improvement in urban facilities and better transport connectivity (Tab. 6).

So far out-migration from N-E India to other parts of India is concerned, although the urban-centric migration is more prominent (67.88%), the contribution of urban to urban migration is significantly high (43.02%). Migration from this region to large urban centres has occurred mostly for reasons related to education and employment due to a shortage of employment and educational opportunities. There was a turning point in Indian economic history during the early 1990s. The post-Cold War international system, along with political instability and severe financial crises compelled India to liberalize its economy and implement extensive privatization, which accelerated the globalization of its markets (Haokip 2012). Multinational companies were drawn to India as its economy opened up, not just to invest but also to discover a sizable market for its goods. These changes create a lot of opportunities for work in the

Tab. 6 Patterns of rural-urban in-migration from other parts of India to N-E India (as per place of last residence), 2011.

State	Rural to Rural (%)	Rural to urban (%)	Urban to rural (%)	Urban to urban (%)
1. Arunachal Pradesh	31.58	42.42	8.22	17.78
2. Nagaland	13.82	52.99	6.38	26.81
3. Manipur	15.69	38.87	12.83	32.61
4. Mizoram	15.01	12.20	10.22	62.57
5. Tripura	63.73	17.75	4.69	13.83
6. Meghalaya	13.63	46.58	8.94	30.85
7. Assam	31.25	37.16	5.32	26.27
N-E India	**30.58**	**37.43**	**6.31**	**25.68**

Source: Migration Table D-2, Census of India, 2011.

private sector in urban areas. Thus, rapid migration from North-East India to the mainland urban cities has been occurring since the start of the new millennium (Haokip 2021). Moreover, there are no large-scale industries in the area other than oil mining and plantations in Assam (Lama 2013). A pool of degree holders in the area lack employment opportunities. People are now heavily dependent on public services because self-employment efforts have not yet reached their full potential. This element additionally motivates youth to take competitive exams such as the civil service test. Delhi, the capital city of India, becomes a favoured location for part-time preparation and employment (Singh 2013).

Among the north-eastern states, the proportion of urban-centric out-migration is found to be the highest in Manipur (82.62%), followed by Tripura (78.31%) and Meghalaya (77.36%), and the lowest in Arunachal Pradesh (60.82%) (Tab. 7 and Fig. 3). The prevalence of such a high urban-centric out-migration from Manipur is largely associated with overall human resource development and frequent disturbances. On the other hand, the state of Meghalaya has witnessed the highest rate of urban to urban out-migration (65.87%) from N-E India Male-female composition in urban to urban stream of out-migration from Meghalaya is to some extent balanced. As per 2011 Census, around 53% of the total urban to urban out-migrants from this state is female and the remaining 47% are male out-migrants. Movement of family is recorded to be the major cause of out migration of female (48.4%). On the other hand, the significant causes of urban to urban male out-migration from Meghalaya to other parts of the country are found to be employment and movement of family (33.87% and 33.83% respectively) (Tab. 7).

4.3 Pattern of male-female composition in inward and outward migration

As elsewhere, the inter-state in-migration to N-E India appears to be male-dominated. In the year 2001 the male in-migrants to this region constituted around 60% of the total interstate in-migrants from outside N-E India (2001 Census). Although there had been a trend of balancing in male-female composition of in-migrants during 2001–2011 in the region, the proportion of male in-migrants is still found to be as high as around 54% as per 2011 Census data. When compared between the rural and urban areas, the proportion of male in-migrants is considerably higher in the urban areas (56%) as compared to that of rural areas (51%). Among the states of N-E India, the proportion of male in-migrants is found to be the highest in Mizoram (69.76%), followed by Arunachal Pradesh (62.44%) and Nagaland (62.12%), and the

Tab. 7 Patterns of rural-urban out-migration from N-E India to other parts of India (as per place of last residence), 2011.

State	Rural to rural (%)	Rural to urban (%)	Urban to Rural (%)	Urban to urban (%)
1. Arunachal Pradesh	24.89	18.53	14.19	42.39
2. Nagaland	15.51	16.84	15.45	52.20
3. Manipur	9.97	27.17	7.41	55.45
4. Mizoram	16.57	18.03	10.97	54.43
5. Tripura	14.62	21.23	7.07	57.08
6. Meghalaya	9.00	11.49	13.64	65.87
7. Assam	26.04	26.36	8.30	39.30
N-E India	**23.31**	**24.86**	**8.81**	43.02

Source: Migration Table D-2, Census of India, 2011.

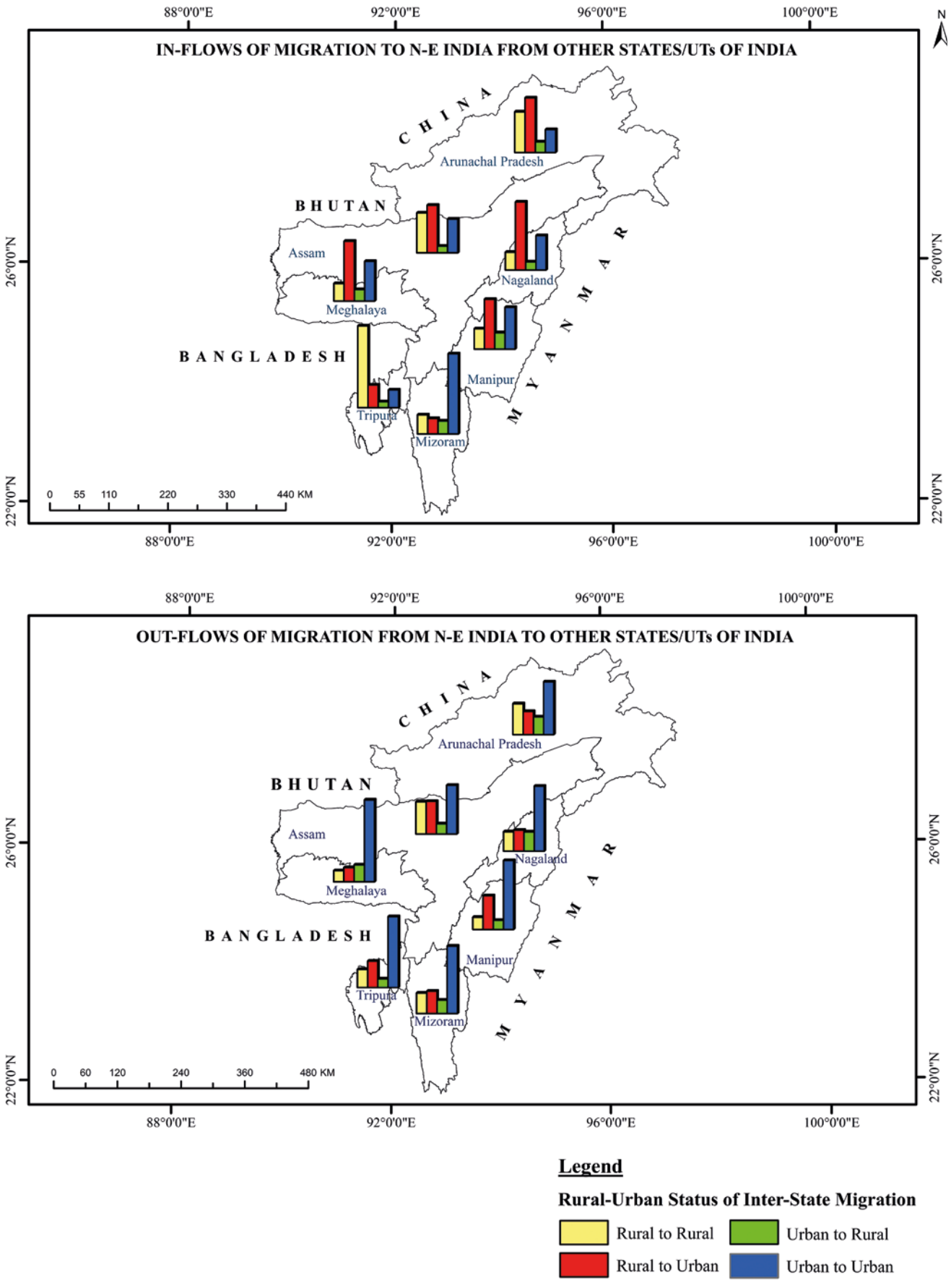

Fig. 3: Rural-urban status of migration flows between N-E India and other states/UTs of India, 2011.
Source: Prepared by the authors.

lowest and somewhat balanced in Assam (51.94%). Moreover, although the gap between the proportions of male and female in-migrants in the rural areas of the region is quite insignificant, it is more than 67% point in Mizoram (Male: 83.83%; Female: 16:17%), followed by 28.58% point in Arunachal Pradesh, and low negative of −5.5% point in Assam (Tab. 8). The prevalence of such a high proportion of male-selective migration particularly in the states of Mizoram, Arunachal Pradesh and Nagaland has been largely associated with in-migration of male workers from outside N-E India for various development activities including construction of roads, etc.

So far male-female composition of out-migration from N-E India is concerned, it is found to be female-dominant with proportion of female out-migrants as 52.06% (2011 Census). It can be associated with the flexibility of gender roles. North-East India has a greater rate of female work participation than the rest of India (Singh 2013). Other than Kerala, North-East India is the only region where female migration has been reported for reasons other than marriage, such as work and education, in contrast to other regions where "marriage" still predominates as the reason for leaving the state (Mukherjee and Dutta 2017). NSSO (64th Round) 2007–2008 reveals that just 0.70 per cent of female migration is related to employment at national level. While almost 25% of all women in North-East India migrate in search of work. The largest percentage of migration related to employment was recorded in Meghalaya (39.20%), followed by Manipur (27.03%), Arunachal Pradesh (26.20%), and Mizoram (22.40%). Again, only 0.50 per cent of women moved across the country in search of higher education opportunities. Conversely, it is revealed in the North-eastern states that roughly one-fourth of them relocated for higher education. This can be an indication that women in these areas enjoyed greater independence due to the matriarchal nature of many tribal cultures (Bango and Kashyap 2018).

When compared between rural and urban areas in this respect, the proportion of female out-migrants is even higher to the rural areas (59.04%) and

Tab. 8 Pattern of male-female composition in inward migration to North-East India from other states/union territories of India (excluding inter-state migration within North-East India) as per Place of Birth, 2011.

State	Proportion of male and female in-migrants (in %)					
	Total		Rural		Urban	
	Male	Female	Male	Female	Male	Female
1. Arunachal Pradesh	62.44	37.56	64.29	35.71	61.11	38.89
2. Nagaland	62.12	37.88	62.14	37.86	62.11	37.89
3. Manipur	58.82	41.18	58.87	41.13	58.80	41.20
4. Mizoram	69.76	30.24	83.83	16.17	66.30	33.70
5. Tripura	55.90	44.10	57.12	42.88	53.28	46.72
6. Meghalaya	54.05	45.95	52.11	47.89	54.66	45.34
7. Assam	51.94	48.06	47.25	52.75	54.80	45.20
N-E India	**54.26**	**45.74**	**51.22**	**48.78**	**56.13**	**43.87**

Source: Migration Table D-1, India, Census of India, 2011.

Tab. 9 Pattern of male-female composition of outward migrants from North-East India to other states/union territories of India (excluding inter-state migration within North-East India) as per place of birth, 2011.

State	Proportion of male and female out-migrants (in %)					
	Total		Rural		Urban	
	Male	Female	Male	Female	Male	Female
1. Arunachal Pradesh	54.34	45.66	55.70	44.30	53.43	46.57
2. Nagaland	49.36	50.64	49.06	50.94	49.49	50.51
3. Manipur	51.96	48.04	53.76	46.24	51.61	48.39
4. Mizoram	46.86	53.14	45.99	54.01	47.10	52.90
5. Tripura	51.87	48.13	47.37	52.63	53.00	47.00
6. Meghalaya	46.34	53.66	43.75	56.25	47.02	52.98
7. Assam	47.15	52.85	39.30	60.70	51.28	48.72
N-E India	**47.94**	**52.06**	**40.96**	**59.04**	**51.21**	**48.79**

Source: Migration Table D-1, India, Census of India, 2011.

lower than male to the urban areas (48.79%). However, there exist some variations in this respect between the male and female out-migrants. Although out-migration from the N-E India is largely female-dominant with highest rate from Meghalaya, it is found to be male dominant from the states of Arunachal Pradesh, Manipur and Tripura. In the case of urban-centric out-migration, it is male dominant from the states of Arunachal Pradesh, Tripura, Manipur and Assam (Tab. 9). In any case, the prevailing rate of female out-migration from different states of N-E India almost equally with male, if not more in some cases, is indicative of the rise in women's socio-economic empowerment (Mahapatro 2014).

4.4 Causes of inter-state inward and outward migration

Analysis of the reasons behind movement of people from one place to another is one of the most important aspects of migration study, because nobody moves without any cause. Among diverse causes of migration, livelihood insecurity is found to be the leading one (Kumar et al. 2022). So far North-East India is concerned; the major cause of its inter-state migration is recorded as employment (work) and business. Marriage is another significant reason for inter-state migration to N-E India.

As per 2011 Census data, North-East India witnessed as high as 35.29% of in-migrants from other parts of India due to employment and business. Marriage, the second most important cause of inter-state in-migration to this region, constitutes 24.30% of the total in-migrants. The migration due to movement of family has contributed 21.04% of total in-migration in the region (Tab. 10). The contribution of education in this respect is quite insignificant (1.06%), as development of educational infrastructures in the region is still much behind many other parts of the country. The choices for modern education are also very limited in the region.

So far the major causes of in-migration from different source regions of the country is concerned, although the pattern appears to be almost the same for most parts of the country, the contribution of employment and business, and marriage is the highest from Eastern India (37.15% and 25.40% respectively) due to its nearness and socio-cultural similarities with N-E India. On the other hand, the major reason behind migration from western India is found to be movement of family, which contributes to as high as 32.69% of the total in-migrants from the western India (Tab. 10).

The dominant cause of inter-state out-migration from North-East India to other parts of the country is found to be movement of family. It constitutes as

Tab. 10 Causes of inward migration to North-East India from different parts of India (as per place of last residence), 2011.

Region of origin of migrants	Percentage distribution of in-migrants due to different causes					
	Employment and business	Education	Marriage	Moved after birth	Movement of family	Other causes
North India	27.82	1.59	18.25	2.77	25.62	23.92
East India	37.15	0.81	25.40	1.68	19.82	15.14
Central India	32.70	0.97	24.23	1.42	24.05	16.63
West India	22.32	2.92	13.77	2.40	32.69	25.90
South India	33.42	3.90	15.39	1.94	25.59	19.76
All India	**35.29**	**1.06**	**24.30**	**1.69**	**21.04**	**16.62**

Source: Migration Table D-3, India, Census of India, 2011.

Tab. 11 Causes of outward migration from North-East India to other parts of India (as per place of last residence), 2011.

Place of destination	Percentage distribution of out-migrants due to different causes					
	Employment and business	Education	Marriage	Moved after birth	Movement of family	Others
North India	24.46	6.30	17.65	1.95	34.82	14.82
East India	13.94	1.69	32.41	2.61	30.77	18.58
Central India	18.68	5.38	28.11	1.34	33.00	13.49
West India	42.49	6.76	8.06	2.41	26.08	14.20
South India	42.50	14.67	5.50	1.84	19.31	16.18
All India	**23.64**	**5.30**	**22.56**	**2.23**	**29.75**	**16.52**

Source: Migration Table D-3, India, Census of India, 2011.

high as 29.75% of the total out-migrants, followed by employment and business (23.61%) and marriage (22.56%). The contribution of education (5.30%) as a driver of out-migration is found to be somewhat significant as compared to in-migration (1.06%) (Tab. 11).

The North-eastern region of India has experienced violent incidents and conflicts related to secessionist movements and insurgencies since the country's independence. People from many racial backgrounds, languages, and socio-cultural traditions live in the area have made these issues more complicated. Their demand for ethnic homelands to safeguard and maintain their own culture and identity has therefore sparked conflict, which has resulted in internal displacement (Phukan 2013). The decades-long ethnic hostilities have once again come to prominence due to a flare-up of violence between the Meiteis and the Kukis in the North-eastern Indian state of Manipur, which started in May, 2023 that has resulted in around 200 fatalities and 60,000 displaced inhabitants (The Hindu). Due to prolonged histories of insurgency and a dearth of economic opportunities, North-eastern states have substantial negative factors that are pushing young people from them to other regions of India. In the areas where insurgencies and wars are prevalent, parents most often send their children out of state to finish their education, not only for security reasons but also to keep them away from joining the local insurgent groups (Hangsing 2023).

The North-Eastern region was declared a "Disturbed Area" under the Disturbed Areas (Special Courts) Acts of 1976, and later under the Armed Forces Special Power Act (AFSPA) of 1958, which finally resulted in a substantial emigration of people as it legitimizes the use of violent means by armed forces to maintain the public order in "disturbed areas" without imposing any time limits in the longevity of its application (Gogoi and Pandov 2022).

So far spatial variation in the contribution of different factors of out-migration from North-East India is concerned, the proportion of out-migration due to movement of family is found to be the highest in North India (34.82%), followed by Central India and East India; in South India and West India due to employment and business (42.50%); in East India due to marriage (32.41%); and in South India due to education (14.67%) (Tab. 11). It means South India and West India owing to massive developments in industrial and IT sectors attract more people from

Tab. 12 Causes of inward migration to North-East India from other states/union territories of India (outside North-East India) as per place of last residence, 2011.

State (place of destination)	Percentage distribution of in-migrants due to different causes					
	Employment and business	Education	Marriage	Moved after birth	Movement of family	Others
1. Arunachal Pradesh	44.13	1.51	9.79	1.85	26.95	15.77
2. Nagaland	42.05	2.11	11.54	1.29	26.06	16.95
3. Manipur	32.69	5.37	14.44	1.57	20.58	25.35
4. Mizoram	45.74	2.72	6.00	1.10	23.18	21.26
5. Tripura	51.70	0.34	7.76	0.42	26.86	12.92
6. Meghalaya	29.70	2.87	19.05	3.25	26.90	18.23
7. Assam	31.40	0.66	30.22	1.91	19.14	16.67

Source: Migration Table D-3, Census of India, 2011.

Tab. 13 Causes of outward migration from North-East India to other states/union territories of India (outside North-East India) as per place of last residence, 2011.

State (place of origin)	Percentage distribution of out-migrants due to different causes					
	Employment and business	Education	Marriage	Moved after birth	Movement of family	Others
1. Arunachal Pradesh	15.87	18.23	9.21	2.53	30.42	23.74
2. Nagaland	21.65	9.56	14.50	3.34	32.32	18.63
3. Manipur	27.25	22.70	7.58	1.45	23.50	17.52
4. Mizoram	23.70	19.60	9.32	1.48	27.52	18.38
5. Tripura	21.75	6.11	18.04	1.85	32.40	19.85
6. Meghalaya	20.96	8.33	13.25	2.17	35.60	19.69
7. Assam	30.87	2.43	21.79	2.02	27.28	15.61

Source: Migration Table D-3, India, Census of India, 2011.

N-E India for employment; East India attracts more out-migration from N-E India for marriage due to nearness and more socio-cultural homogeneity; and South India attracts out-migration of large volume of youths for education due to the availability of modern and diverse educational facilities and associated job opportunities.

4.5 Pattern of spatial variation in the causes of inward and outward migration

So far the causes of migration are concerned; there exists spatial variation with respect to the causes of inward and outward migration in N-E India depending on the prevailing variation in socio-economic conditions in the areas of origin and destination.

Among the states of North-East India, the proportion of in-migrants coming for the purpose of employment and business is found to be the highest in Tripura (51.70%), followed by Mizoram (45.74%), Arunachal Pradesh (44.13%) and Nagaland (42.05%), and the lowest in Meghalaya (29.70%). In the case of marriage as the cause of in-migration, the proportion is found to the highest in Assam (30.22%) and the lowest in Mizoram (6.00%) (Tab. 12). The contribution of education towards in-migration in different states of N-E India is very insignificant.

Among the various causes of out-migration from the states of N-E India, movement of family, employment and business, marriage and education are considered to be important. On the other hand, among the states of out-migration, Assam witnesses the highest proportion due to employment and business (30.87%); Meghalaya due to family movement (35.60%); Assam due to marriage (21.79%); and Manipur due to education (22.70%) (Tab. 13).

5. Conclusion

The foregoing discussion reveals that although there has been no change in the volume of in-migration from different parts of India to North-East India as against marked decline in the volume of out-migration from the region to other parts of the country during 2001–2011, the net migration rate in the region has become low positive from low negative. The decline in out-migration of population from N-E India in recent times is largely due to increased job opportunities and financial support to the different socio-economically marginalized sections of people under various schemes of the state and central governments including MGNREGA. Among the north-eastern states, while the most populous state of Assam handles around three-fourth of total migration, the sparsely populated hill states like Arunachal Pradesh and Nagaland witness considerably high and moderate rate of net migration. As regards the volume and direction of in-migration and out-migration, it has been almost uniformly from and to Eastern India due to its nearness and the socio-cultural similarity with the majority people of Assam and Tripura. While the pattern with respect to in-migration has remained almost the same, the volume of out-migration to Southern India and Western India has been on the rise due to fast growing diverse job opportunities with consequent decline in out-migration to Eastern India in recent times. In the case of rural-urban migration, the in-migration is dominated by rural population, and out-migration is contributed almost uniformly by both urban and rural population. In gender terms, the in-migration from outside N-E India has been slightly male-dominant, and out-migration has been largely female dominant, and more so from rural areas.

The process of in-migration and out-migration and its volume to and from N-E India is associated with a variety of socio-economic factors including the distance between source and destination. In the case of in-migration it is largely contributed by employment and business, and marriage, while the out-migration from N-E India is caused mainly by movement of family, and employment and business. Among the states of N-E India, while all the states witness very high contribution of employment and business towards the volume of in-migration from outside the region with highest being in Tripura, the contribution of marriage in this respect is also quite significant in the case of Assam. The out-migration from N-E India is caused almost equally by both employment and business, and movement of family for better life and living. Although a large size of youths of N-E India moves out to different parts of the country for education, it is quite significant in the case of Manipur, Mizoram and Arunachal Pradesh. Hence, a balanced development in all sectors in most parts of the country including its North-East region shall ensure a balanced pattern of in-migration and out-migration to and from the region.

References

Bango, M., Kashyap, G. C. (2018): Changing trends in work participation of tribal women by education in some selected states of India. International Journal of Arts Humanities and Social Sciences Studies 3(2), 53–59.

Bhagat, R. B., Keshri, K., Ansary, R. (2018): Internal migration in India: Intensity, flows and impact. In Comparing Internal Migration in the Countries of Asia" Conference, Asian Demographic Research Institute, Shanghai University, Shanghai, China, July. Available online https://www.researchgate.net/profile/R-Bhagat/publication/334494446_Internal_Migration_in_India_Intensity_Flows_and_Impact/links/5d2e0806a6fdcc2462e60f42/Internal-Migration-in-India-Intensity-Flows-and-Impact.pdf (accessed on 20 July 2021).

Bhati, R. K. (2015): A Study of Rural to Urban Migration in India. ASM's International E-Journal on Ongoing Research in Management and IT, X, 371–379.

Davis, K. (1951): The Population of India and Pakistan, Princeton University Press, New Jersey, 127–165. Available online https://www.milbank.org/wp-content/uploads/mq/volume-30/issue-02/30-2-The-Population-of-India-and-Pakistan-by-Kingsley-Davis.pdf (accessed on 20 July 2021).

Deotti, L., Estruch, E. (2016): Addressing rural youth migration at its root causes: A conceptual framework, Rome: Food and Agriculture Organization of the United Nations [FAO]. Available online http://www.fao.org/3/a-i5718e.pdf (accessed on 26 June 2023).

Gogoi, J. K., Goswami, H., Borah, K. C. (2009): Problems of border areas in North East India: Implications for the thirteenth finance commission. Department of Economics, Dibrugarh University: Dibrugarh, India. Available online https://fincomindia.nic.in/archive/writereaddata/html_en_files/oldcommission_html/fincom13/Discussion/report14.pdf (accessed on 25 August 2021).

Gogoi, P., Pandov, P. (2022): A study about the implementation of AFSPA against ethnic clashes of North-East India. NeuroQuantology 20(16), 3863–3868, https://doi.org/10.48047/NQ.2022.20.16.NQ880390.

Hangsing, L. (2023): Re-Interpreting Home and Identity: An Ethnographic Study of the Kuki Migration in Delhi (Doctoral dissertation, Ambedkar University Delhi). Available online https://www.researchgate.net/profile/Lunpithang-Hangsing/publication/374117321_Re-Interpreting_Home_and_Identity_An_Ethnographic_Study_of_the_Kuki_Migration_in_Delhi/links/650e7ac082f01628f03d3000/Re-Interpreting-Home-and-Identity-An-Ethnographic-Study-of-the-Kuki-Migration-in-Delhi.pdf (accessed on 14 December 2023).

Haokip, T. (2012): Political integration of northeast India: A historical analysis. Strategic Analysis 36(2), 304–314, https://doi.org/10.1080/09700161.2012.646508.

Haokip, T. (2021): From 'Chinky' to 'Coronavirus': racism against Northeast Indians during the Covid-19 pandemic. Asian Ethnicity 22(2), 353–373, https://doi.org/10.1080/14631369.2020.1763161.

Jaiswal, N. (2017): 'Insurgency' There and 'Identity' Here: A Study of Northeast Indian Migrants in Delhi, M.phil Dissertation, Department of Geography, Delhi School of Economics, University of Delhi. Available online https://www.kuasu.cpier.kyoto-u.ac.jp/wp-content/uploads/2017/03/10-3.Neha-Jasiwal.pdf (accessed on 14 December 2023).

Kumar, S., Sati, V. P., Singh, R., Roy, C. (2023): Patterns and drivers of internal migration: insights from Jharkhand, India. GeoJournal 88(5), 4971–4990, https://doi.org/10.1007/s10708-023-10895-6.

Kumar, T. V., Barman, U., Saikia, H. (2022): Perceived Reasons of Interstate Out-migration of Rural Youth. Multilogic in Science X(XXXV), 1288–1292.

Lama, M. P. (2013): Labour and employment in North-Eastern region: challenges and opportunities. Labour Dev 20, 1–11.

Lusome, R., Bhagat, R. B. (2010): Migration Situation in Northeast India. K. S. James, Arvind Pandey, D. W. Bansod, Lekha Subaiya (eds) Population, Gender and Health in India: methods, Processes and Policies, Academic Foundation, New Delhi, 2010, 167–190.

Lusome, R., Bhagat, R. B. (2020): Migration in Northeast India: Inflows, outflows and reverse flows during pandemic. The Indian Journal of Labour Economics 63, 1125–1141, https://doi.org/10.1007/s41027-020-00278-7.

Mahanta, R. (2016): Inner Line Permit as an Instrument of Protecting Identity: Benefits, Costs and its Effectiveness. Identity Aspirations, Developmental Backlogs and Governance Issues in Northeast India, 55. Available online https://www.researchgate.net/profile/Madhurjya-Bezbaruah/publication/320107830_Identity_Aspirations_Developmental_Backlogs_and_Governance_Issues_in_Northeast_India_Edited_Volume/links/59ee19c3aca272029ddf61e4/Identity-Aspirations-Developmental-Backlogs-and-Governance-Issues-in-Northeast-India-Edited-Volume.pdf#page=63 (accessed on 8 December 2023).

Mahapatro, S. (2014): Contemporary patterns and issues of internal migration in India: Evidence from NSSO. In KNOWMAD conference on Internal Migration and Urbanization, Dhaka, May 1st. Available online https://www.knomad.org/sites/default/files/2018-01/Contemporary%20Patterns.pdf (accessed on 20 July 2021).

Malhotra, N., Devi, P. (2016): Analysis of factors affecting internal migration in India. Amity Journal of Economics 1(2), 34–51.

Mukherjee, M., Dutta, C. (2017): Migration of north-east women in Delhi: A macro level analysis. Journal of Social Inclusion Studies 3(1–2), 95–112, https://doi.org/10.1177/2394481120170107.

Phukan, M. D. (2013): Ethnicity, conflict and population displacement in Northeast India. Asian Journal of Humanities and Social Sciences 1(2), 91–101.

Rajan, S. I., Bhagat, R. B. (2021): Internal migration in India: integrating migration with development and urbanization policies. Policy Brief, 12, 59. Available online https://www.knomad.org/sites/default/files/2021-02/Policy%20Brief%20-%20Internal%20Migrationand%20Urbanization%20-%20India%20Policy%20Brief%2012%20Feb%202021.pdf (accessed on 20 July 2021).

Reimeingam, M. (2018): Migration from North Eastern Region to Bangalore: Evidences from Census Data. Journal of North East India Studies 8(1), 40–56.

Sali, R. S., Astige, S. B. (2015): Causes and consequences of migration in India: a sociological perspective. Golden Research Thoughts 4(7), 1–11.

Sharma, H. N., Kar, B. K. (1997): Pattern of Population Growth in North-East India. Aijazuddin, Ahmad, Daniel Noin, and HN Sharma, eds. Demographic Transition: The Third World Scenario, Rawat Publications, Jaipur, New Delhi, India, 1997, 73–93.

Singh, H. (2016): Increasing rural to urban migration in India: A challenge or an opportunity. International Journal of Applied Research 2(4), 447–450.

Singh, M. A. (2013): Outmigration from North East India: Floating Migrants and Emerging Distinct Identity. Labour & Development 22(2), 30–46.

Taher, M., Ahmed, P. (1998): Geography of North-East India, Mani Manik Prakash, Guwahati, India, 248–270.

Zachariah, K. C. (1964): A historical study of internal migration in the Indian Sub-Continent, 1901–1931. Asia Publishing House, Delhi, India, 34–41.

Morphostructural evolution of the Labe and Jizera rivers confluence area (the Bohemian Massif, Czechia)

Tereza Steklá*, Jan Kalvoda

Department of Physical Geography and Geoecology, Faculty of Science, Charles University, Czechia
* Corresponding author: tereza.stekla@natur.cuni.cz

ABSTRACT
This article investigates the morphostructural evolution of the Labe and Jizera rivers confluence area in the Bohemian Massif of Czechia. The main stages of morphostructural evolution are identified and related landform patterns are described. The lithological and tectonic character of this contact area between the Barrandian and the Bohemian Cretaceous Basin has been gradually evolving since the Early Palaeozoic. Tectonic subsidence of the northeastern part of the Bohemian Massif and the Cretaceous transgression of the sea caused extensive marine sedimentation, which covered the pre-Cenomanian relief. The uplift of the Bohemian Massif during the Santonian initiated a widespread erosion and denudation in the Tertiary. The Labe River valley constitutes a remarkable boundary between the morphostructural plateaus in the south and the system of river accumulation terraces of the Labe and Jizera in the north. The originally extensive and currently considerably eroded III. river terrace of the Labe was formed in the Elsterian glacial period (Cromerian complex c). The conspicuous Jizera alluvial fan developed during the aggradation phase of the VII. river terrace in the Upper Pleistocene. Subsidence along the NW-SE-trending Labe Fault zone, deciphered from the vertical throw of the VII. terrace rock bases of Labe as well as related paleochannels of its local tributaries, which caused the current asymmetry of the Labe valley, reached up to 14 meters prior to the Holocene. The different rock resistance to weathering, arrangement of fault structures and neotectonic movements that took place even during the late Quaternary significantly influenced the intensity of varied climate-morphogenetic processes.

KEYWORDS
morphostructural evolution; landform changes; Labe (Elbe) and Jizera rivers confluence; Mělnická kotlina Basin; Českobrodská tabule Table

Received: 2 January 2024
Accepted: 10 April 2024
Published online: 28 May 2024

Steklá, T., Kalvoda, J. (2024): Morphostructural evolution of the Labe and Jizera rivers confluence area (the Bohemian Massif, Czechia). AUC Geographica 59(1), 35–59
https://doi.org/10.14712/23361980.2024.3

1. Introduction

1.1 Topics and objectives

The study area is situated in the Central Bohemia (Czechia) and it is represented by the confluence of the Labe (Elbe) and Jizera rivers. It is in a territory of natural and archaeological importance on the contact area between the south-eastern edge of the Bohemian Cretaceous Basin and the north-eastern Barrandian region. The main aim of the present paper is to decipher morphostructural evolution of the area. The landforms are studied as part of the relic record of the palaeogeographic evolution of the natural environment. This geomorphological topic about one of the historically unique areas in the Czech part of the Labe basin was chosen because of an extraordinary informative value of its landforms of different development and age. The analytical data on the geomorphological development in the Labe and Jizera confluence area is continuously interpreted in the context of the knowledge about the central part of the Bohemian Massif and the main stages of the development of its river network during the late Cenozoic.

According to the geomorphological classification of the Bohemian Massif (Balatka and Kalvoda 2006), the Labe and Jizera confluence area belongs to the morphostructural unit of the Středolabská tabule Table within the sub-province of the Česká tabule Table and the area of the Středočeská tabule Table. This

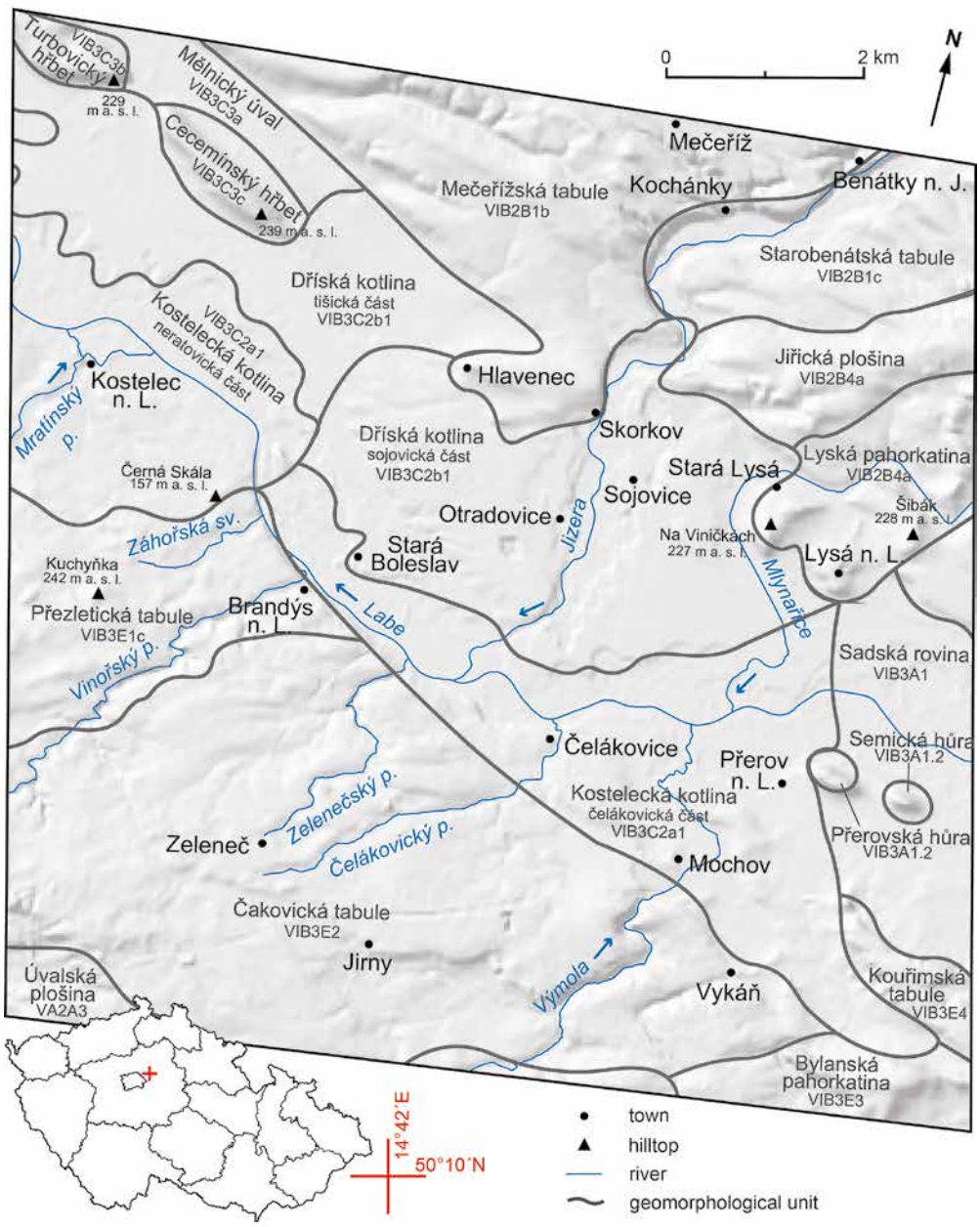

Fig. 1 Geomorphological units in the Labe and Jizera confluence area (169 m a.s.l.; 50°10′21″ N, 14°42′ 56″ E), situated at the morphostructural contact of the Českobrodská tabule Table and Mělnická kotlina Basin (Source: Balatka and Kalvoda 2006; DEM by Czech Office for Surveying, Mapping and Cadastre 2019).

geomorphic division conforms with morphostructures of the 2nd and 3rd order in the Bohemian Massif according to Demek et al. (2009). It concerns block morphostructures on the basement with upland and hilly land as well as complex systems of basin-and-range relief of the Central Bohemia Terrane.

The flat to flat-hilly character of the Středolabská tabule Table is divided by tectonic zones, which determined the formation of the morphologically different subunits of the Mělnická kotlina Basin and Českobrodská tabule Table (Fig. 1). The morphostructural boundary between these subunits runs across the studied area in the SE–NW direction and mostly follows the fault system of the Labe Fault zone (Fig. 2). Differential tectonic movements during the younger Cenozoic also determined other orographic features of the Středolabská tabule Table (Tyráček et al. 2004; Coubal 2010; Grygar 2016). In the neotectonically conditioned depression of the Staroboleslavská kotlina Basin, a flat erosion-accumulation relief was formed, which is bounded in the north both tectonically (Cecemínský and Turbovický Ridges) and in terms of erosion and denudation (Dolnojizerská tabule Table). The flat relief of the Českobrodská tabule Table passes into the hilly terrain at the Kojetický hřbet Ridge and the Bylanská pahorkatina Hilly land (Fig. 1). The higher elevation differences of the relief here were caused by neotectonic movements and varying bedrock resistance to erosion and denudation.

The morphostructural features of the contact area between the Barrandian and the Bohemian Cretaceous Basin have been gradually evolving since the Austrian phase of the Alpine orogeny. During this period of tectonic activity, the subsidence of the northeastern part of the Bohemian Massif accompanied by the Cenomanian and Santonian Sea transgression took place, causing sedimentary processes in the Bohemian Cretaceous Basin (Chlupáč et al. 2002). This ended a palaeo-climatically variable period of erosion and denudation of the pre-Cenomanian planation surface. Triassic terrigenous deposits of the Bohemian Massif are of a kaolinic type, produced by the intensive weathering of exhumed rocks in a humid tropical climate, which took place up until the Lower Cretaceous.

The varied relief in the Labe and Jizera confluence area is a result of the specific geological structure of the southwestern part of the Bohemian Cretaceous

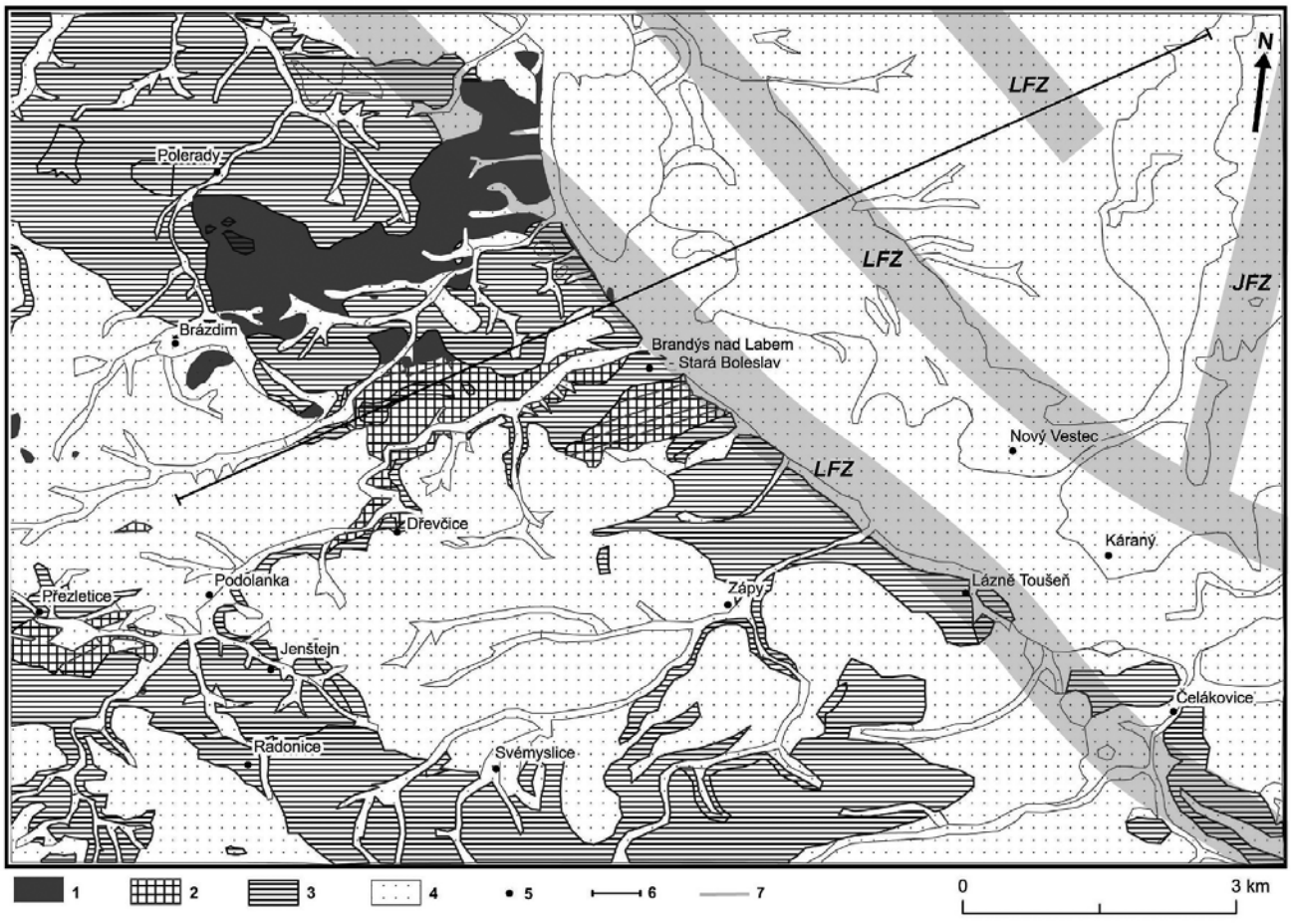

Fig. 2 Scheme of the geological structure in the contact area between the north-eastern zone of the Barrandian and the south-eastern margin of the Bohemian Cretaceous Basin. Key: 1 – Proterozoic (mainly wacke, siltstones and phyllitic schists), 2 – Ordovician (conglomerates, sandstones, clay and sand shales, quartzites), 3 – Cretaceous (quartzose and calcareous sandstones, varied relics of marine and freshwater sediments), 4 – Quaternary (fluvial, slope and aeolian deposits), 5 – town, 6 – geological cross-profile (Fig. 9), 7 – fault zone, LFZ – Labe fault zone, JFZ – Jizera fault zone. Source: Czech Geological Survey: Map applications, version 1B.2, 2019; Uličný et al. 2009; Coubal 2010.

Fig. 3 Boulder conglomerates of the littoral breaker facie of the Korycany layers at the Kuchyňka elevation (242 m a.s.l.), which was created by marine abrasion during the Upper Cenomanian, are unique evidence of the activity of palaeo-morphogenetic processes in the region of the Labe and Jizera confluence. Source: Žítt et al. 1998.

Basin (Fig. 2). In the exhumed part of the basin, Cretaceous and Tertiary platform sediments cover Proterozoic and Palaeozoic rocks of the northeastern zone of the Barrandian complex (Volšan et al. 1990; Holásek et al. 2005). The oldest relics of morphogenetic processes originated in the Upper Cenomanian, when some of the Barrandian Proterozoic outcrops protruded above sea level in the form of cliffs or were affected by abrasion as shallowly submerged elevations (Žítt and Nekovařík 2001). These relics of palaeo-morphogenetic processes were identified mainly on the rock exposures west of Brandýs nad Labem (Fig. 3).

In this paper, we deal with the morphostructural evolution of the Labe and Jizera rivers confluence area. It is based on complex interpretation of our own field data and particulars collected from earlier valuable works. A variety of natural processes during the palaeogeographic history of the contact area between the Barrandian and the Bohemian Cretaceous Basin allowed for an assessment of the main stages of the morphostructural landform evolution (Chapter 2) and an identification of their recent patterns in the Labe and Jizera confluence area (Chapter 3). Furthermore, significant periods of geomorphological changes during the Quaternary (Chapter 4) were verified and/or identified in this area and the main types and intensity of recent morphogenetic processes and phenomena were determined.

1.2 Research methods

The current knowledge of the palaeogeographic development of the central part of the Bohemian Massif is based on remarkable tradition of more than hundred years of natural science research in this area. The systematic evaluation, correlation, and integration of the results of these works are the methodological and knowledge base of recently completed or ongoing research. Extensive and inspiring sets of field and laboratory data, map series and documentary holdings enable both the preparation of comprehensive monographs (e.g., Kovanda et al. 2001; Chlupáč et al. 2002) and the formulation and solution of specific and current research problems in selected localities. Examples include works on Quaternary geological and geomorphological topics (Záruba et al. 1977; Tyráček et al. 2004; Tyráček 2010; Balatka et al. 2015).

The geomorphology of the middle Labe and lower Jizera valleys has been studied by many authors. Most of the works focused on the description and development of morphological formations (Drahota 1931; Balatka 1966; Novotná 1998; Růžičková and Zeman 1994; Mikisková 2009) and/or on climatically and morphogenetically significant periods in the Quaternary (e.g., Balatka 1960; Balatka and Sládek 1965; Hrubeš 1999; Boháčová et al. 2000). Detailed geomorphological research in the Labe and Jizera confluence area is also motivated by recent studies on the evolution of the valley and river accumulation terrace system in the central part of the Bohemian Massif (Balatka and Kalvoda 2008; Balatka et al. 2015), including the Sázava River basin (Balatka and Kalvoda 2010; Balatka et al. 2010).

The methodological procedure of geomorphological research in the Labe and Jizera confluence area is based on a comprehensive approach to the topic under scrutiny, systematic processing, and interpretation of field work results. The basis of this research was field reconnaissance based on the evaluation of available data from geological, geophysical, and geographical publications and map documents. In the studied area, the following sub-thematic areas were gradually addressed: 1) field documentation of morphostructural and climate-morphogenetic landform assemblages and their development, including recent morphogenetic processes; 2) interpretation of geological data and results of geomorphological analysis focused on the morphostructural relief evolution; 3) identification of significant changes in intensity and integration of neotectonic and climate-morphogenetic processes during the Quaternary. Based on existing and newly discovered data, the present paper describes the characteristic features of structural landforms and identifies the main stages of morphostructural evolution of the Labe and Jizera confluence area during the Cenozoic.

The research of river accumulation terraces in the Labe and Jizera confluence area was based on the evaluation of an extensive set of older research works that focused on the river terrace systems of the middle Labe, lower Jizera and their tributaries. The obtained data on fluvial sediments, together with the 1 : 50,000 scale geological map (Czech Geological Survey 2019), were used mainly in the field survey of the studied area to verify the existence and update the delimitation of the extent of the river accumulation terraces. In addition to the localisation of the individual fluvial terraces, the relative heights of their surface and base and the opinions of the individual authors on

the stratigraphic classification of the respective fluvial accumulations were monitored.

In the next stage of the work, the studied river terraces were categorised based on the relative height of their base and/or surface. The surface and base elevations of fluvial accumulations were derived from ZABAGED data (2014), as well as from maps of Quaternary base isolines (Herrmann and Burda Eds. 2016) and from borehole data from the GDO database (2020). The Labe and Jizera river terrace dataset organised in this manner was compared with the river accumulation terraces of the Vltava River, according to the works of Záruba et al. (1977), Tyráček et al. (2004) and Tyráček and Havlíček (2009). The INQUA stratigraphic classification of the Quaternary was used as the current temporal parameter (see, e.g., Gibbard and Cohen 2008; Gibbard et al. 2009).

2. Geological evolution and origin of morphostructural landforms in the study area

2.1 Palaeogeographic history from the Precambrian to the end of the Mesozoic

The oldest rocks of the Středolabská tabule Table and the surrounding areas were formed in the Upper Proterozoic, when the terrestrial weathered rocks were deposited in the marine basin. Proterozoic sediments were consolidated during the Cadomian orogeny (Havlíček 1963; Havlíček et al. 1987; Volšan et al. 1990; Holásek et al. 2005), during which the Barrandian rock complex was formed. The intensity of metamorphosis of Proterozoic rocks varies, but weakly regionally metamorphosed sediments predominate. These rocks of the Kralupy-Zbraslav Group, represented mainly by wacke, siltstones and phyllitic schists, form together with Ordovician sediments the north-eastern Barrandian zone (Fig. 2).

During the Cadomian orogeny at the end of the Upper Proterozoic and the beginning of the Cambrian, the Neratovice body of basic volcanic rocks, which has a volcano-sedimentary character caused by repeated intrusions along tectonically predisposed zones, was formed (Fediuk et al. 1966; Šmejkal and Melková 1969; Volšan et al. 1990). The rocks of the Kralupy-Zbraslav Group are strongly affected by kaolinic weathering up to a depth of several tens of metres (Havlíček et al. 1987) and were therefore exposed to exogenous agents for a long time. In younger geological periods, silicic sediments with higher resistance to weathering rose above the surrounding palaeo-relief or above sea level in the form of cliffs (Loyda 1950). Conversely, sedimentary rocks with a predominance of siltstones and slates formed the lower parts of the pre-Cenomanian relief due their faster weathering and denudation.

The oldest crystalline rocks of the central part of the Bohemian Massif were developed by a long-term sedimentation of material that was transported from the mantle rock of the Precambrian dry land to an epicontinental sea. These marine sediments were repeatedly and to various extents metamorphosed during the Precambrian and the Early Palaeozoic. The complex of sedimentary rocks in the wider area of the present-day Labe and Jizera confluence area has no rocks from the Cambrian period. According to Holásek et al. (2005), this area was outside the sedimentary zone during the Cambrian, or the Cambrian sediments may have been rapidly eroded. The Ordovician sediments of the Barrandian were then discordantly deposited on the tectonically disturbed Cadomian bedrock, of which five formations have been preserved: the Třenice (Tremadocian; conglomerates, sandstones), the Klabava (Arenig; clay shales), the Šárka (Llanvirn; sandy shales), the Dobrotivá (Dobrotiv; clay shales, rock quartzites) and the Beroun (Havlíček et al. 1987; Vaněk 1999). These Ordovician rock formations were formed in shallow marine basins and plateaus, and the character of each formation shows considerable changes in palaeo-relief and sedimentary conditions.

The sediments of the Třenice and Klabava Formations are composed of local material that was transported from the close vicinity of the sedimentary basin by abrasion, occasional flows, mudflows, or slides. The Třenice Formation was created by sedimentation in a shallow sea that was flanked by mountain ranges. The Klabava Formation was created in an environment of isolated marine basins and bays, in the vicinity of which there were already deeply eroded relics of mountain ridges. The sedimentation of the Šárka Formation material took place mainly in lagoons, with its source area likely being more distant parts of the landmass (Havlíček et al. 1987; Vaněk 1999). The Šárka sandy shale formations are rich in siliceous concretions with bio-stratigraphically significant fossil fauna (Röhlich 1952), which confirms their Llarvinian age. The Dobrotivá Formation was formed by sedimentation of weathered rocks in a shallow basin environment with extensive plateaus and deltas (Kukal 1963). According to Holásek et al. (2005), the sedimentation of the north-eastern Barrandian Formation is likely to have continued until the Middle Devonian.

In the Upper Devonian and Lower Carboniferous, the Proterozoic and Early Palaeozoic sediments of the Barrandian area were strongly influenced by Variscan (Hercynian) orogeny. The tectonic disintegration of the Proterozoic rock mass is evidenced by the numerous occurrences of fissures, fractures, fault zones and crushing of some silicate layers (Kovanda et al. 2001; Chlupáč et al. 2002). The Early Palaeozoic rocks were consolidated, folded, and permeated by faults and reverse faults during the Variscan orogeny. For example, in the quarry to the west of Popovice, the so-called Závist-type fault was exposed, according to which

the Upper Proterozoic rocks were pushed onto the younger Třenice Formation. No Závist-type reverse faults developed to the east of Prague, but smaller and younger reverse faults caused by similar tangential pressures were formed there. Havlíček (1963) places the origin of the Závist-type fault in the pre-Westphalian phase of the Variscan folding, and Knížek (2013) specifies the period of its origin to the Tournaisian-Visean boundary in the Lower Carboniferous. Another tectonic reverse fault was discovered by a borehole at the dam of the Hrušovský Pond (Kukal 1963), where the Šárka Formation is covered by younger strata of Dobrotivá shales and Skalec quartzites. The Klabava and Šárka Formations were also disrupted by transverse faults in the NW–SE direction (Havlíček et al. 1987; Holásek et al. 2005).

During the Upper Carboniferous, the north-eastern Barrandian area was probably part of the margin of limnic basins (Holásek et al. 2005). To the NW of the studied Labe and Jizera confluence area, between

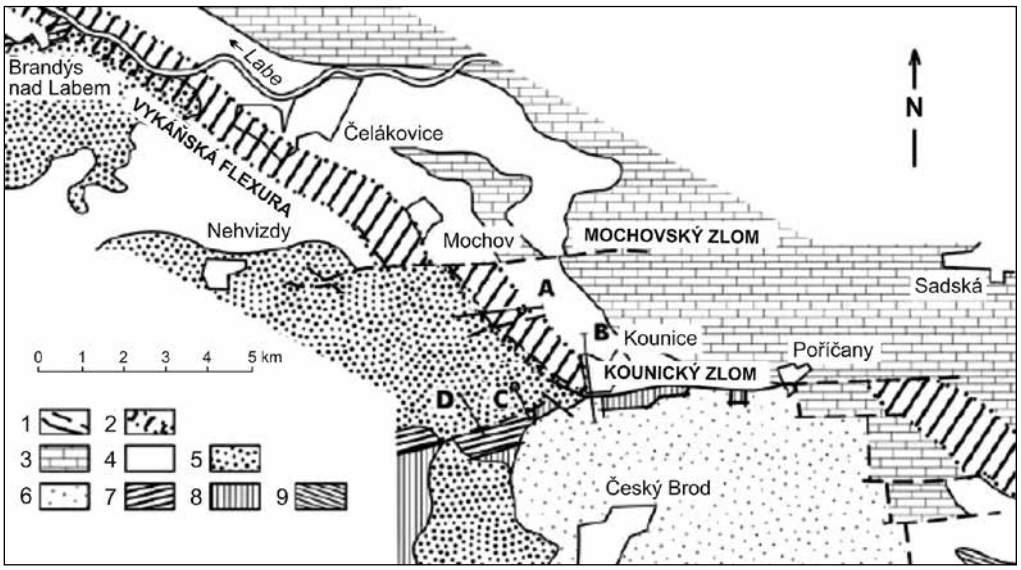

Fig. 4 Scheme of the geological structure of the Vykáň flexure in the southern part of the Bohemian Cretaceous Basin. Key: 1 – fault: identified, expected, 2 – flexural folding, 3 – Jizera formation (Upper Cretaceous), 4 – Bílá hora formation, 5 – Peruc-Korycany formation, 6 – Černý Kostelec formation (Permian), 7 – the Ordovician rocks of the Prague Basin, 8 – Štěchovice group (Upper Proterozoic), 9 – Kutná Hora crystalline complex, A – geological section of the Vykáň flexure (Fig. 5), B – geological section of the Kounice fault (Fig. 6), C, D – geological sections of the western part of the Kounice fault (Fig. 7). Source: Coubal 2010.

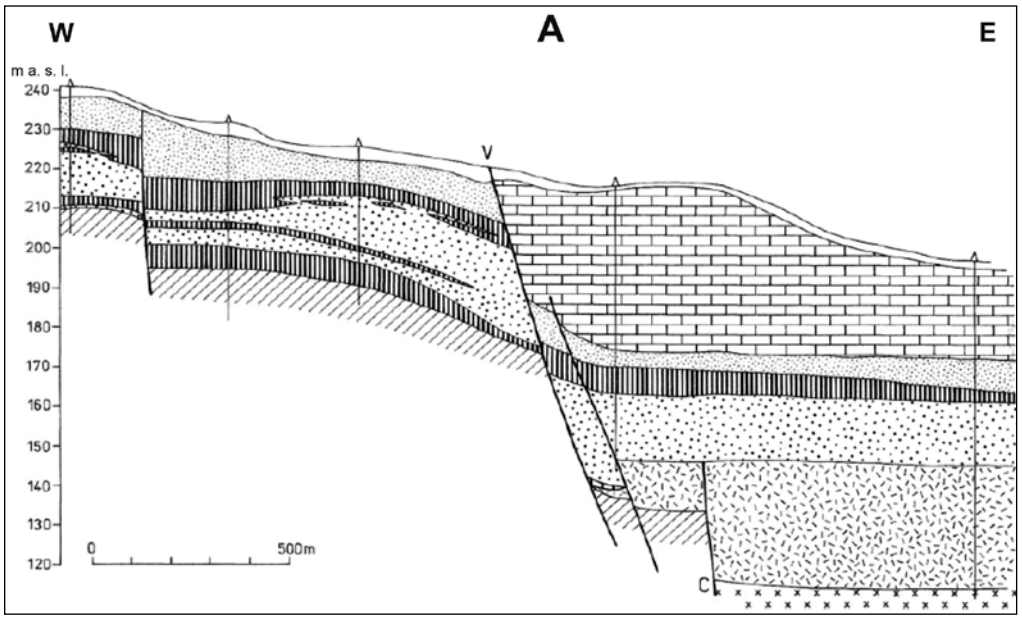

Fig. 5 Geological section of the Vykáň flexure. The location of section A is presented in Fig. 4 and the key is in Fig. 6. Source: Coubal 2010.

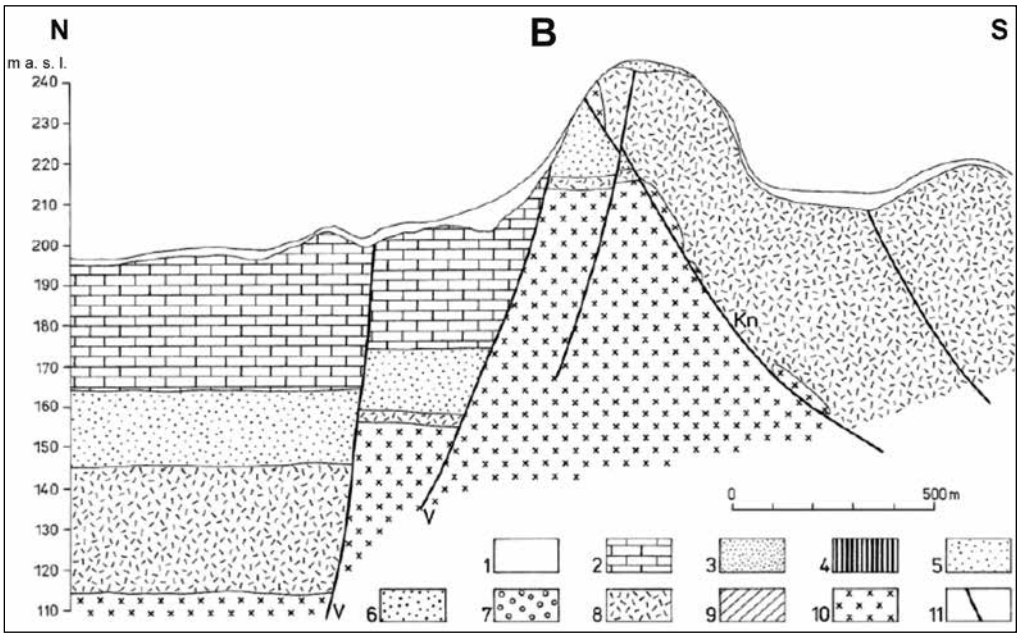

Fig. 6 Geological section of the Kounice fault. The location of section B is presented in Fig. 4. Key: 1 – Quaternary sediments, 2 – Jizera and Bílá hora formation (Upper Cretaceous), 3 – Korycany formation (fine-grained sandstone), 4 – clay parting of the Peruc formation, 5 – fine/medium-grained sandstone of the Peruc formation, 6 – coarse-grained sandstone of the Peruc formation, 7 – conglomerate parting of the Peruc formation, 8 – Černý Kostelec formation (Permian), 9 – the Ordovician rocks of the Prague Basin, 10 – Štěchovice group (Upper Proterozoic), 11 – fault, V – longitudinal fault of the Vykáň flexure, Kn – Kounice fault, C – Černice fault (see Fig. 5). The location of section B is presented in Fig. 4. Source: Coubal 2010.

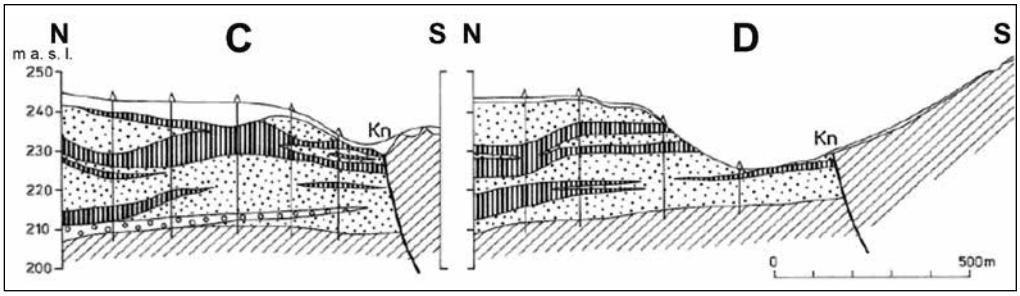

Fig. 7 Geological sections C and D, in the western part of the Kounice fault. The locations of these sections are presented in Fig. 4 and the key is in Fig. 6. Source: Coubal 2010.

Tišice and Dřísy, the southern margin of the Roudnice and Mšeno Carboniferous basins is located. There, in the substratum of Cretaceous sediments, a borehole survey has also revealed the Radnice (silty and coaly claystones, sandstones, conglomerates) and Nýřany layers (arkosic sandstones, siltstones, claystones) of the Kladno Formation (Zelenka et al. 2006). On the other hand, to the southeast of the studied area, in the vicinity of Český Brod, Permo-Carboniferous sediments of the Blanická brázda Furrow have been preserved (Fig. 4). In the Labe and Jizera confluence area, Permo-Carboniferous sediments were found in only one borehole, west of Lysá nad Labem at a depth of 117 m. Their absence in a major part of the studied area is probably caused by erosion during the Lower Cretaceous.

The denudation and erosion of the north-eastern Barrandian zone also continued in the Permian and Lower Cretaceous (Holásek et al. 2005), and this area was part of the Variscan consolidated core of the Bohemian Massif. This is how the pre-Cenomanian planation surface was created in a semiarid and very warm climate, which cuts through both Proterozoic and Palaeozoic rocks (Svoboda 1998). Extensive marine transgressions in the Triassic formed the Hercynian platform into a peninsula and later into an island of the so-called Vindelician Ridge, whose northern part was central Bohemia.

The Jurassic Sea in the Bohemian Massif was a relatively narrow and shallow strait connecting the German and Carpathian Seas. In the Lower Cretaceous, intense rock weathering took place in a humid tropical climate, forming a powerful mantle of tropical weathered rocks. The part of the Bohemian Massif that emerged above the "Cretaceous" sea was still a compact block of Hercynian origin, on the surface of

which a peneplain with a thick mantle of regoliths was largely developed (Demek 2004). This morphostructurally relatively uniform surface, flattened by erosion-denudation processes, had a height of up to approximately 200 m above the then sea level.

The north-eastern part of the Bohemian Massif subsided during the Austrian phase of Alpine orogeny. For this reason, marine sedimentation took place there from the Cenomanian to the Santonian, during which mainly the deposits of the Bohemian Cretaceous Basin were formed. The source areas of mainly clastic Cretaceous sediments were the landmasses of the Central Bohemian and Sudeten Islands (see, e.g., Engel and Kalvoda 2002). The marine Cretaceous sediments cover the Permo-Carboniferous sedimentary formation, which is underlain by the crystalline rocks of the Bohemian Massif, including granitoids. The shallow sea advanced from the Turonian to the Middle Coniacian quite far south of the Prague area (Kovanda et al. 2001; Chlupáč et al. 2002). This transgression of the sea into the central part of the Bohemian Massif, during which for the first time since the Precambrian exhumed crystalline rocks were submerged and the post-Hercynian planation surface on top of them caused by denudation, was terminated by secular epiplatform uplift during the Santonian, 85.5–83 million years ago.

The ruggedness of the relief of the pre-Cenomanian planation surface significantly influenced the extent and nature of marine sedimentation in the Upper Cretaceous (Fig. 2). This extensive marine sedimentation was caused by the subsidence of part of the Bohemian Massif along the Labe Fault zone (i.e., in the NW–SE direction) and by the subsequent eustatic rise of the ocean surface (Uličný 1997). The essential morphostructural landforms of the palaeo-relief of the studied area included mainly two morphostructural elevations of the NW–SE direction. This is the Kojetice elevation, which forms the eastern foreland of the extensive Unhošťsko-Turský hřbet Ridge (Matějka 1936), and the parallel elevation between Prague and Brandýs nad Labem (Žítt et al. 1998). This ridge extended into the area of the present-day Labe and Jizera confluence area from the outskirts of Prague through Kuchyňka and Černá skála to the Labe in the Veleň – Přezletice – Záryby – Brandýs nad Labem zone. In the early stages of Cretaceous sedimentation, the flat ridges rose above sea level (Svoboda 1996) and their complete submergence occurred only during the Upper Cenomanian and Lower Turonian sedimentation stages. In places, abrasion facies were also preserved, showing the position of the then marine coastline (Havlíček et al. 1987; Volšan et al. 1990). In contrast, the areas with Ordovician rocks were in lower areas compared to Proterozoic rocks and thus were part of the marine sedimentary area already for the oldest Peruc layers.

The transition from a continental to marine sedimentary environment during the Upper Cenomanian is evidenced in the Středočeská tabule Table by the character of the sediments of the Peruc Formation, which is made up of fluvial, lacustrine, deltaic, and lagoonal type accumulations. The low thickness of the Peruc layers and their heteropic juxtaposition with younger Korycany layers suggest the Upper Cenomanian age of their sedimentation. However, an older age of the Peruc layers, namely the Lower Cenomanian–Albian layers, cannot be ruled out (Havlíček et al. 1987; Holásek et al. 2005; Volšan et al. 1990). The lower Peruc layers were probably deposited in the fluvial environment of freely meandering and/or braided streams. According to Volšan et al. (1990), the valley of this paleoflow was formed on poorly consolidated Carboniferous sediments. Findings of marine microplankton in the upper clay layers of the Peruc Formation demonstrate that their deposition occurred in the environment of coastal lagoons and estuaries occasionally connected to the sea (Kříž et al. 1984). For example, west of Třeboradice, both lagoonal sediments of the upper clay layer and marine sediments were simultaneously deposited next to each other. According to Svoboda (2004), their synchronous deposition is a consequence of the influence of epeirogenetic movements on the formation of sedimentary basins.

The younger Korycany layers (quartzose sandstones, calcareous sandstones) were already being deposited at the bottom of the shallow Upper Cenomanian Sea. Their age is confirmed by local finds of rich fauna in the highest altitudes of this layer (e.g., Černá skála quarry; Enc 1984). The Upper Cenomanian sediments are absent only in the highest altitudes of the Unhošťsko–Turský hřbet Ridge and the elevation zone Veleň – Přezletice – Záryby – Brandýs nad Labem, which were not flooded during this marine transgression. In the sand pit near Přezletice, it was documented (Havlíček et al. 1987; Volšan et al. 1990) that the Korycany layers were deposited between two bands of Ordovician quartzites, which probably formed islands during the sedimentation of coarse clastics.

The relics of abrasion (surf) facies, which were found on the Proterozoic elevations in the belt between Čakovice and Brázdim (Břízová et al. 2005; Havlíček et al. 1987), also come from the Upper Cenomanian period. The best-preserved remnants of abrasion facies are on Kuchyňka Hill (242 m a.s.l.) east of the village of Brázdim (Fig. 3). The well-sorted and rounded bioclasts, spastic matrix and coarse terrigenous clastics indicate that these sediments were deposited in an environment with a relatively high transport rate. These Upper Cenomanian sediments were probably deposited in the upper part of the sublittoral zone (Havlíček et al. 1987; Volšan et al. 1990), and Žítt et al. (1998) identified at least three sedimentation cycles at the Kuchyňka site. Two of these cycles took place in the Upper Cenomanian and one only in the Lower Turonian. Traces of abrasion deposits have

also been found in the studied area at other elevations formed by Proterozoic silicates, e.g., at Černá skála and Kojetice quarry (Žítt and Nekvasilová 1991).

After an interrupted sedimentation at the beginning of the Turonian, there was a transgression and deepening of the seabed, during which the highest flat ridges were flooded and then the sediments of the Bílá Hora Formation were deposited under open sea conditions (Holásek et al. 2005). The deposition of the Jizera Formation took place in similar marine conditions. In terms of lithofacies, the Cretaceous sediments in the studied area belong to the Prague region (Havlíček et al. 1987; Volšan et al. 1990). Towards the north, the area of the Bílá Hora and Jizera Formations increases substantially, which indicates a deepening of the sedimentary basin after the marine transgression in the Lower Turonian.

Shallow sedimentary basins were formed on crystalline bedrock also in southern Bohemia, and the nature of their Cretaceous sediments shows that they were transported from the surrounding areas together with the products of tropical weathering. The relics of Cenomanian freshwater sediments in the Bohemian Massif are mainly represented by kaolinic sandstones whose material comes from the denuded surface of rising Cretaceous basins with abundant vegetation and newly emerging regolith. The post-Hercynian peneplain was thus covered by kaolin and lateritic regoliths and currently lies beneath the Upper Cretaceous sediments of the Bohemian Cretaceous Basin. The tectonic uplift of the central part of the Bohemian Massif at the end of the Santonian was then caused by the ongoing Alpine and Carpathian orogeny and manifested itself by the complete subsidence of the Upper Cretaceous epicontinental sea.

2.2 The dynamics of Cenozoic evolution of morphostructural landforms

At the end of the Cretaceous period, during the onset of Alpine orogeny, inversion of the Bohemian Cretaceous Basin took place, so the studied area became dry land during the Tertiary. The extent and thickness of the Cretaceous sediments were significantly higher in the beginning of the Tertiary than they are today. These sediments were substantially reduced by the long-term Tertiary erosion and denudation and only the oldest formations have been preserved. The significant denudation of the Cretaceous sediments is also confirmed by the exhumed neovolcanics of Eocene and Lower Miocene age (Holásek et al. 2005). These diatremes, veins and lava plugs of volcanic funnels and principal vents, penetrated the Cretaceous sediments of the Coniacian and Turonian age, but they did not reach the surface of the Tertiary palaeo-relief at the time of their origin. The nearest neovolcanic outcrop to the present-day Labe and Jizera confluence is situated northeast of Neratovice on the Záboří Hill (228 m a.s.l.). It is made of olivine nephelinite, which encloses fragments of Cretaceous sediments. A chart

Tab. 1 A chart of the morphostructural evolution of the Barrandian and Bohemian Cretaceous Table contact area from the Neo-Proterozoic to the Quaternary.

Geological periods	Principal morphostructural and climate-morphogenetic processes and phenomena
Quaternary:	Evolution of river systems of accumulation terraces (see Tab. 2). Differencial tectonic uplift and movements along fault zones.
Neogene:	
Pliocene	Evolution of the oldest relics of fluvial sediments of rivers in Central Bohemia (Klínec stage). Vault uplifts of the Labe and Sázava watershed regions.
Middle Miocene	Rivers from the present-day Polabí region headed eastwards through the Chlum Gate to the East Bohemian Gulf of the Miocene Sea. Mega-syncline fold of the Labská pánev Basin. Formation of the Neogene post-volcanic planation surface and exhumation of neovolcanites. Reduction of sedimentary formations by long-term erosion and denudation.
Lower Miocene Aquitanian – Burdigalian	Tectonic disintegration of the Palaeogene planation surface caused by differential movements of new and revived fault structures (NW-SE, WNW-ESE) during the Saxonian phase of Alpine orogeny.
End of Oligocene and Lower Miocene	Planation processes were interrupted by tectonic movements. The intrusion of plutons of the rifting stage of volcanism into Barrandian, Permo-Carboniferous and Cretaceous rocks. Formation of olivine nephelinite elevations.
Palaeogene:	Palaeo-flows in Central Bohemia form shallow and wide valleys with a low gradient. Development of the Palaeogene planation surface with a cover of lateritic and kaolinic weathering products of rocks (formation of duricrusts). Laramide phase of Alpine orogeny: – Uplift and tectonic dissection of the Bohemian Massif – Formation of graben structures and tectono-volcanic zones Gradual exhumation and reduction of rock complexes of Cretaceous age by long-term erosion and denudation.

Mesozoic: Upper Cretaceous Santonian	Marine sedimentation was terminated by secular epiplatform uplift of the Czech part of the Bohemian Massif during the ongoing Alpine and Carpathian orogeny.
Coniacean	Advance of the shallow sea to the south of the Prague area and submergence of the post-Hercynian planation surface.
Turonian	Sedimentation in the open sea conditions (Bílá Hora Formation). Flooding of the highest elevations of the pre-Cenomanian relief (Jizera Formation). Transgression and deepening of the seabed. Interruption of sedimentation during the sub-Hercynian stage of Alpine orogeny (stratigraphical hiatus).
Cenomanian	Sedimentation in the shallow sea (Korycany layers). The highest parts of the pre-Cenomanian relief rise above the sea level in the form of coastal or island cliffs (relics of the abrasion facies). Epeirogenetic movements influenced the development of sedimentary basins with lagoonal and marine sediments. Transition from continental to marine sedimentary environments with gradual deposition of fluvial, lacustrine, deltaic, and lagoonal-type sediments (Peruc layers).
Lower Cretaceous	The Austrian phase of the Alpine orogeny: – Subsidence of the north-eastern part of the Bohemian Massif along the Labe Fault zone (NW–SE). – Eustatic uplift of the ocean level. Continued erosion and denudation of the consolidated crust of the Bohemian Massif created a pre-Cenomanian planation surface that cuts the rocks of the Barrandian complex and underlies the Cretaceous sediments of the basin.
Jurassic Triassic	Origin of a shallow strait of the Jurassic Sea in the northern and north-eastern part of the Bohemian Massif. Long-term effects of erosion and denudation (stratigraphic hiatus). Central Bohemia is part of the Hercynian platform, a peninsula/island of the so-called Vindelician Ridge.
Palaeozoic: Permian	Formation of the post-Hercynian planation surface in the Bohemian Massif. Sedimentation of a predominantly limnic filling in the Blanická brázda Furrow. Asturian phase of Hercynian (Variscan) orogeny: – Tectonic subsidence in the Labe Fault zone with a NW-SE direction of morpholineaments
Carboniferous	– Formation of the Blanická brázda Furrow and morpholineaments with a NNE-SSW direction. Extensive denudation of the Hercynian (Variscan) mountains of the Bohemian Massif. Formation of sediments in the Roudnická and Mšenská pánve Basins, the Kladno Formation, mainly in the limnic environment. Hercynian (Variscan) orogeny in the Bohemian Massif: – Formation of a chain of mountains with a height of several thousand meters and deep intrusion of granitoids of the Central Bohemian Suture – Tectonic disruption of the Barrandian complex associated with the formation of faults and reverse faults.
Devonian	
Silurian	Marine sedimentation and basic submarine volcanism. Evolution of the Barrandian Formation in the Prague area.
Upper Ordovician Keradoc	Sedimentation of weathered rocks in a shallow marine basin environment with extensive plateaus and deltas (Dobrotivá Formation).
Middle Ordovician Llarvinian	Sedimentation of material from more distant parts of the land in the environment of lagoons (Šárka Formation).
Lower and Middle Ordovician Arenig	Sedimentation of local material into the environment of isolated marine basins and bays fringed by eroded mountain ridge relics (Klabava Formation).
Lower Ordovician Tremadoc	Sedimentation of local material transported by abrasion, occasional flows, mudflows or slides into a shallow sea fringed by mountain ranges (Třenice Formation).
Cambrian	The studied area is outside the sedimentation zone. Extensive erosion and transport of deposited material (stratigraphic hiatus). Cadomian orogeny in the Bohemian Massif: – Consolidation of the Barrandian complex – Repeated lava intrusions along predisposed zones (formation of the Neratovice body).
Neo-Proterozoic: Ediacaran	Sedimentation of the weathering material mantle into the epicontinental sea (Kralupy-Zbraslav group of sediments).

of the morphostructural evolution of the Barrandian and Bohemian Cretaceous Table contact area from the Neo-Proterozoic to the end of the Neogene is presented in Tab. 1.

In the studied area of the Labe catchment, during the Saxonian phase of Alpine orogeny, the development of new faults took place along with reactivation of fault systems with a predominant NW–SE to WNW–ESE direction (Volšan et al. 1990). Along most of the faults, there was subsidence of blocks located closer to the axis of the Cretaceous basin. The main fault zone, with a NW–SE direction, runs along the current watercourse of the Labe. It continues in a south-eastward direction as a remarkable fault system of the Vykáň flexure, whose down-faulted blocks subsided by up to 30 m with an east-northeast flank fold of 3–5° (Figs. 4 and 5). The height of the vertical displacement on this fault zone decreases towards the WNW (Vohanka 1966), so neotectonic movements of only a few meters have been detected NW of Neratovice. Along this main fault zone, the Cretaceous formations of the northeastern subsided block are in direct contact with the Proterozoic and Palaeozoic rocks. Several morpholineaments of the NE–SW direction cut through the rocks of the Barrandian complex and Cretaceous sedimentary formations in the form of straight valley sections. Considering their present location, we conclude that in addition to the vertical component of neotectonic movements, there was also an overall horizontal shift of up to *ca* 400 m along the Labe fault. The fault zone of the Vykáň flexure gave rise to morphologically conspicuous cross faults, such as the Mochov and Kounice faults (Figs. 4, 6 and 7), while a pure left-slip by up to 1400 m was identified at the Mochov fault (Coubal 2010). The convergence of two originally parallel faults, namely the Kounice Fault and the Vykáň Flexure fault, led to the tectonic separation of the Polabí morphostructures from the area of the Permian rocks of the Český Brod and the Blanická brázda Furrow.

According to Volšan et al. (1990), tectonic movements during the Quaternary are linked to NE–SW faults, which affected the considerable thickness of the fluvial sediments of the Mělnický úval Basin. Havlíček et al. (1987) agree with this opinion; young tectonic movements in the younger Quaternary explain the higher fluvial sediment strengths on the right bank of the Labe River. In the Labe and Jizera confluence area, it is more difficult to identify the evolution of fault structures precisely because of the extensive cover of Quaternary sediments, especially the fluvial accumulation terraces of the Labe River.

3. Identification of Quaternary morphostructural landforms in the Labe and Jizera confluence area

The geological structure and lithology of the rocks in the Labe and Jizera confluence area played a significant role in the development of the current morphostructural landforms (Fig. 8). Particularly striking is the asymmetry of the slopes of the Labe valley (Fig. 9),

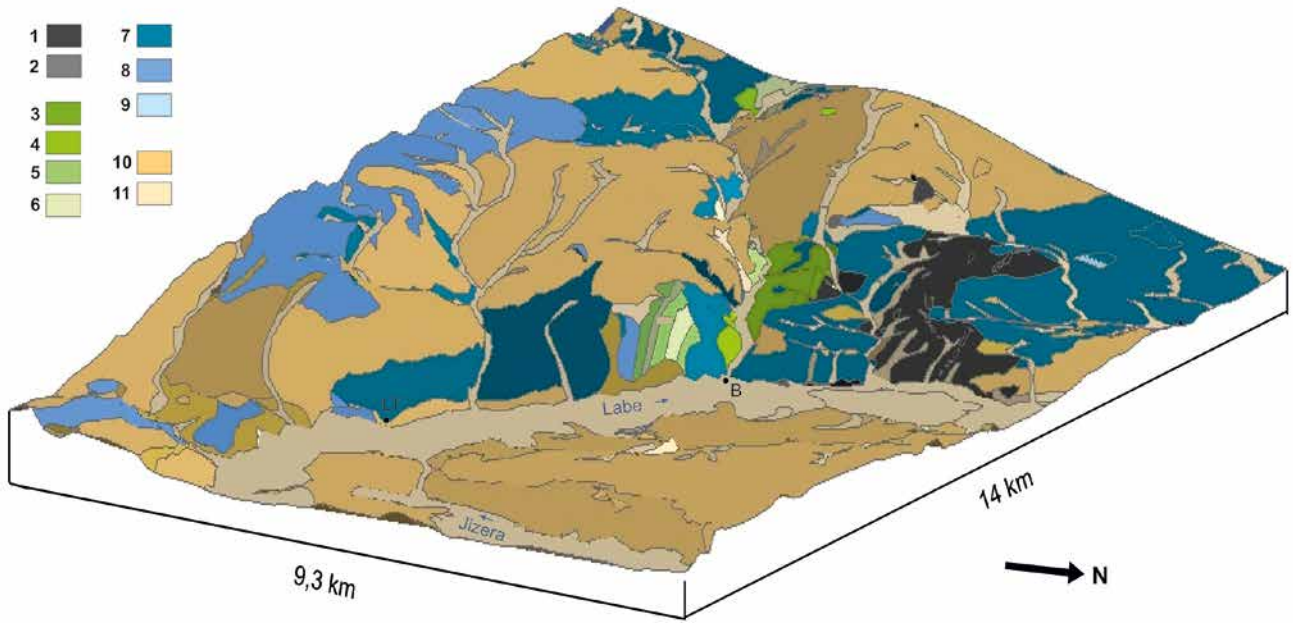

Fig. 8 Digital model of the terrain featuring the geological structure of the Labe and Jizera confluence area, viewed from NE to SW. Key: 1 – Kralupy-Zbraslav group (Proterozoic), 2 – Štechovice group (Proterozoic), 3 – Klabava formation (Ordovician), 4 – Šárka formation (Ordovician), 5 – Dobrotiv and Libeň formations (Ordovician), 6 – Dobrotiv formation (Ordovician), 7 – Peruc-Korycany formation (Cretaceous), 8 – Bílá hora formation (Cretaceous), 9 – Jizera-Bílá hora formation (Cretaceous), 10 – Pleistocene sediments, 11 – Holocene sediments, B – Brandýs nad Labem, LT – Lázně Toušeň. A detailed description of the rock assemblages from the marked geological periods is presented in the 2nd chapter. Source: Tereza Steklá, ZABAGED 2014.

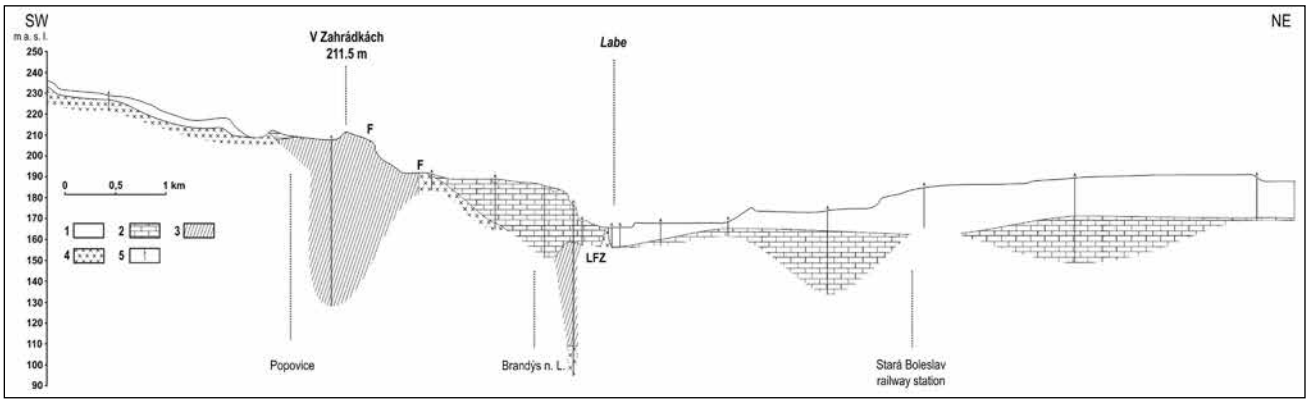

Fig. 9 Topographical cross-profile through the asymmetrical Labe valley with relief of the morphostructural plateaus on the left bank and the moderate stepped slopes formed of the Quaternary river accumulation terraces on the right bank. The steep structural slope of the left bank of the Labe River developed along the tectonic fault of the Labe Fault zone. Key: 1 – Quaternary (fluvial and aeolian sediments), 2 – Cretaceous (sandstones, marlites, limestones, claystones), 3 – Ordovician (black shales, quartzites), 4 – Proterozoic (wacke, siltstones and phyllitic schists), 5 – borehole, F – fault, LFZ – Labe Fault zone. Source: Tereza Steklá; Uličný et al. 2009; Czech Geological Survey: Map applications, version 1B.2, 2019; GDO 2020.

which was formed by fluvial erosion along the fault system of the Labe Fault zone (Fig. 2). The Labe valley thus represents a morphological boundary between different types of relief on its right (NE) and left (SW) banks.

A relatively steep tectonically controlled left bank of the Labe valley gradually transitions into a structurally denudation relief with relics of planation surfaces in the south-western part of the studied area (Fig. 9). The Proterozoic and Palaeozoic rocks of the Barrandian are close to the surface and already exhumed in denudation windows. The most pronounced are bodies of Neo-Proterozoic silicates, which are more resistant to weathering and form knobs and elongated elevations mainly in the SW–NE direction (Volšan et al. 1990; Holásek et al. 2005). Most of these structural ridges occur in the Veleň – Brandýs nad Labem zone. The most important localities of Neo-Proterozoic lydites are the Kuchyňka (242 m a.s.l.) and Černá skála (157 m a.s.l.) knobs. The original size of most knobs and silicate elevations was often substantially reduced by quarrying.

The Barrandian rocks with a predominance of siltstones and slates have not yet been exhumed by denudation of the overlying layers. Ordovician rocks crop out in Brandýs nad Labem and its western surroundings, close to the erosional edge of the Labe valley, the Vinořský potok Brook, the Záhořská svodnice Brook and their tributaries. Elevations of Ordovician rocks occur only at the south-western edge of the studied area, where Upper Cretaceous sediments were less thick (Havlíček et al. 1987). Distinctive is a structural monadnok called Zabitý kopec Hill (264 m a.s.l.) near Miškovice, where the Třenice Formation has been preserved together with the prevailing Proterozoic silicates.

Cretaceous sediments in this part of the Polabí region have less thickness and area, due to both the ruggedness of the pre-Cenomanian relief and tectonic movements during the late Cenozoic (Havlíček et al. 1987; Volšan et al. 1990). The erosional activity of the Vinořský potok and Mratínský potok Brooks has exhumed the Korycany layers, while the older Peruc Formation does not crop out at all. Extensive areas of the Bílá Hora Formation (Turonian, calcareous claystones and marlstones) are denuded in the vicinity of Zeleneč and Svémyslice, as part of the Neogene planation surface, which is markedly dissected by the valleys of the Zelenečský potok Brook and Svémyslická svodnice Brook. The Bílá Hora Formation is preserved in varying thickness on the left bank of the Labe and is largely overlain by Quaternary aeolian and fluvial sediments (Holásek et al. 2005). Relatively deeply incised valleys of the Labe tributaries suggest their increased erosional activity during the late Quaternary (Fig. 8), which resulted from both the gradual deepening of the Labe valley and neotectonic movements in the area of the Labe Fault zone and Vykáň Flexure.

On the right bank of the Labe, the accumulation landforms are more pronounced. The rocks of the Barrandian complex do not crop out in any place there and have been detected only by a few boreholes (Coubal 2010; Zelenka et al. 2006). Also, the base of the Cretaceous sediments decreases towards the NE, while the Bílá Hora Formation has been detected here beneath Quaternary sediments in the tectonically subsiding block (Havlíček et al. 1987; Volšan et al. 1990). Therefore, structurally conditioned landforms are not as frequent in this part of the studied area as in the southwestern region. Their occurrence increases towards the NE, i.e., deep down into the Bohemian Cretaceous Basin. An example is the Na Viničkách locality northeast of Lysá nad Labem (Fig. 10), where the Jizera Formation crops out and, together with fluvial sediments of Pleistocene age, forms a morphologically distinct level of the Hlavenec Terrace

Fig. 10 The erosion-denudational slopes of the southern edge of the morphostructural plateau Na Viničkách, which is situated NW of Lysá nad Labem, are built by the Cretaceous rocks of the Jizera formation. The surface of the platform is covered by the relics of the river terrace IV (Hlavenec, 222–225 m a.s.l.) belonging to the terrace system of the Labe and Jizera. Source: Tereza Steklá.

(Holásek et al. 2005, Tab. 2). A similar morphostructural character of coarse-grained siltstones to fine-grained sandstones is also present in the transverse sill in the Jizera River basin approximately 2 km south of Otradovice. However, the stratigraphic assignment of these sediments has not yet been paleontologically documented (Břízová et al. 2005). The evolution of the present-day accumulation relief was conditioned by neotectonic subsidences of this part of the Polabí region along the main fault of the Labe Fault zone and Vykáň Flexure (Figs. 2, 4 and 5). In the overlying Upper Cretaceous sediments, a system of river accumulation terraces (sometimes strikingly asymmetrical) was formed during the Quaternary, which is interconnected with slope and aeolian sediments.

Part of the identification of the morphostructural features of the Labe and Jizera confluence area were the measurements of morphologically distinct lineaments of tectonic and lithological origin. The Barrandian rocks and Cretaceous sediments are divided there by valleys that follow lineaments in four main directions, namely ENE–WSW (Rudohorský direction), WNW–ESE (Sudeten direction), NNE–SSW (Vltava or Jizera direction) and NW–SE. The location of the main morpholineaments on both banks of the Labe River is shown in Fig. 11 and the frequency of their occurrence in these directions in Fig. 12.

Morpholineaments of the Sudeten WNW–ESE direction are found on both banks of the Labe River, i.e., in all local types of geological structure. On the right bank of the Labe, the WNW–ESE morpholineaments run in a relatively dense network. Most of the morphologically distinct lineaments on the left bank of the Labe occur close to the erosional edge of the Labe valley, which indicates their relation to the morphostructures of the Labe Fault zone and Vykáň Flexure. NW–SE morpholineaments (Fig. 12), which are mainly pronounced in the Labe valley, are likely to be linked to these fault zones as well. This is also suggested by the frequent overlapping of lineaments with proven faults and their length, which reaches even more than 10 km.

The morpholineaments in the NNE–SSW direction are not frequent in the studied area – only the lineament in the Jizera River valley and southwest of the Labe River is more pronounced in this direction (Fig. 11). The lineaments in the ENE–WSW direction are more pronounced in the relief on the left bank of the Labe River, where they are mostly bound to the Proterozoic bedrock. Their position suggests that they indicate fault lines or lithological boundaries. The NE–SW morpholineaments are of similar origin, occurring more frequently to the northeast of the Labe and follow parts of the Jizera valley. In the north-western part of the area, NE–SW morpholineaments are bound to the Proterozoic rocks of the Kojetický hřbet Ridge and in its south-eastern part they occur on a structurally and lithologically similar ridge near Úvaly.

The current morphostructural landforms in the Labe and Jizera confluence area are conditioned by the extent of exhumation of the pre-Cenomanian relief. This exhumation of the rocks and palaeo-relief was influenced by the depth of denudation and erosion of the Cretaceous formations, the arrangement of the fault systems and neotectonic movements in the late Cenozoic. The influence of the pre-Cenomanian relief

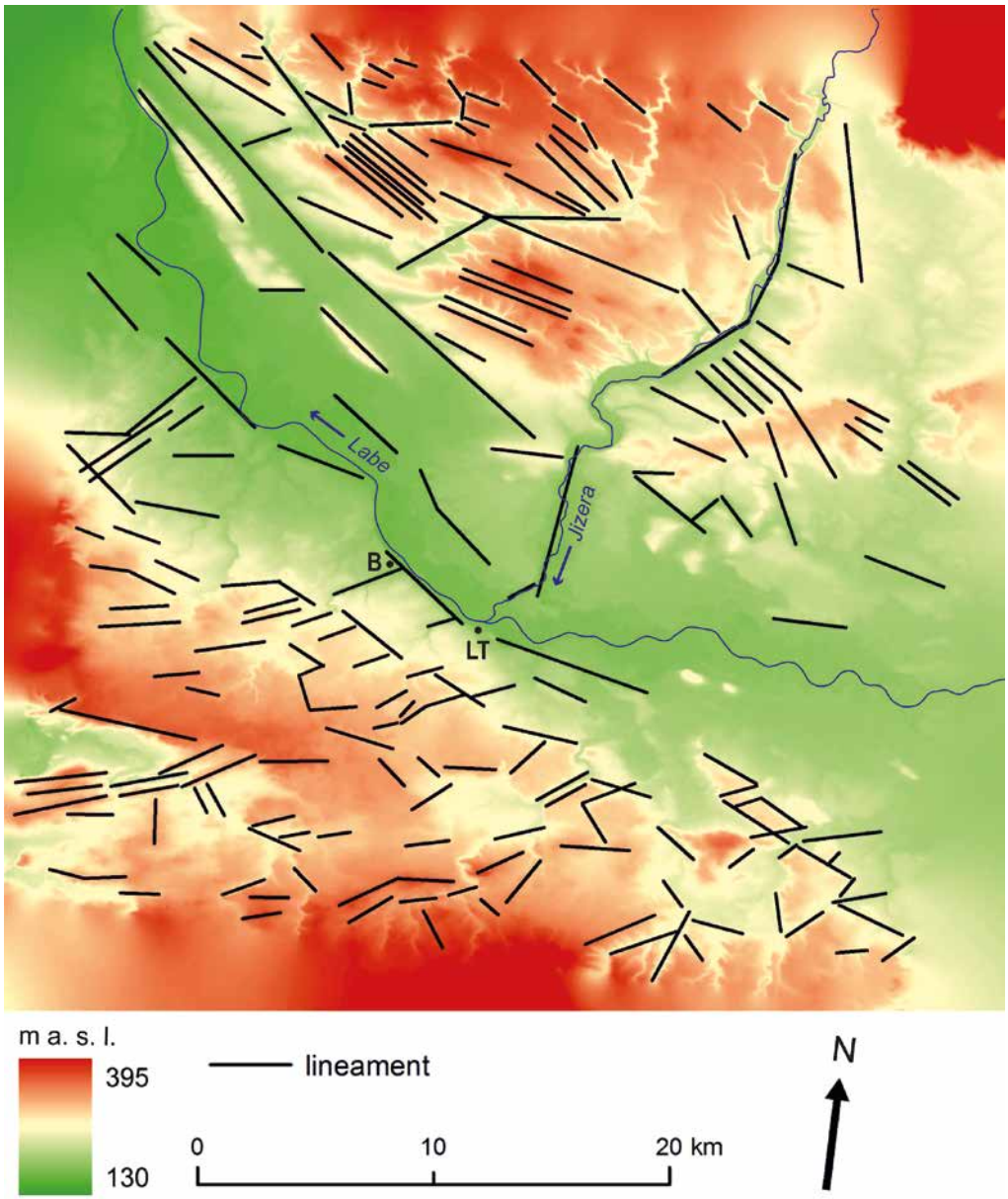

Fig. 11 Topographical situation and morpholineaments in the Labe and Jizera confluence area.
B – Brandýs nad Labem, LT – Lázně Toušeň. Source: Tereza Steklá.

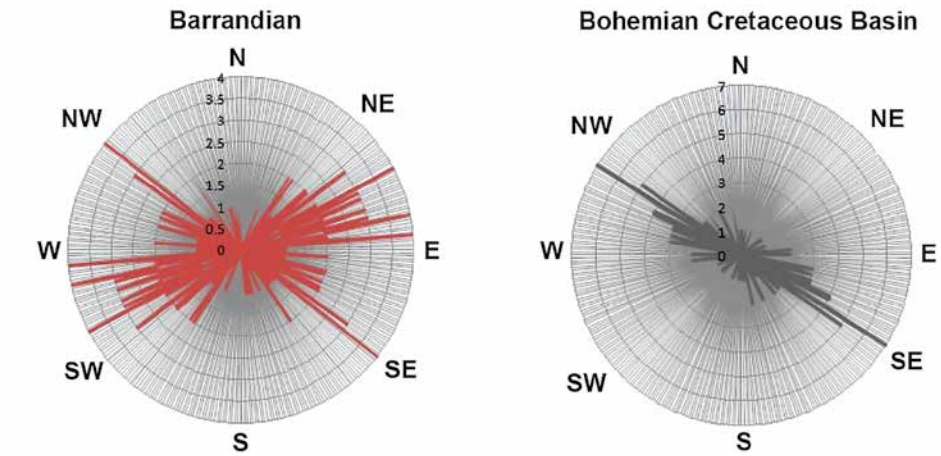

Fig. 12 Circular diagrams of identified morpholineaments in the Labe and Jizera confluence area. Source: Tereza Steklá.

on the development of the present-day landforms is more pronounced to the SW of the Labe valley. This is mainly due to the late Quaternary tectonic subsidence of the north-eastern part of the studied area.

The denudation of Cretaceous rocks on the right bank of the Labe has not yet reached the level of the pre-Cenomanian relief. Significant morphostructural landforms here mainly take the form of structural plateaus and witness hills. They were formed by the joint action of neotectonic movements and erosion processes on the base of the Cretaceous formations during the Quaternary. These are, for example, the striking elevations called Turbovický hřbet Ridge (229 m a.s.l.), Cecemín (239 m a.s.l., Na Viničkách (227 m a.s.l.) and Šibák (227.8 m a.s.l.). Towards the north, the rocks of the Jizera Formation form a large table broken up by erosional activity of the right-side tributaries of the Labe and the left-side tributaries of the Jizera.

To the SW of the Labe valley, the long-term denudation of the Cretaceous sediments has created a relief of low structural tables with relics of planation surfaces of Tertiary age, with knobs made of resistant Proterozoic lyddites cropping out in places. These low erosion-denudation platforms are dissected by the activity of the left-side tributaries of the Labe, with deep and backward erosion having already reached the bedrock formed by the Barrandian rocks in several locations. The most pronounced exhumation of the Barrandian complex has occurred near the erosional edge of the Labe valley, which in this area is a significant divide between the relief of low structural tables

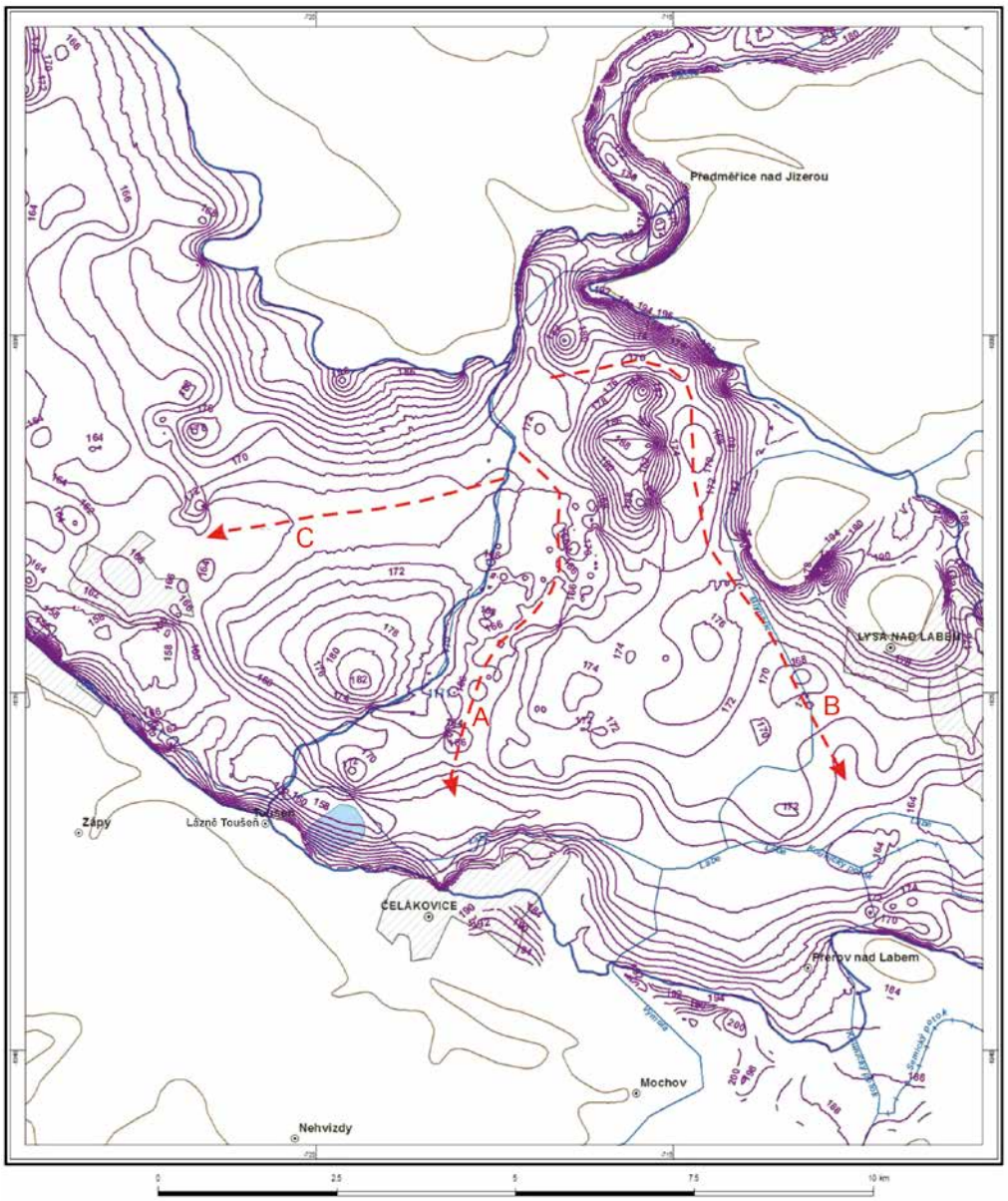

Fig. 13 Isolines (in m a. s. l.) of the base of the Quaternary sediments in the confluence area of the Labe and Jizera.
The red arrows indicate the direction of the Jizera paleobeds during the different development phases of the VII. terrace (see Tab. 2).
A – initial incision phase, B – maximum deepening, C – main accumulation phase. Source: Herrmann and Burda Eds., 2016.

on the left bank of the Labe and the Quaternary system of fluvial accumulation terraces of the Labe and Jizera rivers.

4. Morphological manifestations of tectonic activity in the Labe and Jizera confluence area during the Quaternary

The main geomorphological testimony of exogenic processes in the Labe and Jizera confluence area during the Quaternary are river accumulation terraces. The terrace system of the studied part of the Labe and Jizera rivers is characterised by advanced erosion of the terrace accumulations and by the sporadically preserved group of older (higher) terraces. The highest fluvial sediments developed as accumulations of the Labe tributaries and their morphological position gives evidence of a gradual deepening of the river network during the Pleistocene (Tyráček et al. 2004; Tyráček 2010). The activity of fault systems in the NE–SW to WNW–ESE directions is evidenced by tectonic disruption of Quaternary sediments noted by Coubal (2010) on a geological section of the Vykáň Flexure near Vykáň (Fig. 5). Quaternary tectonic movements along these faults were already envisaged by Havlíček et al. (1987) and Volšan et al. (1990).

To determine the extent and progression of neotectonic subsidence, an analysis of the position of the base of the Quaternary sediments was first used (Fig. 13). The neotectonic subsidence near Brandýs n. L. was determined by comparing the present level of the higher rock base of VII_2 Terrace (166 m a.s.l.), which was formed by lateral erosion before the subsidence of the valley floor, and the surface of the Cretaceous formations near the erosional edge of the Labe valley (*ca* 180 m a.s.l.). At Stará Lysá, it was possible to determine the extent of tectonic subsidence by finding the difference in height between the paleochannel of Mlynařice (188 m a.s.l.) and the paleochannel of Jizera B (172 m a.s.l.), which were probably at the same elevation during the maximum deepening of the Labe (Fig. 14). At present, the difference in height at both sites is *ca* 14 m.

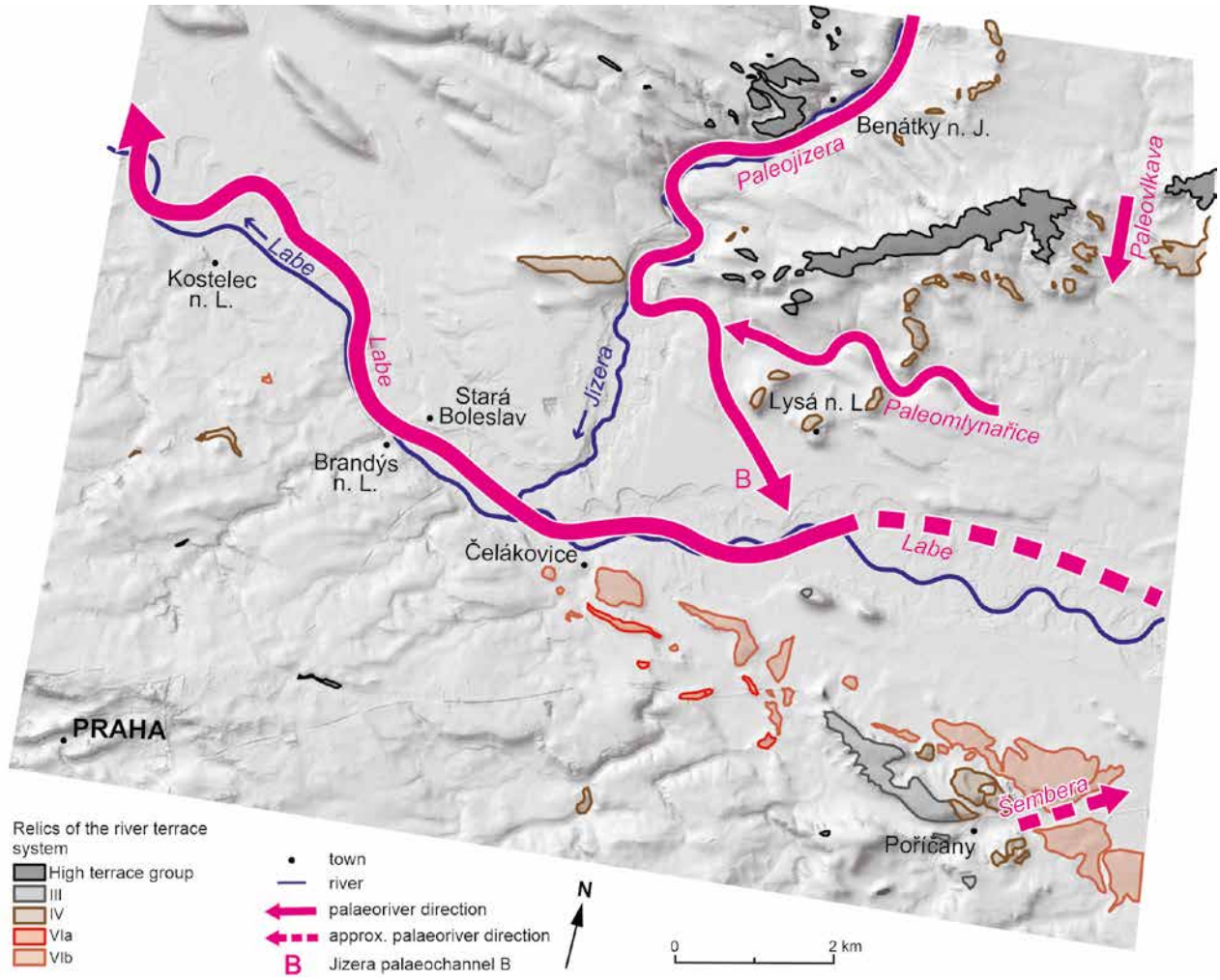

Fig. 14 The directions of paleoflows in the area of today's Labe and Jizera confluence in the period of maximum deepening during the development of the VII. Terrace. Source: Tereza Steklá; DEM by Czech Office for Surveying, Mapping and Cadastre 2019.

Indications of differential neotectonic movements were also found by analysis of isolines of the base of Quaternary sediments and longitudinal profiles of the Labe and Jizera paleochannels. These isolines have a very uneven course with frequent steps. As regards the Jizera paleochannel, these changes in elevation may have been caused by neotectonic movements linked to the NE–SW Jizera fault. In the Labe paleochannel, we compared the elevated steps of Quaternary sediments base with morpholineaments of the same direction, i.e., NE–SW (Figs. 11 and 12).

The morphostratigraphic classification of the river terraces according to the current Quaternary classification system is proposed in Tab. 2 and Fig. 15. The geomorphological analysis of the river accumulation terraces, and their morphostratigraphic classification are made more difficult in this area by neotectonic and erosional interventions, relatively extensive covers of aeolian sediments in the form of loess and drift sands and, moreover, the effects of anthropogenic activity.

The current state of the relics of fluvial sediments and the structure of river terraces in the Jizera and Labe confluence area demonstrate morphologically significant tectonic activity in the younger Quaternary. Five main river accumulation terraces are preserved in this area, two of which are further subdivided by secondary levels of erosional or erosional-accumulation origin (Tab. 2). These river terraces were formed in a climatically determined alternation of erosional and accumulation phases of the valley development (Balatka and Kalvoda 2008; Hradecký and Brázdil 2016), which were supported by differential tectonic uplifts of the central part of the Bohemian Massif. The fluvial accumulations were substantially dissected by post-sedimentary erosion processes resulting in sporadic preservation of older (higher) terraces. The neotectonic subsidence of a part of the Labe valley in the Upper Pleistocene then caused a marked asymmetry in the extent and position of river accumulation terraces, with the predominance of accumulation of fluvial sediments of Terrace VII on the right bank of the Labe (Fig. 15).

The highest, and therefore the oldest preserved fluvial sediments in the Labe and Jizera confluence area were deposited by paleotributaries of the Labe.

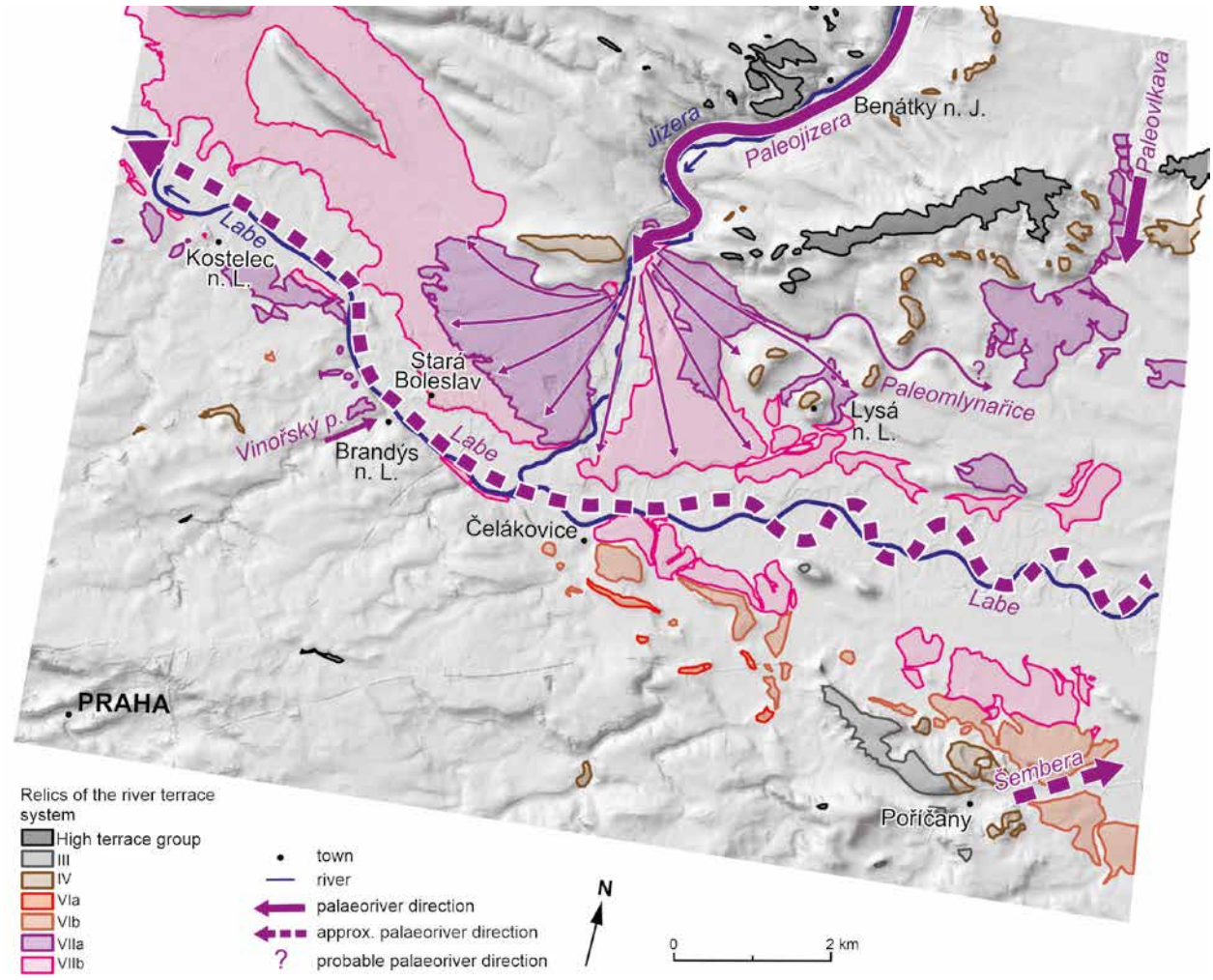

Fig. 15 The directions of paleoflows around today's Labe and Jizera confluence during the main accumulation phase of the VII. terrace after the tectonic subsidence of the Labe valley. Source: Tereza Steklá; DEM by Czech Office for Surveying, Mapping and Cadastre 2019.

Tab. 2 The arrangement of river accumulation terraces in the Labe and Jizera confluence area and their morphostratigraphic correlation with the Vltava river terrace system. The surface (s.) and base (b.) heights are given in metres above sea level, the relative height in metres is given in brackets. Source: Tereza Steklá.

Stratigraphical division (stage/substage) of the Quaternary (Gibbard and Cohen 2008; Gibbard et al. 2009)	Labe river km 854–891	Jizera river km 0–20	Labe and Vltava Confluence river km 803–840, 0–22 Záruba et al. (1977) Tyráček et al. (2004) Tyráček, Havlíček (2009)	Vltava in Prague river km 204 Záruba et al. (1977) Tyráček et al. (2004) Tyráček, Havlíček (2009)
Holocene -------- 0.0117 mil. years	Lower alluvial level s. 165–179 b. 156–164 (−10 to −6)	Alluvial level s. 171–180 b. 158–178 (−20 to −2)	Alluvial level s. (5) b. (−10)	Alluvial level s. 180 b. 168 (−8)
	Higher alluvial level s. 166–181 b. 156–164 (−10 to −6)			
Upper Pleistocene Weichsel -------- 0.12 mil. years	VIIb s. 170–185 (8–13) b. 156–184 (−10 – 12)	Jizera Fan s. 180–196 (9–22) b. 164–196 (−7 – 22)	VII Hostín Terrace s. (12) b. (−10)	VII Maniny Terrace s. 187 (11) b. 168 (−8)
	VIIa s. 180–196 (14–24) b. 166–196 (1–24)			
Middle Pleistocene saale, warthe -------- 0.19 mil years	VIb s. 188–201 (16–29) b. 186–200 (14–28)	The relics of Terrace VI can be buried here by the Jizera Fan[2]	VI Veltrusy Terrace s. (25) b. (0)	VI Veltrusy Terrace s. 193 (17) b. 174 (–2)
	VIa (Čelákovice) s. 199–208 (27–36) b. 198–205 (26–33)			
Middle Pleistocene saale, drenthe -------- 0.20 mil years	Terrace V was eroded here during the erosion phase of Terrace VI [1]	Terrace V was not deposited on the erosional and tectonic right bank of the Jizera valley. On the left bank it was eroded during the erosion phase of Terrace VI[3]	V Cítov Terrace s. (40) b. (16)	V Dejvice Terrace s. 214 (38) b. 194 (18)
Middle Pleistocene saale, fuhne -------- 0.38 mil. years	IV Hlavenec Terrace s. 218–225 (53–56) b. 217–220 (49–52)	IV Hlavenec Terrace s. 218–225 (41–44) b. 217–220 (37–40)	IV Hněvice Terrace s. (60) b. (43)	IV Letná Terrace s. 226 (50) b. 215 (39)
Middle Pleistocene elster -------- 0.48 mil. years	III Přerov Terrace s. 232–236 (59–63) b. 230–234 (57–61)	III Jiřice Terrace s. 242–256 (62–68) b. 234–248 (54–60)	III Straškov Terrace s. (75) b. (55)	IIIb Vinohrady Terrace s. 240 (64) b. 225 (49)
Middle Pleistocene Cromer Complex, Glacial C				IIIa Kralupy Terrace s. 249 (73) b. 240 (64)
Middle Pleistocene Cromer Complex, Glacial C	Terrace II was eroded during younger development phase [1]	II Sedlec Terrace s. 266 (84) b. 253 (71)	II Ledčice Terrace s. (90) b. (75)	II Pankrác Terrace s. 262 (86) b. 249 (73)
Middle Pleistocene Cromer Complex, Glacial B	Terrace I was eroded during younger development phase[1]	The palaeo-flow of the Jizera River was located further to the E from its present course[4]		Ib Suchdol Terrace s. 272 (96) b. 260 (84)
Middle Pleistocene Cromer Complex, Glacial A -------- 0.78 mil. years			I Krabčice Terrace s. (115) b. (105)	Ia Lysolaje Terrace s. 288 (112) b. 268 (92)

[1] The nearest preserved fluvial sediments of Labe Terraces I (Krabčice Terrace), II (Ledčice Terrace) and V (Cítov Terrace) are located in the Labe and Vltava confluence area. [2] The nearest fluvial sediments of Terrace VI of the Jizera River were found near Nová Ves u Bakova. [3] The nearest relics of deposits of Terrace V of the Jizera are near Mladá Boleslav. [4] Terrace I accumulations have not been found in the Jizera basin.

On the right bank of the Labe, the highest fluvial accumulations are located near the village of Mečeříž and in the locality of Na Zlatě (surface: 278–290 m a.s.l., r. h. 106–118 m; base: 275 m a.s.l., r. h. 103 m), which Balatka and Sládek (1962) identified as the accumulations of the Mohelka paleostream. Near the village of Sedlec, there are relics of lower-level fluvial accumulations preserved (Sedlec Terrace, surface: 266 m a.s.l., r. h. 94 m; base: 253 m a.s.l., r. h. 81 m), which Zelenka et al. (2006) described as sediments of the Jizera paleostream. Tyráček (2010) classified all fluvial accumulations of the high terrace group at Mečeříž, Sedlec and Kochánky as Lower Pleistocene to upper part of Middle Pleistocene.

Fig. 16 View to the asymmetric valley of the Jizera in Skorkov towards the NE, i.e. upstream of the river. The erosion-denudation slope of the structural plateau formed by Cretaceous rocks (in the foreground) drops steeply to the valley floor with alluvial sediments. On the left bank of the Jizera, now forested fluvial sediments of the VII. terrace occur (in the right part of the picture). Behind this accumulation, three elevations built by the Jizera formation (Čihadla 240.2 m, Na vrších 245.8 m and Raštice 241.4 m a.s.l.) are striking on which relics of III. (Jiřice) terrace of the Jizera remain. Source: Tereza Steklá

The oldest relics of the fluvial accumulations of Terrace IV (Hlavenec, 222–225 m a.s.l.) contain admixture of crystalline rock from the upper Jizera catchment. These fluvial sediments were probably developed in the locality of earlier Labe and Jizera confluence (Holásek et al. 2005; Tyráček 2010). Main occurrences of these deposits were identified on the plateau between Hlavenec and Skorkov and Na Viničkách (Fig. 10), *ca* 8 km away from the current confluence of the Labe and Jizera. The deposits of Terrace V have not been preserved in the studied area due to following intensive deep erosion and widening of the Labe valley (Balatka and Sládek 1965; Tyráček 2010). On the left bank of the Labe river, two levels of Terrace VI have been preserved, their distinction being mainly reflected at the level of their bases (Záruba et al. 1977; Holásek et al. 2005; Tyráček 2010).

River accumulation terrace VII in the Labe and Jizera confluence area is characterised by a complex internal structure and surface morphology (Fig. 16). In the main erosion phase during the younger Pleistocene, the Labe formed a deepened riverbed about 10 m below its present level (Figs. 13 and 14). To the N of Sojovice, Paleojizera diverted its flow from the original N–S direction to the E, namely to the former valley of the lower Paleomlynařice. The paleobed of the Jizera (B) formed a wide arch here, namely south from the buried elevation of Cretaceous rocks between Sojovice and Stará Lysá. This paleobed B continues in the southern direction towards Dvorce and then in a straight section to the SE. Due to antecedent deepening in the resistant rocks of the Cretaceous formations, the valleys of Paleomlynařice and Paleovlkava near Jiřice have been preserved in the same position as during former periods. After the riverbed was filled with younger fluvial sediments, the river valley was widened by lateral erosion and a higher bed was formed, on which aggradation sediments were

deposited by the raging flow. Based on the reconstruction of the local Labe and Jizera terrace system (Tab. 2) and its relationships to morphostructural landforms, it is concluded that a neotectonic subsidence took place during the main aggradation phase of Terrace VII in the Upper Pleistocene (Weichselian).

In the late Pleistocene, an extensive accumulation of fluvial sediments in the form of an alluvial fan was formed in the last 10 km of the Jizera valley (Fig. 15). These sediments were deposited by the Jizera River at its entering to the broad and flat Labe valley and covered the older erosional relief (Balatka 1966; Hrubeš 1999; Tyráček 2010). This extensive fluvial accumulation overwhelmed the earlier relief, including the paleobed of the Jizera C (Fig. 13) and elevations of the Cretaceous bedrock up to 188 m a.s.l. Higher elevations in the vicinity of Lysá nad Labem, on which the relics of the IV. river terrace remain, rose above the surface of the Jizera fan at this time. They diverted the transported material of the Paleojizera to the Paleomlynařice valley. The morphology of the massive alluvial fan of the Jizera indicates that it was formed mainly in the environment of shallowly raging flow and flat streams. They caused the Labe flow to be gradually shifted to the south. At the present-day confluence of the Labe and the Jizera, the Labe floodplain was significantly narrowed, which slowed down its flow between Lysá and Labem and Přerov and Labem and wide meanders were formed (Fig. 15). Less marked erosion levels preserved in the fluvial sediments of the alluvial fan were formed only during the Late Glacial and Holocene.

5. Discussion of geomorphic patterns in the Labe and Jizera confluence area related to the morphostructural evolution of the Bohemian Massif

Objective of presented research was to find out the key phases of the morphostructural evolution of the Labe and Jizera confluence area. Current landforms in the region provide a reliable record of palaeogeographical changes in the natural environment. For this reason, it was possible to carry out a detailed historical-genetic analysis of the landforms. Special attention was paid to the influence of neotectonic activity and climate-morphogenetic processes on the changes in the drainage pattern. The morphostratigrafical system of the river terraces was updated and applied as a primary timeline.

Tectonic uplift of the Bohemian Massif, which has started at the end of the Santonian, led to a complete retreat of the Upper Cretaceous epicontinental sea. The extent of denudation of the Bohemian Cretaceous Basin sediments during the Neogene is estimated at 500–600 m by the morphological position of the sediments and volcanics (Kovanda et al. 2001; Balatka and Kalvoda 2006). In the region of the Labe and Jizera confluence, the thickness of the Cretaceous sediments is influenced by a vertical differentiation of the pre-Cenomanian relief.

The palaeogeographical record of the morphostructural evolution of the contact area between the north-eastern Barrandian zone and the south-eastern margin of the Bohemian Cretaceous Basin shows that the main lithological and tectonic features of the present relief have been gradually formed since the Palaeozoic (Tab. 1). Geological structures and landforms of Central European region testifies to a very dynamic evolution of the relief in the palaeogeographical history of the Bohemian Massif (e.g., Chlupáč et al. 2002; Balatka and Kalvoda 2006; Pánek and Hradecký Eds., 2016). The Hercynian orogenic processes united the Bohemian Massif into a structurally complex unit, the central part of which consists of the collisionally deformed and metamorphosed crystalline rocks of the Moldanubic age.

During the main phase of the Hercynian orogeny, extensive deep-seated intrusions of granitoid rocks took place, and in its final phase 290–260 million years ago, shear movements with the formation of fault systems also took place. This is how tectonic subsidence in the Lower Permian occurred in the NW–SE direction in the Labe Fault zone and in the Blanická, Jihlavská and Boskovická brázda Furrows in the NW–SE direction. During the Hercynian orogenetic processes, the Moldanubicum was not only the central part of the gradually consolidated Bohemian Massif, but also an area where mountain ranges with heights of several thousand metres were formed (Chlupáč et al. 2002). However, the extensive denudation of these mountain ranges caused the exposure of deep metamorphic rock masses as early as at the end of the Permian. In the Upper Permian, the palaeo-relief of the Bohemian Massif took the form of a post-Hercynian planation surface, the denudation of which took place in a semiarid and very warm climate (Demek 2004).

The Triassic sedimentation and its termination can be interpreted as the beginning of the next platform development of the Bohemian Massif (Grygar 2016), because erosion and planation of its surface took place until the end of the Jurassic period. This period of extensive denudation of the Bohemian Massif was ended first by continental and then by marine sedimentation (especially in its northern part) as late as during the eustatic uplift of the world ocean level during the Cretaceous period.

In terms of palaeo-climate, the changes in the position of the Bohemian Massif as part of the Pangea palaeocontinent in the Mesozoic and Palaeogene were significant, when it was moved from the tropical zone to the north of the equator to about 45° N, i.e., west of the current zero meridian (Chlupáč et al. 2002). It was only the dynamic development of the rift in the northern part of the Atlantic Ocean, and the associated opening of oceanic plates, that moved the

Hercynian and older crystalline basement of the continental plate of Europe at the end of the Palaeogene to approximately its present geographic position.

The tectonic uplift of the Bohemian Massif from the end of the Cretaceous period were a response to the continuing Alpine and Carpathian orogeny, which consisted mainly in the retreat of the continental sea. It was shown by radiometric dating and modelling using a combination of zircon (U-Th)/He and apatite (AFT and U-Th-[Sm])/He thermochronology methods on rock samples from planation surfaces in the Krkonoše and other Sudetic Mountains ridges (Danišík et al. 2010, 2012) that these peneplains were probably formed by extensive exhumation of a Late Permian planation surface originally located under a several kilometre-thick layers of Cretaceous sediments.

The current orography and landform assemblage of the Bohemian Massif developed as late as during the Neogene and Quaternary periods, i.e., in the last 20–25 million years of its palaeogeographical history. The Palaeogene planation of the relief of the Bohemian Massif was interrupted at the end of the Oligocene by tectonic movements, which were accompanied in its western and north-western parts by the formation of the Oherský Rift and intense volcanic activity 35–17 million years ago (e.g., Grygar 2016). The evolution of the Bohemian Massif relief was also substantially influenced by two other phases of volcanic activity, namely in the Upper Miocene between 9.0 and 6.4 million years ago, and from the Upper Pliocene to the Pleistocene between 2.7–0.17 million years ago (Wagner et al. 1998). The extent of denudation of the sediments of the Bohemian Cretaceous Basin from the beginning of the Miocene to the present is documented by the morphostructural position of the volcanic massifs. The extent of erosion and denudation in the Central Bohemian Uplands during the Neogene is estimated at 500–600 m assessed from the layers of sedimentary rock relics and volcanic bodies (Malkovský 1975; Chlupáč et al. 2002).

The primary arrangement of the river network of the Bohemian Massif originated as late as in the Neogene (e.g., Balatka and Kalvoda 2006; Tyráček and Havlíček 2009). The main differences between the Early Miocene river network and the present-day relief comprise: 1) the upper part of the Labe basin drained into the Carpathian foredeep, 2) the upper part of the Vltava basin drained to the south into the Alpine foredeep, and 3) the West Bohemian rivers, including the Berounka, flowed into freshwater lakes, which were formed in the basins of the Oherský Rift (Tyráček and Havlíček 2009). Along the south-eastern edge of the Bohemian Massif, deep river valleys were formed in the Neogene (Czudek 1997; Pánek and Kapustová 2016). Today, they are filled with and partly covered by Miocene sediments.

The combined effect of changes in climate-morphogenetic processes and long-term neotectonic uplift created systems of river accumulation terraces during the Pliocene and Quaternary in the valleys of most of the main streams of the Bohemian Massif. These fluvial deposits are, together with the overall arrangement of the river network and other manifestations of epigenetic and antecedent evolution of watercourse valleys, an important source of data on the relief history of the Bohemian Massif (Balatka and Kalvoda 2006; Kalvoda and Balatka 2016). The evolution of the Labe and Jizera terrace system has been studied by numerous authors and their findings are evaluated in several older papers (e.g., Balatka and Sládek 1962; Růžičková and Havlíček 1981).

The geomorphological analysis of the longitudinal profile of the river terrace system and the development of the river valley assumes that the individual parts of the river terraces maintained a constant slope corresponding to their longitudinal profile. The flow and transport capacity of the stream are in dynamic equilibrium with the material input. Therefore, the river does not erode or accumulate in this section of the stream and all its energy is concentrated on material transport (Mackin 1948). This condition is substantially influenced by tectonic movements (uplift and subsidence) and/or climatic changes that determine the sedimentary regime. Individual sites of fluvial sediments must therefore be assessed with respect to their lithological characteristics, including petrographic composition, and to the landforms in their wider vicinity.

The distinct morphostructural segmentation of the area around the Labe and Jizera confluence, which is manifested on both banks of the Labe by block subsidence and uplift both in the relief and at the height of the base of Quaternary sediments, supports the view of the formation of an interaction zone between two significant fault systems. The interaction zone development principles are described by, e.g., Peacock (2001), Peacock et al. (2017) and van Gent and Urai (2020). In the studied area it is the interaction between the faults of the Labe Fault zone (WNW–ESE) and the Jizera Fault (N–S). The described morphostructural features of the near-surface geological structure testify to the action of high stress and friction in the rocks of the contact zone between both fault systems. The main Labe Fault and the compact rocks of the Barrandian complex limited the extension of the Jizera Fault further to the south, but older morphostructural zones were activated and secondary block-type deformations occurred.

The specific morphostructural conditions in the Labe and Jizera confluence area conditioned the formation of asymmetrical system of river terraces, in which fluvial sediments deposited on the right bank of the Labe predominate. Due to the action of post-accumulation erosion processes, the relics of the river terraces of the Labe and its tributaries have been preserved only in a limited morphostratigraphic sequence (Table 2). The disruption of the relics of

fluvial sediments by erosion indicates that the Labe and Jizera confluence area has undergone significant changes in the natural environment from the Upper Pleistocene to the present day, influencing the development of the river network.

In the upper glacial phases, aeolian material was drifted away from slopes and from fluvial sediments and deposited on fluvial sediments of Middle to Upper Pleistocene age. In this respect, discontinuous covers of drift sands, often in the form of dunes and dune banks, are striking (Hrubeš 1999; Břízová et al. 2005). Most of the drift sands was stabilised by vegetation during the Holocene. To the east of the Labe and Jizera confluence area, near the village of Písty, an unconsolidated sandbank up to 8 m high has been preserved (Čech et al. 2009).

The deposition of fluvial sediments continued during the Holocene in the form of flood clays, loams, and fluvial sands (Růžičková and Zeman 1994). Palynological analysis of the organic sediments of oxbows confirms the long-term human influence on the natural environment of this area, e.g., by changes in the natural composition of vegetation since the Middle Holocene (Hrubeš 1999; Břízová et al. 2005). In recent centuries, there have been extensive anthropogenic influences on the natural environment. These include intensive farming, large-scale housing developments, alterations to watercourse routes and banks, construction of transport networks, gravel extraction and creation of detritus heaps.

6. Conclusions

The presented research in the Labe and Jizera confluence area contributes to the determination of remarkable changes in the landform patterns of the Bohemian Massif during the Quaternary. Morphostructures of the contact area between the Barrandian and the Bohemian Cretaceous Basin has been gradually evolving from the Early Palaeozoic to the Quaternary.

Tectonic subsidence of the northeastern part of the Bohemian Massif and the Cretaceous transgression of the sea caused extensive marine sedimentation, which covered pre-Cenomanian relief. The uplift of the Bohemian Massif during the Santonian initiated widespread erosion and denudation in the Tertiary. Neotectonic activity and climate-morphogenetic processes determined the evolution of present landforms during the Upper Cenozoic (Tab. 1).

Historical-genetical relations between morphostructural landforms of the studied area and Quaternary deposits indicate significant influence of different rock resistance to weathering, the arrangement of fault structures and neotectonic movements on the intensity of varied climate-morphogenetic processes. The location and the depositional character of the river terraces in the Labe and Jizera confluence area were used to determine the changes in direction of the paleoriver flows in the Quaternary. The morphostructural platform surfaces on the left bank of the Labe River are dissected by erosion of its tributaries, which has reached the Barrandian bedrock at several sites.

Regional geomorphic research revealed that most of the relics of fluvial deposits in the Labe and Jizera confluence area are younger than reported in the previous studies (Tab. 2). Originally extensive and currently already considerably eroded III. river terrace of Labe River was formed in the Elster glacial period. The conspicuous Jizera River alluvial fan developed during the aggradation phase of the VII. river terrace in the Upper Pleistocene.

The degree of river incision between several accumulation phases of the river terraces development and the extent of backward erosion through the valleys of the Labe and Jizera tributaries reflect the changes of the erosional basis caused by neotectonic and climate-morphogenetic processes. Down-slip tectonic movements along the Labe fault zone, which caused the current asymmetry of the Labe valley, reached up to 14 m even before the beginning of the Holocene.

Acknowledgements

The presented paper was prepared in the framework of the Charles University Project Cooperatio "Geography".

References

Balatka, B. (1960): Terasy Jizery. Kandidátská disertační práce. PřF UK v Praze, Praha. (in Czech).

Balatka, B. (1966): Ke středopleistocénnímu a mladopleistocénnímu vývoji údolní nejdolejší Jizery. Sborník České Společnosti zeměpisné 71(3), 217–230, https://doi.org/10.37040/geografie1966071030217.

Balatka, B., Gibbard, P., Kalvoda, J. (2010): Morphostratigraphy of the Sázava river terraces in the Bohemian Massif. AUC Geographica 45(1–2), 3–34, https://doi.org/10.14712/23361980.2015.54.

Balatka, B., Kalvoda, J. (2006): Geomorfologické členění reliéfu Čech. Kartografie Praha. (in Czech).

Balatka, B., Kalvoda, J. (2008): Evolution of Quaternary river terraces related to the uplift of the central part of the Bohemian Massif. Geografie 113(3), 205–222, https://doi.org/10.37040/geografie2008113030205.

Balatka, B., Kalvoda, J. (2010): Vývoj údolí Sázavy v mladším kenozoiku. Česká geografická společnost, Praha.

Balatka, B., Kalvoda, J., Gibbard, P. (2015): Morphostratigraphical correlation of river terraces in the central part of the Bohemian Massif with the European stratigraphical classification of the Quaternary. AUC Geographica 50(1), 63–73, https://doi.org/10.14712/23361980.2015.87.

Balatka, B., Sládek, J. (1962): Říční terasy v českých zemích. Československá akademie věd. Praha. (in Czech).

Balatka, B., Sládek, J. (1965): Pleistocénní vývoj údolí Jizery a Orlice. Rozpravy Československé akademie věd, Řada matematických a přírodních věd 11, 3–26. (in Czech).

Boháčová, I., Břízová, E., Nývlt, D., Růžičková, E. (2000): Holocene flood plain of the Labe river (past climatic changes and their impact on natural and human development). Excursion Guide, the International Conference on Past Global Changes, September 6–9, 2000, Prague.

Břízová, E., Dušek, K., Havlíček, P., Holásek, O., Manda, Š., Vodrážka, R. (2005): Geologie středního Polabí: Předběžné výsledky geologického mapování na listu 13–131 Brandýs nad Labem – Stará Boleslav. Zprávy o geologických výzkumech v roce 2004, 19–22. (in Czech).

Coubal, M. (2010): Tektonické založení jižního okraje české křídové pánve v okolí Kounic. Zprávy o geologických výzkumech v roce 2009, Česká geologická služba, 27–30. Available online https://app.geology.cz/img /zpravyvyzkum/fulltext/2009-8.pdf (accessed on 12. 11. 2019).

Czech Office for Surveying, Mapping and Cadastre (2019): Analýza výškopisu. Prohlížecí služba WMS – DMR 5G. Available online https://ags.cuzk.cz/av/ (accessed on 3. 12. 2022).

Czudek, T. (1997): Reliéf Moravy a Slezska v kvartéru. Sursum, Tišnov. (in Czech)

Czech Geological Survey: Map applications, version 1B.2. Available online http://www.geology.cz/app/ciselniky /lokalizace/show_map.php?mapa=g50&y=724200&x =1034400&r=7000&s=1&legselect=0 (accessed on 12. 11. 2019).

Čech, S., Holásek, O., Havlíček, P., Skácelová, Z. (2009): Kvartérní a křídové sedimenty na území listu Nymburk. Zprávy geologického výzkumu v roce 2008, 59–61. Available online https://app.geology.cz/img /zpravyvyzkum/fulltext/2008-15.pdf (accessed on 20. 12. 2022).

Danišík, M., Migoń, P., Kuhlemann, J., Evans, N. J., Dunkl, I., Frisch, W. (2010): Thermochronological constraints on the long-term erosional history of the Karkonosze Mts., Central Europe. Geomorphology 117(1–2), 78–89, https://doi.org/10.1016/j.geomorph.2009.11.010.

Danišík, M., Štěpančíková, P., Evans, N. J. (2012): Constraining long-term denudation and faulting history in intraplate regions by multisystem thermochronology: An example of the Sudetic Marginal Fault (Bohemian Massif, central Europe). Tectonics 31(2), TC2003, https://doi.org/10.1029/2011TC003012.

Demek, J. (2004): Etchplain, rock pediments and morphostructural analysis of the Bohemian Massif (Czech Republic). In: Drbohlav, D., Kalvoda, J., Voženílek, V.: Czech Geography at the Dawn of the Millenium. Czech Geographical Society, Palacky University in Olomouc, Olomouc, 69–81.

Demek, J., Kirchner, K., Mackovčin, P., Slavík, P. (2009): Morphostructures on the territory of the Czech Republic (Europe). Zeitschrift fur Geomorphologie 53, Supplementary Issue 2, 1–10, https://doi.org /10.1127/0372-8854/2009/0053S3-0001.

Drahota, F. (1931): Spádová křivka Jizery se zřetelem k morfologickému vývoji její oblasti. Disertační práce. Geografický ústav UK v Praze, Praha (in Czech).

Enc, P. (1984): Flora a fauna nejstarších geologických útvarů na Brandýsku. Studie a zprávy 1981–1982, 5–19. (in Czech).

Engel, Z., Kalvoda, J. (2002): Morphostructural development of the sandstone relief in the Bohemian Cretaceous Basin. In: Přikryl, R., Viles, H. (Eds.): Understanding and managing stone decay. SWAPNET, Karolinum, Praha, 225–231.

Fediuk, F., Ichinkhorloo, B., Ciniburk, M. (1966): Neratovice Komplex – product of metasomatic transformation of volcanites into rocks of plutonic appearance. Paleovolcanites of the Bohemian Massif, 51–60.

Gent, H. van, Urai, J. L. (2020): Abutting faults: a case study of the evolution of strain at Courthouse branch point, Moab Fault, Utah. Solid Earth 11(2), 513–526, https:// doi.org/10.5194/se-11-513-2020.

GDO (2020): Database of the geologically documented objects in the Czech Republic. Czech Geological Survey. Available online http:// www.geology.cz/app/gdo /d.php?item=3 (accessed on 17. 12. 2020).

Gibbard, P. L., Cohen, K. M. (2008): Global chronostratigraphical correlation table form the last 2.7 million years. Episodes 31(2), 243–247, https:// doi.org/10.18814/epiiugs/2008/v31i2/011.

Gibbard, P. L., Head, M. J., Walker, M. J. L. and the Subcomission on Quaternary Stratigraphy (2009): Formal ratification of the Quaternary System/Period and the Pleistocene Series/Epoch with a base at 2.58 Ma. Journal of Quaternary Science 25(2), 96–102, https:// doi.org/10.1002/jqs.1338.

Grygar, R. (2016): Geology and Tectonic Development of the Czech Republic. In: T. Pánek, J. Hradecký (Eds.): Landscapes and Landforms of the Czech Republic. World Geomorphological Landscapes. Springer Verlag, 7–18, https://doi.org/10.1007/978-3-319-27537-6_2.

Havlíček, V. (1963): Tektogenetické porušení barrandienského paleozoika. Sborník geologických věd – Geologie 1, 77–102. (in Czech).

Havlíček, P., Brunnerová, Z., Hrkal, Z., Kříž, J., Růžičková, E., Šalanský, K., Valečka, J., Volšan, V., Zeman, M., Zoubek, J. (1987): Vysvětlivky k základní geologické mapě ČSSR, list 12-242 Čakovice. Ústřední ústav geologický, Praha. (in Czech).

Herrmann, Z., Burda, J. (Eds., 2016): Závěrečná zpráva o řešení geologického úkolu s výpočtem zásob podzemních vod v hydrogeologických regionech 1151 – Kvartér Labe po Kolín, 1152 – Kvartér Labe po Nymburk, 1171 – Kvartér Labe po Jizeru, 1172 – Kvartér Labe po Vltavu. MS archiv Česká geologická Služba. (in Czech).

Holásek, O., Adamová, M., Břízová, E., Čáp, P., Dušek, K., Havlíček, P., Hradecká, L., Kadlecová, R., Kolejka, V., Krupička, J., Majer, V., Manda, Š., Nývlt, D., Rajchl, M., Rudolský, J., Stehlík, F., Svobodová, I., Šebesta, J., Táborský, Z., Tyráček, J., Vodrážka, R. (2005): Vysvětlivky k základní geologické mapě České republiky, list 13–131 Brandýs nad Labem – Stará Boleslav. Česká geologická služba, Praha. (in Czech).

Hrubeš, M. (1999): Výzkum kvartéru mezi Lysou nad Labem a Čelákovicemi – předběžné výsledky studia archivních materiálů. Zprávy o geologických výzkumech v roce 1998, 111–114. (in Czech).

Hradecký, J., Brázdil, R. (2016): Climate in the Past and Present in the Czech Lands in the Central European Context. In: T. Pánek, J. Hradecký (Eds.): Landscapes

and Landforms of the Czech Republic. World Geomorphological Landscapes. Springer Verlag, 19–28, https://doi.org/10.1007/978-3-319-27537-6_3.
Chlupáč, L. et al. (2002) Geologická minulost České republiky. Academia, Praha. (in Czech).
Kalvoda, J., Balatka, B. (2016): The Geomorphological Evolution and Environmental Hazards of the Prague Area. In: T. Pánek, J. Hradecký (Eds.): Landscapes and Landforms of the Czech Republic. World Geomorphological Landscapes. Springer Verlag, 43–57, https://doi.org/10.1007/978-3-319-27537-6_5.
Knížek, M. (2013): Radiální tektonika barrandienu. Disertační práce. PřF MU v Brně, Brno. (in Czech).
Kovanda, J. et al. (2001): Neživá příroda Prahy a jejího okolí. Academia, Český geologický ústav, Praha. (in Czech).
Kříž, J. et al. (1984): Vysvětlující text k základní geologické mapě 1:25 000 13-133 Úvaly. Ústřední ústav geologický, Praha. (in Czech).
Kukal, Z. (1963): Výsledky sedimentologického výzkumu barrandienského ordoviku. Sborník Geologických Věd – Geologie 1, 103–132. (in Czech)
Loyda, L. (1950): Buližníkové kamýky v Barrandienu. Diplomová práce. PřF UK v Praze, Brandýs nad Labem. (in Czech).
Mackin, J. H. (1948): Concept of the graded river. Geological Society of America Bulletin 59(5), 463–512, https://doi.org/10.1130/0016-7606(1948)59[463:COTGR]2.0.CO;2.
Malkovský, M. (1975): Paleogeography of the Miocene of the Bohemian Massif. Věstník ústředního ústavu geologického 50(1), 27–31.
Matějka, A. (1936): Svrchní křída. In: Čepek, L. et al.: Vysvětlivky ke geologické mapě Československé republiky, list Kladno 3952. Knihovna Státního geologického úřadu Československé republiky 17, 63–70. (in Czech).
Mikisková, I. (2009): Paleokoryto řeky Jizery. Magisterská práce. PřF UK v Praze, Praha. (in Czech).
Novotná, R. (1998): Geomorfologická analýza a vývoj reliéfu opuštěného pleistocenního údolí Jizery v úseku Domousnice – Všejany. Magisterská práce. PřF UK v Praze, Praha. (in Czech).
Pánek, T., Hradecký, J. (Eds., 2016): Landscapes and Landforms of the Czech Republic. World Geomorphological Landscapes, Springer Verlag, https://doi.org/10.1007/978-3-319-27537-6.
Pánek, T., Kapustová, V. (2016): Long-Term Geomorphological History of the Czech Republic. In: T. Pánek, J. Hradecký (Eds.): Landscapes and Landforms of the Czech Republic. World Geomorphological Landscapes. Springer Verlag 29–42, https://doi.org/10.1007/978-3-319-27537-6_4.
Peacock, D. C. P. (2001): The temporal relationship between joints and faults. Journal of Structural Geology 23(1–2), 329–341, https://doi.org/10.1016/S0191-8141(00)00099-7.
Peacock, D. C. P., Nixon, C. W., Rotevatn, A., Sanderson, D. J., Zuluaga, L. F. (2017): Interacting faults. Journal of Structural Geology 97, 1–22, https://doi.org/10.1016/j.jsg.2017.02.008.
Röhlich, P. (1952): Zpráva o biostratigrafickém výzkumu ordoviku mezi Prahou a Brandýsem nad Labem. Zprávy geologického výzkumu v roce 1952, 99–102. (in Czech).
Růžičková, E., Havlíček, P. (1981): Fluviální sedimenty soutokové oblasti Labe a Jizery. Výzkumné práce ústředního ústavu geologického, Praha. (in Czech).
Růžičková, E., Zeman, A. (1994): Paleogeographical developmemnt of the Labe flood plain during the Holocene. In: E. Růžičková, A. Zeman (Eds.): Holocene flood plain of the Labe River. Geological Institute of the Czech Academy of Science, Prague, 104–112.
Svoboda, P. (1996): Facie s Exogyra sigmoidea Reuss a Cidaris soriqneti Desor ve svrchním cenomanu a spodním až středním turonu české křídové pánve. Studie a zprávy Okresního muzea Praha – východ 12, 81–90. (in Czech).
Svoboda, P. (1998): Transgrese svrchní křídy mezi Kralupy nad Vltavou a Korycany. Studie a zprávy Okresního muzea Praha – východ 13, 129–154. (in Czech).
Svoboda, P. (2004): Vznik, vývoj a fauna předbřežních svrchnocenomanských a spodnoturonských sedimentů české křídové pánve a sousedních oblastí. Vliv klimatu, paleogeografie a tektoniky střední Evropy a severní Tethydy. Studie a zprávy Okresního muzea Praha – východ 15, 115–170. (in Czech).
Šmejkal, V., Melková, J. (1969): Notes on some potassium argon dates of magmatic and metamorphic rocks from the Bohemian Massif. Časopis pro Mineralogii a Geologii 14(3–4), 331–338.
Tyráček, J. (2010): Geologie kvartérních fluviálních sedimentů na soutoku Labe s Jizerou. Zprávy o geologických výzkumech 43, 133–138 (in Czech).
Tyráček, J., Havlíček, P. (2009): The fluvial record in the Czech Republic: A review in the context of IGCP 518. Global and Planetary Change 68(4), 311–325, https://doi.org/10.1016/j.gloplacha.2009.03.007.
Tyráček, J., Westaway, R., Bridgland, D. (2004): River terraces of the Vltava and Labe (Elbe), and their implications for the uplift history of the Bohemian Massif. Proceedings of the Geological Association 115(2), 101–124, https://doi.org/10.1016/S0016-7878(04)80022-1.
Uličný, D. (1997): Sedimentation in a reactivated, intra-continental strike slipe fault zone: the Bohemian Cretaceous Basin, Central Europe. Gaea Heidelbergensis 3, 347.
Uličný, D., Špičáková, L., Grygar, R., Svobodová, M., Čech, S., Laurin, J. (2009): Palaeodrainage systems at the basal unconformity of the Bohemian Cretaceous Basin: Roles of inherited fault systems and basement lithology during the onset of basin filling. Bulletin of Geosciences 84(4), 576–610, https://doi.org/10.3140/bull.geosci.1128.
Vaněk, J. (1999): Ordovician in the easternmost part of the Prague Basin (Úvaly and Brandýs areas) and its comparison with Rokycany area (westernmost part of the basin). Palaeontographica Bohemiae 5(2), 5–20.
Vohanka, L. (1966): Vyšehořovicko 1966. Závěrečná zpráva a výpočet zásob žáruvzdorných jílů. MS Česká geologická služba, Geofond. Praha. (in Czech).
Volšan, V., Havlíček, P., Hrkal, Z., Kovanda, J., Lochmann, Z., Pašava, J., Pražák, J., Růžičková, E., Shrbený, O., Straka, J., Šalanský, K., Valečka, J., Vejlupek, M., Vítek, J., Zeman, A., Zoubek, J. (1990): Vysvětlivky k základní geologické mapě ČSSR, list 12-224 Neratovice. Ústřední ústav geologický, Praha. (in Czech).
Wagner, G. A., Gögen, K., Jonckheere, R., Kämpf, H., Wagner, I., Woda, C. (1998): The age of Quaternary

volcanoes Železná hůrka and Komorní hůrka (western Eger Rift), Czech Republic: alpha-recoil track, TL, ESR and fission track chronometry. Excursion guide and Abstracts of Workshop, Intern. Geol. Correl. Progr. No 369 "Magmatism and Rift Basin Evolution", 7.9.–11.9. 1998, Liblice, Czech Geological Survey, 95–96.

ZABAGED® (2014) – výškopis. Praha: ČÚZK, 2014.

Záruba, Q., Bucha, V., Ložek, V. (1977): Significance of the Vltava terrace system for the Quaternary chronostratigraphy. Rozpravy Československé Akademie Věd, Řada matematických a přírodních věd 87(4), 1–89.

Zelenka, P., Adamová, M., Břízová, E., Čáp, P., Čech, S., Dušek, K., Havlíček, P., Holásek, O., Hroch, T., Hradecká, L., Kadlecová, R., Koleka, V., Krupička, J., Mlčoch, B., Prouza, V., Rajchl, M., Rudolský, J., Smolíková, L., Stehlík, F., Táborský, Z., Tyráček, J., Valečka, J. (2006): Vysvětlivky k základní geologické mapě České republiky, list 13-113 Sojovice. Česká geologická služba, Praha. (in Czech).

Žítt, J., Nekovařík, Č. (2001): Nové poznatky o lokalitě Kuchyňka u Brázdimi (česká křídová pánev). Studie a zprávy okresního muzea Praha – východ v Brandýse nad Labem a Staré Boleslavi 14, 250–255. (in Czech).

Žítt, J., Nekvasilová, O. (1991): Kojetice – nová lokalita svrchnokřídových epibiontů přisedlých na buližníkových klastech. Bohemia centralis, 20, 7–27. (in Czech).

Žítt, J., Nekovařík, Č., Hradecká, L., Záruba, B. (1998): Svrchnokřídová sedimentace a tafocenózy na proterozoických elevacích okolí Brandýsa nad Labem, s hlavním důrazem na lokality Kuchyňka u Brázdimi (česká křídová pánev). Studie a zprávy Okresního muzea Praha – východ 13, 189–206. (in Czech).

An open geospatial database as a tool for geoheritage management at national scale: The case study of Greece

Zoe Pantazopoulou[1,2,*], Antonios Mouratidis[1,2], Dimitrios D. Alexakis[3], Vasileios Tsioukas[4], Triantafyllia-Maria Perivolioti[1,2], Dimitrios Terzopoulos[5], Panagiotis Kalaitzis[6]

[1] Aristotle University of Thessaloniki, Department of Physical and Environmental Geography, Greece
[2] Center for Interdisciplinary Research and Innovation (CIRI-AUTH), Greece
[3] Institute for Mediterranean Studies, Foundation for Research and Technology Hellas (FORTH), Greece
[4] Aristotle University of Thessaloniki, Department of Geodesy and Surveying, Greece
[5] Aristotle University of Thessaloniki, School of Physics, Greece
[6] University of the Aegean, Department of Geography, Greece
* Corresponding author: zpantazo@geo.auth.gr

ABSTRACT

Geological heritage or geoheritage is of at least equal significance to – and sometimes also interwoven with – cultural heritage. Hence, it holds the potential of scientific, educational, cultural, aesthetic, and touristic value. Nevertheless, geoheritage has not attracted the same level of attention as cultural heritage to date, especially regarding its sustainable management and suitable conservation strategies. Yet actions and measures are mandatory to preserve and highlight geological heritage and to reduce threats that may cause its deterioration or even extinction. To this end, geospatial science and technology provide the means for documenting and dealing with geological heritage throughout the individual steps of the geoheritage management process. In this study, we present a holistic approach to geoheritage management at the national level for Greece, based on the implementation of a Geographical Information Systems (GIS) database that also enables the coupling of geoheritage with a plethora of readily available geospatial information from remote sensing and other sources. The results demonstrate that an appropriate, geospatial record of geological heritage can have a crucial contribution to geoheritage management from its identification, to its monitoring, protection, and exploitation for educational, scientific, recreational, and other purposes.

KEYWORDS

geoheritage; geoheritage management; GIS; Remote Sensing; Greece

Received: 4 January 2024
Accepted: 28 February 2024
Published online: 14 March 2024

Pantazopoulou, Z., Mouratidis, A., Alexakis, D. D., Tsioukas, V., Perivolioti, T.-M., Terzopoulos, D., Kalaitzis, P. (2024): An open geospatial database as a tool for geoheritage management at national scale: The case study of Greece. AUC Geographica 59(1), 60–76
https://doi.org/10.14712/23361980.2024.4

1. Introduction

1.1 Definition of geoheritage

The term "geoheritage" has evolved from the notion of "geological heritage". The first use of the term was at the First International Symposium on the Conservation of our Geological Heritage, which took place in France, in 1991 (Brilha 2015). Since then, many different interpretations have been proposed for the aforementioned term.

Geoheritage is defined as the group of geological elements (items) or geological sites (geosites or geotopes) with outstanding scientific, cultural, and educational value (Fassoulas et al. 2012; Herrera-Franco et al. 2022; Thomas 2016). The term geological site or geosite comes from the Greek root "geo" (= Earth) and the Latin word "situs'' (= sites) and refers to locations of geological interest. However, the geological elements should be evaluated for their uniqueness to be characterized as geological heritage (Brilha, 2018). Additionally, geosites with high touristic value can also be known as "geomonuments", a term already used to promote some items of geoheritage to the general public (Brilha 2016).

Some authors suggested that geoheritage refers to those aspects of the Earth, which are important to our understanding of Earth history. By their nature, the geoheritage sites, which are akin to cultural heritage sites or documents, are among non-renewable resources (Bradbury 1993). Others (Semeniuk 1997) referred to geoheritage as nationally significant features of geology, including igneous, metamorphic, sedimentary, structural, paleontological, geomorphic, pedologic or hydrologic attributes that offer important information or insight into the formation or development of a continent, or that can be used for research, teaching or as a reference site. However, it has also been argued that "geoheritage consists of all the significant Earth features and continuing processes that we wish to keep, sustain, conserve, manage and interpret for their natural heritage value" (Osborne 2000). According to several authors (Brilha 2002; Gonggrijp 1999; Zagorchev and Nakov 1998), geoheritage relates to the importance of the site (locally, regionally, nationally, and internationally), and its use (educational, scientific, and recreational), as well as the need to conserve it. Education is here perceived in its broader sense of education, training, capacity building and outreach, including all levels and types (formal, informal, non-formal) of education in a lifelong learning context.

For the present study, geoheritage is considered as the global, regional, and local geological elements, such as igneous, metamorphic or sedimentary rocks, minerals, fossils, stratigraphic, tectonic, pedologic, paleontological structures and other geosites (or geotopes). It also encompasses important sites and specimens, which offer information and insights into the formation and evolution of the Earth, the evolution of life, the climate and landscapes of the past and present, along with the geological history of the sites where they are found (Brocx and Semeniuk 2007; Carcavilla et al. 2009; Zafeiropoulos et al. 2021).

Geomonuments have equivalent significance as historical and archaeological monuments. Consequently, they have scientific, educational, cultural, aesthetic and touristic value. Thus, sustainable management and suitable conservation strategies are mandatory to preserve geoheritage and to reduce threats that may cause the deterioration of geological heritage and its surrounding environment. Moreover, the links and integration between geological and cultural heritage are recently being more and more discussed (Bollati et al. 2023; Pijet-Migoń and Migoń 2022).

1.2 Management of geoheritage

The management process of geological heritage includes a variety of steps or stages, which depend on the type of geoheritage as well as the cartographic scale used – the latter not being independent from the type/size/geographic scale of each geological heritage item (Burlando et al. 2011; Theodosiou 2010; Zouros 2004, 2005; Zouros and Valiakos 2010). Nevertheless, some of these stages are common and applicable to most geoheritage elements (Fig. 1). These span from the original investigation/identification, mapping and/or scanning, monitoring and protecting, to "higher-level" management activities related to its sustainable exploitation for various purposes (education, culture, tourism, promotion of local products etc.), as well as an overall assessment for the value of each geoheritage element.

For example, a petrified tree trunk is first found (Identification), spatially described (Delineation) and scanned with a terrestrial laser scanner (Mapping or

Fig. 1 Stages (steps) of geological heritage management process applicable to most types of geoheritage. The process starts at the bottom of the pyramid with the most fundamental (lower) stages (e.g. identifying, mapping) and follows through the final (higher) steps such as exploitation and promotion for various purposes (aesthetic, touristic, educational etc.).

Scanning). Subsequently, it is defined for its characteristics and determined for its origin (Interpretation), preserved locally with technical and/or chemical measures (Protection) and continually followed for its potential degradation and changes (Monitoring). In higher (later) stages of management, it may be highlighted e.g. by building roads for securing access to the specific geosite (Exhibition), evaluated for its scientific, educational or touristic importance (Assessment), used for different purposes such as research, education, tourism etc. (Exploitation) and finally, communicated and disseminated together with all the relevant activities, developed material and other outputs related to the specific geoheritage (Promotion).

1.3 The role of geospatial science and technology

Geospatial information has become the backbone of modern society and one of the main drivers of decision making. The traditional technologies of Remote Sensing (spaceborne, airborne, or ground-based), Global Navigation Satellite Systems (GNSS) and Geographical Information Systems (GIS) have been used for the collection and processing of large volumes of geospatial information since decades, at ever increasing resolution and accuracy. In today's era of Big Data, these fundamental elements of what is broadly defined as "Geospatial Science and Technology" are now coupled with web-mapping, Artificial Intelligence (AI), Internet of Things (IoT) and related capabilities. Together with smartphones, tablets, other internet and geolocation-enabled devices, equipment and related applications, they constitute a geospatially-enabled ecosystem that is continuously changing everyday life and opening new horizons in practically every sector of the economy worldwide (Goodchild 2022; Liu et al. 2022; Mouratidis and Koutsoukos 2016).

The increasing development of terrestrial/ground-based (e.g. 3D laser scanners) (Fassoulas et al. 2022; Marsico et al. 2015; Pasquaré Mariotto et al. 2023; Perotti et al. 2020; Ravanel et al. 2014), aerial (e.g. Unmanned Aerial Vehicles/UAVs) (Papadopoulou et al. 2022; Santos et al. 2018) and space-based (e.g. multispectral optical or Synthetic Aperture Radar/SAR) Remote Sensing techniques (AbdelMaksoud et al. 2019; Németh 2022; Singh et al. 2021), together with the tremendous advancement of GIS technologies (Bendaoud et al. 2015) have the potential to contribute significantly to the effective management of geoheritage. Remote Sensing technologies have thus great prospects as a low-cost, non-destructive tool for dealing with geoheritage. Nevertheless, to date, in the majority of scientific publications, the use of geospatial science and technology refers to applications for the management of cultural heritage (Agapiou et al. 2015; Elfadaly et al. 2020; Stewart 2017; Wilson 2021). Remote Sensing data of varied spectral and spatial resolutions have been interpreted to detect, identify, monitor, map and prospect cultural heritage (or the cultural aspects of heritage) sites or objects, but also their surrounding landscape. Remote Sensing has also been used for the investigation and prediction of environmental change and scenarios through the development of GIS-based models and decision-support instruments (Ayad 2005; Hadjimitsis et al. 2013).

1.4 Geoheritage databases in the world

Some efforts for creating geoheritage databases have been implemented around the world (Ballesteros et al. 2022; Bendaoud et al. 2015; Martin et al. 2014; Suma and Cosmo 2011). These focused on different geographical scales, from national, to regional or local level and/or to specific or generic geoheritage types. They have also typically addressed just some of the aspects of geoheritage management (e.g. identification, interpretation, visualization, assessment, promotion or exploitation) and rarely the full spectrum of management stages. GIS has inherently received a prominent role in most of these cases and has been often combined with web mapping services. Thus, there is hardly any experience from studies that address a wide geographical area, all types of geoheritage and all stages of geoheritage management at the same time.

1.5 Study Area

As per the geographical area investigated, owing to its geotectonically privileged location at the convergence of two tectonic plates, Greece has a very complex geological history and geodiversity, which is complemented by an even richer historical and cultural background.

Located between the converging African and Eurasian plates, Greece is characterized by an abundance of geosites and is therefore considered a "natural geological laboratory" (Papanikolaou 2021; Spyrou et al. 2022) that is unveiling insights on geodynamics and related phenomena as well as geological processes. Rocks, fossils and other geological elements reveal the palaeogeography of the broader Greek territory, which is today reflected in a complex geomorphological environment shaped mainly by active tectonics, but also exogenous processes. Mountains, mountain ranges, island complexes, lakes, rivers, caves, beaches consist some of the rich geomorphological features extending up to almost 3,000 m of elevation and contributing to the geodiversity of the country (Drinia et al. 2022).

As a result, though occupying a relatively small area, the Greek territory is scattered with a variety of geological formations, landforms, fossils and other geoheritage elements. These are in many cases interwoven with elements of cultural heritage – with some of the latter being of global importance and

recognition and thus also of high scientific, educational and touristic value. All this is reflected in the 19 UNESCO World Heritage Sites (Centre n.d.), as well as 8 geoparks with global recognition listed in the World Network of UNESCO Geoparks (UNESCO Global Geoparks | UNESCO n.d.), located in the country. For the ensemble of the aforementioned reasons, Greece provides an excellent test site the purposes of this study.

1.6 Objectives

In this context, the goal of this study is to use Greece as a paradigm of the contribution to a geospatially-enabled management of geoheritage over a large geographic area, with the specific objectives of:

a) Producing an open geoheritage GIS database at national level.
b) Highlighting the benefits of having such a database as a stand-alone infrastructure.
c) Demonstrating the added value and immense further potential of exploiting the database together with additional geospatial data (both remotely-sensed and other).

2. Methodology

2.1 Retrieval and verification of information regarding geoheritage in Greece

The original information for creating the database for geological heritage sites was drawn from a variety of sources, such as research articles, other publications, official websites of local management authorities (municipalities or other organizations), other internet sources, and in some cases from personal communication and testimonies from local communities.

The location of each geoheritage site was recognized and thoroughly verified with the maximum possible accuracy (in the order of a few meters), by exploiting national geospatial data as well as publicly available layers, such as Google Earth™, Google Maps™ and OpenStreetMap, in an open-source GIS software (QGIS) environment. Only these verified entries were considered for registration in the database. Nevertheless, the inherent geolocation uncertainty of some types of geoheritage (e.g. caves, quarries etc.), when represented by a point feature/geometry, was considered later and is discussed further within the geospatial analysis section. With these considerations, approximately 350 entries were qualified for this first version of the database.

2.2 Creation of the GIS Database

As a general methodological concept for the content and structure of a GIS geoheritage database, the following elements ought to be considered:

a) Availability of a GIS software (commercial or open source).
b) Choice of a Coordinate Reference System (national or international).
c) Storage of the database (locally or online).
d) Source(s) from which the infomation for geoheritage will be retrieved (may be official national records or not, in situ observations, publications etc.).
e) Attributes to be included for each geoheritage entry (can be relatively easily amended at a later stage).
f) Categorisation (possibly including sub-categories) of the geoheritage entries, which may be different

Tab. 1 Fields created in the attribute table of the geoheritage GIS database and their respective description.

No	Field Name	Type	Description
1	Id	Integer	A unique number given to each entry, in order to identify it in the database.
2	Name	Text	A name for each geoheritage location or element.
3	Details	Text	Some basic characteristics (e.g. properties, history, value etc.) of the geoheritage element are provided. Practically endless information can be added, if a geodatabase (*.gdd) format is being used for the database.
4	Link	Text	Link(s) to official website(s) in which reference is made to the specific geoheritage element either by local bodies or by the managing authority.
5	Ingest date	Date	The date of ingestion or last modification of the geoheritage element in the database.
6	Access	Text	If the location/element is freely accessible then it is designated as “Open”, while if there is an entrance fee or other restrictions it is designated as “Restricted”. In case it is not at all possible to visit the site, it is then classified as “Inaccessible”.
7	Price	Double	The general admission fee price information (in Euros) is given for sites with restricted access.
8	Museum	Text	Information is given on whether there is an associated exhibition or a museum (Yes/No).
9	Type	Text	General category of geological heritage to which the site belongs.
10	Code	Text	Short code corresponding to the aforementioned type/category of geoheritage.
11	Culture	Text	Reference to any connections with cultural heritage e.g. geomythological and/or archaeological sites (Yes/No).

Tab. 2 Snapshot of the attribute table containing the first 20 entries of the database.

Id	Name	Details	Link	Ingestdate	Access	Price	Museum	Type	Code	Geo-mythology
1	Nymfo-petres	A series of rocks, standing upright and creating the impression of a "stone forest".	–	23-12-20	Open	0	No	Geomorpho-logical	NG 06	Yes
2	The Petrified Forest of Lesvos	The Petrified Forest of Lesvos is a fossilized ecosystem that includes hundreds of standing and lying petrified tree trunks.	http://www .petrifiedforest .gr/	24-12-20	Restricted	5	Yes	Paleonto-logical	NG 03	No
3	Vatika Petrified Palm Forest Agios Nikolaos	Petrified palm forest of the coastal zone of Agios Nikolaos	https://www .visitvatika.gr /el/nature /petrified -forest.html	24-12-20	Open	0	Yes	Paleonto-logical	NG 03	No
4	Cave of Lakes-Kastria	Cave of Lakes consist of 13 in total small or large lakes succeed one another.The terrestrial areas alternate with lakes ones until the cave's end. The total lenh of cave is nearly 2Km.	https://www .kastriacave .gr/	28-12-20	Restricted	9	Yes	Cave	NG 05.1	No
5	Meteora	The gigantic rocks of Meteora resulted from the conglomerates erosion and the rapid uplift	https://whc .unesco.org /en/list/455/	04-01-21	Open	0	Yes	Geomorpho-logical	NG 06	No
8	Cave St. Georgiou Kilkis	St.Georgiou Kilikiw is one of the most important cave in Greece. THe cave has great paleontological value	–	04-01-21	Open	0	Yes	Cave	NG 05.1	No
6	Thracian Meteora	Thracian Meteora is located 15Km to the north Iasmos. The rocks of the Astrean rock formations are the same material with Meteora in Kalabaka.	–	04-01-21	Open	0	No	Geomorpho-logical	NG 06	No
7	Boucharia-Nohtaria	At the area of Mikrovalto and Livadero 40Km south of Kozani are the natural formations of rocks that lave been created dy the corrosion of the ground. Boucharia resemble chimneys,Nohtaria tall pyramid	–	04-01-21	Open	0	No	Geomorpho-logical	NG 06	No
9	Mirror rift Arkitsa	A rare geological phenomenon is a vertical rocky (limastone) surface over the highway. The surface is 300m length and 80m heigh.	–	04-01-21	Open	0	No	Structural	NG 01	No
10	Thermal Springs of Edipsos	The springs of Edipsos are more than 80. The temperature of the water ranges from 28oC-86oC and it is rich in magnesium,calcium and iron.	–	11-01-21	Open	0	No	Thermal Springs	NG 08	No

Id	Name	Details	Link	Ingestdate	Access	Price	Museum	Type	Code	Geo-mythology
11	Gorge Samaria	The Gorge of Samaria and a large area has been characterized as National Park. Along the gorge you will find 22 sources of drinking water.	https://www.samaria.gr/en/tips-crossing-samaria/	11-01-21	Restricted	5	No	Gorge	NG 09.5	No
12	Gorge Ha	The Gorge of Ha is a beautiful technical gorge in Crete. The gorge is about 1.5 Km long, very narrow and the walls rise up hundreds of meters.	https://petraoncrete.com/ha-gorge/	11-01-21	Open	0	No	Gorge	NG 09.5	No
13	Gorge Nekroi	The gorge of Nekroi in Zakros is an important archaeological gorge due to the large number of the graves found in the caves allong the gorge.	–	11-01-21	Open	0	No	Gorge	NG 09.5	No
14	Gorge Kotsyfos	The gorge starts at Kannevos village and ends at Plakias. The total length is 1800 m	–	11-01-21	Open	0	No	Gorge	NG 09.5	No

in each country, depending on the special geoenvironmental context, number of geoheritage sites, significance of the geoheritage items, purpose of the databse etc.

In this study, QGIS version 3.16 (Hannover) and Google Earth™ were used to implement the database and register all entries, with the initial coordinate reference system being Geographic WGS 1984 (EPSG 4326). During this first implementation, the database has been stored and processed locally. The coupling with external information such as national databases and Copernicus data (e.g. topography, land cover etc.) was carried out through Web Map Services (WMS) or direct downloading and importing in a GIS.

The table of elements (or attribute table) included eleven fields (Tab. 1) with the respective type (number, text, date etc.) and related information (Tab. 2).

2.3 Categorization of geoheritage in the database

The strategy for dividing geoheritage into broad categories (types) was to cover the variety of geological heritage elements in Greece, in a relatively simple, but comprehensive approach. To this end, 14 distinct categories were identified, covering both natural and anthropogenic geosites (Tab. 3 and Fig. 2).

More specifically, the type NG01 of natural geosites includes places of tectonic interest, such as seismic faults, folds, or tectonic windows. Category NG02 is related to outcrops of formations with specific interest/meaning for the prevailing processes in the area's geological history. NG03 is intended to cover locations of invertebrate or vertebrate fossils and/or excavation sites. Places of (visible to the naked eye) special or rare mineralogical and petrological composition are categorized in geoheritage type NG04. Type NG05 is associated with surficial or underground karstic features like sinkholes, poljes and caves. Other features formed by geomorphological processes like weathering, erosion and deposition are categorized under NG06. Places of (active or historical) volcanic activity (craters, phreatic explosions,

Tab. 3 Basic categorization of geoheritage sites of Greece for the GIS database, under the two broad categories of natural and anthropogenic geosites.

Natural Geosites (NG)	
1	Structural sites (NG01)
2	Stratigraphic sites (NG02)
3	Paleontological sites (NG03)
4	Mineralogical-Petrographical sites (NG04)
5	Karstic features (NG05)
6	Geomorphological features (NG06)
7	Volcanic sites (NG07)
8	Thermal Springs (NG08)
9	Other Environments (NG09)
10	Glacial and Periglacial features and processes (NG10)
11	Landscapes (NG11)
Anthropogenic Geosites (AnG)	
12	Mines (AnG01)
13	Quarries (AnG02)
14	Development projects sites (AnG03)

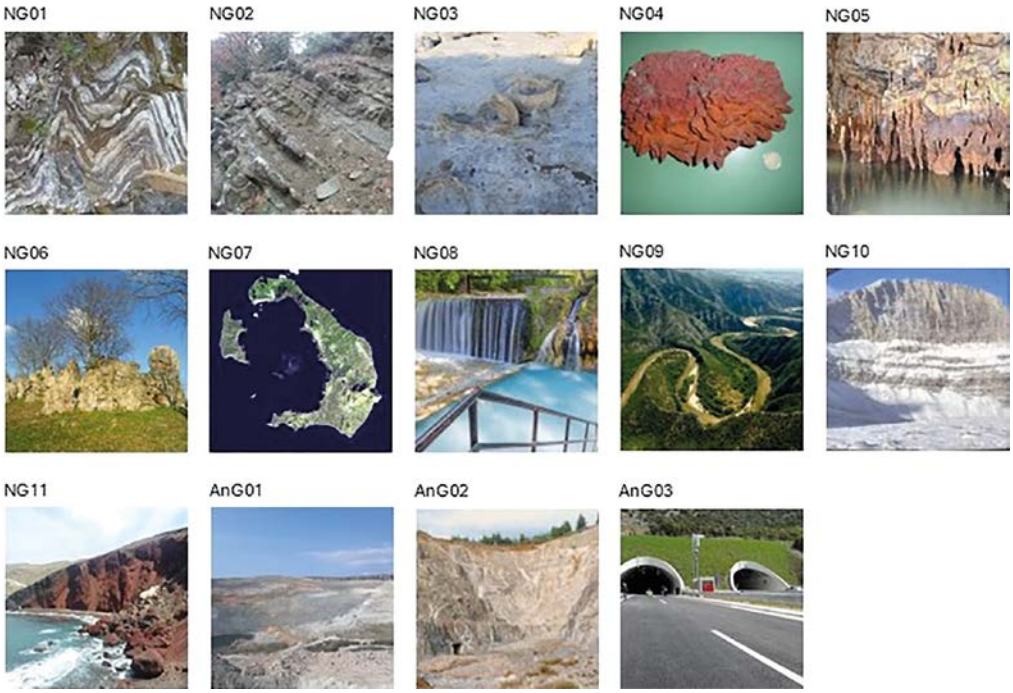

Fig. 2 Indicative examples of geological heritage sites, belonging to each of the 14 distinct categories identified in Tab. 3.

volcanic gas releases) fall under geoheritage category NG07. Thermal springs are considered as a special category under NG08. Special, extensive, and dynamic environments with their associated structures and processes, which unveil essential geological elements of the area where they are encountered and are not very commonly regarded as geoheritage (e.g. rivers, lakes, coastal areas, deserts, gorges, waterfalls etc.), form a separate category (NG09). Glacial and periglacial formations and processes (for Greece, it essentially concerns remnants of glacial activity from the last ice age – 100,000–10,000 years ago) are included in within type NG10. The last natural geoheritage category (NG11) is related to large geographic scale landscapes (e.g. mountains or mountain ranges, plains, basins, trenches, islands) that provide some vital information or constitute a unique and special geological appearance that reveals an important element of the geological history of the Earth.

Regarding anthropogenic geosites, they include active or inactive mines (AnG01) and quarries (AnG02), which, apart from the given geological interest, may also have considerable touristic, educational and historical value. The last category (AnG03) includes sites of other ancient and modern development projects and artificial structures, which constitute tangible proof of power of humans to shape the geo-environment. This category may e.g. encompass tunnels, canals, drainage works, road constructions etc. Quarries and mines could also have been included in this category; however, the separation is considered useful because of Greece's historically intense mining activity.

2.4 Geospatial analysis

Geospatial analysis was performed, in order to demonstrate the significance and prospective uses of the database at national level. To this end the Administrative Regions of Greece were taken into consideration (Fig. 3), along with some other basic, meaningful parameters (elevation, land cover, climate change) from EU's Copernicus Programme that could indicatively be of value to potential users. Additionally, as an indicative demonstration of local (site-level) usage of the database, a case study from the Island of Milos was implemented. Both open-source GIS (QGIS) and commercial GIS (ArcGIS™) software were used for the analyses.

More specifically, the Copernicus Land Monitoring Services were used to retrieve elevation data from the European Union Digital Elevation Model (EU-DEM) (Copernicus Land Monitoring Service – Reference Data: EU-DEM 2017), whereas the most recent Land Cover Change data between 2012–2018 were retrieved from Corine Land Cover (CORINE Land Cover n.d.).

Regarding climate change/sea level rise information, it was accessed via the Copernicus Climate Change Service. In particular, it was taken into account that for the next 100 years the average sea level rise for Europe will be between 20 cm and 40 cm (Copernicus Climate Change Service n.d.).

The land use change data underwent geospatial analysis in conjunction with the geoheritage database, to identify land use changes affecting or likely to disrupt sites of geological heritage. In this process, a

buffer zone of 1 km was used to account for the inherent geolocation uncertainty of certain types of geoheritage (caves, quarries etc.).

Each geoheritage element was assigned the corresponding orthometric elevation using the available DEM. Subsequently, the geological heritage sites potentially at risk from sea level rise in the next 100 years were identified, by adopting the extreme 40 cm sea level rise scenario.

In total, the ensemble geospatial analyses of all the aforementioned parameters with the geoheritage database yielded indicative new insights, such as:

a) Number of geoheritage items per administrative district.
b) Geoheritage density.
c) Density of geoheritage sites, normalized per area of Administrative Region.
d) Distribution of geoheritage, in terms of type and elevation (surface relief).
e) Correlation of geoheritage sites with land cover change.
f) Impact of projected sea level rise on geoheritage sites in the next 100 years.

For the site-specific (local level) example, the famous cove of Kleftiko (meaning "Bandit's Lair" in Greek) was selected from the geoheritage database (Fig. 4). In particular, the focus was on an impressive limestone formation of about 65 m × 20 m × 10 m (length × width × height), just a few meters off the coast, which is one of the most popular tourist attractions on the island. The purpose was to demonstrate the monitoring potentialities with geospatial technologies (Remote Sensing and GIS). For this reason, three very high resolution (0.5–0.6 m) optical satellite data were used from the Worldview-2™ and Pleiades satellites™ for the years 2010, 2014 and 2023. These images were processed with the Sentinel Application Platform (SNAP) to retrieve the Natural Difference Water Index (NDWI) (McFeeters 1996), classify the result with K-Means unsupervised classification and calculate the area and perimeter of the rock formation for each image in a GIS.

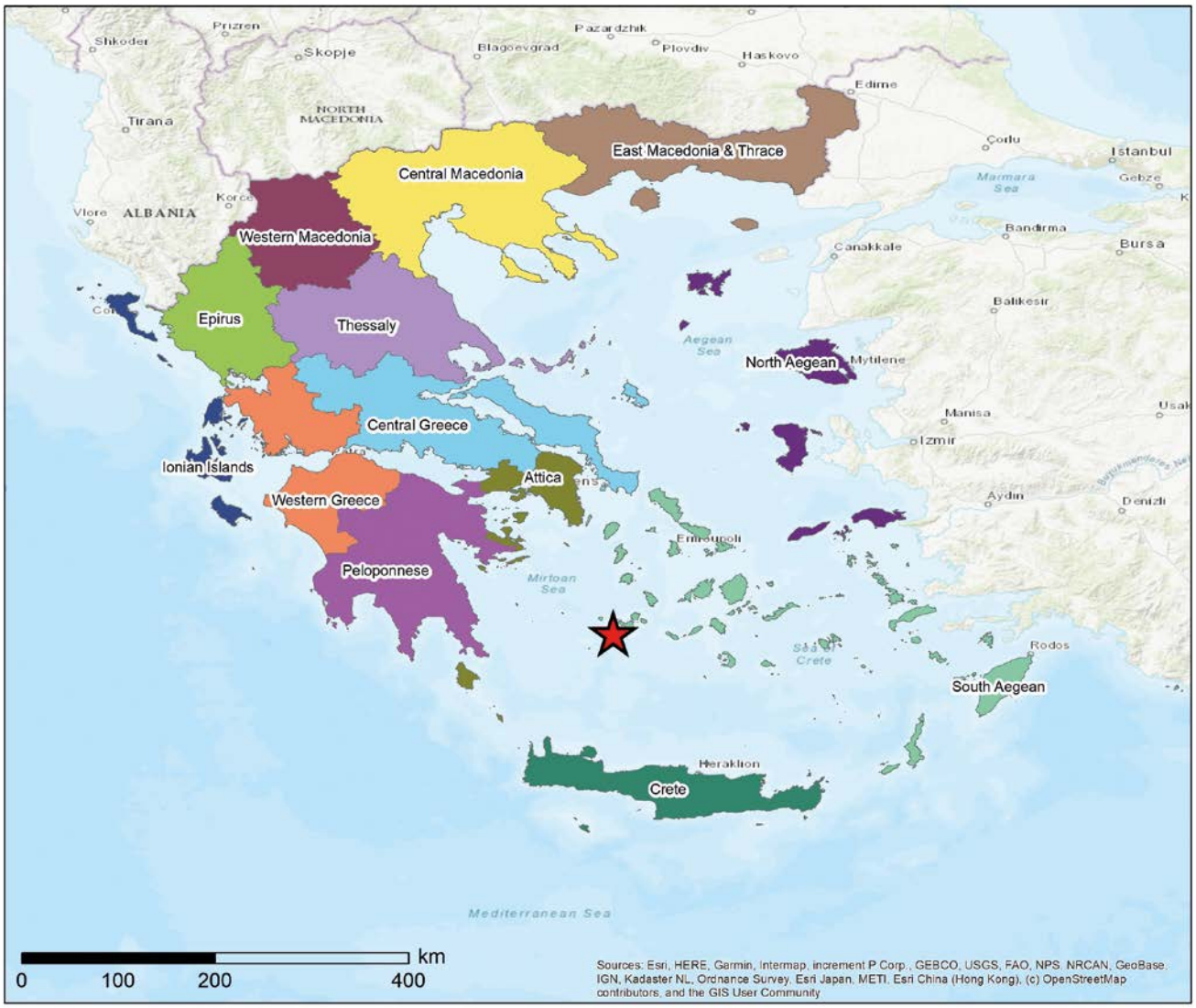

Fig. 3 The 13 Administrative Regions of Greece, which were considered as a basis for an initial geospatial analysis of geoheritage information. The red star indicates the location of "Kleftiko" on Milos Island, which was chosen to demonstrate a site-level usage of the database.

Fig. 4 Left: Google Earth image of the limestone formation in the area of Kleftiko on Milos Island, which falls under the NG06 (Geomorphological features) type of geoheritage. Right: Photo (view from the South) of the same rock mass from in situ observations (Source: A. Mouratidis).

3. Results

The open GIS database already includes a few hundreds of geological heritage elements all over Greece and is continually expanding. The database itself (or information regarding its migration) will be permanently available at the "Open Geospatial Database" of the Aristotle University of Thessaloniki (https://gis.web.auth.gr/), freely accessible for all purposes. A demo of the relevant web map is already available at the aforementioned website under https://gis.web.auth.gr/Webmaps/Geoheritage_171023_v3/index.html.

The geospatial analysis of geoheritage sites in conjunction with the Administrative Regions provides an overview of the number of geoheritage items per Administrative Region (Fig. 5), which can be also normalized by the area of each Region (Fig. 6), in order to yield more comparative results thereto. Disregarding the boundaries of Administrative Regions, an overall density of geoheritage sites at National level can be extracted (Fig. 7), which shows the concentration of geological heritage in specific areas. Another basic output is the distribution of geoheritage per type, which can be easily visualized through the database (Fig. 8).

By using a DEM, the geoheritage sites can also be classified based on the surface relief where they occur and thus categorized from lowland to mountainous geosites, which adds another layer of useful information for various purposes (Fig. 9).

With respect to the land cover change data, it can be observed (and quantified) that several geoheritage sites are in the vicinity of land cover changes between 2012 and 2018 (Fig. 10), which may indicate a potential threat for the geoheritage.

Regarding the climate change impact assessment, the endangered geoheritage sites can be identified for

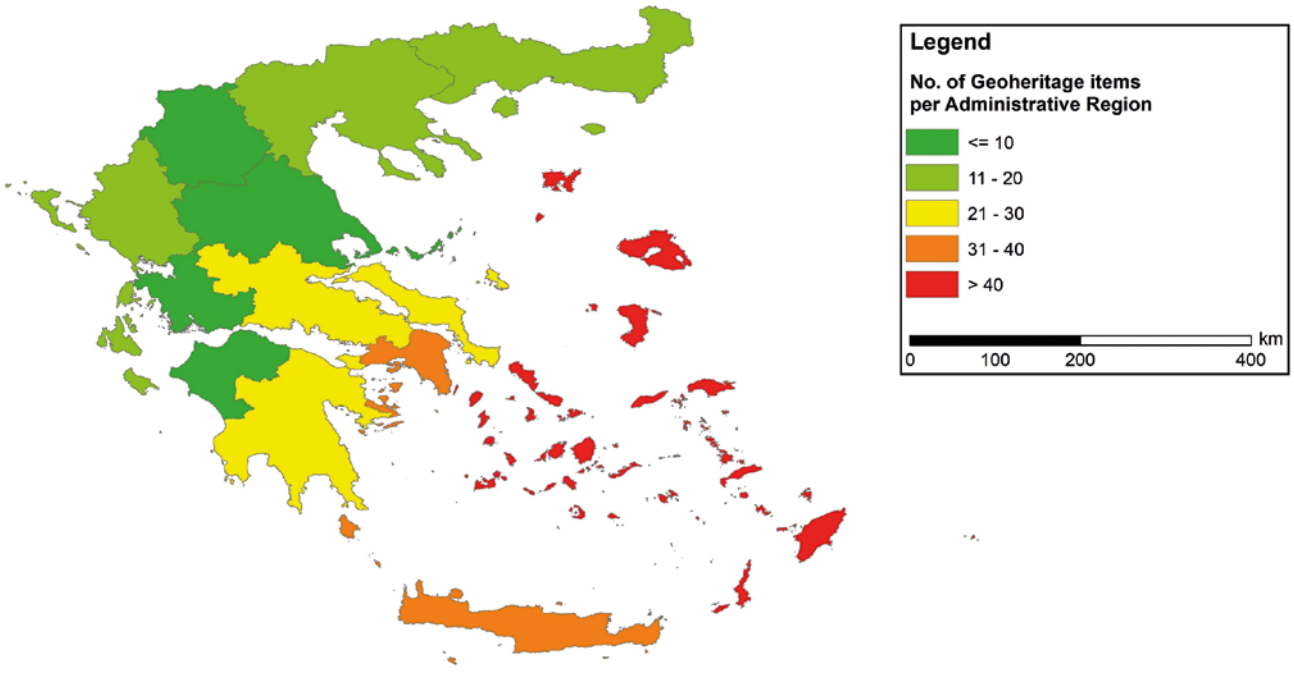

Fig. 5 Number of geoheritage items per Administrative Region.

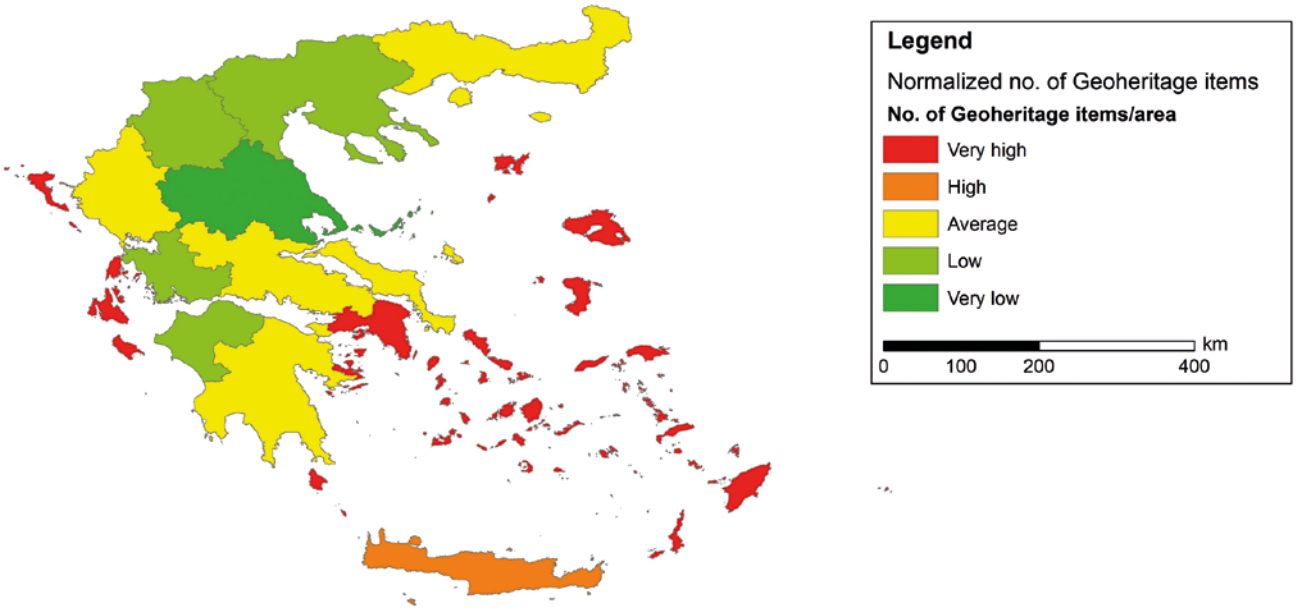

Fig. 6 Number of geoheritage sites normalized per Administrative Region area.

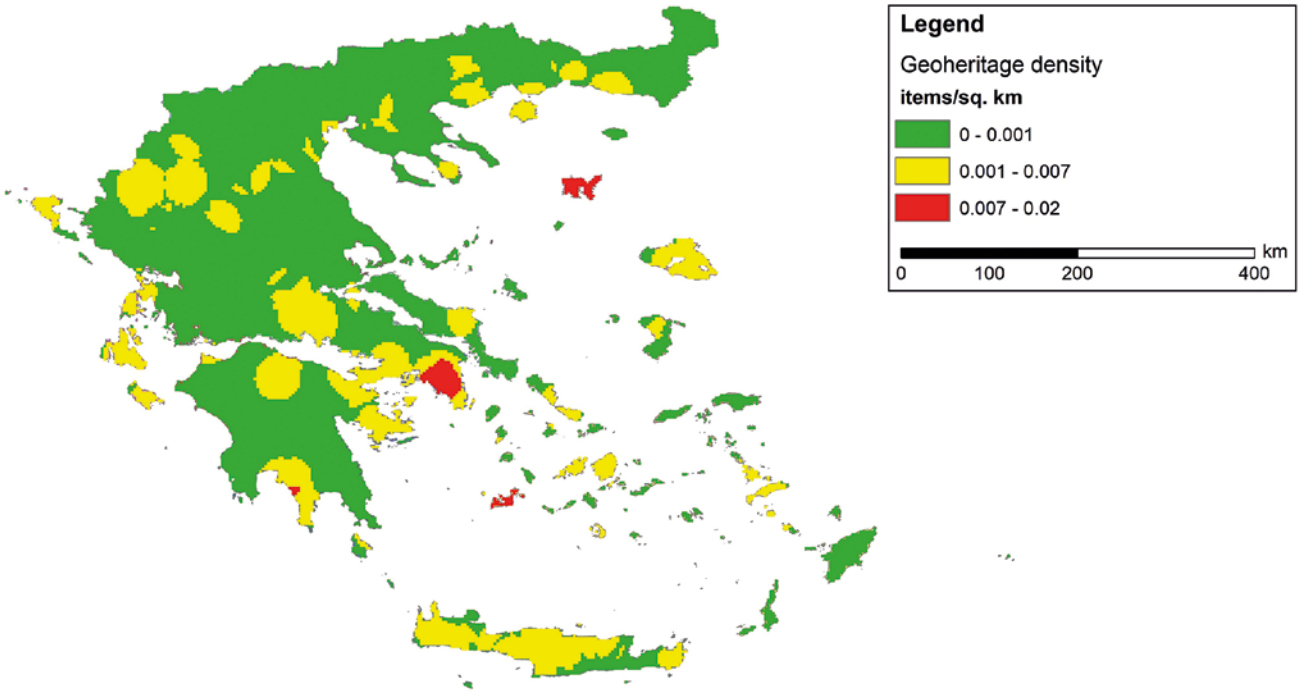

Fig. 7 Geoheritage density throughout the country.

different climatic projections and sea level rise scenarios (e.g. Fig. 11).

Finally, for the site-specific application demonstration on Milos Island, the Kleftiko rock mass was delineated from the satellite imagery in three processing steps (Fig. 12). This allowed the monitoring of this major rock formation, providing evidence for assessing the progress of erosional processes (and thus the degradation of the geoheritage site), by measuring the changes in its area and perimeter (Tab. 4).

4. Discussion

The geological heritage database developed in this study is a dynamic tool aimed at highlighting all kinds of geoheritage from local to global impact. It is a rare example of addressing the topic in such a holistic approach, by covering a relatively large geographical scale, while including all types of geoheritage and all stages of geoheritage management. The database was developed within the framework of a PhD research,

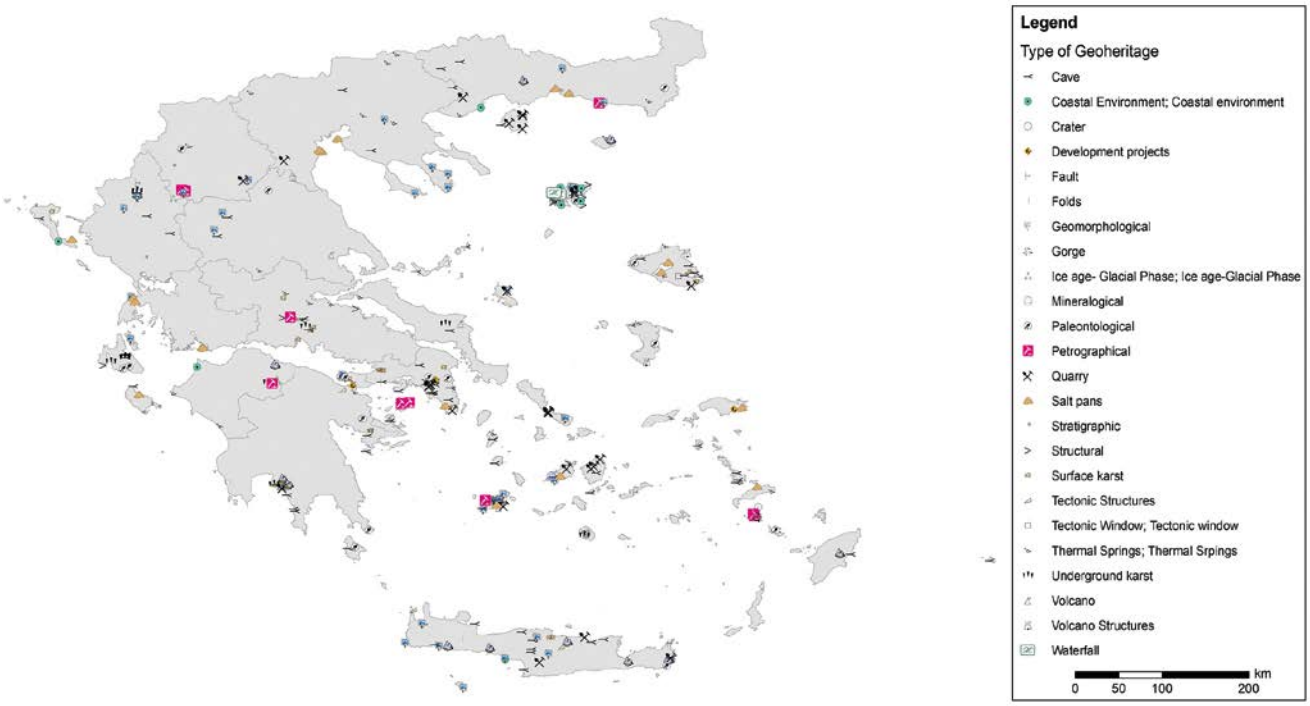

Fig. 8 Distribution of geoheritage sites per type.

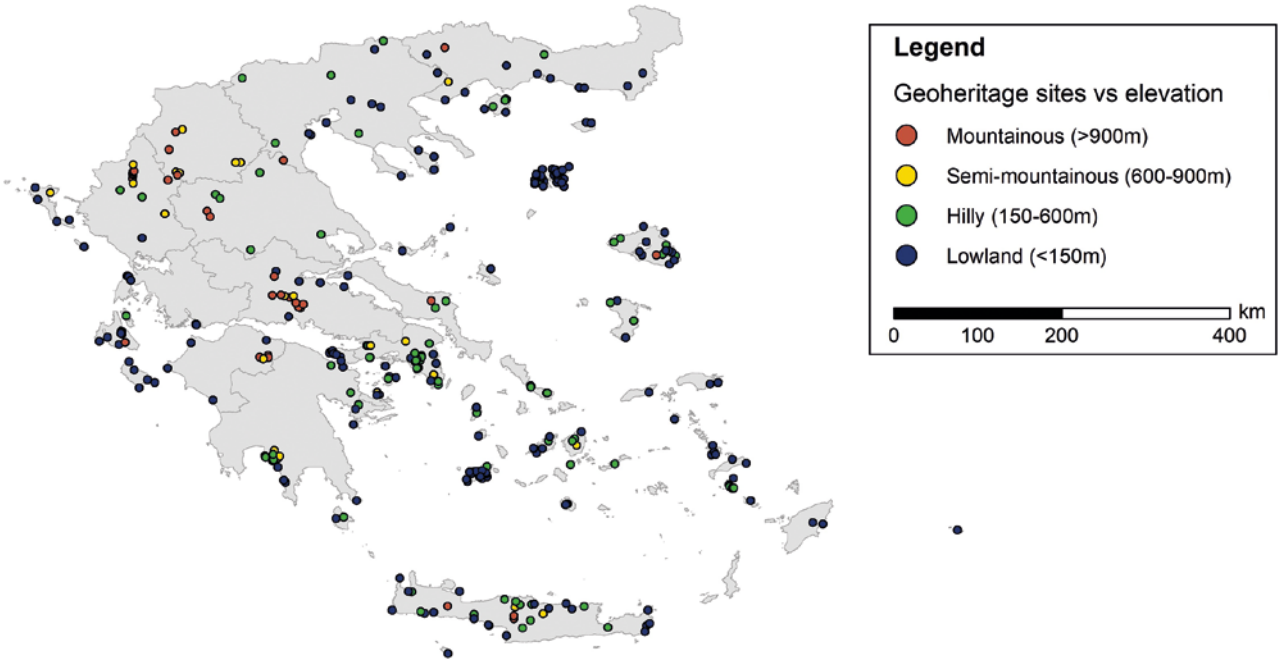

Fig. 9 Classification of geoheritage sites per surface relief according to Dikau's classification (Dikau 1989).

but aims at continuous enrichment, development, correction when deemed necessary and foremost at its exploitation by national or local authorities as well as the general public. This will not only contribute to the optimization of the overall geoheritage management but will also render the registered geosites more widely known and further develop the citizens' sense of responsibility in maintaining geological heritage elements for future generations. In this context, education in its very broad sense is of paramount importance and can maximize its potential through the use of open data (Coughlan 2020) – which is the case for the geoheritage database.

The number of entries (about 350 to date) in the database has been sufficient to demonstrate the value and potential uses of a geospatially-enabled database, but it is envisaged that it will increase to higher numbers in the near future. In any case, what is more

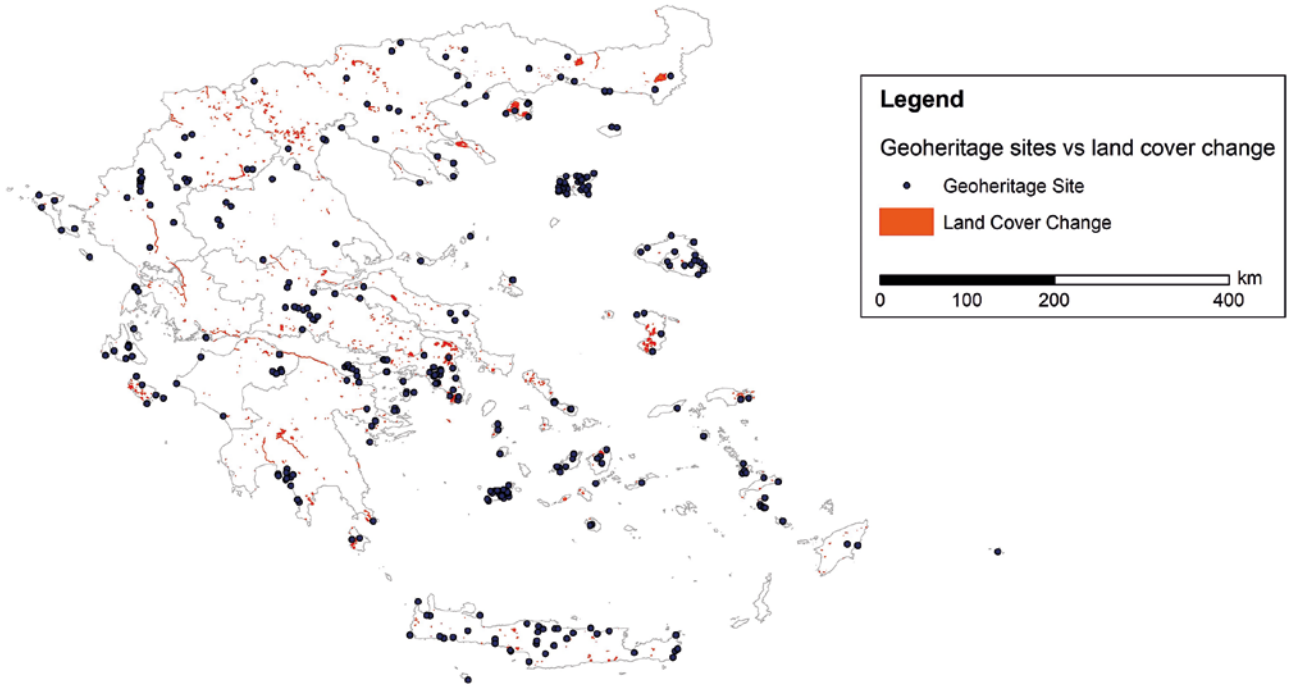

Fig. 10 Geoheritage sites vs Corine Land Cover Chance between 2012 and 2018.

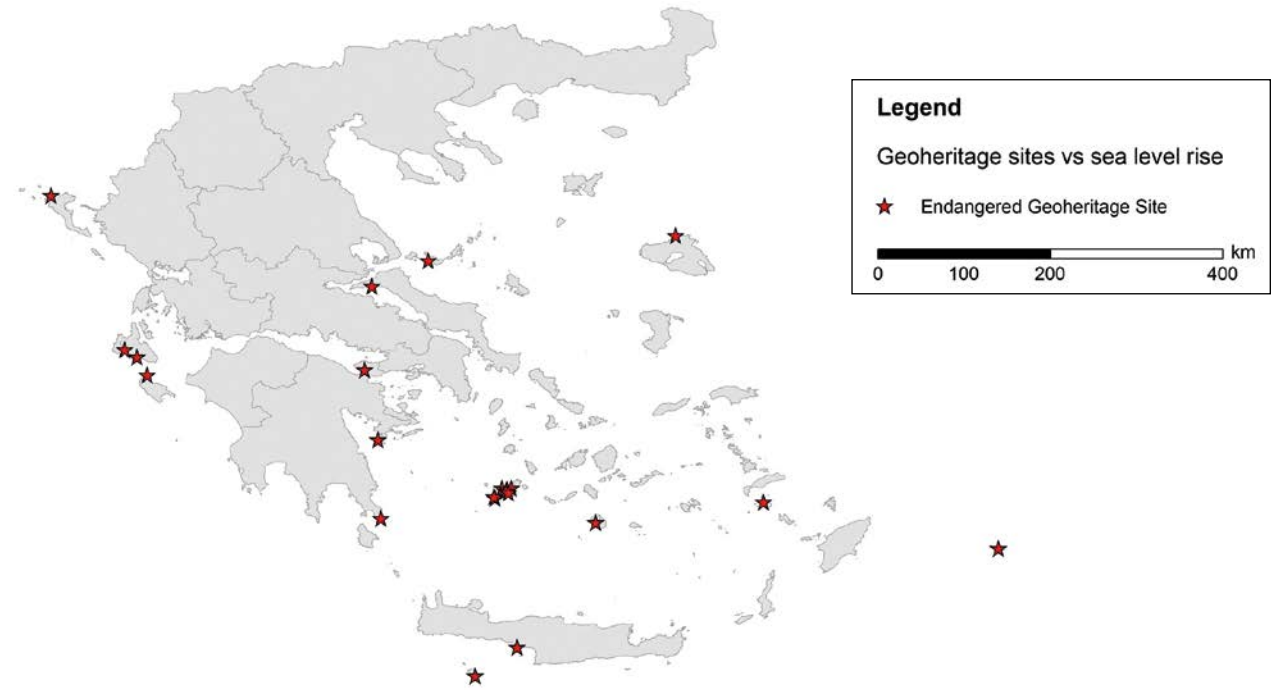

Fig. 11 Impact of 40 cm sea level rise on geoheritage sites in the next 100 years.

important is to maintain or even raise the quality standards set from the beginning (especially regarding verification and geolocation) rather than focusing on quantitative aspects.

GIS is the sine qua non for all the analyses and the fundamental connecting resource of all geospatial technologies and information for the purposes of this study. Due to the availability of all options, but also for reasons of convenience, both open source and commercial GIS were used. Nevertheless, it ought to be clarified that all the procedures presented herein, and many more, are feasible to be performed with freely available GIS software and related tools. This is considered particularly important, as it consolidates that the database if fully "open" at all stages, from its original assemblage to its operational use.

Apart from hosting the database at institutional level, it shall also be made available via National storage

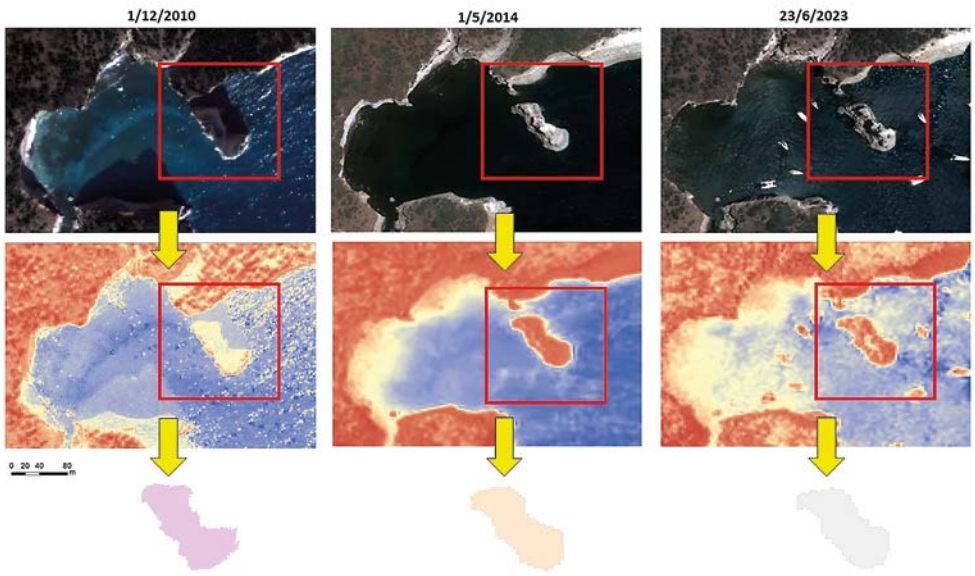

Fig. 12 Mapping and monitoring of the Kleftiko rock formation between 2010 and 2023. The set of three very high resolution images (first row) was used to extract NDWI (second row) and subsequently to isolate the relevant non-water area via K-Means supervised classification (third row).

Tab. 4 Monitoring changes of area and perimeter for the rock structure of Kleftiko on Milos Island during 2010–2023.

Date	Source	Area			Perimeter		
		Area (m^2)	Change (m^2)	Change (%)	Perimeter (m)	Change (m)	Change (%)
1 December 2010	Worldview-2	1747	–	–	341.65	–	–
1 May 2014	Pleiades	1692	−55	−3.1	237.35	−104.30	−30.5
23 June 2023	Pleiades	1643	−49	−2.9	242.00	4.65	2.0
		Total	−104	−6.0	Total	−99.70	−28.6

resources – such as the Hellenic Academic Research Data Management Initiative (HARDMIN) https://hardmin.heal-link.gr/en/about. This will ensure its viability as well as visibility at national level. The database will also be made available on ArcGIS online™, Environmental Systems Research Institute's (ESRI®) web-based mapping software for even higher visibility and possibility to combine it with a plethora of other readily available geospatial information online.

The results from the demo of geospatial analysis presented herein provide various insights into the geoheritage elements that would otherwise be very difficult or time consuming to retrieve. For example, if only absolute numbers of geological heritage sites are considered (Fig. 5), it can be deducted that there is a dividing line between a "rich" in geoheritage South and a relatively "poorer" North in the country. Conversely, the nomalization of geoheritage items by area (Fig. 6) reveals that almost all of the Greek islands and the Administrative Region of Attica have a proportionally higher number of geoheritage.

The main spatial reference unit used as a logical initial basis was that of the Administrative Regions, but more or less detailed spatial units can be used at will, like e.g. city boundaries, metropolitan areas, or any other meaningful spatial boundaries. This means that the operational scale of the database is very flexible and is only limited by the geolocation accuracy by which the geoheritage items were registered. As an indication, considering the few (3–5) meters of accuracy in this case, these correspond to a maximum cartographic scale of about 1 : 10,000 to 1 : 25,000. Regardless of spatial sub-units, when the ensemble of geoheritage entry locations is used, the density of geological heritage can be revealed in more specific areas, like particular islands or part of Attica in this case (Fig. 7).

The distribution of geoheritage by type (Fig. 8) and elevation (Fig. 9) throughout the country reveals spatial aspects of geological heritage which may be e.g. useful for touristic or educational purposes, but also of interest to the general public. For example, the concentration of specific types of mountainous geosites in Central Greece may indicate increased potential for revenues or educational field trips in the winter season, by exploiting the added value of geoheritage together with other cultural highlights in the area.

More advanced analyses incorporating external data like land cover or climate change information may produce higher level results, connecting geoheritage with a multitude of other parameters. For example, they reveal that geoheritage are indeed prone to

land cover changes (Fig. 10), whereas more details on the nature of change can be easily retrieved from the attribute table of the Corine Land Cover dataset, which indicates the exact change in each case (from one land cover class to another), therefore being able to further assess the importance of each change concerning the nearby geoheritage site. In the case of sea level rise, 22 geoheritage sites are found to be endangered within the next decades (Fig. 11), an information that would prioritize interventions by the relevant protection authorities. Other risks, degradation and changes to geoheritage sites may also be assessed, with respect to their sensitivity, fragility, natural and anthropogenic vulnerability (García-Ortiz et al. 2014; Pelfini and Bollati 2014). Indicative additional options for exploiting the database in conjunction with other geospatial information and GIS capabilities include, but are not limited to:

- The detection of deformation over geoheritage sites with satellite-based Interferometric Synthetic Aperture Radar (InSAR) products from Copernicus (EGMS n.d.) or similar services (Foumelis et al. 2022).
- Implementation of vegetation, water, snow or other indices from satellite data, for accessing/monitoring the status of geoheritage sites.
- Combination with earthquake databases, to assess the seismic risk over geoheritage sites.
- Story telling (Antoniou et al. 2023) linked with georoute creation for enhancing public awareness of geoheritage in specific places (Georoutes of Nisyros n.d.).

The importance of the database is more evident when many (e.g. hundreds) of geoheritage sites are included in the analysis. Thus, its impact generally decreases with the decreasing geographical scale of reference, i.e. it is very high at national level, medium at regional level, and smaller at local level. Nevertheless, in case of existence of many geoheritage sites (high density) at regional or local level, the impact can also be equally high for relatively small geographical areas.

In site-level examples, such as that from Kleftiko on Milos Island, the contribution of the database itself is limited to the knowledge of geolocation for the (few or single) specific geoheritage item(s) that is (are) investigated. These examples are mainly highlighting the contribution of GIS analysis, not of the database, but mainly of the external geospatial data (remotely sensed or other) that are being used.

5. Conclusions

In terms of time and effort, the investment of constructing a thematically and geospatially accurate geoheritage database at National level is rather large. Nevertheless, once this complex and to a certain extend tedious task has been completed, having the GIS database available immediately provides practically infinite, relatively effortless, possibilities of extracting very useful information, depending on the user needs.

The GIS database offers practically endless possibilities for combining its data with remotely-sensed or other geospatial information, rendering it particularly useful in the overall management of geoheritage as well as in the decision-making process.

The geolocation accuracy of geoheritage sites in the database is of outmost importance, to fully harness its potential. Therefore the registration of entries in only meaningful when it adheres to the minimum accuracy standards set for the whole dataset, otherwise the functionality of the database as an ensemble is compromised.

The results of geospatial analysis presented herein indicate the potential uses of database and are subject to change, should more entries be registered and/or higher resolution information or accuracy is available (e.g. in terms of the land cover change or elevation of each geoheritage site).

Future work on the database itself, apart from increasing the number of records, may include the delineation of certain types of geoheritage in the form of polygon (e.g. caves, quarries), for increasing the accuracy of geospatial analysis, without the necessity of using buffer zones. Also, geolocating geoheritage sites with very precise (cm level) in situ Global Navigation Satellite System (GNSS) measurements, will also add value to the detailed analysis and combination with more refined geospatial information. Crowdsourcing and volunteering is another serious consideration for enlarging the database in terms of data volume and accuracy across the country, and, although it entails some higher risks of credibility, it will be explored in the near future.

The ultimate objective or vision behind and beyond the effective management of geoheritage with geospatially-enabled information is to raise public awareness on its value and at the same time contribute significantly to the development of local societies.

Acknowledgements

The study was supported by ESA Network of Resources (NoR) Initiative, in the context of a project on "Geospatial Data and Technology for Education (Geo-4Edu)" and in particular for accessing very high resolution satellite imagery.

References

AbdelMaksoud, K. M., Al-Metwaly, W. M., Ruban, D. A., Yashalova, N. N. (2019): Sand dune migration as a factor of geoheritage loss: Evidence from the Siwa Oasis (Egypt) and implications for geoheritage management.

Proceedings of the Geologists' Association 130(5), 599–608, https://doi.org/10.1016/j.pgeola.2019.07.001.

Agapiou, A., Lysandrou, V., Alexakis, D. D., Themistocleous, K., Cuca, B., Argyriou, A., Sarris, A., Hadjimitsis, D. G. (2015): Cultural heritage management and monitoring using remote sensing data and GIS: The case study of Paphos area, Cyprus. Computers, Environment and Urban Systems 54, 230–239, https://doi.org/10.1016/j.compenvurbsys.2015.09.003.

Antoniou, V., Panousis, D., Nikoli, E., Katsigera, A., Vlasopoulos, O., Nomikou, P. (2023): The Geo-Cultural Heritage of Kos Revisited: Web-GIS Applications and Storytelling Promoting the Well-Known Island of Dodecanese, Greece. Resources 12(7), https://doi.org/10.3390/resources12070074.

Ayad, Y. M. (2005): Remote sensing and GIS in modeling visual landscape change: A case study of the northwestern arid coast of Egypt. Landscape and Urban Planning 73(4), 307–325, https://doi.org/10.1016/j.landurbplan.2004.08.002.

Ballesteros, D., Caldevilla, P., Vila, R., Barros, X. C., Rodríguez-Rodríguez, L., García-Ávila, M., Sahuquillo, E., Llorente, M., Diez, J. B., Fuertes-Fuente, M., Timón-Sánchez, S. M., de Lombera-Hermida, A., Álvarez, I., Pérez-Cáceres, I., Acebo, M., Orche Amaré, P., García, J. H., Martín-González, F., Alemparte, M. (2022): A GIS-supported Multidisciplinary Database for the Management of UNESCO Global Geoparks: The Courel Mountains Geopark (Spain). Geoheritage 14(2): 41, https://doi.org/10.1007/s12371-022-00654-3.

Bendaoud, A., Chabou, M. C., Kolli, O., Bouzidi, O., Djemaï, S., Kaabeche, H. (2015): Use of Website and GIS Databases for Enhancement of Geosites in Algeria. In E. Errami, M. Brocx, V. Semeniuk (Eds.), From Geoheritage to Geoparks: Case Studies from Africa and Beyond (pp. 145–156). Springer International Publishing, https://doi.org/10.1007/978-3-319-10708-0_10.

Bollati, I. M., Caironi, V., Gallo, A., Muccignato, E., Pelfini, M., Bagnati, T. (2023): How to integrate cultural and geological heritage? The case of the Comuniterrae project (Sesia Val Grande UNESCO Global Geopark, northern Italy). AUC Geographica 58(1), 129–145, https://doi.org/10.14712/23361980.2023.10.

Bradbury, J. (1993): A preliminary geoheritage inventory of the eastern Tasmania terrane (p. 46). Parks and Wildlife Service, Tasmania. https://nla.gov.au/nla.obj-2840460609/view.

Brilha, J. (2002): Geoconservation and protected areas. Environmental Conservation 29(3), 273–276, https://doi.org/10.1017/S0376892902000188.

Brilha, J. (2015): Geoconservation, History of. In G. Tiess, T. Majumder, and P. Cameron (Eds.), Encyclopedia of Mineral and Energy Policy (pp. 1–3). Springer Berlin Heidelberg, https://doi.org/10.1007/978-3-642-40871-7_3-1.

Brilha, J. (2016): Inventory and Quantitative Assessment of Geosites and Geodiversity Sites: A Review. Geoheritage 8(2), 119–134, https://doi.org/10.1007/s12371-014-0139-3.

Brilha, J. (2018): Chapter 4 – Geoheritage: Inventories and Evaluation. In E. Reynard and J. Brilha (Eds.), Geoheritage (pp. 69–85). Elsevier, https://doi.org/10.1016/B978-0-12-809531-7.00004-6.

Brocx, M., Semeniuk, V. (2007): Geoheritage and geoconservation – History, definition, scope and scale. Journal of the Royal Society of Western Australia.

Burlando, M., Firpo, M., Queirolo, C., Rovere, A., Vacchi, M. (2011): From Geoheritage to Sustainable Development: Strategies and Perspectives in the Beigua Geopark (Italy). Geoheritage 3(2), 63–72, https://doi.org/10.1007/s12371-010-0019-4.

Carcavilla, L., Durán, J. J., García-Cortés, Á., López-Martínez, J. (2009): Geological Heritage and Geoconservation in Spain: Past, Present, and Future. Geoheritage 1(2), 75–91, https://doi.org/10.1007/s12371-009-0006-9.

Centre, U. W. H. (n.d.): UNESCO World Heritage Centre – World Heritage List. UNESCO World Heritage Centre. Retrieved January 1, 2024, from https://whc.unesco.org/en/list/.

Copernicus Climate Change Service. (n.d.): Retrieved January 2, 2024, from https://climate.copernicus.eu/.

Copernicus Land Monitoring Service – Reference Data: EU-DEM. (2017): https://land.copernicus.eu/user-corner/publications/eu-dem-flyer/view.

CORINE Land Cover. (n.d.): Retrieved January 2, 2024, from https://land.copernicus.eu/en/products/corine-land-cover.

Coughlan, T. (2020): The use of open data as a material for learning. Educational Technology Research and Development 68(1), 383–411, https://doi.org/10.1007/s11423-019-09706-y.

Dikau, R. (1989): The application of a digital relief model to landform analysis in geomorphology. In J. Raper (Ed.): Three Dimensional Applications in Geographic Information Systems. Taylor and Francis, Chichester.

Drinia, H., Tripolitsiotou, F., Cheila, T., and Zafeiropoulos, G. (2022): The Geosites of the Sacred Rock of Acropolis (UNESCO World Heritage, Athens, Greece): Cultural and Geological Heritage Integrated. Geosciences 12(9): 9, https://doi.org/10.3390/geosciences12090330.

Elfadaly, A., Shams eldein, A., Lasaponara, R. (2020): Cultural Heritage Management Using Remote Sensing Data and GIS Techniques around the Archaeological Area of Ancient Jeddah in Jeddah City, Saudi Arabia. Sustainability 12(1): 240, https://doi.org/10.3390/su12010240.

European Ground Motion Service. (n.d.): Retrieved January 2, 2024, from https://egms.land.copernicus.eu/.

Fassoulas, C., Mouriki, D., Dimitriou-Nikolakis, P., Iliopoulos, G. (2012): Quantitative Assessment of Geotopes as an Effective Tool for Geoheritage Management. Geoheritage 4(3), 177–193, https://doi.org/10.1007/s12371-011-0046-9.

Fassoulas, C., Nikolakakis, E., Staridas, S. (2022): Digital Tools to Serve Geotourism and Sustainable Development at Psiloritis UNESCO Global Geopark in COVID Times and Beyond. Geosciences 12(2): 78, https://doi.org/10.3390/geosciences12020078.

Foumelis, M., Delgado Blasco, J. M., Brito, F., Pacini, F., Papageorgiou, E., Pishehvar, P., Bally, P. (2022): SNAPPING Services on the Geohazards Exploitation Platform for Copernicus Sentinel-1 Surface Motion Mapping. Remote Sensing 14(23): 6075, https://doi.org/10.3390/rs14236075.

García-Ortiz, E., Fuertes-Gutiérrez, I., Fernández-Martínez, E. (2014): Concepts and terminology for the risk of

degradation of geological heritage sites: Fragility and natural vulnerability, a case study. Proceedings of the Geologists' Association 125(4), 463–479, https://doi.org/10.1016/j.pgeola.2014.06.003.

Georoutes of Nisyros. (n.d.): Retrieved January 3, 2024, from https://gaia.igme.gr/portal/apps/webappviewer/index.html?id=ae496200ef81413b93f01b59fb111383.

Gonggrijp, G. (1999): Geodiversity: The key to a holistic approach in renaturation. In Towards the balanced Management and conservation of the geological heritage in the new millennium (pp. 77–80). Sociedad Geologica de Espana.

Goodchild, M. F. (2022): Commentary: General principles and analytical frameworks in geography and GIScience. Annals of GIS 28(1), 85–87, https://doi.org/10.1080/19475683.2022.2030943.

Hadjimitsis, D., Agapiou, A., Alexakis, D., Sarris, A. (2013): Exploring natural and anthropogenic risk for cultural heritage in Cyprus using remote sensing and GIS. International Journal of Digital Earth 6(2), 115–142, https://doi.org/10.1080/17538947.2011.602119.

Herrera-Franco, G., Carrión-Mero, P., Montalván-Burbano, N., Caicedo-Potosí, J., Berrezueta, E. (2022): Geoheritage and Geosites: A Bibliometric Analysis and Literature Review. Geosciences 12(4): 4, https://doi.org/10.3390/geosciences12040169.

Liu, X., Chen, M., Claramunt, C., Batty, M., Kwan, M.-P., Senousi, A. M., Cheng, T., Strobl, J., Cöltekin, A., Wilson, J., Bandrova, T., Konecny, M., Torrens, P. M., Zhang, F., He, L., Wang, J., Ratti, C., Kolditz, O., Klippel, A., Li, S., Lin, H., Lü, G. (2022): Geographic information science in the era of geospatial big data: A cyberspace perspective. The Innovation 3(5): 100279, https://doi.org/10.1016/j.xinn.2022.100279.

Marsico, A., Infante, M., Iurilli, V., Capolongo, D. (2015): Terrestrial Laser Scanning for 3D Cave Reconstruction: Support for Geomorphological Analyses and Geoheritage Enjoyment and Use. In B. Andreo, F. Carrasco, J. J. Durán, P. Jiménez, J. W. LaMoreaux (Eds.), Hydrogeological and Environmental Investigations in Karst Systems (pp. 543–550). Springer Berlin Heidelberg, https://doi.org/10.1007/978-3-642-17435-3_61.

Martin, S., Reynard, E., Pellitero Ondicol, R., Ghiraldi, L. (2014): Multi-scale Web Mapping for Geoheritage Visualisation and Promotion. Geoheritage 6(2), 141–148, https://doi.org/10.1007/s12371-014-0102-3.

McFeeters, S. K. (1996): The use of the Normalized Difference Water Index (NDWI) in the delineation of open water features. International Journal of Remote Sensing 17(7), 1425–1432, https://doi.org/10.1080/01431169608948714.

Mouratidis, A., Koutsoukos, M. (2016): Use of ESA Earth observation educational resources in vocational education and training – Lifelong learning: Towards STEM promotion and development of skills. Bulletin of the Geological Society of Greece L(3), 1652–1661, https://doi.org/10.12681/bgsg.11888.

Németh, K. (2022): Geoheritage and geodiversity aspects of catastrophic volcanic eruptions: Lessons from the 15th of January 2022 Hunga Tonga – Hunga Ha'apai eruption, SW Pacific. Special Issue on Geodiversity 10(4), 546–568, https://doi.org/10.1016/j.ijgeop.2022.08.003.

Osborne, R. (2000): Geodiversity: "Green" geology in action-Presidential address for 1999–2000. Proceedings of the Linnaean Society of New South Wales, 122, 149–173, https://biostor.org/reference/68401.

Papadopoulou, E. E., Papakonstantinou, A., Vasilakos, C., Zouros, N., Tataris, G., Proestakis, S., Soulakellis, N. (2022): Scale issues for geoheritage 3D mapping: The case of Lesvos Geopark, Greece. International Journal of Geoheritage and Parks 10(3), 435–446, https://doi.org/10.1016/j.ijgeop.2022.08.006.

Papanikolaou, D. I. (2021): The Geology of Greece. Springer International Publishing, https://doi.org/10.1007/978-3-030-60731-9

Pasquaré Mariotto, F., Corti, N., Drymoni, K. (2023): Advanced Technologies for Geosite Visualization and Valorization: A Review. Applied Sciences 13(9): 5598, https://doi.org/10.3390/app13095598.

Pelfini, M., Bollati, I. (2014): Landforms And Geomorphosites Ongoing Changes: Concepts And Implications For Geoheritage Promotion. Quaestiones Geographicae 33(1), 131–143, https://doi.org/10.2478/quageo-2014-0009

Perotti, L., Bollati, I. M., Viani, C., Zanoletti, E., Caironi, V., Pelfini, M., Giardino, M. (2020): Fieldtrips and Virtual Tours as Geotourism Resources: Examples from the Sesia Val Grande UNESCO Global Geopark (NW Italy). Resources 9(6): 63, https://doi.org/10.3390/resources9060063.

Pijet-Migoń, E., Migoń, P. (2022): Geoheritage and Cultural Heritageandmdash;A Review of Recurrent and Interlinked Themes. Geosciences, 12(2): 98, https://doi.org/10.3390/geosciences12020098.

Ravanel, L., Bodin, X., Deline, P. (2014): Using Terrestrial Laser Scanning for the Recognition and Promotion of High-Alpine Geomorphosites. Geoheritage 6(2), 129–140, https://doi.org/10.1007/s12371-014-0104-1.

Santos, I., Henriques, R., Mariano, G., Pereira, D. I. (2018): Methodologies to Represent and Promote the Geoheritage Using Unmanned Aerial Vehicles, Multimedia Technologies, and Augmented Reality. Geoheritage 10(2), 143–155, https://doi.org/10.1007/s12371-018-0305-0.

Semeniuk, V. (1997): The linkage between biodiversity and geodiversity. In Pattern and Processes: Towards a Regional Approach to National Estate assessment of geodiversity (pp. 51–58). Environment Australia.

Singh, B. V. R., Sen, A., Verma, L. M., Mishra, R., Kumar, V. (2021): Assessment of potential and limitation of Jhamarkotra area: A perspective of geoheritage, geo park and geotourism. Exploration of Geoheritage, Geoparks and Geotourism 9(2), 157–171, https://doi.org/10.1016/j.ijgeop.2021.04.001.

Spyrou, E., Triantaphyllou, M. V., Tsourou, T., Vassilakis, E., Asimakopoulos, C., Konsolaki, A., Markakis, D., Marketou-Galari, D., Skentos, A. (2022): Assessment of Geological Heritage Sites and Their Significance for Geotouristic Exploitation: The Case of Lefkas, Meganisi, Kefalonia and Ithaki Islands, Ionian Sea, Greece. Geosciences 12(2): 55, https://doi.org/10.3390/geosciences12020055.

Stewart, C. (2017): Detection of Archaeological Residues in Vegetated Areas Using Satellite Synthetic Aperture Radar. Remote Sensing 9(2): 118, https://doi.org/10.3390/rs9020118.

Suma, A., Cosmo, P. (2011): Geodiv Interface: An Open Source Tool for Management and Promotion of the Geodiversity of Sierra De Grazalema Natural Park (Andalusia, Spain). GeoJournal of Tourism and Geosites 8(2), 309–318.

Theodosiou, I. (2010): Designation of Geosites – Proposals for Geoparks in Greece. Bulletin of the Geological Society of Greece 43(2), 926–938, https://doi.org/10.12681/bgsg.11258.

Thomas, M. F. (2016): New keywords in the geosciences – some conceptual and scientific issues. Revista do Instituto Geológico (Descontinuada) 37(1): 1, https://doi.org/10.5935/0100-929X.20160001.

UNESCO Global Geoparks | UNESCO. (n.d.): Retrieved January 1, 2024, from https://www.unesco.org/en/iggp/geoparks/about.

Wilson, A. (2021): The use of remote sensing and digital tools for cultural heritage management and archaeological research. Levant 53(3), 384–388, https://doi.org/10.1080/00758914.2022.2051901.

Zafeiropoulos, G., Drinia, H., Antonarakou, A., Zouros, N. (2021): From Geoheritage to Geoeducation, Geoethics and Geotourism: A Critical Evaluation of the Greek Region. Geosciences 11(9): 381, https://doi.org/10.3390/geosciences11090381.

Zagorchev, I., Nakov, R. (1998): Geological Heritage of Europe. Geologica Balcanica, 28, 3–4.

Zouros, N. (2004): The European Geoparks Network–Geological heritage protection and local development. International Union of Geological Sciences 27(3), 165–171, https://doi.org/10.18814/epiiugs/2004/v27i3/002.

Zouros, N. (2005): Assessment, protection, and promotion of geomorphological and geological sites in the Aegean area, Greece. OpenEdition Journals 11(3), 227–234, https://doi.org/10.4000/geomorphologie.398.

Zouros, N., Valiakos, I. (2010): Geoparks Management And Assessment. Bulletin of the Geological Society of Greece 43(2), 965–977, https://doi.org/10.12681/bgsg.11262.

Hazards profile of the Shigar Valley, Central Karakoram, Pakistan: Multicriteria hazard susceptibility assessment

Munazza Afreen[1], Fazlul Haq[2,*], Bryan G. Mark[2]

[1] Government College University Faisalabad, Department of Geography, Pakistan
[2] Ohio State University, Byrd Polar and Climate Research Center, USA
* Corresponding author: haq.47@osu.edu

ABSTRACT

The rapid deglaciation in the Upper Indus Basin (UIB) significantly impacts local landscapes, watersheds, and basin-wide hydrology. While creating new opportunities, such as emerging landscapes and hydrological changes, deglaciation simultaneously heightens the risk of glacio-hydrological hazards in adjacent and downstream regions. With limited available land for agriculture and settlements, communities around glaciers expand human activities toward newly formed floodplains and deglaciating valleys, necessitating a comprehensive understanding of associated risks and vulnerabilities. This study employs Geographical Information System (GIS) and Remote Sensing products for a multicriteria hazards susceptibility assessment in the Shigar Valley, located in the downstream of major Himalayan glaciers – the Baltoro (63 km) and Biafo (67 km) glaciers. The research reveals that 28.3% of the valley is highly susceptible to multiple hazards, emphasizing the urgency of informed decision-making in the region. Only 0.03% area lies in the very low susceptible category, 9.7% in the low susceptible, 60.6% in the moderately susceptible, and 1.04% in the very highly susceptible categories. These findings highlight the need for proactive measures, adaptive strategies, and sustainable development in the Shigar Valley to mitigate the escalating risks posed by deglaciation and changing hydrological patterns.

KEYWORDS

glacial hazards; landslides; snow avalanches; floods; multi-hazards; hazard susceptibility

Received: 23 January 2024
Accepted: 6 May 2024
Published online: 22 May 2024

Afreen, M., Haq, F., Mark, B. G. (2024): Hazards profile of the Shigar Valley, Central Karakoram, Pakistan: Multicriteria hazard susceptibility assessment. AUC Geographica 59(1), 77–92
https://doi.org/10.14712/23361980.2024.5

1. Introduction

The Hindukush-Karakoram-Himalayan (HKH) region, one of the most geologically active and environmentally sensitive areas on our planet, has consistently been the focus of various scientific investigations, primarily due to its inherent geological complexity, climatic variability, and susceptibility to natural hazards (Richardson and Reynolds 2000; Wang et al. 2021; Chowdhury et al. 2021; Kropáček et al. 2021). Cryo-hydro-climatic dynamics in the Upper Indus Basin (UIB), have been producing severe consequences in the proximal areas as well as in the Lower Indus Basin throughout history in the form of water shortages and catastrophic flooding (Lutz et al. 2016; Ishaque et al. 2022; Yao and Khan 2022). Following the history's most devastating flooding in 2010 (Khattak et al. 2012), the recent floods of 2022 resulted into the displacement of millions of people when almost two third of the country was under water (Saifi et al. 2022). With only a gap of 2 years, several areas in the HKH region were recently hit by severe flash floods in April 2024, causing widespread damages especially to standing crops, agricultural land, and other property. Besides such large-scale catastrophic flooding, the local communities have been suffering the impacts of these changes in the form of glacial lake outburst floods (GLOFs), water stress associated with fluctuating and uncertain snowmelt, landslides, and river blockages etc. (Iqbal et al. 2014; Gao et al. 2021).

The Shigar Valley in Pakistan is one of the most dynamic areas in the HKH exposed to a complex set of hazards, challenging its inhabitants and the environment. This valley is not only home for the local population but also a region of great cultural, economic, and ecological significance. Yet, it is distressed by multiple natural hazards, including landslides, glacial lake outburst floods (GLOFs), earthquakes, and avalanches, which pose a constant threat to the lives of the local and downstream populations, as well as to the infrastructure, and sustainability of the valley (Sangha et al. 2019; Kumar et al. 2018; Kumari et al. 2016). Located in the Karakoram Range, this valley is a region characterized by diverse topographic, climatic, and geological conditions. Its location near the converging boundaries of the Indian and Eurasian tectonic plates makes it particularly susceptible to seismic events (Mondal et al. 2021). Moreover, the presence of numerous glaciers in the region increases the risk of GLOFs, a hazard that has claimed lives and caused significant damage in the past (Bajracharya et al. 2015; Shrestha et al. 2019). Landslides, often triggered by a combination of factors including precipitation, thawing of permafrost, and seismic activity, further compound the vulnerability of the area being (Adhikari et al. 2019; Bajracharya et al. 2020). In addition, avalanches represent a constant threat to transportation routes and residential areas, especially during the winter months (Bhutiyani et al. 2008).

Understanding and mitigating these hazards are critical for the resilience and long-term survival of the communities residing in the Shigar Valley and the downstream communities. As climate change accelerates, the frequency and magnitude of these hazards are likely to increase, making it imperative to adopt advanced methodologies for assessing vulnerability and risk in this region (Clark-Ginsberg et al. 2021; Jaiswal et al. 2010). This study seeks to address this pressing need by employing advanced Multi-criteria Hazard Assessment (MHA) methods, leveraging the power of Geographic Information Systems (GIS) and Remote Sensing (RS) technologies to provide a comprehensive understanding of the vulnerability of the Shigar Valley to a range of natural hazards.

The existing literature on hazard assessment in the Shigar Valley provides valuable insights but lacks the comprehensive, integrated approach required to address this multifaceted challenge. Past studies have often focused on individual hazards in isolation or have relied on limited data sources and traditional vulnerability assessment methods, which may not capture the complex interplay of factors affecting the region's vulnerability to multiple hazards (Mokarram et al. 2021; Yang et al. 2021). Furthermore, the landscape is continuously evolving, both due to natural processes and human activities, making it essential to have up-to-date, accurate, and dynamic information for effective hazard assessment and risk management (Kaur et al. 2019).

The utility of GIS-based susceptibility maps cascades into illuminating the geographical distribution of multi-hazard risks for the perusal of decision-makers and stakeholders. The techniques range from overlay analysis and weighted overlays to the efficacy of machine learning algorithms (Chen et al. 2018; Li et al. 2020). These utilities manifest their worth in guiding the scale of land-use planning, infrastructure development, disaster management and response, and targeted mitigation measures (Wenwu Chen and Zhang 2021; Piao et al. 2022; Ha-Mim et al. 2022; Kornejady et al. 2019). Multi-hazard analyses entail the integration of various factors and methodologies to assess the susceptibility of an area to multiple hazards simultaneously. These analyses employ advanced techniques such as Geographic Information Systems (GIS) and Remote Sensing (RS) to incorporate diverse parameters such as topography, geology, climate, land use, and infrastructure into the assessment process (van Westen 2000; Abella et al. 2008; Olaya Calderon et al. 2024). By considering multiple hazards in conjunction, these analyses provide a more comprehensive understanding of the overall risk landscape, allowing for better-informed decision-making and proactive risk reduction strategies (Jaiswal et al. 2010; Kaur et al. 2019). Furthermore, multi-hazard analyses enable the identification of synergies and interactions between different hazards, which may exacerbate overall risk levels (Ward

et al. 2020; Pham et al. 2021). This holistic approach is particularly crucial in regions like the Shigar Valley, where various hazards coexist and intersect, necessitating a nuanced understanding of their combined impacts on local communities and ecosystems. By conducting multi-hazard analyses, researchers and stakeholders can effectively prioritize resources, implement targeted interventions, and enhance the resilience of vulnerable areas to a wide range of natural hazards. However, it is important to recognize that GIS-based multi-hazard assessments encounter several challenges, including issues of data heterogeneity, uncertainty, and the compelling need for the evolution of advanced modeling methodologies (Ujjwal et al. 2019; Ward et al. 2020; Pham et al. 2021).

The purpose of this study is to utilize advanced multi-criteria decision analysis methods, integrating Geographic Information Systems (GIS) and Remote Sensing (RS) products, to assess the vulnerability of the Shigar Valley, Himalayas, Pakistan, to a spectrum of natural hazards. This research aims to perform a comprehensive analysis of various natural hazards in the Shigar Valley by incorporating multi-criteria, including topography, geology, climate, land use, and infrastructure, in the vulnerability assessment process, enabling a holistic understanding of the region's susceptibility to hazards. The methodology for multi-criteria hazard susceptibility assessment in the Shigar Valley integrates geographical considerations and the unique conditions of the Shigar Valley. The criteria for hazard mapping are formulated with a specific focus on the valley's characteristics, recognizing its importance in the execution of Multi-Criteria Decision Analysis (MCDA). The assessment criteria are established through a comprehensive review of relevant literature and consultations with experts. The literature review aims to gather information applicable to GIS-based MCDA, drawing from primary sources obtained through reputable research databases (Belay et al. 2022). Different MCDA methodologies, including Analytic Hierarchy Process (AHP), Analytic Network Process (ANP), Technique for Order of Preference by Similarity to Ideal Solution (TOPSIS), and Weighted Sum Model (WSM), are explored for assessing multi-hazard susceptibility.

This analysis will establish risk zones within the Shigar Valley, which can serve as a foundation for informed decision-making and the development of hazard-specific risk reduction strategies. By achieving these objectives, this study aims to offer a comprehensive and up-to-date understanding of the vulnerabilities that the Shigar Valley faces, enabling local authorities, policymakers, and stakeholders to enhance proactive measures for disaster risk reduction and sustainable development.

2. Study area

The Shigar Valley is located in the central part of the Karakoram Range stretching from 35°29′14″ N to 35°23′54″ N latitude and 75°41′56″ E to and

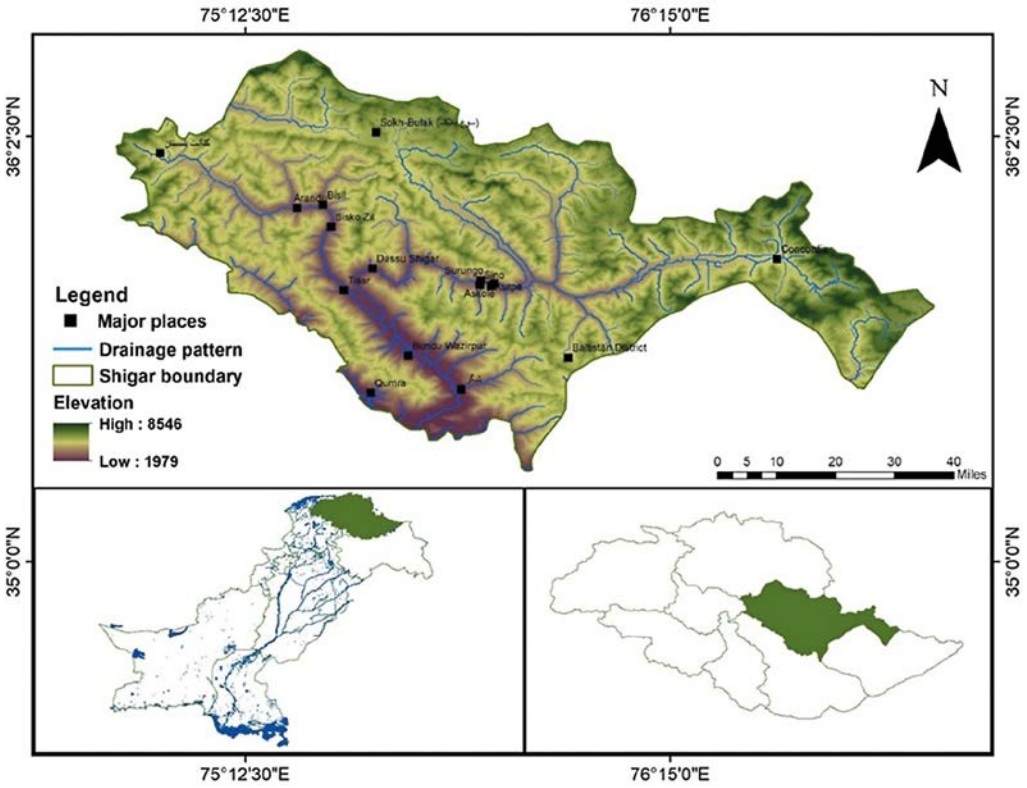

Fig. 1 (a) Location map of the study area. Elevation was calculated in ArcGIS using SRTM data, while the boundary layers were obtained from DivaGIS.com.

75°44′57″ E longitude (Fig. 1a). The Shigar Valley shares a border with China and is characterized by high peaks such as K-2 (8611 meters), Broad Peak (8047 meters), Angel Peak (6858 meters), and Skil Brum (7360 meters) with a population of 75 thousand according to the census of 2017 (Abbas et al. 2017). The valley consists of several small villages situated on alluvial fans, terraces, and gentle slopes along the river and its tributaries at altitudes ranging from 2300 m (Marapi) to 3050 m (Askole) (Schmidt 2008). It is one of the best tourism destinations in the northern areas of Pakistan (Khan et al. 2023).

The Shigar River drains the valley and is supplemented by numerous smaller tributaries flowing from the surrounding mountains, primarily sourced from glaciers. This river takes its origin from the Hispar glacier situated at the base of the Haramosh and Kanjut Sar peaks in the Shigar valley. A vital tributary of the Shigar River originates from the Baltoro Glacier near Masherbrum Peak, flowing westward to join the main channel. This river drains the meltwaters of the significant Baltoro and Biafo glaciers in the Karakoram Range. The catchment area is shaped by glaciers, with a deep upper valley that widens near the mouth. A small river island forms at the junction of the main river and the Baltoro Glacier tributary. The high-altitude, low-rainfall catchment area is sparsely vegetated, and human habitation is limited. The valley is characterized by moraines and glacial deposits resulting from the presence of these glaciers (Seong et al. 2009). Additionally, the Shigar Valley hosts several glacial lakes, often formed by the meltwater originating from the surrounding glaciers (Ali et al. 2023).

Shigar Valley's physiography is distinguished by its numerous landforms (Fig. 1b), which include valleys, mountains, glaciers, and river systems (Ali et al. 2023; Fatima et al. 2022). This area was selected for this study because of geophysical settings making it susceptible to a variety of natural hazards and the fact that it is home to a considerable population. Geologically, the area spans the northern end of the Kohistan-Ladakh Island Arc (KLIA) and the southern edge of the Asian plate. The Main Karakoram Thrust (MKT), situated at the northern suture and passing through the Shigar Valley, acts as a dividing line between the meta-sediments of the Asian plate and the volcano-clastic rocks of the KLIA. Seismic activity not only makes it susceptible to earthquakes but also induced landslides and historically the area has been hit by severe landslide t (Calligaris et al. 2017). Furthermore, the area is highly susceptible to snow avalanches and glacial hazards. Several disastrous events can be noted from history such as the debris flow on Jul 27, 2000, which destroyed 124 houses, and a gigantic glacial flow on Apr 7, 2012 that took the lives of 139 people along with infrastructure and livestock damages (Gilany and Iqbal 2017).

Fig. 1 (b) Pictures captured by the first author during a recent visit to the study area in November 2023. The left image depicts Arando Village in the Shigar Valley, an area prone to recurrent flash floods in recent years. These floods have caused substantial damage, including sedimentation on agricultural land and accelerated erosion. The right image showcases a newly discovered granite complex near Bisil, Shigar, presenting potential economic prospects. However, this area is also susceptible to landslides and avalanches.

2. Methodology

This study recognizes the importance of selecting factors influencing susceptibility to various hazards, including elevation, slope, flow accumulation, rainfall, distance from river, topographic wetness index, land use, lithology, normalized difference vegetation index (NDVI), curvature, distance from fault, stream power index, aspect, distance from road, and drainage density.

2.1 Data collection and preprocessing

Different sources and methods were used to extract and process the data for different factors considered for the multicriteria analysis. Several factors related to the characteristics of physical landscape (Tab. 1) were extracted from digital elevation model (DEM). These factors include elevation, slope, curvature, slope aspect, stream power index, flow accumulation, and drainage density. Curvature is classified into three classes: concave slope (negative value), flat plane (value −0.1 to 1.0), and convex slope (value greater than 0.1) (Gizaw et al. 2023). The stream power index calculates the erosive force of water in rivers or streams which was also extracted from the DEM (Okoli et al. 2023; Olii et al. 2023). Likewise, flow accumulation was extracted from DEM. The topographic wetness index (TWI) quantifies terrain moisture availability. TWI was obtained from DEM (Moharir et al. 2023) using ArcGIS and divided into 5 groups. Drainage density was also extracted from DEM with 250 m intervals (Ozegin et al. 2023; Upwanshi et al. 2023).

Tab. 1 Description of spatial data for different parameters.

Parameter	Source	Description
Elevation	ALOS-PALSAR DEM	12.5 m^2 resolution DEM image
Slope	ALOS-PALSAR DEM	12.5 m^2 resolution DEM image
Distance to fault	ALOS-PALSAR DEM	12.5 m^2 resolution DEM image
Aspect	ALOS-PALSAR DEM	12.5 m^2 resolution DEM image
Flow accumulation	ALOS-PALSAR DEM	12.5 m^2 resolution DEM image
Distance to river	ALOS-PALSAR DEM	12.5 m^2 resolution DEM image
Drainage density	ALOS-PALSAR DEM	12.5 m^2 resolution DEM image
Curvature	ALOS-PALSAR DEM	12.5 m^2 resolution DEM image
LULC	Sentinel-2 image	10 m^2 resolution from USGS
NDVI	Sentinel-2 image	10 m^2 resolution from USGS
Soil type	FAO	Soil shape files
Geology	Geological map	1 : 50,000 from GSP
Lithology	Geological map	1 : 50,000 from GSP
Topographic wetness index	ALOS-PALSAR DEM	12.5 m^2 resolution DEM image
Distance to road	Topgraphical map	1 : 50,000 from GSP
Rainfall	Metrological department	30-years data from PDM

Data for rainfall was collected for local meteorological stations from the Pakistan Meteorological Department (PMD) Lahore head office (Tab. 1). Rainfall was mapped using the Inverse Distance Weightage (IDW) method in ArcGIS (Al-Taani et al. 2023; Li et al. 2023) and classified into three classes. Proximity to rivers provides valuable insights into flood risk (Majeed et al. 2023; Shekar and Mathew 2023). In this study, five classes, with intervals of 250 m extracted from DEM, were generated in ArcGIS (Fig. 2).

Land use and land cover (LULC) and NDVI data were acquired using Sentinel-2 satellite imagery and supervised image classification, six classes – glaciers, water bodies, agricultural land, vegetation cover, and built-up areas – were identified (Belazreg et al. 2023; Bandyopadhyay et al. 2023; Meshram et al. 2023). Lithology layer ws created using the geological survey data in ArcGIS (Farhat et al. 2023; Mushtaq et al. 2023), while soil type layer was generated from the Food and Agriculture Organization (FAO) shape files.

Another crucial geological characteristic in multicriteria hazard assessment, distance from fault, is measured in intervals of 200 meters using the geological survey of Pakistan data, with five classes generated in ArcGIS (Faryabi 2023; Ke et al. 2023; Kumar et al. 2023). Additionally, distance from road was extracted from 1 : 50,000 topographic map.

2.2 Analytical Hierarchy Process (AHP) method

Susceptibility maps based on AHP provide a quantitative representation of areas vulnerable to various threats (Hu et al. 2018). It involves pairwise comparisons of criteria and sub-criteria to determine their relative relevance. A preference scale, inspired by Saaty (2008) and Kursunoglu et al. (2021), is employed to assign weightings reflecting the perceived importance of each factor. The AHP-based susceptibility evaluation relies on the collection and preparation of spatial data, organized within the hierarchical structure of the AHP framework (Bui et al. 2019; Javidan et al. 2021). Pairwise comparison matrices and weightings are utilized to assign priority scores to locations based on their susceptibility to threats. Higher scores indicate greater vulnerability, aiding decision-making by highlighting areas requiring targeted risk reduction actions (Cheng et al. 2020; Lee and Seo 2016; Youssef and Pourghasemi 2021).

The consistency ratio in AHP is a critical metric assessing the dependability of decision-makers' judgments during pairwise comparisons of criteria and alternatives (Scapozza and Bartelt 2003). It is calculated as the Consistency Index (CI) divided by the Random Index (RI) (Scapozza et al. 2019).

The CI measures the degree of consistency in the pairwise comparison assessment. It is determined by comparing the largest eigenvalue (λ_max) of the matrix to its order (n), expressed as:

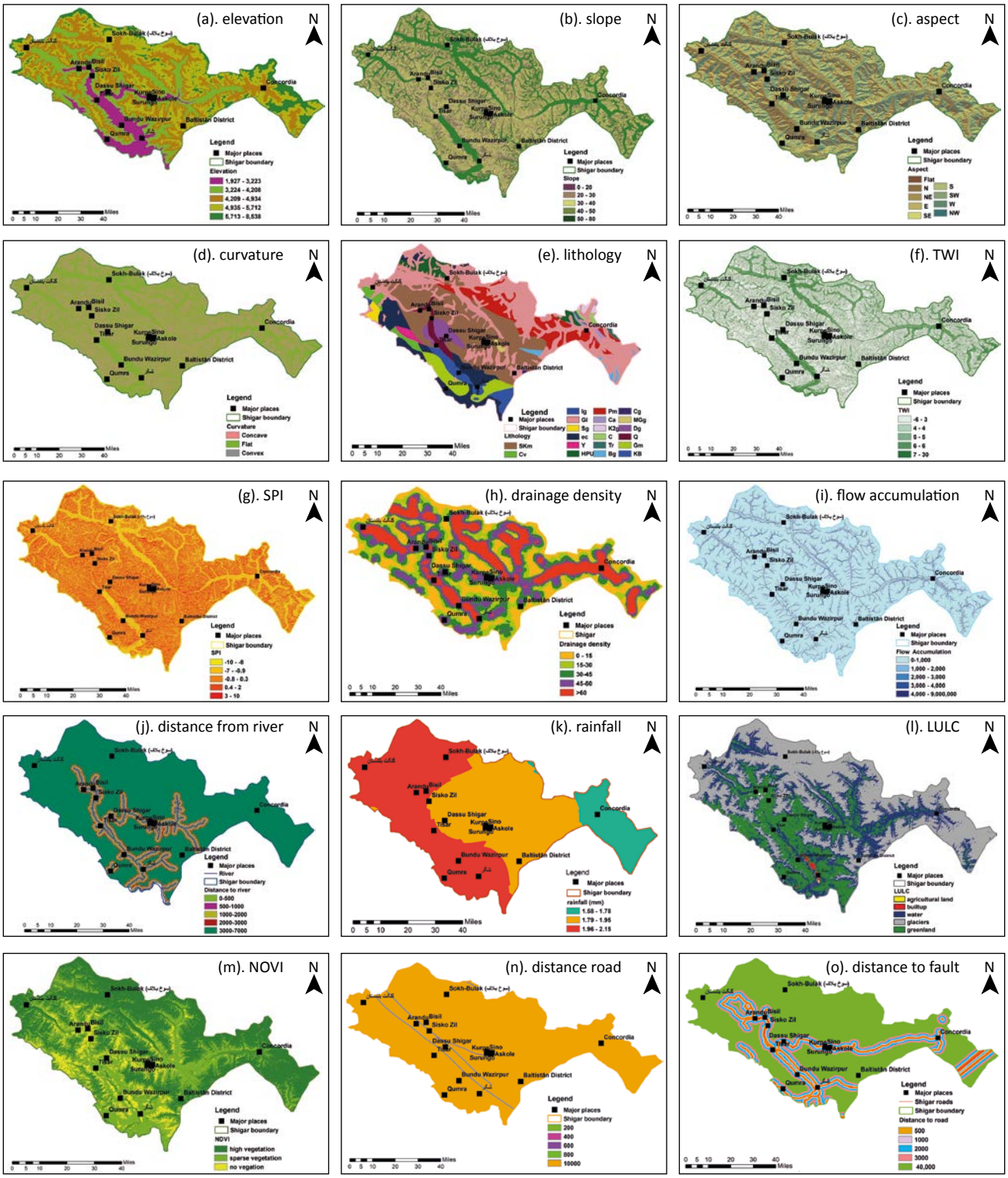

Fig. 2 Layers for multicriteria hazards susceptibility assessment. Detail methods and sources of data have been discussed in the methodology description.

$$\text{Consistency ratio} = \frac{\text{Consistency Index (CI)}}{\text{Random Index (RI)}}$$

The Random Index (RI) serves as a reference value to estimate the consistency level of randomly generated matrices, ensuring the reliability of decision-making judgments. If the calculated CR is close to or less than 0.10, the judgments are considered reasonably consistent and acceptable. However, if the CR exceeds 0.10, it suggests inconsistencies in the pairwise comparisons, requiring further scrutiny or revisions.

The CR is computed to ensure consistent judgments, defining the ratio. If the calculated CR is less than or near 0.10, judgments are deemed reasonably

Tab. 2 Conversion of language preferences into numerical scores.

Scale value	Importance of scale	Example in detail
1	Equally important	Both variables are equally significant
3	Moderately important	One variable is slightly significant
5	Strongly important	One variable is strongly significant
7	Very strongly important	One variable is dominantly significant
9	Absolutely important	One variable is entirely significant
2,4,6,8	Intermediate	Intermediate value

Tab. 3 Random index values to calculate consistency ratio.

N	1	2	3	4	5	6	7	8	9	10	9	10
RI	0	0	0.58	0.90	1.12	1.24	1.32	1.41	1.45	1.49	1.45	1.49

consistent and acceptable. A CR exceeding 0.10 indicates inconsistencies, necessitating further inspection or revisions.

Decision-makers use a scale created by Saaty, ranging from 1 to 9. These scale values are logarithmically separated to maintain qualitative comparisons. Tab. 2 illustrates the numerical scale used to convert language preferences into numerical score values (Rehman et al. 2022).

Tab. 3 presents random index values used to calculate the consistency ratio. The CI, expressing the degree of consistency in pairwise comparisons, is determined by comparing λ_max to its order (n). The Random Index (RI) is a reference value assessing the consistency level of randomly generated matrices.

2.3 Multi-hazards weight assignment

Weights assigning is a crucial step in developing the multi-hazards index map to reflect the varying degrees of risk in the research area with high degree of accuracy. In this study, we employed a weighted overlay in ArcGIS, to ensure integration of multiple hazard factors. Given the region's varying susceptibility to different hazards, each hazard category was carefully considered. This integrated approach ensures that the contribution of each hazard factor is adequately considered in the multi-hazards index map. The following weights were assigned to different hazards based on experts' observations drawing from different literature sources (Park et al. 2018; Rehman et al. 2022).

Flood Weight (40%)

The study area, situated in a high-risk zone, experiences frequent flooding events and therefore it was assigned the highest weight (40%) to conduct a final multi-hazards susceptibility map.

Landslide Weight (30%)

A weight of 30% was assigned to landslides due to the region's topographical characteristics aligning with the observed vulnerability of the area to slope failures and associated risks.

Earth Snow Avalanches Weight (25%)

Considering the substantial risk of snow avalanches, particularly at higher steep slopes, a weight of 25% was assigned acknowledging the threats associated with this landscape.

Earthquake Weight (5%)

While earthquakes contribute to the overall hazard profile, the weight assigned to this factor was set at 5%. This decision reflects the seismic activity in the region but acknowledges that other hazards pose comparatively greater risks.

Using weighted overlay analysis, the individual hazard indices were integrated to generate an overall susceptibility index map, depicting the varying degrees of susceptibility across different areas (Rahman et al. 2022). The resulting polygons were then converted into a projected coordinate system to facilitate the calculation of areas corresponding to different susceptibility categories using the field calculator tool in ArcGIS.

3. Result and discussion

Flood hazards, exacerbated by glacial-fed drainage and the formation of glacial lakes in the upper catchment of the Shigar River and its tributaries, pose a significant threat in the study area, making it susceptible to Glacial Lake Outburst Floods (GLOFs) (Campbell 2004; Batool et al. 2016). To comprehensively assess flood susceptibility, detailed mapping was conducted, integrating multiple factors (Afreen et al. 2022) such as elevation, slope, flow accumulation, rainfall, distance to river, drainage density, topographic wetness index, land use, soil type, lithology, NDVI, and curvature.

The resultant flood susceptibility index map provides insights into the vulnerability of the study area, particularly concerning the very high and high categories (Fig. 3a). Notably, the downstream region in the densely populated lowland exhibits a pronounced susceptibility to floods. Conversely, areas characterized by very low flood susceptibility are limited and predominantly situated in high steep slopes. A significant portion of the landscape falls within the moderately to low susceptible categories.

Statistically, the analysis reveals that a total of 59.3 km^2, constituting 1.04% of the total area, falls under the very highly susceptible category in terms of flood hazards. The heightened flood risk in this region is compounded by its dense population and its role as the primary cultivation zone in the valley. Similarly, 1604.9 km^2 or 28.3% of the area is classified as highly susceptible (Tab. 4), primarily concentrated in the floodplains of the main Shigar River and its major tributaries. These zones, observed through inventory

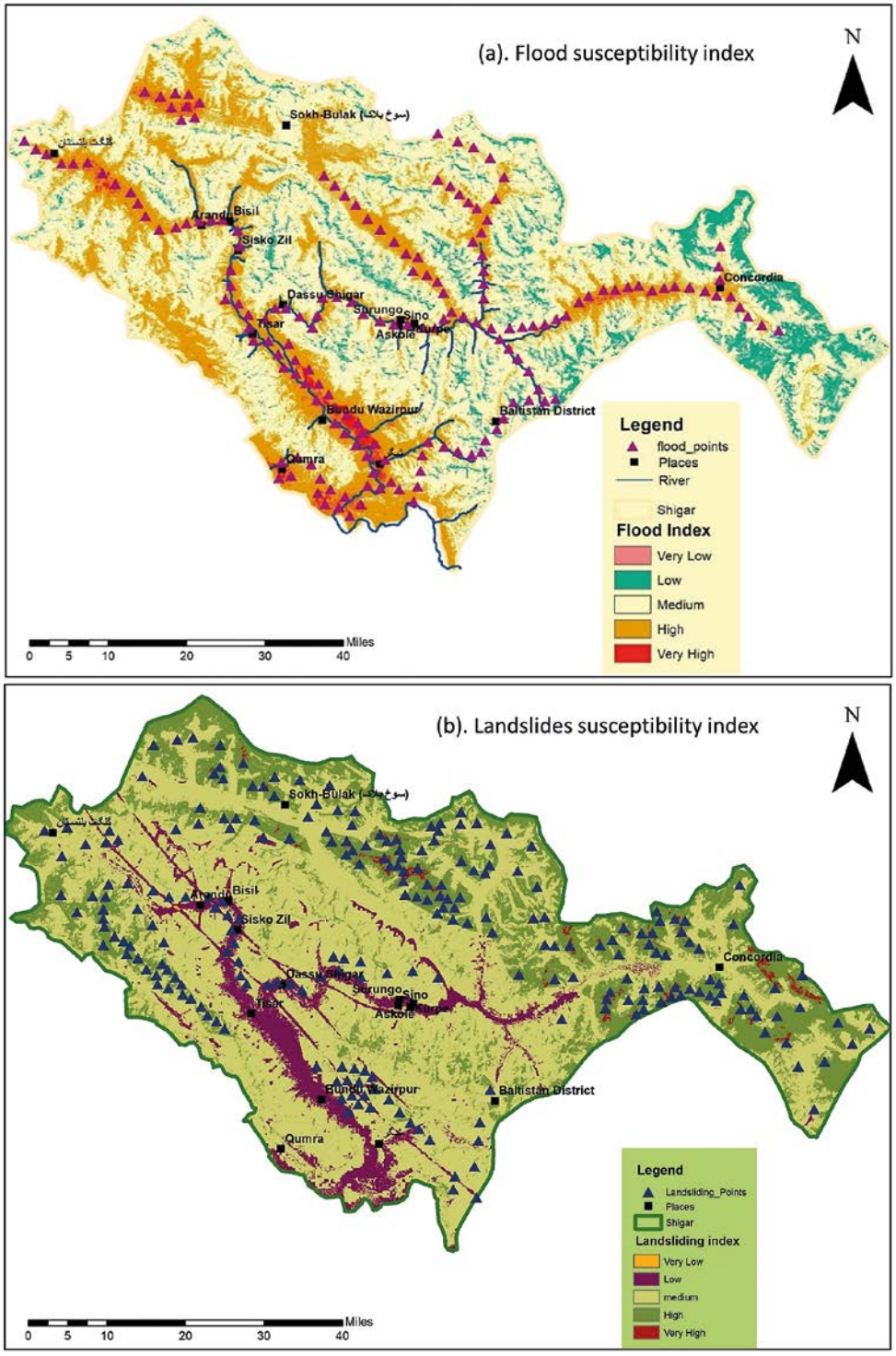

Fig. 3 Flood and landslide susceptibility index maps. The maps were created in ArcGIS using the relevant layers.

points and previous studies, have experienced frequent inundation events (Gilany and Iqbal 2016). In particular, several major villages are located within the high to very high susceptible zones, including Chaqpo, Tissar, Churtron, Haiderabad, Lansa, Marapi, Churka, Alchori, Qulpur, and Kashmal.

Landslides, with the second-highest weight in the hazard susceptibility index, emerge as a frequent and impactful hazard within the study area. A comprehensive approach to landslide hazard mapping involved the consideration of ten key parameters, including lithology, soil type, slope, land use, distance to road, distance to river, distance to fault, elevation, aspect, and precipitation. The intricate interplay of these factors in the region's topography and climatic conditions establishes a substantial susceptibility to landslides, as corroborated by existing literature (Hewitt 1999; Calligaris et al. 2017).

The results of the study elucidate that a significant portion of the study area, 1459 km^2, which makes

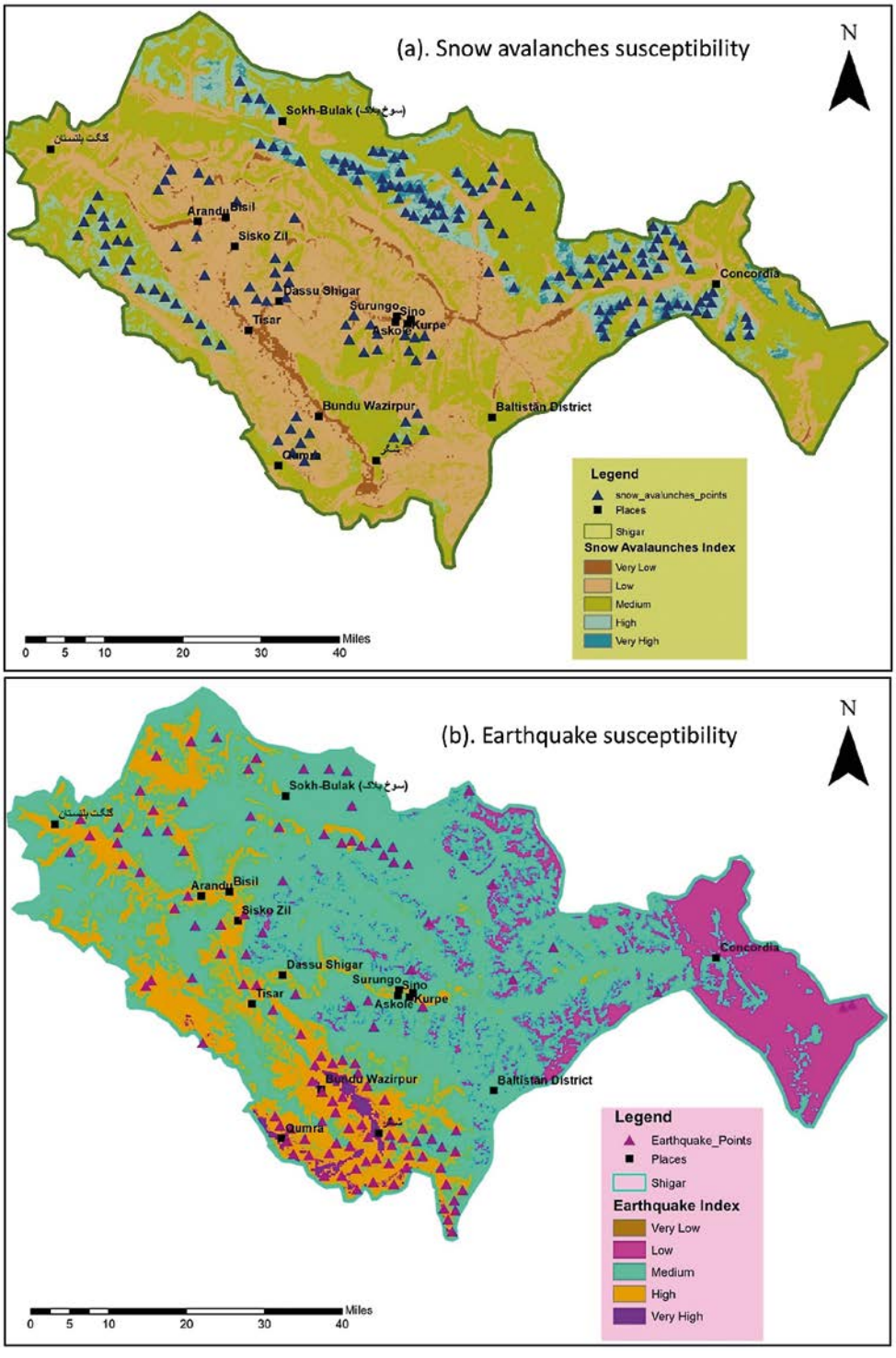

Fig. 4 Earthquake and snow avalanches susceptibility index maps. The maps were created in ArcGIS using the relevant layers.

25.8% of the total land, is characterized by a high susceptibility to landslide hazards (Tab. 4). The resultant landslide susceptibility index map provides a representation of vulnerability distribution across the study area (Fig. 3b). The susceptibility to landslides demonstrates an escalating trend toward higher elevations and steeper slopes, accentuating the topographic influence on landslide occurrence. Within the highly susceptible zones, notable villages such as Hoto, Daso, Demal, Haiderabad, and Arandu are situated, underscoring the threat to populated areas. A substantial yet distinct portion, comprising 64.6% of the total, falls within the moderately susceptible classification. This delineation reflects the nuanced topographic hostility inherent in the region.

Despite the prevalence of moderately susceptible areas, a closer examination reveals that only a select few out of approximately 50 villages are positioned in the high to very high susceptible zones. This underscores the concentrated nature of landslide vulnerability, with specific communities facing heightened risks. Navigating the landscape challenges posed by landslides necessitates a tailored understanding of the localized susceptibility patterns, enabling targeted mitigation efforts and community resilience strategies.

In exploring the hazards prevalent in our study area, snow avalanches emerge as a significant concern (Hewitt 1988; Hewitt et al. 2011; Hasson et al. 2014; Gilany and Iqbal 2017), demanding a detailed evaluation (Shroder et al. 2011). We adopted a thorough approach, considering twelve factors like slope, distance to fault, lithology, and others to create a Snow Avalanche Susceptibility Index (Ali et al. 2023). The susceptibility index, depicted in Tab. 3, assigns different levels ranging from low to very high vulnerability.

Examining the map (Fig. 4a), it's evident that high and very high susceptibility zones cluster in elevated terrains, primarily in the upper northern and northwestern parts of our study area. Zooming in, villages such as Wazir Pur, Churka, Hasnupi, and others fall within these high-risk zones. These findings highlight the localized nature of avalanche susceptibility, emphasizing that certain communities face elevated risks due to where they're situated.

On the flip side, most low-lying regions showcase low susceptibility. This spatial distribution of susceptibility levels points to areas where avalanche risks are comparatively lower, providing valuable insights for targeted safety measures and community planning. Breaking down the stats, areas with very high susceptibility cover 40.7% of the total land, while high susceptibility areas account for 11.8%. On the lower end, low susceptibility areas make up 2.35%. This statistical breakdown gives us a clearer picture of the varying risk levels across the landscape. Our assessment of snow avalanche susceptibility helps uncover the mix of factors influencing risk. Identifying high-risk zones and areas of lower susceptibility is vital for crafting safety measures tailored to specific communities. This down-to-earth understanding is crucial for decision-makers working to safeguard our communities from the challenges posed by alpine hazards.

In our study, our primary aim was to create a comprehensive picture of the risks in the Shigar Valley by looking at multiple hazards simultaneously. We achieved this by assigning weights based on expert opinions from existing literature, ensuring a well-rounded analysis (Zhou et al. 2016; Rehman et al. 2021; 2022). By doing this, we move beyond just individual hazards and gain a holistic understanding of how various threats come together, influencing the overall risk profile of the study area. Our holistic approach allows us to look at the bigger picture, giving us insights into how different hazards interact. This in-depth exploration provides a detailed view of vulnerability, crucial for managing and planning human activities in the region.

Looking at the results, the susceptibility of the study area to combined hazards is quite worrisome. A significant portion of the valley, about 28.3%, falls into the highly susceptible category, and an additional 1.04% is classified as very highly susceptible (Tab. 4). These areas are predominantly along the floodplains of the Shigar River and its tributaries, which are crucial zones for human activities (Fig. 5). Moving beyond the high susceptibility zones, we find that approximately 60% of the total land in the study area is moderately susceptible to multi-hazards. This moderate susceptibility is spread throughout the valley, presenting challenges for a range of activities. It's not just about the extremes; even the moderate risk areas demand attention and planning. In contrast,

Tab. 4 Area susceptible to various hazards and overall multi-hazards susceptibility index.

Susceptibility index →	Low		Very low		Medium		High		Very high	
Hazards ↓	Area (km²)	%age	Area (km²)	%age	Area (km²)	%age	Area (km²)	%age	Area (km²)	%age
Floods	1.73	0.030	550.2	9.70	3436.0	60.7	1604.9	28.3	59.3	1.04
Landsides	1.61	0.020	494.8	8.70	3654.5	64.6	1459.7	25.8	40.3	0.70
Avalanches	135.50	2.300	2410.1	42.65	2304.5	40.7	667.8	11.8	132.8	2.35
Earthquake	0.34	0.005	866.3	15.30	3507.1	61.9	1229.1	21.7	58.7	1.03
Multi-hazard	1.73	0.030	548.6	9.70	3432.0	60.8	1602.1	28.3	59.2	1.04

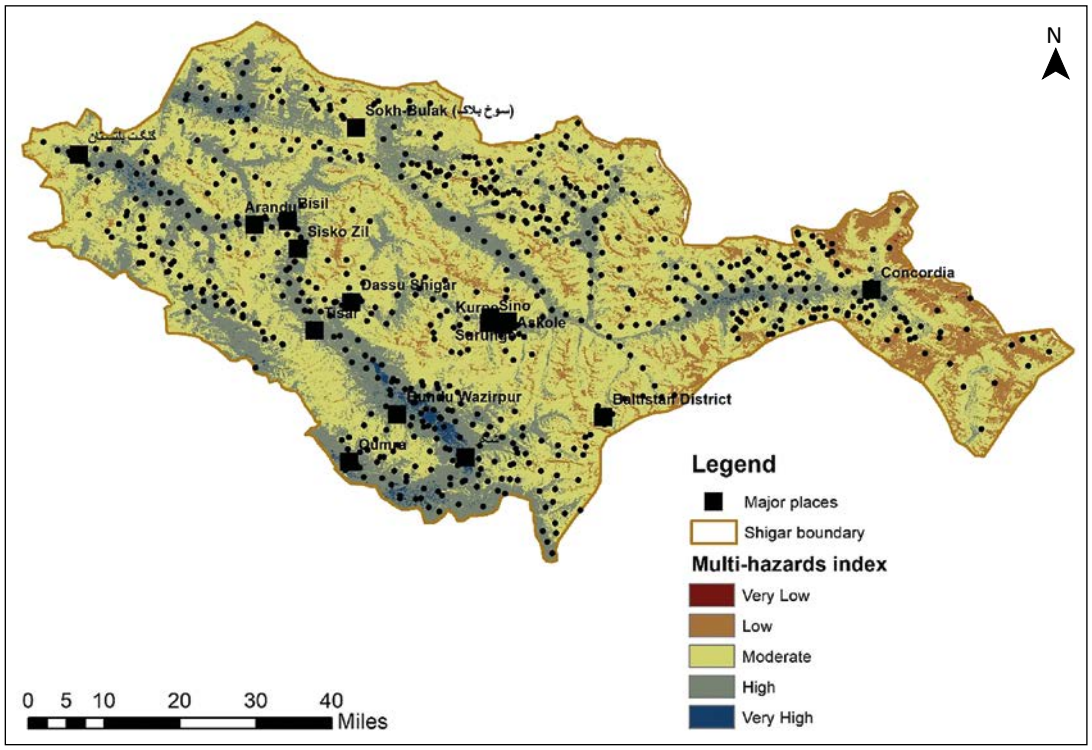

Fig. 5 Multi-hazards susceptibility index of the study area. The map was created using weighted overlay in ArcGIS combining all the hazards susceptibility indices.

the low and very low susceptibility categories cover a relatively small proportion of the total land. Most of these areas are located in uninhabited high mountains and glacial terrain.

Understanding the dynamics of highly susceptible zones along with moderately and less susceptible areas is crucial for adapting resilient strategies. The valley's vulnerability is not just about the extreme risks but also about managing day-to-day activities in areas that might seem less risky but still demand attention. Balancing these aspects is key to ensuring a secure and sustainable future for the Shigar Valley.

4. Conclusion

In undertaking a comprehensive multi-hazard susceptibility assessment for the Shigar Valley, our study has provided invaluable insights into the complex risk landscape of this region. As we conclude, it becomes evident that navigating the hazards in the Shigar Valley requires a nuanced understanding and strategic planning to foster sustainable resilience. Our research delved into individual hazards, uncovering the specific threats posed by floods, landslides, snow avalanches, and earthquakes. By carefully mapping susceptibility indices for each hazard, we laid the groundwork for a detailed exploration of the challenges faced by the Shigar Valley.

Floods emerged as a recurrent and severe hazard, particularly in lowland areas adjacent to the Shigar River and its tributaries. The susceptibility mapping illuminated the vulnerabilities of densely populated regions, emphasizing the need for targeted risk reduction strategies and preparedness measures. Landslides, with their significant weight in the susceptibility index, showcased a substantial portion of the study area as highly susceptible. The distribution of vulnerabilities revealed a correlation with higher elevations and steeper slopes, impacting villages like Hoto, Daso, Demal, Haiderabad, and Arandu. The susceptibility map for snow avalanches unveiled high and very high susceptibility in the elevated regions, affecting villages like Wazir Pur, Churka, Hasnupi, Daso, Dasonid, Doka, Zil, and Surungo. Low susceptibility prevailed in low-lying areas, emphasizing the need for specific mitigation strategies based on local terrain. Given the historical significance of earthquakes in the HKH region, our earthquake susceptibility assessment indicated considerable vulnerability. Highly susceptible zones were concentrated in populated southern and southwestern lowlands, emphasizing the need for resilient infrastructure and emergency preparedness.

Moving beyond individual hazards, we adopted a holistic approach by combining all hazards into a multi-hazard susceptibility index. Assigning weights based on expert opinions enabled us to capture the interconnectedness of these threats. This approach not only identified highly susceptible zones but also highlighted moderate risk areas that demand attention for comprehensive hazard planning. Our integrated analysis painted a concerning picture, with a

substantial area classified as highly and very highly susceptible. Balancing the need for development and human activities in these areas requires meticulous planning, emphasizing the importance of community awareness and engagement. As we conclude, it is imperative to consider our findings in guiding sustainable development and resilience strategies in the Shigar Valley. Additionally, our study emphasizes the need for ongoing monitoring and adaptive management to address the dynamic nature of hazards in this region. In navigating the multi-hazard landscape of the Shigar Valley, our research lays the groundwork for informed decision-making, fostering a resilient future for the communities that call this vulnerable yet picturesque landscape home.

References

Abbas, Z., Khan, S., Alam, J. et al. (2017): Medicinal plants used by inhabitants of the Shigar Valley, Baltistan region of Karakorum range-Pakistan. J Ethnobiology Ethnomedicine 13: 53, https://doi.org/10.1186/s13002-017-0172-9.

Abella, E. A. C., Van Westen, C. J. (2008): Qualitative landslide susceptibility assessment by multicriteria analysis: A case study from San Antonio del Sur, Guantánamo, Cuba. Geomorphology 94(3–4), 453–466, https://doi.org/10.1016/j.geomorph.2006.10.038.

Adhikari, R., Gautam, D., Jha, P., Aryal, B., Ghalan, K., Rupakhety, R., Dong, Y., Rodrigues, H., Motra, G. (2019): Bridging multi-hazard vulnerability and sustainability: approaches and applications to Nepali highway bridges. In: Noroozinejad Farsangi, E., Takewaki, I., Yang, T., Astaneh-Asl, A., Gardoni, P. (eds) Resilient Structures and Infrastructure. Springer, Singapore, https://doi.org/10.1007/978-981-13-7446-3_14.

Afreen, M., Haq, F., Mukhtar, Z. (2022): Flood susceptibility analysis of the Panjkora Valley Northern Pakistan, using frequencyratio approach. International Journal of Disaster Resilience in the Built Environment 13(5), 601–614, https://doi.org/10.1108/IJDRBE-09-2020-0104.

Ahmed, T., Rehman, K., Shafique, M., Ali, W. (2023): GIS-based earthquake potential analysis in Northwest Himalayan, Pakistan. Environmental Earth Sciences 82(4), 113, https://doi.org/10.1007/s12665-023-10798-2.

Ali, F., Zhang, J.-H., Alam, M., Sajjad, M., Abbas, S., Hussain, A., Ramzan, M., Hussain, F. (2023): Avalanche Susceptibility mapping of District Shigar, Pakistan using GIS-based MCDA–AHP modeling, 16 January 2023, PREPRINT (Version 1) available at Research Square, https://doi.org/10.21203/rs.3.rs-2237380/v1.

Ali, S., Khan, G., Qureshi, J. A., Hassan, M., Kheirandish, S. (2023): Climatic and topographic controls on glacial changes (1973–2020) in Shigar Basin, Central Karakoram, Northern Pakistan. Environmental Science and Pollution Research 30, 74889–74899, https://doi.org/10.1007/s11356-023-27648-0.

Al-Taani, A., Al-husban, Y., Ayan, A. (2023): Assessment of potential flash flood hazards. Concerning land use/land cover in Aqaba Governorate, Jordan, using a multi-criteria technique. The Egyptian Journal of Remote Sensing and Space Science 26(1), 17–24, https://doi.org/10.1016/j.ejrs.2022.12.007.

Andrabi, T., Daniels, B., Das, J. (2023): Human capital accumulation and disasters: Evidence from the Pakistan earthquake of 2005. Journal of Human Resources 58(4), 1057–1096, https://doi.org/10.3368/jhr.59.2.0520-10887R1.

Aslam, B., Zafar, A., Qureshi, U. A., Khalil, U. (2021): Seismic investigation of the northern part of Pakistan using the statistical and neural network algorithms. Environmental Earth Sciences 80, 1–18, https://doi.org/10.1007/s12665-020-09348-x.

Baig, S. U., Rehman, M. U., Janjua, N. N. (2021): District-level disaster risk and vulnerability in the Northern mountains of Pakistan. Geomatics, Natural Hazards and Risk 12(1), 2002–2022, https://doi.org/10.1080/19475705.2021.1944331.

Bajracharya, R. M., Shrestha, H. L., Shakya, R., Sitaula, B. K. (2015): Agro-forestry systems as a means to achieve carbon co-benefits in Nepal. Journal of Forest and Livelihood 13(1), 59–68, https://doi.org/10.3126/jfl.v13i1.15366.

Bajracharya, S. R., Maharjan, S., Shrestha, F., Sherpa, T., Wagle, N., Shrestha, A. (2020): Inventory of glacial lakes and identification of potentially dangerous glacial lakes in the Koshi, Gandaki, and Karnali River Basins of Nepal, the Tibet Autonomous Region of China and India. International Centre for Integrated Mountain Development, United Nations Development Programme, Kathmandu, Nepal, https://doi.org/10.53055/ICIMOD.773.

Bandyopadhyay, J., Rahaman, S. H., Karan, C. (2023): Agricultural potential zone mapping with surface water resource management using geo-spatial tools for Jhargram district, West Bengal, India. Knowledge-Based Engineering and Sciences 4(1), 1–18.

Batool, S., Khan, T., Karim, R., Zafar, M., Ahmed, S. (2016): Climate Change and Agricultural Transformation in Shigar Valley, Gilgit-Baltistan, Pakistan: A Commune-Scientific Perception. International Journal of Environment, Agriculture and Biotechnology 1(4), 902–906, https://doi.org/10.22161/ijeab/1.4.39.

Belay, S., Goedert, J., Woldesenbet, A., Rokooei, S. (2022): AHP based multi criteria decision analysis of success factors to enhance decision making in infrastructure construction projects. Cogent Engineering 9(1): 2043996, https://doi.org/10.1080/23311916.2022.2043996.

Belazreg, N. E. H., Hasbaia, M., Şen, Z., Ferhati, A. (2023): Flood risk mapping using multi-criteria analysis (MCA) through AHP method case of El-Ham wadi watershed of Hodna basin (Algeria): Natural hazards 120, 1023–1039, https://doi.org/10.1007/s11069-023-06239-9.

Bhutiyani, M., Kale, V. S., Pawar, N. (2008): Changing streamflow patterns in the rivers of northwestern Himalaya: implications of global warming in the 20th century. Current Science, 618–626.

Bui, D. T., Ngo, P.-T. T., Pham, T. D., Jaafari, A., Minh, N. Q., Hoa, P. V., Samui, P. (2019): A novel hybrid approach based on a swarm intelligence optimized extreme learning machine for flash flood susceptibility mapping.

Catena 179, 184–196, https://doi.org/10.1016/j.catena.2019.04.009.
Calligaris, C., Tariq, S., Khan, H., Poretti, G. (2017): Landslide Susceptibility Analysis in Arandu Area Shigar Valley, CKNP (Gilgit-Baltistan- Pakistan): In: Mikos, M., Tiwari, B., Yin, Y., Sassa, K. (eds) Advancing Culture of Living with Landslides. WLF 2017. Springer, Cham, https://doi.org/10.1007/978-3-319-53498-5_103.
Campbell, J.G. (2004): Inventory of Glaciers and Glacial Lakes and the Identification of Potential Glacial Lake Outburst Floods (GLOFs) Affected by Global Warming in the Mountains of India, Pakistan and China/Tibet Autonomous Region. International Centre for Integrated Mountain Development (ICIMOD) G. P. O. Box 3226, Kathmandu, Nepal.
Chen, W., Zhang, S. (2021): GIS-based comparative study of Bayes network, Hoeffding tree and logistic model tree for landslide susceptibility modeling. Catena 203: 105344, https://doi.org/10.1016/j.catena.2021.105344.
Chen, W., Shahabi, H., Zhang, S., Khosravi, K., Shirzadi, A., Chapi, K., Pham, B. T., Zhang, T., Zhang, L., Chai, H. (2018): Landslide susceptibility modeling based on GIS and novel bagging-based kernel logistic regression. Applied Sciences 8(12): 2540, https://doi.org/10.3390/app8122540.
Cheng, X., Cheng, Y., Zhang, N., Zhao, S., Cui, H., Zhou, H. (2020): Purification of flavonoids from Carex meyeriana Kunth based on AHP and RSM: Composition analysis, antioxidant, and antimicrobial activity. Industrial Crops and Products 15: 112900, https://doi.org/10.1016/j.indcrop.2020.112900.
Chowdhury A., Kroczek T., Kumar De S., Vilímek V., Chand Sharma M., Debnath M. (2021): Glacial Lake Evolution (1962–2018) and Outburst Susceptibility of Gurudongmar Lake Complex in the Tista basin, Sikkim Himalaya (India): Water 13(24): 3565, https://doi.org/10.3390/w13243565.
Clark-Ginsberg, A., Easton-Calabria, L. C., Patel, S. S., Balagna, J., Payne, L. A. (2021): When disaster management agencies create disaster risk: a case study of the US's Federal Emergency Management Agency. Disaster Prevention and Management: An International Journal 30(4/5), 447–461, https://doi.org/10.1108/DPM-03-2021-0067.
Farhat, B., Souissi, D., Mahfoudhi, R., Chrigui, R., Sebei, A., Ben Mammou, A. (2023): GIS-based multi-criteria decision-making techniques and analytical hierarchical process for delineation of groundwater potential. Environmental Monitoring and Assessment 195(2): 285, https://doi.org/10.1007/s10661-022-10845-8.
Faryabi, M. (2023): A fuzzy logic approach for land subsidence susceptibility mapping: the use of hydrogeological data. Environmental Earth Sciences 82(9): 209, https://doi.org/10.1007/s12665-023-10909-z.
Fatima, S. U., Khan, M. A., Shaukat, S. S., Alamgir, A., Siddiqui, F., and Sulman, N. (2022): Geo-Spatial Assessment of Water Quality in Shigar Valley, Gilgit Baltistan, Pakistan. Health 14(5), 535–552, https://doi.org/10.4236/health.2022.145040.
Gao, Y., Liu, S., Qi, M., Xie, F., Wu, K., Zhu, Y. (2021) Glacier-Related Hazards Along the International Karakoram Highway: Status and Future Perspectives. Frontiers in Earth Science 9:611501, https://doi.org/10.3389/feart.2021.611501.
Gilany S.N., Iqbal, J. (2016): Geospatial analysis of glacial hazard prone areas of Shigar and Shayok basins. International Journal of Innovation and Applied Studies 14(3), 623–644.
Gilany, S. N., Iqbal, J. (2017): Glacial avalanche hazard's comparative geospatial analysis in Shigar and Shyok basins. In 2017 Fifth International Conference on Aerospace Science and Engineering (ICASE), Islamabad, Pakistan, 1–7, https://doi.org/10.1109/ICASE.2017.8374279.
Gizaw, E. A., Bawoke, G. T., Alemu, M. M., Anteneh, Z. L. (2023): Spatial analysis of groundwater potential using remote sensing and GIS-based multi-criteria decision analysis method in Fetam-Yisir catchment, Blue Nile Basin, Ethiopia. Applied Geomatics 15, 659–681, https://doi.org/10.1007/s12518-023-00518-7.
Ha-Mim, N. M., Rahman, M. A., Hossain, M. Z., Fariha, J. N., Rahaman, K. R. (2022): Employing multi-criteria decision analysis and geospatial techniques to assess flood risks: A study of Barguna district in Bangladesh. International Journal of Disaster Risk Reduction 77: 103081, https://doi.org/10.1016/j.ijdrr.2022.103081.
Hasson, S., Lucarini, V., Khan, M. R., Petitta, M., Bolch, T., and Gioli, G. (2014): Early 21st century snow cover state over the western river basins of the Indus River system. Hydrology and Earth System Sciences 18(10), 4077–4100, https://doi.org/10.5194/hess-18-4077-2014.
Hewitt, K. (1998): Catastrophic landslides and their effects on the Upper Indus streams, Karakoram Himalaya, northern Pakistan. Geomorphology 26(1–3), 47–80, https://doi.org/10.1016/S0169-555X(98)00051-8.
Hewitt, K. (1999): Quaternary Moraines vs Catastrophic Rock Avalanches in the Karakoram Himalaya, Northern Pakistan. Quaternary Research 51(3), 220–237, https://doi.org/10.1006/qres.1999.2033.
Hewitt, K., Gosse, J., Clague, J. J. (2011): Rock avalanches and the pace of late Quaternary development of river valleys in the Karakoram Himalaya. GSA Bulletin 123(9–10), 1836–1850, https://doi.org/10.1130/B30341.1.
Hu, J., Chen, J., Chen, Z., Cao, J., Wang, Q., Zhao, L., Zhang, H., Xu, B., Chen, G. (2018): Risk assessment of seismic hazards in hydraulic fracturing areas based on fuzzy comprehensive evaluation and AHP method (FAHP): A case analysis of Shangluo area in Yibin City, Sichuan Province, China. Journal of Petroleum Science and Engineering 170, 797–812, https://doi.org/10.1016/j.petrol.2018.06.066.
Iqbal, J. M., Shah, H. F., Chaudhry, A. H., Baig, N. M. (2014): Impacts of Attabad Lake (Pakistan) and its future outlook. European Scientific Journal 10(8), 107–120.
Ishaque, W., Tanvir, R., Mukhtar, M. (2022): Climate Change and Water Crises in Pakistan: Implications on Water Quality and Health Risks. Journal of Environment and Public Health 22: 5484561, https://doi.org/10.1155/2022/5484561.
Jaiswal, K., Wald, D., Porter, K. (2010): A global building inventory for earthquake loss estimation and risk management. Earthquake Spectra 26(3), 731–748, https://doi.org/10.1193/1.3450316.
Jaiswal, P., van Westen, C. J. (2010): Use of remote sensing data for landslide susceptibility mapping

in central Nepal. Proceedings of the International Conference on Geoinformatics for Disaster Management 4–6.

Javidan, N., Kavian, A., Pourghasemi, H. R., Conoscenti, C., Jafarian, Z., Rodrigo-Comino, J. (2021): Evaluation of multi-hazard map produced using MaxEnt machine learning technique. Scientific reports 11(1): 6496, https://doi.org/10.1038/s41598-021-85862-7.

Kaur, H., Gupta, S., Parkash, S., Thapa, R., Gupta, A., Khanal, G. C. (2019): Evaluation of landslide susceptibility in a hill city of Sikkim Himalaya with the perspective of hybrid modelling techniques. Annals of GIS 25(2), 113–132, https://doi.org/10.1080/19475683.2019.1575906.

Kaur, P., and Singh, B. (2019): Multi-hazard vulnerability assessment of Indian Himalayan region using geospatial technique. Natural Hazards 98(1), 435–456.

Ke, C., He, S., Qin, Y. (2023): Comparison of natural breaks method and frequency ratio dividing attribute intervals for landslide susceptibility mapping. Bulletin of Engineering geology and the Environment 82: 384, https://doi.org/10.1007/s10064-023-03392-0.

Khan, A., Farah, H., Khan, S., Azmat, M. (2023): Comparative assessment of spatiotemporal variability in cryosphere and hydro-climatic regime of the Hunza, Astore and Shigar Basins (Hindukush-Karakoram–Himalaya Region) in Pakistan. Arabian Journal of Geosciences 16(5), 350–365, https://doi.org/10.1007/s12517-023-11440-y.

Khattak, I., Rahman, F., Haq, F. (2012): The Flood Event of July 2010: Socioeconomic Disruptions in Lower Dir District. The Journal of Humanities and Social Sciences 20(2), 57–76.

Khurshid, A., Yielding, G., Ahmad, S., Davison, I., Jackson, J. A., King, G. C. P., Zuo, L. B. (1984): The seismicity of northernmost Pakistan. Tectonophysics 109(3–4), 209–226, https://doi.org/10.1016/0040-1951(84)90141-0.

Kornejady, A., Pourghasemi, H. R., Afzali, S. F. (2019): Presentation of RFFR New Ensemble Model for Landslide Susceptibility Assessment in Iran. In: Pradhan, S., Vishal, V., Singh, T. (eds) Landslides: Theory, Practice and Modelling. Advances in Natural and Technological Hazards Research 50. Springer, Cham, https://doi.org/10.1007/978-3-319-77377-3_7.

Kropáček J., Vilímek V., Mehrishi P. (2021): A preliminary assessment of Chamoli ice and rock fall in Indian Himalayas by remote sensing. Landslides 18, 3489–3497, https://doi.org/10.1007/s10346-021-01742-1.

Kumar, A., Gupta, A. K., Bhambri, R., Verma, A., Tiwari, S. K., Asthana, A. (2018): Assessment and review of hydrometeorological aspects for cloudburst and flash flood events in the third pole region (Indian Himalaya): Polar Science 18, 5–20, https://doi.org/10.1016/j.polar.2018.08.004.

Kumar, M., Singh, P., Singh, P. (2023): Machine learning and GIS-RS-based algorithms for mapping the groundwater potentiality in the Bundelkhand region, India. Ecological Informatics 74: 101980, https://doi.org/10.1016/j.ecoinf.2023.101980 .

Kumari, N., Chowdary, V., Waghaye, A., Tiwari, K. (2016): Assessment of surface Runoff and Sediment Yield using WEPP model. Nature Environment and Pollution Technology 15(2), 491.

Kursunoglu, S., Kursunoglu, N., Hussaini, S., Kaya, M. (2021): Selection of an appropriate acid type for the recovery of zinc from a flotation tailing by the analytic hierarchy process. Journal of Cleaner Production 283: 124659, https://doi.org/10.1016/j.jclepro.2020.124659.

Lee, S., Seo, K. K. (2016): A hybrid multi-criteria decision-making model for a cloud service selection problem using BSC, fuzzy Delphi method and fuzzy AHP. Wireless Personal Communications 86, 57–75, https://doi.org/10.1007/s11277-015-2976-z.

Li, R., Huang, S., Dou, H. (2023): Dynamic Risk Assessment of Landslide Hazard for Large-Scale Photovoltaic Power Plants under Extreme Rainfall Conditions. Water 15(15): 2832, https://doi.org/10.3390/w15152832.

Li, X., Sovilla, B., Jiang, C., Gaume, J. (2020): The mechanical origin of snow avalanche dynamics and flow regime transitions. The Cryosphere 14(10), 3381–3398, https://doi.org/10.5194/tc-14-3381-2020.

Lutz, A.F., Immerzeel, W., Kraaijenbrink, P., Shrestha, A.B., Bierkens, M.F. (2016): Climate change impacts on the upper Indus hydrology: sources, shifts and extremes. PloS ONE 11(11): e0165630, https://doi.org/10.1371/journal.pone.0165630.

Majeed, M., Lu, L., Anwar, M. M., Tariq, A., Qin, S., El-Hefnawy, M. E., El-Sharnouby, M., Li, Q., Alasmari, A. (2023): Prediction of flash flood susceptibility using integrating analytic hierarchy process (AHP) and frequency ratio (FR) algorithms. Frontiers in Environmental Science 10: 1037547, https://doi.org/10.3389/fenvs.2022.1037547.

Meshram, S., Tirivarombo, S., Meshram, C., Alvandi, E. (2023): Prioritization of soil erosion-prone sub-watersheds using fuzzy-based multi-criteria decision-making methods in Narmada basin watershed, India. International Journal of Environmental Science and Technology 20(2), 1741–1752, https://doi.org/10.1007/s13762-022-04044-8.

Moharir, K. N., Pande, C. B., Gautam, V. K., Singh, S. K., Rane, N. L. (2023): Integration of hydrogeological data, GIS and AHP techniques applied to delineate groundwater potential zones in sandstone, limestone and shales rocks of the Damoh district, (MP) central India. Environmental Research 228: 115832, https://doi.org/10.1016/j.envres.2023.115832.

Mokarram, M., Negahban, S., Abdeldjalil, B. (2021): GIS-based fuzzy-analytic network process (FAHP), fuzzy-analytic hierarchy process (FANP) methods and feature selection algorithm (FSA) to determine earthquake-prone areas in Kermanshah Province. Environmental Earth Sciences 80: 633, https://doi.org/10.1007/s12665-021-09934-7.

Mondal, M., Haldar, S., Biswas, A., Mandal, S., Bhattacharya, S., Paul, S. (2021): Modeling cyclone-induced multi-hazard risk assessment using analytical hierarchical processing and GIS for coastal West Bengal, India. Regional Studies in Marine Science 44: 101779, https://doi.org/10.1016/j.rsma.2021.101779.

Mushtaq, F., Farooq, M., Tirkey, A. S., Sheikh, B. A. (2023): Analytic Hierarchy Process (AHP) Based Soil Erosion Susceptibility Mapping in Northwestern Himalayas: A Case Study of Central Kashmir Province. Conservation 3(1), 32–52, https://doi.org/10.3390/conservation3010003.

Okoli, J., Nahazanan, H., Nahas, F., Kalantar, B., Shafri, H. Z. M., Khuzaimah, Z. (2023): High-Resolution Lidar-Derived

DEM for Landslide Susceptibility Assessment Using AHP and Fuzzy Logic in Serdang, Malaysia. Geosciences 13(2): 34, https://doi.org/10.3390/geosciences13020034.

Olaya Calderon, L. J., Cocuccioni, S., Romagnoli, F., Atun, F., Pittore, M., Schneiderbauer, S., van Westen, C., Sliuzas, R., Armas, I., Mocanu, R., and Kundak, S. (2024): Analysing historical disasters to support multi-hazard risk assessment: enhancing forensic analysis through Impact Chains, EGU General Assembly 2024, Vienna, Austria, 14–19 Apr 2024, EGU24-10177, https://doi.org/10.5194/egusphere-egu24-10177.

Olii, M. R., Olii, A., Pakaya, R., Olii, M. Y. U. P. (2023): GIS-based analytic hierarchy process (AHP) for soil erosion-prone areas mapping in the Bone Watershed, Gorontalo, Indonesia. Environmental Earth Sciences 82(9), 1–14, https://doi.org/10.1007/s12665-023-10913-3.

OpenAI. (2023): ChatGPT: Language Models for Drafting Assistance. OpenAI, Available at: https://chat.openai.com/.

Ozegin, K., Ilugbo, S., Ogunseye, T. (2023): Groundwater exploration in a landscape with heterogeneous geology: an application of geospatial and analytical hierarchical process (AHP) techniques in the Edo north region, in Nigeria. Groundwater for Sustainable Development 20: 100871, https://doi.org/10.1016/j.gsd.2022.100871.

Park, S., Son, S., Han, J., Lee, S., Kim, J. (2018): Groundwater vulnerability assessment using an integrated DRASTIC model using frequency ratio and analytic hierarchy process in GIS. In Proceedings of the EGU General Assembly Conference Abstracts, Vienna, Austria, 4–13 April 2018.

Pham, Q. B., Achour, Y., Ali, S. A., Parvin, F., Vojtek, M., Vojteková, J., Al-Ansari, N., Achu, A., Costache, R., Khedher, K. M. (2021): A comparison among fuzzy multi-criteria decision making, bivariate, multivariate and machine learning models in landslide susceptibility mapping. Geomatics, Natural Hazards and Risk 12(1), 1741–1777, https://doi.org/10.1080/19475705.2021.1944330.

Pham, B. T., Bui, D. T., Prakash, I., Indrajit, I., and Revhaug, I. (2021): GIS-based multi-hazard susceptibility assessment in Central Vietnam. Natural Hazards 105(3), 3113–3140.

Piao, Y., Lee, D., Park, S., Kim, H. G., Jin, Y. (2022): Multi-hazard mapping of droughts and forest fires using a multi-layer hazards approach with machine learning algorithms. Geomatics, Natural Hazards and Risk 13(1), 2649–2673, https://doi.org/10.1080/19475705.2022.2128440.

Rehman, A., Song, J., Haq, F., Ahamad, M. I., Sajid, M., Zahid, Z. (2021): Geo-physical hazards microzonation and suitable site selection through multicriteria analysis using geographical information system. Applied Geography 135: 102550, https://doi.org/10.1016/j.apgeog.2021.102550.

Rehman, A., Song, J., Haq, F., Mahmood, S., Ahamad, M. I., Basharat, M., Mehmood, M. S. (2022): Multi-hazard susceptibility assessment using the analytical hierarchy process and frequency ratio techniques in the Northwest Himalayas, Pakistan. Remote Sensing 14(3), 554, https://doi.org/10.3390/rs14030554.

Richardson, S. D., Reynolds, J. M. (2000): An overview of glacial hazards in the Himalayas. Quaternary International 65, 31–47, https://doi.org/10.1016/S1040-6182(99)00035-X.

Saaty, T. L. (2008): Decision making with the analytic hierarchy process. International Journal of Services Sciences 1(1), 83–98, https://doi.org/10.1504/IJSSCI.2008.017590.

Saifi, S., Turner B., John, T. (2022): Over 900 killed by Pakistan monsoon rains and floods, including 326 children. CNN, August 24, 2022.

Sangha, K. K., Evans, J., Edwards, A., Russell-Smith, J. (2019): Measuring environmental losses from natural disasters: A case study of costing bushfires in the Northern Territory. Australian Journal of Emergency Management 34(4), 31–39.

Scapozza, C., Bartelt, P. (2003): Triaxial tests on snow at low strain rate. Part II. Constitutive behaviour. Journal of Glaciology 49(164), 91–101, https://doi.org/10.3189/172756503781830890.

Scapozza, C., Ambrosi, C., Cannata, M., Strozzi, T. (2019): Glacial lake outburst flood hazard assessment by satellite Earth observation in the Himalayas (Chomolhari area, Bhutan). Geographica Helvetica 74(1), 125–139, https://doi.org/10.5194/gh-74-125-2019.

Schmidt, M. (2008): Land use, land administration and land rights in Shigar, Baltistan. In Modern Ladakh, 241–266. Brill, https://doi.org/10.1163/ej.9789004167131.i-313.90.

Seong, Y. B., Bishop, M. P., Bush, A., Clendon, P., Copland, L., Finkel, R. C., Shroder, J. F. (2009): Landforms and landscape evolution in the Skardu, Shigar and Braldu valleys, central Karakoram. Geomorphology 103(2), 251–267, https://doi.org/10.1016/j.geomorph.2008.04.026.

Shekar, P. R., Mathew, A. (2023): Assessing groundwater potential zones and artificial recharge sites in the monsoon-fed Murredu river basin, India: An integrated approach using GIS, AHP, and Fuzzy-AHP. Groundwater for Sustainable Development 23: 100994, https://doi.org/10.1016/j.gsd.2023.100994.

Shrestha, H. L., Poudel, N. S., Bajracharya, R. M., Sitaula, B. K. (2019): Mapping and Modelling of Land Use Change in Nepal. Journal of Forest and Livelihood 18 (1), 39–53, https://doi.org/10.3126/jfl.v18i1.59621.

Shroder, Jr., Owen, J. F., Seong, L. A., Bishop, Y. B., Bush, M. P., Caffee, A., Kamp, U. (2011): The role of mass movements on landscape evolution in the Central Karakoram: Discussion and speculation. Quaternary International 236(1–2), 34–47, https://doi.org/10.1016/j.quaint.2010.05.024.

Ujjwal, K., Garg, S., Hilton, J., Aryal, J., Forbes-Smith, N. (2019): Cloud Computing in natural hazard modeling systems: Current research trends and future directions. International Journal of Disaster Risk Reduction 38: 101188, https://doi.org/10.1016/j.ijdrr.2019.101188.

Upwanshi, M., Damry, K., Pathak, D., Tikle, S., Das, S. (2023): Delineation of potential groundwater recharge zones using remote sensing, GIS, and AHP approaches. Urban Climate 48: 101415, https://doi.org/10.1016/j.uclim.2023.101415.

Usman, M. (2016): A study on the enhancing earthquake frequency in northern Pakistan: is the climate change responsible? Natural Hazards 82, 921–931, https://doi.org/10.1007/s11069-016-2226-z.

Van Westen, C. J. (2000): The modelling of landslide hazards using GIS. Surveys in geophysics 21(2), 241–255, https://doi.org/10.1023/A:1006794127521.

Wang, S. W., Munkhnasan, L., Lee, W.-K. (2021): Land use and land cover change detection and prediction in Bhutan's high altitude city of Thimphu, using cellular automata and Markov chain. Environmental Challenges 2: 100017, https://doi.org/10.1016/j.envc.2020.100017.

Ward, P. J., Blauhut, V., Bloemendaal, N., Daniell, J. E., de Ruiter, M. C., Duncan, M. J., Emberson, R., Jenkins, S. F., Kirschbaum, D., Kunz, M. (2020): Natural hazard risk assessments at the global scale. Natural Hazards and Earth System Sciences 20(4), 1069–1096, https://doi.org/10.5194/nhess-20-1069-2020.

Ward, P. J., Jongman, B.,Weiland, F. S., Bouwman, A., van Beek, R., Bierkens, M. F., … and Winsemius, H. C. (2020): Strong influence of El Niño Southern Oscillation on flood risk around the world. Proceedings of the National Academy of Sciences, 117(37), 22952–22958.

Yang, L., Luo, W., Zhao, P., Zhang, Y., Kang, S., Giesy, J. P., Zhang, F. (2021): Microplastics in the Koshi River, a remote alpine river crossing the Himalayas from China to Nepal. Environmental Pollution 290: 118121, https://doi.org/10.1016/j.envpol.2021.118121.

Yao, Y., Khan, A. Z. (2022): Predicting Pakistan's next flood. Science 378 (6619), https://doi.org/10.1126/science.ade7824.

Youssef, A. M., Pourghasemi, H. R. (2021): Landslide susceptibility mapping using machine learning algorithms and comparison of their performance at Abha Basin, Asir Region, Saudi Arabia. Geoscience Frontiers 12(2), 639-655, https://doi.org/10.1016/j.gsf.2020.05.010.

Zhou, S., Chen, G., Fang, L., Nie, Y. (2016): GIS-based integration of subjective and objective weighting methods for regional landslides susceptibility mapping. Sustainability 8(4): 334, https://doi.org/10.3390/su8040334.

Agricultural land suitability analysis in Manipur, India using GIS and AHP

Letminthang Baite[1,*], Niranjan Bhattacharjee[1], Jimmi Debbarma[2], Anup Saikia[1]

[1] Gauhati University, Department of Geography, India
[2] Tripura University, Department of Geography and Disaster Management, India
[*] Corresponding author: khokounmimin@gmail.com

ABSTRACT

This article aims to identify potential sites for agricultural use in the state of Manipur of north east India by employing the analytic hierarchy process in a geographic information system environment in conjunction with the use of remote sensing and soil data. Within the analytic hierarchy process, each terrain variable underwent a pairwise comparison and criteria weights were assigned according to their relative importance. Eight variables were selected and used in land suitability analysis for agriculture. It was found that Manipur had 57% (12,660 km^2) of its total geographical area suitable for agriculture. However, 8126 km^2 (37%) and 1374 km^2 (6%) of the total geographical area was currently and permanently unsuitable land respectively. The distribution of suitable land varied greatly, with highly, moderately and marginally suitable land covering only 8%, 16% and 33% respectively of the total geographical area. The highly suitable agricultural land is predominantly concentrated in the Imphal valley (70%), though 90% of moderately suitable and 96% of marginally suitable land also exist in the hills. The hilly areas constitute 96% and 97% respectively of currently unsuitable and permanently unsuitable land in the state. Suitable land comprises of land with low to medium altitude, gentle to moderate slopes, soil of fine or acceptable quality, and with minimal flood risk. Unsuitable lands tend to be diametrically opposite to these attributes with steep hill slopes. The nature of distribution of land suitability types influences the agricultural pattern in Manipur. Agriculture in the hill areas comprises mainly of shifting cultivation on hill slopes, whereas in the valley region it is irrigated and permanent. This analysis of Manipur has a wider applicability since the shifting cultivation-irrigated agriculture combination is similar to that which exists across much of the highlands of South East Asia.

KEYWORDS

agriculture; analytic hierarchy process; geographic information systems; land suitability, terrain; Manipur, India

Received: 10 November 2023
Accepted: 6 May 2024
Published online: 22 May 2024

Baite, L., Bhattacharjee, N., Debbarma, J., Saikia, A. (2024): Agricultural land suitability analysis in Manipur, India using GIS and AHP. AUC Geographica 59(1), 93–107
https://doi.org/10.14712/23361980.2024.6

1. Introduction

Terrain evaluation assesses land features such as topography, geology, soil quality, water availability, vegetation, and current land usage to determine its appropriateness for a specific activity (Beckett et al. 1972). Land evaluation analyses the essential properties of the terrain and its ability to support specific land uses sustainably over extended periods (Bandyopadhyay et al. 2009). Topographic characteristics are key to land capability and suitability analyses as they influence the irrigation system, soil quality, cost of land development, forms of agricultural plots, and crop diversity (Akinci et al. 2013; FAO 1985; Mahato et al. 2024). Topography influences the hydrological regime, climatic and meteorological conditions of a particular terrain which are important determinants of soil (Florinsky 2012; Nath et al. 2021). Soil and climate data are crucial for land evaluation and land capability classification (Sitorus 2010).

Land suitability (LS) analysis is a process of determining inherent land capabilities, its quality, potential, and suitability for different purposes (Zolekar and Bhagat 2015). Agricultural LS analysis is a way of ensuring food security in line with the United Nations sustainable development goals (SDG) (Akpoti et al. 2019). Indigenous communities leverage their traditional ecological knowledge and environmental acumen in the assessment and selection of agricultural land plots. Crops to be cultivated are chosen based on soil characteristics, insolation, and moisture availability. Relatively better agriculture sites are selected for the cultivation of rice, the principal crop. Indigenous knowledge is crucial in agricultural land suitability analysis (Feizizadeha and Blaschkeb 2013), but this method of land evaluation has limitations in the formal land use assessment. LS analyses have been undertaken concerning agroforestry in NEI (Nath et al. 2021), paddy cultivation (Mahato et al. 2024), vegetable farming (Sarkar et al. 2023), betel nut cultivation and crop acreage expansion (Hudait and Patel 2022). Being determined by several factors, LS requires a multicriteria assessment in its approach.

Multicriteria decision making is a method of processing a set of criteria into a single index of evaluation (Feizizadeh and Blaschke 2013). Numerous methods are available for multicriteria decision making such as artificial neural networks (Wang 1994), criteria matching process (Ritung et al. 2007), logical integration (Martin and Saha 2009), logic scoring preferences (Montgomery et al. 2016) and Analytic Hierarchy Process (AHP). AHP has proven to be an effective and methodical means of assessing intuition and subjective personal choices and incorporating them into objective mathematics (Saaty 2001). It provides a method to make assessments and decisions objectively using a simple pairwise comparison. The combination of GIS and AHP techniques is widely used across different disciplines (Podvezko 2009; Tempa 2022). The latter involves breaking down a decision into a hierarchy of criteria and sub-criteria and then assigning weights to each of these based on their relative importance (Saaty 2008). LS analyses deal with multiple factors that influence agriculture in varying ways. AHP uses pairwise comparison of data in which the criteria involved are compared in pairs which is simpler than taking all criteria considered at a time (Podvezko 2009).

The integration of AHP in a GIS environment has proved to be a versatile tool that has been used in a range of studies like LS analysis, groundwater potential mapping, and decision-making in diverse fields (Canco et al. 2021; Bozdağ et al. 2016; Akinci et al. 2013; Melese and Belay 2022; Hassan et al. 2020). Similar studies on paddy cultivation on parts of NEI (Mahato et al. 2024; Pawe and Saikia 2022) have been carried out. However, no such studies on Manipur have been undertaken. The majority of the population depends on agriculture and allied economic activities where shifting cultivation is the dominant agriculture method. Therefore, the objective of the present study is to evaluate LS for agricultural land use optimization using AHP in a GIS environment and to determine the distribution of land resource availability in Manipur. The hills of NEI of which the current study area (CSA) is a part are ethnically and physiographically similar to SE Asia (SEA). Therefore, this analysis has significantly wider applicability.

2. Study area

Manipur, in north-east India (NEI), extends from 23°83′N to 25°68′N latitude and 93°03′E to 94°78′E longitude (Fig. 1). The state has been referred to as a "Mini-Amazon" (Ganguly et al. 2023) being part of the India Burma biodiversity hotspot (Rai and Vanlalruati 2022) and is ecologically vulnerable (Jin et al. 2021). Imphal Valley (IV) consists of 10% of the state's TGA (22,327 square kilometers) while the surrounding Hills of Manipur (MH) constitute 90% of the tract. Geological formations in the state include Tipam, Surma, Barail, and Disang, while IV is formed of recent alluvium soils (GSI 2011). The Tipam and Surma are soft, friable and poorly consolidated arenaceous rocks forming highly dissected hills and valleys. The Barail predominantly comprises coarse, massive, well-bedded sandstone and shales. Disang is composed mainly of shales and occasional limestone blocks interbedded by sandstones. The Barail and Disang are depicted by moderately dissected hills and valleys. Each geological group exhibits varying base cation exchange capacity (CEC) of soil. The CEC (cmol/kg) in the A horizon of major soil series in the state are 9.2 (Surma), 11 (Disang), 14 in Suongpeh series and 17.3 in Leimakhong series at the adjoining zone of Disang, and Barail rocks (Sahoo et al. 2020). The hill areas generally exhibit higher soil organic

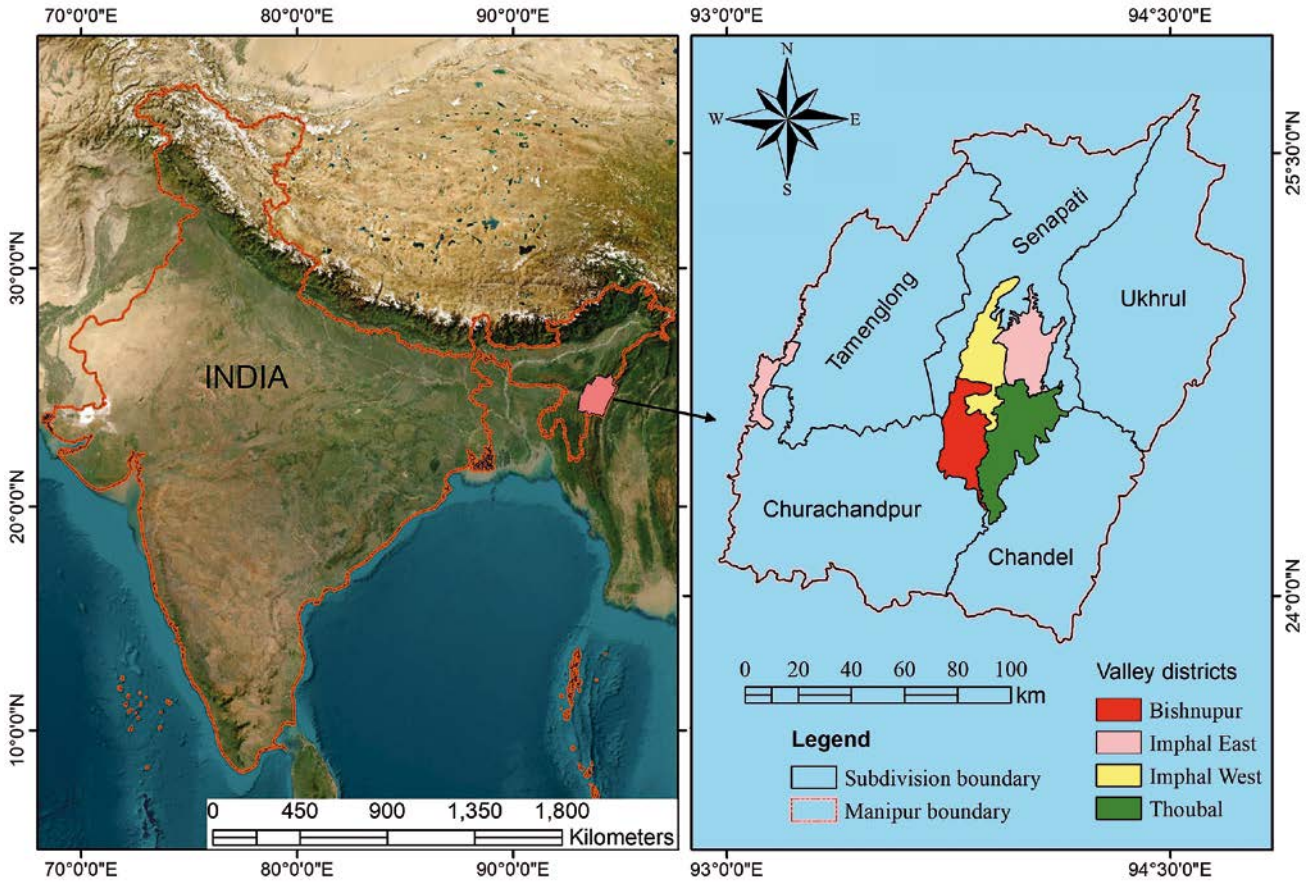

Fig. 1 Location of thestudy area.

carbon (SOC) content than IV (Roy et al. 2018). Inceptisols, Ultisols, Entisols, and Alfisols which constituted 38.4%, 36.4%, 23.1%, and 0.2% respectively of TGA are the dominant soil types (Sen et al. 1996).

Geomorphological landforms are categorized into four types based on their origin: structural, denudational, fluvial, and lacustrine. Structural origin hills and valleys are highly or moderately dissected, but some low dissected hills and valleys belong to this group. Denudational landforms, here, are usually pediplains, piedmont slopes, low hills, and valleys. The fluvial origin landforms are the old alluvial flood plain, the young alluvial flood plain, and the active flood plain. Lastly, lacustrine plains are found mostly around Loktak Lake (GSI and NRSC 2012). Fig. 2 illustrates the topography and relief of Manipur while Tab. 1 summarizes the spatial distribution. The flat and gently sloping landforms accounted for 16% of the TGA while hills and mountains make up the rest of the state. Topographically, about 84% of the TGA of Manipur is formed of hilly and mountainous terrain.

NEI has a monsoon climate (Ganguly et al. 2023). Manipur lies close to the Tropic of Cancer and acquired the characteristics of a tropical climate but north of the 25°N latitude, it has a warm temperate mesothermal climate (Dikshit and Dikshit 2014). It has a mean annual temperature of 19 °C to 20 °C and an average rainfall of 2000 mm to 2400 mm. The CSA falls within the Eastern Himalayan agroclimatic region, but it has three distinct agro-ecological zones (AEZ) (https://horticulture.mn.gov.in/soil_of_manipur.html). The warm and humid AEZ with a thermic ecosystem has a length of growing period (LGP) of 300–330 days. The hot and humid AEZ has a hyperthermic ecosystem and LPG of 270–300 days. The warm and perihumid AEZ has an LGP of 330–365 days. The AEZs are characterized by deep and fine red and lateritic soils that

Tab. 1 Areal distribution of different landforms.

Relief Types	Slope (in degrees)	Area (in km^2)	Area (in %)
Flat	< 1.5	1657	7.45
Undulating/ Gently Sloping	1.5–4.0	780	3.51
Rolling/Sloping	4.0–7.5	1252	5.63
Hilly	7.5–15	4928	22.17
Mountainous	15–20	4754	21.38
Steep/Mountainous	20–30	7029	31.62
Very Steep/Highly Mountainous	> 30	1831	8.24
Total Area		22231	100

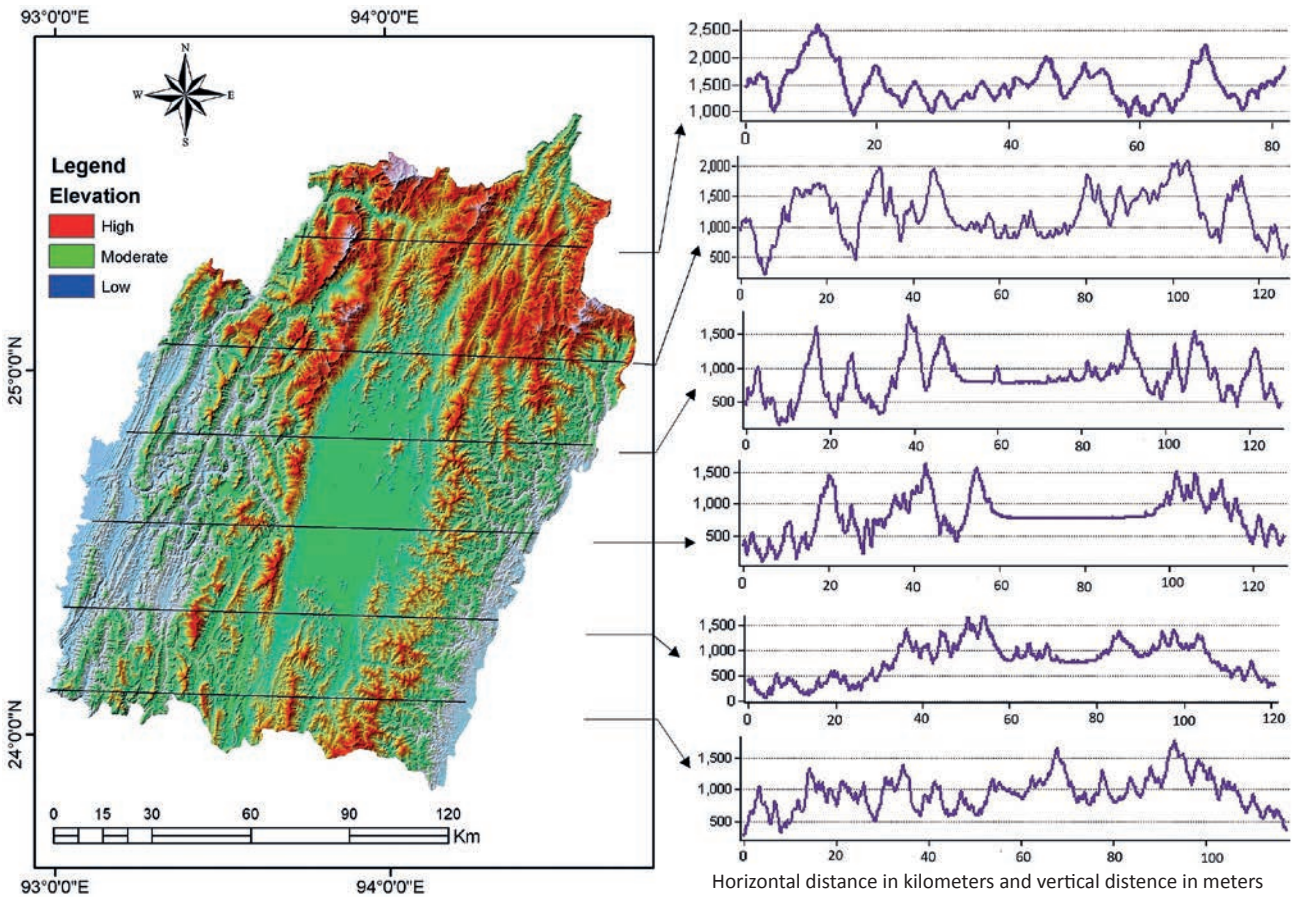

Fig. 2 Relief and elevation profile of the study area.

have available water capacity of 200–300 millimeters per meter (Sen et al. 1996).

The soils are generally hyperthermic and have low cation exchange capability and base saturation, yet it has high exchangeable calcium and magnesium ions and high organic carbon content (Sahoo et al. 2020). Despite the prevalent shifting cultivation and soil loss, agriculture can effectively continue due to the constant replenishment of soil organic through the fall of litter. The AEZ and associated soil characteristics of Manipur show the prospects for crop diversity (Sen et al. 1996). However, there are concerns regarding the effect of climate change on water resources, forests, the environment (GoM 2013), and agricultural productivity in the state (Takhell 2023). According to the CEEW (Council on Energy, Environment and Water) Report 2021, Manipur ranks 6th in the climate vulnerability index. The dependence of the population on activities like agriculture, forestry, and fishing makes them particularly vulnerable to climate change (Devi et al. 2023).

3. Data and methods

Topographic data and soil information were the main datasets used in the analysis (Fig. 3). The Shuttle Radar Topographic Mission (SRTM) (https://earthexplorer.usgs.gov) Digital Elevation Model (DEM) was used to extract topographic information (i.e. slope and altitude). The altitude and slope map of the study area were prepared using the 30 meter DEM in ArcGIS 10.8 (www.esri.com). Geomorphologic attributes such as alluvial plains, flood plains, piedmont slopes, lacustrine swamps, and marshes were acquired from the Geomorphology of Manipur (1 : 50,000 scale) from the Bhuvan web portal (https://bhuvan-app1.nrsc.gov.in/thematic/thematic/index.php). The data was prepared jointly by the Geological Survey of India (GSI) and the National Remote Sensing Centre (NRSC). We manually digitized the geomorphic units of the study area in ArcGIS. The vector file of the data was assigned separate grid codes for each geomorphic unit and converted to raster. We derived soil attributes from the soil map of Manipur available at the scale of 1 : 500,000. The map was prepared by the National Bureau of Soil Survey and Land Use Planning (NBSS & LUP) and the Directorate of Horticulture and Soil Conservation, Manipur (https://esdac.jrc.ec.europa.eu/content/manipur-soils). The soil mapping units consisted of dominant (50% or more of the delineated area) and subdominant soil families (Sen et al. 1996). Four soil attributes – depth, erosion, drainage, and flood hazards – were digitized manually

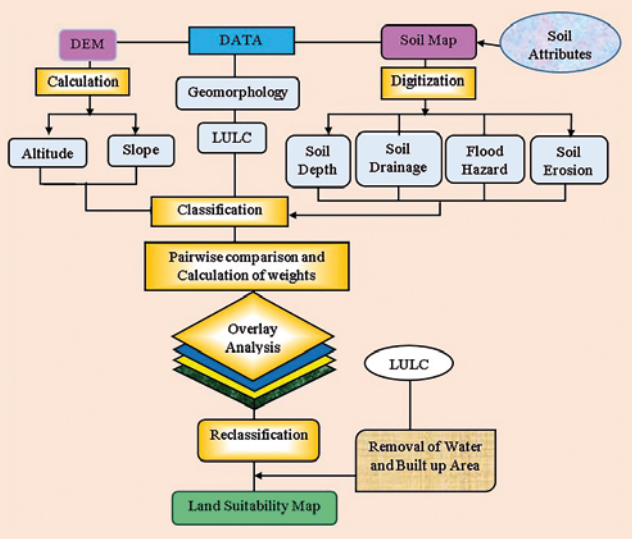

Fig. 3 Flow chart and methodology.

from the soil map in ArcGIS. Subsequently, the digitized vector shapefile representing these soil characteristics was converted into raster datasets. The global land use and land cover (LULC) data available at 15-meter resolution was downloaded from the ESRI website (https://livingatlas.arcgis.com/landcover). The LULC classes used in this analysis were built-up, bare ground, crop or fallow lands, flood vegetation, range and open grassland, and dense forest. Of these, the extent of the bare ground class was negligible, crops and fallow land constitute irrigated permanent agricultural lands (PAL). The LULC was reclassified into five classes after combining similar classes for the present study. Finally, all the raster data prepared for LS analysis were resampled into a uniform spatial resolution of 100 meters and projected into a uniform UTM coordinate system (Fig. 4).

3.1 Analytic Hierarchy Process (AHP)

AHP decision making involves several steps: identification of variables, hierarchical structuring of the variables, pairwise comparison of each element, and calculation of weights. The involvement of multiple criteria and intricate relations among the elements in AHP makes the assignment of criteria weight a complex process. However, AHP arranges criteria in a hierarchical structure and enables a pairwise comparison of the elements. This technique is simple and efficient as it allows qualitative estimates of experts to be converted to quantitative ones (Podvezko 2009; Gupta and Dixit 2022).

A comparison between two elements was performed to determine how many times one element was dominant over the others (Saaty 2008). The pairwise comparison was based on subjective assessment and intuitive judgment among the criteria (Saaty 2001). The criteria used in LS were judged based on their relative importance (Tab. 2) Saaty (2008). We performed a pairwise comparison based on information about altitudes (Allan 1986), slopes (FAO 1976) and soil attributes (FAO 1967; Grose 1999) and the pairwise judgment in similar studies (Hudait and Patel 2022; Mahato et al. 2024; Zolekar and Bhagat 2015). The opinions of elderly farmers, especially in hill agriculture, and the authors' intuition during the field observations played a crucial role in pairwise judgment. Based on Saaty's preference scale, slope exacted a significant importance over soil depth, drainage, erosion, and LULC respectively (Tab. 3). The pairwise matrix consists of n (n − 1)/2 elements of comparison for n numbers of elements (Akinci et al. 2013). Interpretation of other elements in the pairwise matrix was the same as detailed above.

When performing pairwise comparisons inconsistencies often occur. The logical consistency of the pairwise comparison can be determined by the consistency ratio (CR) as suggested by Saaty (Akinci et al. 2013). The validity of the pairwise comparison matrix was confirmed by CR with an upper limit of 0.10 (Saaty 2008). The calculated CR of the pairwise matrix was 0.028 (Tab. 4) well within the threshold value of 0.1. Therefore, the pairwise matrix obtains a sufficient degree of logical consistency in the pairwise comparison.

Tab. 2 Fundamental scale of comparison for pairwise comparision (Saaty 2008).

Intensity of importance	Definition	Explanation
1	Equal importance	Two activities contribute equally to the objective
3	Moderate importance	Experience and judgment strongly favor one activity over another
5	Strong importance	Experience and judgment strongly favor one activity over another
7	Very strong or demonstrated importance	An activity is favored very strongly over another; its dominance demonstrated in practice
9	Extreme importance	Preference for one activity over the other is highest
2, 4, 6 and 8	Intermediate values	When compromise is needed
Reciprocals	If activity i has one of the above numbers assigned to it when compared with activity j, then j has the reciprocal value when compared with i.	

Tab. 3 Pairwise comparison matrix of criteria based on Saaty's fundamental scale (2008).

Criteria	Slope	Soil depth	GM	Altitude	Soil drainage	Flood	Soil erosion	LULC	Criteria weight (CW)
Slope	1	3	4	4	5	6	7	9	0.34
Soil depth	1/3	1	3	4	5	6	5	8	0.24
GM	1/4	1/3	1	1	3	5	5	7	0.13
Altitude	1/4	1/4	1	1	3	4	3	5	0.11
Soil Drainage	1/5	1/5	1/3	1/3	1	3	3	5	0.07
Flood	1/6	1/6	1/3	1/4	1/3	1	2	3	0.06
Soil Erosion	1/7	1/5	1/5	1/3	1/3	1/2	1	2	0.03
LULC	1/9	1/8	1/7	1/5	1/5	1/3	1/2	1	0.02

3.2 Description of criteria used in LS evaluation

Altitude: Altitude significantly influences agricultural land use and cropping patterns, offering opportunities for specialized agriculture tailored to specific elevation zones (Allan 1986; Bonan 2015). The altitude of the CSA was categorized into five classes (Tab. 5). Crops and livestock thrive at altitudes below 180 meters but above this zone, some crops are vulnerable to frost (Grose 1999). Limited crops thrive at 380–500 meters and there is little grazing ground available at 600–900 meters. Beyond 900 meters elevation, no activities are possible.

Slope: Slopes are the basis for the FAO classification of agricultural LS based on the degree of limitation of mechanization, trafficability, and accessibility. Slopes are a primary factor in site selection for agricultural land use (FAO 1976) since they are related to soil depth, texture, moisture, and nutrient availability. They can be categorized into five classes (Tab. 5) based on the limitations they present to different agricultural activities (FAO 1976). For instance, slopes less than 4° have more than 90% tractor efficiency while only primitive implements can be used on slopes greater than 35°.

Geomorphology (GM): Geomorphic units like alluvial and flood plains are ideal for agriculture due to the high soil fertility in these zones. It is an important component of LS analyses for paddy cultivation (Mahato et al. 2024; Anusha et al. 2023). Eight geomorphic units are available in the CSA which were assigned weights and ranked according to their importance for agriculture (Tab. 5).

Soil depth: It determines the volume of soil that can be used by crops. Deep soils are preferred for agriculture (FAO 1967). Types of soil depth in CSA are deep (> 100 cm), moderately deep (75–100 cm), moderately shallow (50–75 cm), and shallow (25–50 cm). The effective rooting in crops is restricted by soil depth in varying degrees as severe, moderate, slight, and no limitations depending on the thickness of the soil horizon (Bhaskar et al. 2021). Soil depth as provided in the soil mapping units is given in Tab. 5.

Soil drainage: It is determined by soil texture, topography, and water table which control air and nutrient availability thus determining soil productivity (Sen et al. 1996). Soil drainage efficiency was interpreted from an earlier analysis (Grose 1999) and were assigned weights accordingly. Soil drainage classes found in CSA ranged from extremely poor to excessively drained soils (Tab. 5).

Flood hazard: The state has slight, moderate, and severe flood hazard zones and most of the MH faces slight or no flood hazards. However, areas along the river banks are prone to seasonal flooding. IV is vulnerable to occasional severe flooding due to heavy runoff and low infiltration capacity of the soil as a result of land degradation in the catchment area (https://mastec.nic.in/images/Completed_projects/ReportFloodHazard.pdf).

Soil erosion: Soil erosion in the CSA ranged from slight to severe (Tab. 5). The IV has very slight or no erosion but the rest of Manipur faces moderate to severe erosion attributable to the hilly topography, land degradation, and heavy rainfall (Roy et al. 2018). Slight erosion manifests as damaged surface horizons, yet soil biotic conditions remain undisturbed (Jahn et al. 2006). Moderate erosion displays evident signs of soil loss, impacting biotic functions. The annual soil loss in terms of tons per hectare through slight, moderate, and severe erosion amounted to 10–20, 20–40, and >40 tons/ha/year respectively (NRSC 2019).

LULC: Cropland lies fallow during the post-harvest or off-season. Rangeland is an open area covered by homogeneous plants such as grass and stunted vegetation that is open to other land uses. On the other hand, built-up and water bodies cannot be converted into PAL. Flooded vegetation is covered with a variety of plants like paddy, grass, and shrubs in seasonally flooded areas (Karra et al. 2021). Forests with trees higher than 15 meters were identified as dense forests.

Tab. 4 Pairwise comparison result.

Maximum Eigen Value (λ_{max})		8.280
Consistency Index (CI)	CI = (λ_{max} – n)/(n–1)	0.040
Consistency Ratio (CR)	CR = CI/RI	0.028
Random Index (RI)		1.410

Tab. 5 Criteria and sub-criteria weight assignment.

Main criteria	CWCW	Criteria level two	Score (x)
Slope classes	0.34	Level to gentle	9
		Gentle slope	7
		Moderate slope	5
		Steep slope	3
		Very steep slope	1
Soil depth	0.24	Deep soil	7
		Deep associated with moderately deep soil	6
		Deep associated with shallow soil	5
		Moderately shallow and deep soil	4
		Other soils	1
Geo-morphology	0.13	Alluvial plain	9
		Flood plain	9
		Pediment pediplain complex	7
		Piedmont slope	7
		Low dissected hills and valleys	5
		Moderately dissected hills and valleys	5
		Lacustrine swamp and marsh	3
		Highly dissected hills and valleys	3
		Water body	1
Altitude zones	0.11	0-150	5
		150-300	4
		300-450	3
		450-600	2
		600 Above	1
Drainage effectiveness	0.07	Well drained	7
		Well drained associated with poorly drained	5
Drainage effectiveness	0.07	Well drained associated with excessively drained	5
		Somewhat excessively drain associated with well drain	4
		Poorly drained associated with well drained	3
		Excessively drained associated with well drained	3
		Others	1
Flood hazard	0.06	None	5
		Slight flooding	4
		Moderate and severe	3
		Moderate to severe	2
		Severe and slight	1
Soil erosion	0.03	No erosion	9
		Very slight erosion	9
		Slight erosion	7
		Moderate erosion	5
		Moderate	5
		Low erosion	3
		Moderate to severe erosion	3
		Moderate erosion; severe in parts	3
		Severe erosion, moderate in parts	1
		Severe	1
LULC	0.02	Crops/fallow lands	7
		Range, open grassland, expose soil/rocks	5
		Flood vegetation, rice paddy	4
		Trees higher than15m, dense vegetation	3
		Others	1

Criteria weights (Fig. 4) of the elements were calculated by normalizing the pairwise comparison matrix (Tab. 3). The normalized pairwise matrix was created by dividing the column elements of the matrix by the sum of the respective columns. The sum of the elements of the rows in the matrix was calculated, then each sum of a row was divided by the sum of their total (Akinci et al. 2013; Podvezko 2009). The weight vector of the criteria ranged from 0 to 1 the sum of which equalled 1 (Tab. 5). Assignment of the sub-criteria rank was done on a scale between 1 and 10. For instance, slope < 4° was assigned a score of 9, slope 8–20° was given 5 while very steep slopes > 35° scored only 1. The higher the score the more favourable the sub-criteria and minimal constraints were posed for agriculture. Similarly, the ranks for other elements of the sub-criteria were assigned based on their importance to agriculture. Scores were allocated based on the degree of suitability or constraints of the sub-criteria for agricultural application. These were in concordance with similar analyses (Anusha et al. 2023; Bandyopadhyay et al. 2009; FAO 1976; Grose 1999; Hudait and Patel 2022; Mahato et al. 2024; Zolekar and Bhagat 2015).

The weighted sum overlay analysis for LS evaluation was run in the Spatial Analyst tool of ArcGIS 10.8 using the formula (Zolekar and Bhagat 2015; Mahato et al. 2024):

$$LSI = \sum_{i=1}^{n} CWiXi$$

Where LSI is the land suitability index, *CWi* indicates the weight of the main criteria, *Xi* represents the assigned sub-criteria score of the i^{th} land suitability criteria, and *n* denotes the total number of selected parameters.

The output of the weighted sum overlay analysis yielded continuous raster data where the maximum value indicated the most suitable land and the least

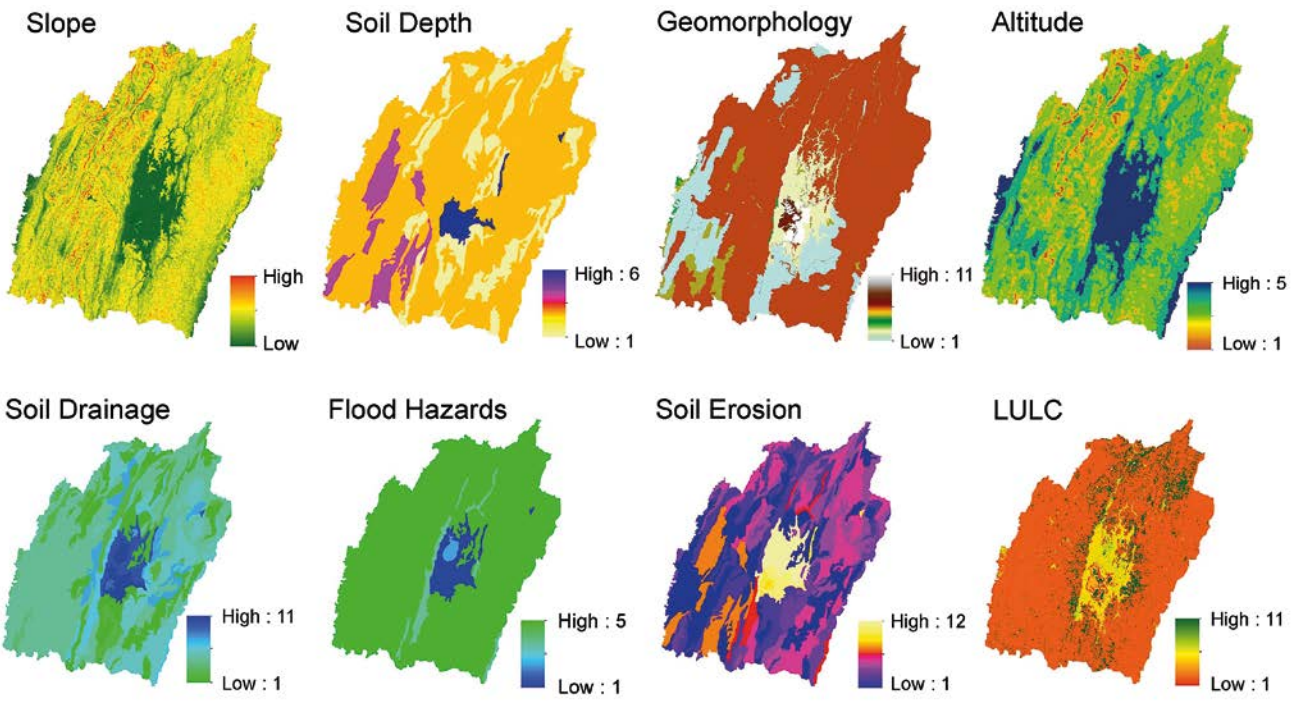

Fig. 4 Ranked criteria.

value represented unsuitable land. The continuous data was reclassified into five classes according to FAO (1976) as highly suitable, moderately suitable, marginally suitable, currently unsuitable, and permanently unsuitable (Fig. 5). The LS classification system of FAO was employed since it has been adopted by several studies (Hudait and Patel 2022; Kazemi and Akinci 2018; Zolekar and Bhagat 2015). The assignment of different suitability classes was based on Jenk's classification method. This method works on the principle of maximum homogeneity of values within a class. Jenk's classification has become a standard geographic classification algorithm (North 2009) in which the geographical environmental unit has a minimum deviation from the mean class. It is a "data classification method designed to determine the best arrangement of values into different classes" (Chen et al. 2013) giving optimal results. To determine the extent of LULC in different LS categories, the latter were overlaid on the former. The area covered by each LULC class overlapped by the LS classes was evaluated.

4. Results and discussion

Land Suitability is divided into two sub-groups – suitable land (S) and not suitable land (N). The former was further subdivided into three classes, namely, highly suitable (S1), moderately suitable (S2), and marginally suitable (S3). N was divided into currently unsuitable (N1) and permanently not suitable (N2) categories (Fig. 5). The areal distribution of different land suitability classes in Manipur exhibited significant variation (Tab. 6).

S1 was characterized by level or gentle slopes, deep soils, and was situated in the low altitude zone. Soils were either well or poorly drained and experienced slight to moderate flooding, and slight to no erosion. This land category enabled the cultivation of wet paddy during the monsoon season and vegetables in other seasons (Fig. 7A). S1 was well-suited for agriculture and had immense potential for intensive agriculture (Zolekar and Bhagat 2015). S2 land had a gentle slope and occurred at slightly higher altitudes (Fig. 7B). Soils were moderately deep to deep and were generally associated with slight to moderate erosion. Such lands were cultivable and productive provided suitable conservation and management system were practiced on them (Zolekar and Bhagat 2015). Areas under S2 with moderate to gentle slopes were used in terrace cultivation while those prone to flooding and waterlogging were suitable for paddy cultivation. S3 land was the most widespread suitability

Tab. 6 Area under different land suitability classes.

Suitability Class	Area in km²	Area in %
Highly Suitable Land (S1)	1793	8
Moderately Suitable Land (S2)	3588	16
Marginally Suitable Land (S3)	7297	33
Currently Not Suitable (N1)	8126	37
Permanently Not Suitable (N2)	1374	6
Total	22158	100

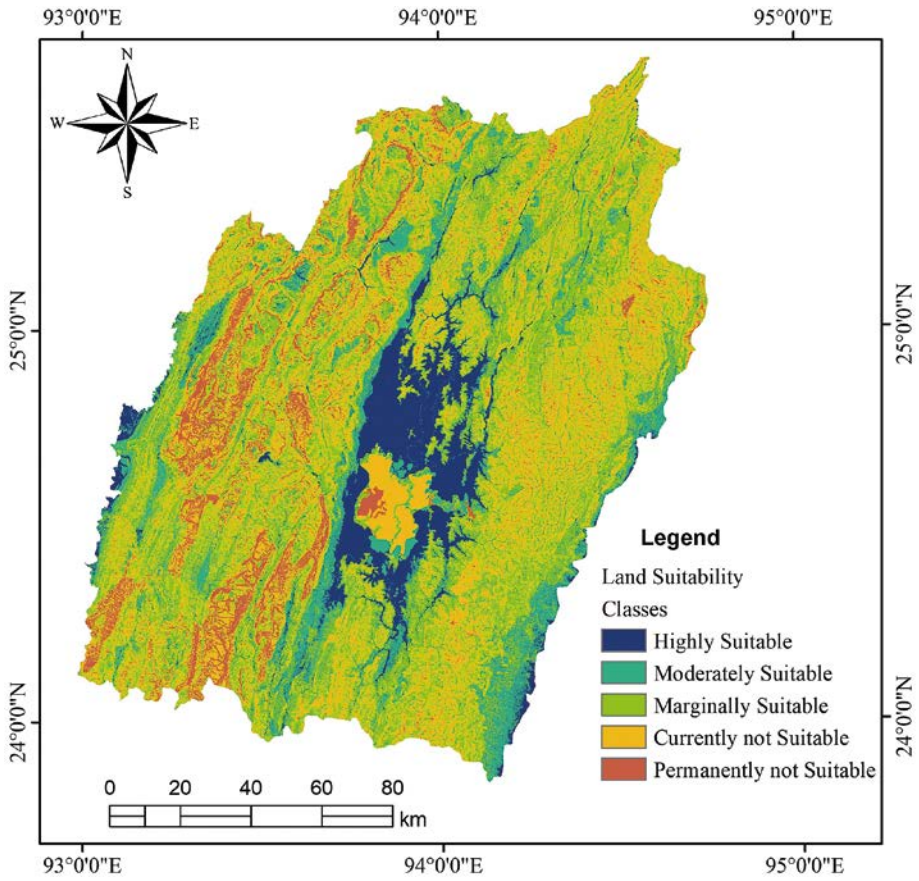

Fig. 5 Land suitability.

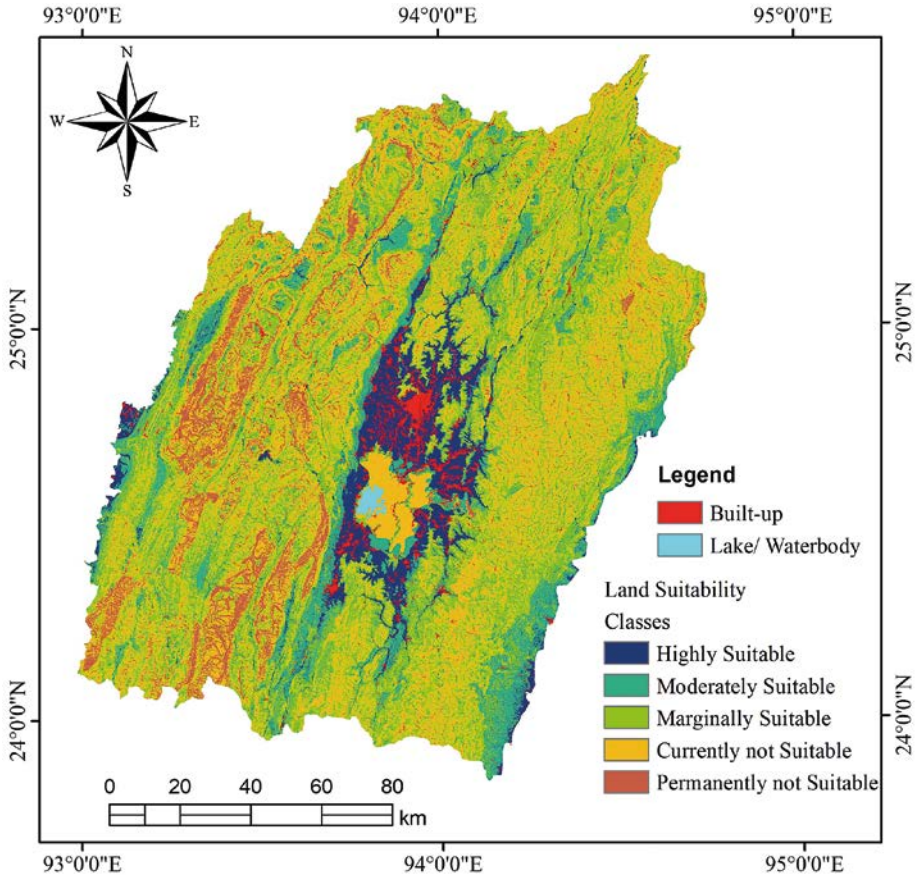

Fig. 6 Land suitability (built-up and water-body removal).

Fig. 7A Wet paddy cultivation on highly suitable land (Date: 20/8/2019).

Fig. 7B Paddy cultivation on moderately suitable land (Date: 04/10/2021).

Fig. 7C Paddy cultivation on marginally suitable land (Date: 02/10/2021).

Tab. 7 Land use land cover distribution in different districts of Manipur.

Districts	Area of LULC in square kilometres					
	Built-Up	Agriculture	Scrub	Flood vegetation	Forest	Water
Bishnupur	71	203	32	88	23	63
Chandel	30	35	322	0	2795	2
Churachandpur	56	55	347	0	4234	19
East Imphal	107	200	37	0	250	4
Senapati	95	84	755	0	3960	9
Tamenglong	37	12	176	0	3960	9
Thoubal	119	342	73	24	111	45
Ukhrul	46	6	529	0	3870	1
West Imphal	130	239	30	18	50	20

class found on moderate to steep slopes of hills at higher altitudes, with no flood hazards, characterized by excessive soil drainage and moderate to severe soil erosion. Agriculture, especially terrace farming, was possible on marginally suitable land with proper conservation and management strategies (Zolekar and Bhagat 2015). S3 were devoted mainly to shifting cultivation in MH (Fig. 7C). Due to significant limitations in S3, production was low, and also expenditure on farm inputs tended to rise. As a consequence, the profit of farm production was adversely affected (Ritung et al. 2007). N1 and N2 lands were characterized by steep slopes and found at higher altitudes where soils were shallow and prone to severe erosion. Although the N1 and N2 classes were of little value from the agricultural perspective, they were generally undisturbed and perennially under vegetation. Thus, different LULC classes (Tab. 7) distributes across various LS categories.

The area suitable for agriculture constitutes roughly 57% of the TGA of Manipur, with the remaining 43% land being unsuitable for cultivation. Of the total 1793 km^2 of S1 class, 23% was built-up and about 1% had reservoir water from construction of dams resulting in the submergence of fertile plains along the river course. The area of LULC under different LS classes is given below (Tab. 8). The bulk of S3 (86%) was under forest and scrubland (12%) while built-up and cropland were insignificant. Manipur had 4565 km^2 highly suitable and 10482 km^2 suitable for agroforestry (Nath et al. 2021). The estimate of land capability Class II in the state stood at 9% of its TGA (Sen et al. 1993). The soils in this capability class had slight limitations but were cultivable with proper management strategies. The S1 (highly suitable land) in this study (8%) was close to the area of IIws and IIIw combined (9.1%). Manipur has 52.87% of S1 devoted for PAL (Tab. 8). This LS class was characterized by gentle slopes, high annual rainfall on floodplains and was conducive to paddy cultivation (Mahato et al. 2024).

About 7% (119 km^2) of S1 land in Manipur was scrub forest or range land. Scrub or range lands are degraded forests with minimal vegetation cover. Therefore, S1 has the potential to be converted as PAL without unduly adverse effects occurring on the green cover. The extent of S1 within forest cover is 16% or 288 km^2 and can be expanded for PAL. The share of S1 available for expansion into PAL is small compared to S2. Additionally, conversion from forest land to PAL is not an environmentally friendly course of action. Although 3243 km^2 of S2 class is available for conversion into PAL it remains under-utilized. S2 has the potential for expansion and improved sustainable agriculture. Manipur depends on imported food grains from other Indian states yet 52% of the state's population is engaged in agriculture and allied sectors (GoM 2015). One important reason for the limited expansion of PAL is the high cost of land development and maintenance. There is a pressing need for the expansion of sustainable agriculture. Currently, agriculture expansion is feasible in S1 and S2 LS classes,

Tab. 8 Area of LS class under different LULC classes in Manipur.

Land suitability class	LULC classes (area in km^2)						
	Built-up	Fallow / crop (PAL)	Flood vegetation	Range / scrub	Dense forest	Water-body	Total
S1	413	948	1	119	289	23	1793
S2	130	168	10	439	2804	36	3588
S3	121	14	6	854	6251	31	7279
N1	22	41	78	785	7123	77	8126
N2	3	2	35	94	1236	4	1374

however, it entails adequate financial investment. The S3 class in the MH (Hills of Manipur) is used for shifting or jhum cultivation. Among the NEI states, Manipur has the highest area under shifting cultivation and the minimum annual area under it is 900 km^2 (Choudhury and Sundriyal 2003). It is not suitable for PAL due to topographic constraints. Floods and water logging are the main limitations in the IV of Manipur. Yet the latter contributes a major share of the state's agricultural output due to favourable climatic, hydrogeologic and topographic conditions (Thockchom and Kshetrimayum 2019).

The share of S1 class is highly inequitable among the districts (Tab. 9). The four districts in IV account for 71% of the S1 land in Manipur. However, due to the concentration of population and large scale developmental activities in the IV, S1 lands were converted to other land use. The MH accounts for only 29% of S1 exhibiting the hill-valley contrast in the availability of suitable agricultural land in the state. In terms of spatial extent, the former spreads over 20,089 km^2 i.e. 89.98% of the TGA of the state. Our analysis shows that S1 land for PAL is inadequate in Manipur, though the average size of operational land holding was 1.14 hectares in 2015–2016 (MoA&FW 2018). According to the latest Agriculture Census (2015–2016), the total operational land holding in the state was 1720 km^2 out of which 45.9% lie in the hill areas (MoA&FW 2018). In the MH, irrigable lands suitable for PAL are scarce, therefore, people have little option than to take recourse to shifting cultivation. The latter is an age-old practice rooted in their culture. Additionally, people are involved in economic activities such as fuelwood collection, charcoal making, and collection of forest products. In the valley region, the S1 class is prevalent, and wet paddy cultivation dominates agriculture, while animal husbandry, fish farming, and vegetable crops are practiced as well.

The man-land ratio is high but the quality of land is poor in MH due to topographic constraints. The availability of S1 land in IV and MH is highly inequitable (Tab. 10). This resulted in limited accessibility, high cost of agriculture management, difficulties in the transportation of farm produce. In the IV of Manipur land is scarce and the man-land ratio is low. Yet, it is endowed with favourable natural conditions such as low soil erosion and fertile alluvial soil, and social factors like accessibility, market, and modern agriculture equipment. Historically, the hill and valley people were one people but the preference for an agricultural system as a result of distinct geographical attributes has caused an economic gap and other cultural differences to develop over time (Phanjoubam 2005). The distinct geographical entity in Manipur, now, forms culturally and economically different populations in the state. The hill dwellers are at a relatively disadvantageous position vis-vis their counterparts in the valley in terms of agriculture and allied opportunities.

In addition to the terrain factors, the effect of global climate change on agriculture production remains an unavoidable issue. The erratic and changing pattern of precipitation in the past few years resulted in low crop yield (Takhell 2023). There are perceptions of climate change effects on agriculture among the farmers in the NEI region (Devi et al. 2023; Baruah et al. 2021). That Manipur is vulnerable to floods and designated as a flood hotspot (Mohanty and Wadhawan 2021) poses a challenge to its agricultural sector. Additionally, extreme weather events that are projected to get accentuated are slated to affect crop yields (Roy et al. 2018). The situation Manipur is faced with is not dissimilar to that faced in other parts of highland SEA (Boral and Moktan 2022).

Topographic and soil data are essential criteria in the LS analysis (Akinci et al. 2013; Kazemi and Akinci 2018; Zolekar Bhagat 2015) and climatic data are sometimes, but not always, incorporated in studies dealing with specific crops (Nath et al. 2021). The selection of criteria for LS analysis varies among authors based on the specific objectives of their study and the geographical characteristics of the study area

Tab. 9 Area of land suitability classes in different districts.

Districts	S1		S2		S3		N1		N2	
	km^2	%	km^2	%	km^2	%	km^2	%	km^2	%
Bishnupur	234	13	53	2	35	1	118	1	40	3
Imphal East	329	18	116	3	104	1	42	1	0	0
Imphal West	342	19	47	1	28	0	71	1	0	0
Thoubal	359	20	137	4	92	1	120	1	6	0
Chandel	145	8	727	20	1187	16	1079	13	16	1
Churachandpur	150	8	802	22	1541	21	1644	20	539	39
Senapati	140	8	655	18	1269	17	1294	16	112	8
Tamenglong	42	2	502	14	1311	18	1739	21	585	43
Ukhrul	52	3	549	15	1712	24	2018	25	75	5
Total	1793	100	3588	100	7279	100	8126	100	1374	100

Tab. 10 Absolute man-land ratio.

Regions	District	Population (2011)	S1 Area (km²)	Person / km²
Imphal valley	Imphal East	456113	709	643
	Imphal West	517992	558	928
	Bishnupur	221422	496	446
	Thoubal	422168	514	821
Manipur hills	Senapati	479148	3271	146
	Churachandpur	274142	4570	60
	Ukhrul	183998	4544	40
	Tamenglong	140651	4391	32
	Chandel	144182	3313	44

(Mahato et al. 2024). The present analysis being concerned with agriculture suitability in general in both the tropical (Awb) and humid warm temperate (Cfb) climates of Manipur (Dikshit and Dikshit 2014) felt that climatic data was not an overriding requirement. The climatic conditions in Manipur are typically conducive to agriculture (Sen et al. 1996) hence climatic parameters was not included in the LS analyses.

5. Conclusion

The rationale behind this analysis was to consider agriculture land suitability in Manipur that would have applicability to other hill regions in SEA. The use of the AHP technique in a GIS environment has simplified the terrain evaluation process by analyzing soil and topographic data. The findings show that S1 is scarce: about half of its area is devoted to cropping and settlement. In the remaining portion of S1, there is potential for expansion of PAL at the cost of forest and scrubland. The majority of the S2 and S3 lands are found in the MH where shifting cultivation has been a traditional practice for sustenance. However, the operation of shifting cultivation accelerates deforestation and environmental degradation in the state, calling for the need for research to identify a more suitable and sustainable method of cultivation. Soil erosion is a major concern in the hills whereas flooding and water logging are the challenges in the valley. The analyses of land capability is necessary in the hill-valley complex of Manipur and it is hoped would add to the scanty literature pertaining to Manipur in this respect.

Acknowledgements

The authors acknowledge using the computing facilities at the Prof. M.M. Das Advanced Study and Resource Cell at the Dept. Of Geography, Gauhati University.

References

Akinci, H., Özalp, A. Y., Turgut, B. (2013): Agricultural land use suitability analysis using GIS and AHP technique. Computers and Electronics in Agriculture 97, 71–82, https://doi.org/10.1016/j.compag.2013.07.006.

Akpoti, K., Kabo-bah, A. T., Zwart, S. J. (2019): Agricultural land suitability analysis: State-of-the-art and outlooks for integration of climate change analysis. Agricultural systems 173, 172–208, https://doi.org/10.1016/j.agsy.2019.02.013.

Allan, N. J. R. (1986): Accessibility and altitudinal zonation models of mountains. Mountain Research and Development 6(3), 185–194, https://doi.org/10.2307/3673384.

Anusha, B. N., Babu, K. R., Kumar, B. P., Sree, P. P., Veeraswamy, G., Swarnapriya, C., Rajasekhar, M. (2023): Integrated studies for land suitability analysis towards sustainable agricultural development in semi-arid regions of AP, India. Geosystems and Geoenvironment 2(2): 100131, https://doi.org/10.1016/j.geogeo.2022.100131.

Bandyopadhyay, S., Jaiswal, R. K., Hegde, V. S., Jayaraman, V. (2009): Assessment of land suitability potentials for agriculture using a remote sensing and GIS based approach. International Journal of Remote Sensing 30(4), 879–895, https://doi.org/10.1080/01431160802395235.

Baruah, U. D., Saikia, A., Robeson, S. M., Mili, N., Chand, P. (2021): Perceptions and adaptation behaviour of farmers to climate change in the upper Brahmaputra Valley, India. Environment, Development and Sustainability 23(10), 15529–15549, https://doi.org/10.1007/s10668-021-01309-z.

Beckett, P. H. T., Webster, R., McNeil, G. M., Mitchell, C. W. (1972): Terrain Evaluation by Means of a Data Bank. The Geographical Journal 138(4), 430–449, https://doi.org/10.2307/1795497.

Bhaskar, B. P., Srinivas, S., Kumar, S. C. R., Ramamurthy, V., Maske, S., Sujatha, K, Rajendra, H. (2021): Visual signs of Biophysical indicators for assessing the status of degradation in drylands of Pulivendula tehsil, Kadapa district, Andhra Pradesh. NBSS publication No.1151, NBSS & LUP, Nagpur.

Bonan, G. (2015): Earth's Climate. In: Ecological climatology: concepts and applications. 3rd Ed. 73–100.

Cambridge University Press, https://doi.org/10.1017/CBO9781107339200.

Boral, D., Moktan, S. (2022): Mapping the spatial distribution of the invasive Mexican Sunflower Tithonia diversifolia (Asteraceae) in South East Asia. Journal of Asia-Pacific Biodiversity 15(3), 425–434, https://doi.org/10.1016/j.japb.2022.03.006.

Bozdağ, A., Yavuz, F., Günay, A. S. (2016): AHP and GIS based land suitability analysis for Cihanbeyli (Turkey) County. Environmental Earth Sciences 75: 813, https://doi.org/10.1007/s12665-016-5558-9.

Canco, I., Kruja, D., Iancu, T. (2021): AHP, a reliable method for quality decision making: A case study in business. Sustainability 13(24): 13932, https://doi.org/10.3390/su132413932.

Chen, J., Yang, S. T., Li, H. W., Zhang, B., Lv, J. R. (2013): Research on geographical environment unit division based on the method of natural breaks (Jenks). The International Archives of the Photogrammetry, Remote Sensing and Spatial Information Sciences 40, 47–50, https://doi.org/10.5194/isprsarchives-XL-4-W3-47-2013.

Choudhury, D., Sundriyal, R. C. (2003): Factors contributing to the marginalization of shifting cultivation in north-east India: Micro-scale issues. Outlook on Agriculture 32(1), 17–28, https://doi.org/10.5367/000000003101294226.

Devi, C. K., Das, P., Nath, M. Mishra, B. K. (2023): Attitude of Farm Women towards the Effects of Climate Change in Agriculture and Allied Activities: A Study in Imphal, East Districts of Manipur, India. International Journal of Environment and Climate Change 13(10), 3843–3849, https://doi.org/10.9734/ijecc/2023/v13i103057.

Dikshit, K. R., Dikshit, J. K. (2014): Weather and Climate of North-East India. In: North-East India: Land, People and Economy. Advances in Asian Human-Environmental Research. Springer, Dordrecht, https://doi.org/10.1007/978-94-007-7055-3_6.

FAO. (1967): Soil Survey Interpretation and Its Use. FAO Soils Bulletin 8, 1–16. http://www.fao.org/docrep/018/64247e/64247e.pdf (accessed on 12 June 2023).

FAO. (1976): A framework for land evaluation. FAO Soils Bulletin 32, 36–47, https://www.fao.org/3/X5310E/X5310E00.htm (accessed on 08 June 2023).

FAO. (1985). Guidelines: Land Evaluation for Irrigated Agriculture. FAO Soils Bulletin 55, 45–46, https://www.fao.org/3/x5648e/x5648e07.htm#TopOfPage.

Feizizadeh, B., Blaschke, T. (2013): Land suitability analysis for Tabriz County, Iran: a multi-criteria evaluation approach using GIS. Journal of Environmental Planning and Management 56(1), 1–23, https://doi.org/10.1080/09640568.2011.646964.

Florinsky, I. V. (2012): Influence of Topography on Soil Properties. In I. V. Florinsky (Ed.), Digital Terrain Analysis in Soil Science and Geology, 1st ed., 145–150. Academic Press, https://doi.org/10.1016/C2010-0-65718-X.

Ganguly, A., Oza, H., Padhya, V., Pandey, A., Chakra, S., Deshpande, R. D. (2023): Extreme local recycling of moisture via wetlands and forests in North-East Indian subcontinent: a Mini-Amazon. Scientific Reports 13: 521, https://doi.org/10.1038/s41598-023-27577-5.

Government of Manipur, GoM (2013): Manipur State Action Plan on Climate Change. Directorate of Environment, Government of Manipur. Climate Change and Vulnerability Assessment. Available online: https://moef.gov.in/wp-content/uploads/2017/09/Manipur.pdf (accessed on 25 July 2023).

Government of Manipur, GoM (2015): Economic Survey of Manipur 2016-17. Directorate of Economic and Statistics, Government of Manipur, 49–70.

Grose, C. J. (1999): Guidelines for the Classification of Agriculture Land in Tasmania (C. J. Grose (ed.); 2nd ed.). Department of Primary Industries, Water and Environment. Available online: https://nre.tas.gov.au/Documents/Land_Cap_Revised-handbook.pdf (accessed on 08 June 2023).

Geological Survey of India (GSI). (2011): Geology and Mineral Resources of Manipur, Mizoram, Nagaland and Tripura, Miscellaneous Publications 30(1). Available online: https://www.scribd.com/document/342438079/Geology-of-mani-mizo-naga-tripura-pdf (accessed on 08 June 2023).

GSI and NRSC (2012): National geomorphological and Lineament mapping on 1 : 50,000 scale.

Natural Resources Census Project. National Remote Sensing Centre, ISRO, Hyderabad. Available online: https://bhuvan-app1.nrsc.gov.in/thematic/thematic/index.php (accessed on 21 September 2023).

Gupta, L., Dixit, J. (2022): A GIS-based flood risk mapping of Assam, India, using the MCDA-AHP approach at the regional and administrative level. Geocarto International 37(26), 11867–11899, https://doi.org/10.1080/10106049.2022.2060329.

Hassan, I., Javed, M. A., Asif, M., Luqman, M., Ahmad, S. R., Ahmad, A., Akhtar, S., Hussain, B. (2020): Weighted overlay based land suitability analysis of agriculture land in Azad Jammu and Kashmir using GIS and AHP. Pakistan Journal of Agricultural Sciences 57(6), 1509–1519.

Hudait, M., Patel, P. P. (2022): Site suitability assessment for traditional betel vine cultivation and crop acreage expansion in Tamluk Subdivision of Eastern India using AHP-based multi-criteria decision making approach. Computers and Electronics in Agriculture 200, 107220, https://doi.org/10.1016/j.compag.2022.107220.

Jahn, R., Blume, H. P., Asio, V. B., Spaargaren, O., Schad, P. (2006): Guidelines for soil description. FAO. Available online: https://www.fao.org/3/a0541e/a0541e.pdf (accessed on 20 October 2023).

Jin, Y., Li, A., Bian, J., Nan, X., Lei, G., Muhammad, K. (2021): Spatiotemporal analysis of ecological vulnerability along Bangladesh-China-India-Myanmar economic corridor through a grid level prototype model. Ecological Indicators 120: 106933, https://doi.org/10.1016/j.ecolind.2020.106933.

Kazemi, H., Akinci, H. (2018): A land use suitability model for rainfed farming by Multi-criteria Decision-making Analysis (MCDA) and Geographic Information System (GIS). Ecological Engineering 116, 1–6, https://doi.org/10.1016/j.ecoleng.2018.02.021.

Karra, K., Kontgis, C., Statman-Weil, Z., Mazzariello, J. C., Mathis, M., Brumpi, S. P. (2021): Global land use/land cover with Sentinel 2 and deep learning. 2021 IEEE International Geoscience and Remote Sensing

Symposium IGARSS, Brussels, Belgium, 4704–4707, https://doi.org/10.1109/IGARSS47720.2021.9553499.
Mahato, R., Bushi, D., Nimasow, G., Dai Nimasow, O. (2024): Remote sensing and geographic information system–based land suitability analysis for precision agriculture: a case of paddy cultivation in East Siang district of Arunachal Pradesh (India). In Remote Sensing in Precision Agriculture (pp. 151-173). Academic Press, https://doi.org/10.1016/B978-0-323-91068-2.00023-0.
Martin, D., Saha, S. K. (2009): Land evaluation by integrating remote sensing and GIS for cropping system analysis in a watershed. Current Science, 569–575. Available online: https://www.jstor.org/stable/pdf/24105472.pdf (accessed on 10 November 2023).
Melese, T., Belay, T. (2022): Groundwater Potential Zone Mapping Using Analytical Hierarchy Process and GIS in Muga Watershed, Abay. Global Challenges, 2100068(6), 1–13, https://doi.org/10.1002/gch2.202100068.
Ministry of Agriculture and Farmers Welfare (MoA&FW), (2018): Agriculture Census 2015–16.
In Department of Agriculture, Cooperation and Farmers Welfare (Vol. 1), Government of India. Available online: http://agcensus.nic.in/document/agcen1516/T1_ac_2015_16.pdf (accessed on 10 November 2023).
Mohanty, A., Wadhawan, S. (2021): Mapping India's Climate Vulnerability: A District Level Assessment. State of vulnerability of Indian districts and states, pp: 29–42 New Delhi: Council on Energy, Environment and Water (CEEW).
Montgomery, B., Dragićević, S., Dujmović, J., Schmidt, M. (2016): A GIS-based Logic Scoring of Preference method for evaluation of land capability and suitability for agriculture. Computers and Electronics in Agriculture, 124, 340–353, https://doi.org/10.1016/j.compag.2016.04.013.
Nath, A. J., Kumar, R., Devi, N. B., Rocky, P., Giri, K., Sahoo, U. K., ... Pandey, R. (2021): Agroforestry land suitability analysis in the Eastern Indian Himalayan region. Environmental Challenges, 4, 100199, https://doi.org/10.1016/j.envc.2021.100199.
North, M. A. (2009): A Method for Implementing a Statistically Significant Number of Data Classes in the Jenks Algorithm," 2009 Sixth International Conference on Fuzzy Systems and Knowledge Discovery, Tianjin, China, 35-38, https://doi.org/10.1109/FSKD.2009.319.
NRSC (2019): Status of Land Degradation in India: 2015-16 National Remote Sensing Centre ISRO, Govt. of India, Hyderabad.
Pawe, C. K., Saikia, A. (2022): These hills called home: quantifying urban forest dynamics in the hills of the Guwahati metropolitan area, india. Geografisk Tidsskrift-Danish Journal of Geography, 122(2), 87-102, https://doi.org/10.1080/00167223.2022.2157853.
Phanjoubam, P. (2005): Manipur: fractured land. India International Centre Quarterly, 32(2/3), 275–287. Available online: https://www.jstor.org/stable/pdf/23006034.pdf (accessed on 06 October 2023).
Podvezko, V. (2009): Application of AHP technique. Journal of Business Economics and Management 10(2), 181–189, https://doi.org/10.3846/1611-1699.2009.10.181-189.
Rai, P. K., Vanlalruati (2022): Societal perception on environmental and socio-economic implications of Tithonia diversifolia (Hemsl.) A. Gray invasion in an Indo-Burma biodiversity hotspot. Environmental and Socio-Economic Studies 10(3), 59–66, https://doi.org/10.2478/environ-2022-0017.
Ritung, S., Wahyunto, Hidayat, F. (2007): Land suitability evaluation with a case map of Aceh Barat District. World Agroforestry Centre, https://apps.worldagroforestry.org/downloads/Publications/PDFS/MN15224.pdf (accessed on 06 October 2023).
Roy, S. S., Ansari, M. A., Sharma, S. K., Sailo, B., Devi, C. B., Singh, I. M., … Ngachan, S. V. (2018): Climate resilient agriculture in Manipur. Current Science, 115(7), 1342–1350, https://www.jstor.org/stable/26978408.
Saaty, T. L. (2001): Fundamentals of the analytic hierarchy process. In: Schmoldt, D.L., Kangas, J., Mendoza, G. A., Pesonen, M. (eds) The Analytic Hierarchy Process in Natural Resource and Environmental Decision Making. Managing Forest Ecosystems 3. Springer, Dordrecht, https://doi.org/10.1007/978-94-015-9799-9_2.
Saaty, T. L. (2008): Decision making with the analytic hierarchy process. International Journal of Services Sciences 1(1), 83–98, https://doi.org/10.1504/IJSSCI.2008.017590.
Sahoo, S., Vasu, D., Paul, R., Sen, T. K., Ray, S. K., Chandran, P. (2020): Acid soils of Manipur of the north-eastern region of India: their mineralogy, pedology, taxonomy and edaphology. Clay Research 39(1), 31–43, https://doi.org/10.5958/0974-4509.2020.00005.4.
Sarkar, D., Saha, S., Mondal, P. (2023): Modelling agricultural land suitability for vegetable crops farming using RS and GIS in conjunction with bivariate techniques in the Uttar Dinajpur district of Eastern India. Green Technologies and Sustainability 1(2): 100022, https://doi.org/10.1016/j.grets.2023.100022.
Sen, T. K., Chamuah, G. S., Maji, A. K., Sehgal, J. (1996): Soils of Manipur for Optimising Land Use. NBSS Publ. 56b (Soils of India Series), National Bureau of Soil Survey and Land Use Planning, Nagpur, India.
Sitorus, S. R. P. (2010): Land Capability Classification for Land Evaluation: a Review. Journal Sumberdaya Lahan 4(2), 69–78. Available online: https://scholar.google.com (accessed on 30 April 2023).
Takhell, D. (2023): Manipur farmers blame institutional failures for low yield and demand compensation. Mongabay-India, 6 January 2023.
Tempa, K. (2022): District flood vulnerability assessment using analytic hierarchy process (AHP) with historical flood events in Bhutan. PLoS ONE 17(6): e0270467, https://doi.org/10.1371/journal.pone.0270467.
Thockchom, L., Kshetrimayum, K. S. (2019): Assessment of quality contributing parameters using hydrochemistry and hydrogeology for irrigation in intermontane Manipur valley in northeast India. Groundwater for Sustainable Development 8, 667–679, https://doi.org/10.1016/j.gsd.2018.08.003.
Wang, F. (1994): The use of artificial neural networks in a geographical information system for agricultural land-suitability assessment. Environment & Planning A 26(2), 265–284, https://doi.org/10.1068/a260265.
Zolekar, R. B., Bhagat, V. S. (2015): Multi-criteria land suitability analysis for agriculture in hilly zone: Remote sensing and GIS approach. Computers and Electronics in Agriculture 118, 300–321, https://doi.org/10.1016/j.compag.2015.09.016.

Short-term geomorphic adjustments of bars in the Elbe, a large regulated river in Czechia

Tomáš Galia*, Václav Škarpich, Adriana Holušová, Jan Hradecký

University of Ostrava, Department of Physical Geography and Geoecology, Czechia
* Corresponding author: tomas.galia@osu.cz

ABSTRACT
Gravel and sandy bars constitute critical components of river channel morphology, yet their morphodynamics in large, heavily regulated rivers during periods without significant flows remain poorly understood. This study investigates changes in surface heterogeneity and sediment sizes through a two-year field monitoring program, focusing on the frontal, central, and distal sections of four bars along the Elbe River in Czechia. Despite the absence of high-flow events reaching at least a one-year recurrence interval, observable changes in surface heterogeneity and sediment sizes were noted across all bars. However, the changes did not follow a uniform pattern; individual bars and their sections exhibited varying degrees of surface sediment coarsening or fining, alongside increases or decreases in surface heterogeneity. These findings highlight the necessity for site-specific management strategies for individual bars within such human-impacted rivers, recognizing their value as ecological hotspots. Furthermore, the methodology presented in this study may serve as a blueprint for the cost-effective monitoring of bar dynamics in channelized river sections.

KEYWORDS
regulated river; bar; river morphodynamics; the Elbe

Received: 18 April 2024
Accepted: 29 May 2024
Published online: 10 June 2024

Galia, T., Škarpich, V., Holušová, A., Hradecký, J. (2024): Short-term geomorphic adjustments of bars in the Elbe, a large regulated river in Czechia. AUC Geographica 59(1), 108–119
https://doi.org/10.14712/23361980.2024.7

1. Introduction

Channel depositional forms are a key element in the natural evolution of river channels (Bridge 1993; Lewin 1976). These deposits can be represented by gravel or sandy bars formed from fluvial sediments settled either along the banks (such as lateral or point bars) or within the central channel (such as transverse, mid-channel, or diagonal bars). They are shaped through the deposition and reworking of loose sedimentary material transported by the water flow to locations where there is a local decrease in transport capacity. This process is typically associated with the channel geometry, with deposits most often found on the inner banks of bends, in areas of local channel widening, or in zones with flow obstacles that allow for the dispersion of the flow energy (e.g., downstream transversal structures like check dams and weirs or behind stable large wood) (Abbe and Montgomery 1996; Hey et al. 1982; Jaballah et al. 2015; Škarpich et al. 2019). These bars are typically described as "forced" due to their formation process, in contrast to "periodic bars", which are large sediment deposits formed as a result of morphodynamic instability (Duró et al. 2016).

The ratio of channel width to flow depth is a critical parameter for the formation of the bars (Cordier et al. 2020; Duró et al. 2016; Redolfi et al. 2020). In cases of periodic lateral bars, which can be observed in straight channel reaches, their relative height above the level of common flows is proportional to the depth of the channel (Tubino et al. 1999). In general, the bars are highest in their central sections and the elevation above water surface correlates with flow characteristics related to the river transport capacity, where higher flows usually lead to the formation of relatively lower deposits (Redolfi et al. 2020). The bars also often exhibit specific characteristics in terms of grain size distribution. Typically, bars are made up of finer sediments than those found in the permanently submerged parts of the channel (Smith 1974). It has been frequently observed in natural channels that the surface layer of bars becomes finer in downstream direction, with the coarsest material present in the frontal (i.e., upstream) bar segment and the finest sediments found in the distal (i.e., downstream) segment (Ashworth and Ferguson 1986; Li et al. 2014; Smith 1974). Additionally, there is usually a gradual fining of sediments from the water level to the outer edge of the bar as the depth and flow velocity decrease during bar flooding (Parker and Andrews 1985). Surface layer armoring on bars can also occur, meaning that the sediments beneath this layer contain finer grain-size fractions (Hey et al. 1982; Smith 1974). However, all these morphological or sedimentological trends can be disrupted by the presence of vegetated patches on the bars, which acts as a hydraulic roughness element facilitating the deposition of particularly fine sediments (Corenblit et al. 2015; Edwards et al. 1999). Similarly, bars in human-impacted, channelized channel reaches (Holušová and Galia 2020), or those directly affected by sediment dredging (Zawiejska et al. 2015), can exhibit significant differences in sedimentary structure and morphology.

The formation and morphodynamics of bars depends on the availability of a sufficient quantity of fluvial sediment, whose characteristics (volume, grain-size, and the frequency and intensity of its movement) are influenced not only by natural conditions (e.g., lithology, energy of relief, and hydrological regime) but also by various types of direct and indirect anthropogenic interventions that are quite typical for European cultural landscapes and human-impacted fluvial systems. Examples of such interventions include bank reinforcements that prevent the delivery of sediments to the channel through bank erosion, the construction of longitudinal barriers that slow down or prevent the downstream movement of sediments, or changes in land use, such as afforestation, which stabilizes sediment sources across the entire catchment area (Syvitski et al. 2005). Another important factor is the presence of vegetation in the river channel, which can stabilize the banks or bars through root systems and reduce flow velocity due to increased hydraulic roughness (Corenblit et al. 2015). In this regard, a variable hydrological regime and the regular occurrence of flows capable of transporting sediments, and thus actively reshaping these bars, are crucial for the occurrence and sustainability of bars. Low variability in flows (e.g., due to the presence of valley dams regulating peak discharges or water abstraction), with the absence of transport-efficient flows, can lead to complete colonization of the bars by vegetation and their integration into the floodplain, resulting in a reduction of both the width and flow capacity of the channel (Adami et al. 2016; Crosato and Mosselman 2020).

From the ecological point of view, bars provide an environment essential for certain plant species that require periodic flooding (Gilvear and Willby 2006; Zeng et al. 2015). The presence of bars also influences water temperature variability and nutrient deposition in the streambed (Claret et al. 1997; Ock et al. 2015). However, as suggested, bars are sensitive to human interventions in channels and anthropogenic influence on flows. The recent decades have seen trends of decreased frequency or loss of bars due to channelization leading to increase of river transport capacity, construction of valley reservoirs, and gravel and sand extraction from rivers (Arróspide et al. 2018; Kondolf 1997). In this context, obtaining information on the current morphodynamics of bars in regulated rivers is crucial to direct management efforts towards preserving these valuable components of river channels that are subject to significant anthropogenic pressure and climate change.

Interannual changes in surface sediment sizes and bar morphology in large regulated rivers during

periods without high flow events have not been thoroughly investigated. Furthermore, some water authorities debate the stability of these bars, their overgrowth by vegetation, and their formation as obstacles to flow during floods. To assess the current morphodynamics of these bars with potential implications for enhancing current management practices in relation to the sustainability of these habitats, we conducted a two-year (September 2021 – September 2023) geomorphic monitoring of four bars in the Elbe River near the border between Czechia and Germany. We utilized a comprehensive approach, including repeated geodetic measurements, observations of scour chains, and repeated grain-size sampling, to gather field evidence of potential recent activity of geomorphic processes.

2. Materials and Methods

2.1 Study area

The Elbe River, one of Europe's longest rivers, spans 1,094 km and encompasses a catchment area of 148,268 km^2. It originates in the Giant Mountains in Czechia and flows into the North Sea near Hamburg, Germany. Characterized by a pluvio-nival flow regime within a temperate climate, the Elbe experiences its highest discharges during the spring months due to melting snow and rainfall, while the lowest water levels are observed in summer period.

Our study investigates four bars located in the Czech portion of the Elbe River, near the state boundary between Germany and Czechia. These bars approximately extend from 760 to 730 river km, with distances measured upstream from the Elbe outflow into the North Sea (contributing catchment area ca. 48,500–51,000 km^2). This reach traverses terrain uplifted by tectonic activity. During the Neogene and Quaternary periods, significant river erosion occurred, resulting in the formation of a predominantly confined channel, incised 200–300 m into the surrounding terrain and characterized by narrow floodplain strips (Balatka and Kalvoda 1995). From the perspective of the channel's planform shape, the Elbe River in the studied reach is characterized by a single-thread river pattern (sinuosity = 1.21) with the occurrence of lateral bars composed of gravel-sand material. Bars typically form along the inner banks of river bends as relatively narrow, elongated strips of exposed sediment. Their formation is sometimes influenced by the artificial addition of material from channel dredging intended for ship navigation. Additionally, bars infrequently develop at confluence points with streams draining the adjacent hilly terrain. This part of the river, like much of its length, is subject to significant modifications due to ship navigation, including bank stabilization efforts and above mentioned maintenance of the shipping channel through dredging. Outer banks of bends and channel segments within the intravilane are stabilized using riprap. As the result, local channel width varies between 110 and 150 m and flow depth between 2–3 m during base flow conditions. The natural flow regime is affected by large dams in the Vltava River (the main tributary in Czechia) and the presence of weirs with navigation locks. At the same time, the studied reach is under environmental protection as part of a site of European significance. It is adjacent to the České Švýcarsko National Park and the České Středohoří protected area.

The studied bars show some variations in their planform morphology and can be classified as forced bars sensu Duró et al. (2016) due to their location on the inner bank of a distinctly curved river bend (Fig. 1). Hre and Dzb are characterized as relatively long and flat lateral bars (Tab. 1). In contrast, Val shows characteristics of a point bar morphology, attributed to its location in a pronounced river bend and the noticeable difference in elevation between the water surface and the outer edge of the bar. The fourth bar, Tech, is a lateral bar but is considerably shorter than both Hre and Dzb. All bars are recently covered with patchy herbaceous vegetation and their surface and sub-surface layers are composed of gravel-size fractions, with varying amounts of sand and mud. Gravel-size fraction dominates the surface sediments, comprising 71–94% of the mass sample. However, at the distal part of Hre, this proportion decreases to 59% due to its local flat, low surface characterized by an abundant presence of sand and mud (Hradecký et al. 2024).

Our monitoring of bar dynamics and their sediment composition spanned from September 2021 to September 2023. The nearby gauging station in Děčín (located between Tec and Dzb bars at 740.5 river km)

Tab. 1 Positions and morphometric parameters of the studied bars; morphometric parameters are related to a bar surface delineated by base flow (approximately 130–150 m^3/s) and bounded externally by continuous vegetation during the 2023 inventory.

Bar	Geographical position	River (km)	Length (m)	Maximal width (m)	Elevation over water surface (m)
Val	50.6762N, 14.1272E	759	250	20	1.4
Tech	50.6953N, 14.2001E	752	100	10	0.5
Dzb	50.8363N, 14.2261E	733	790	16	0.8
Hre	50.8496N, 14.2172E	731	730	25	1.1

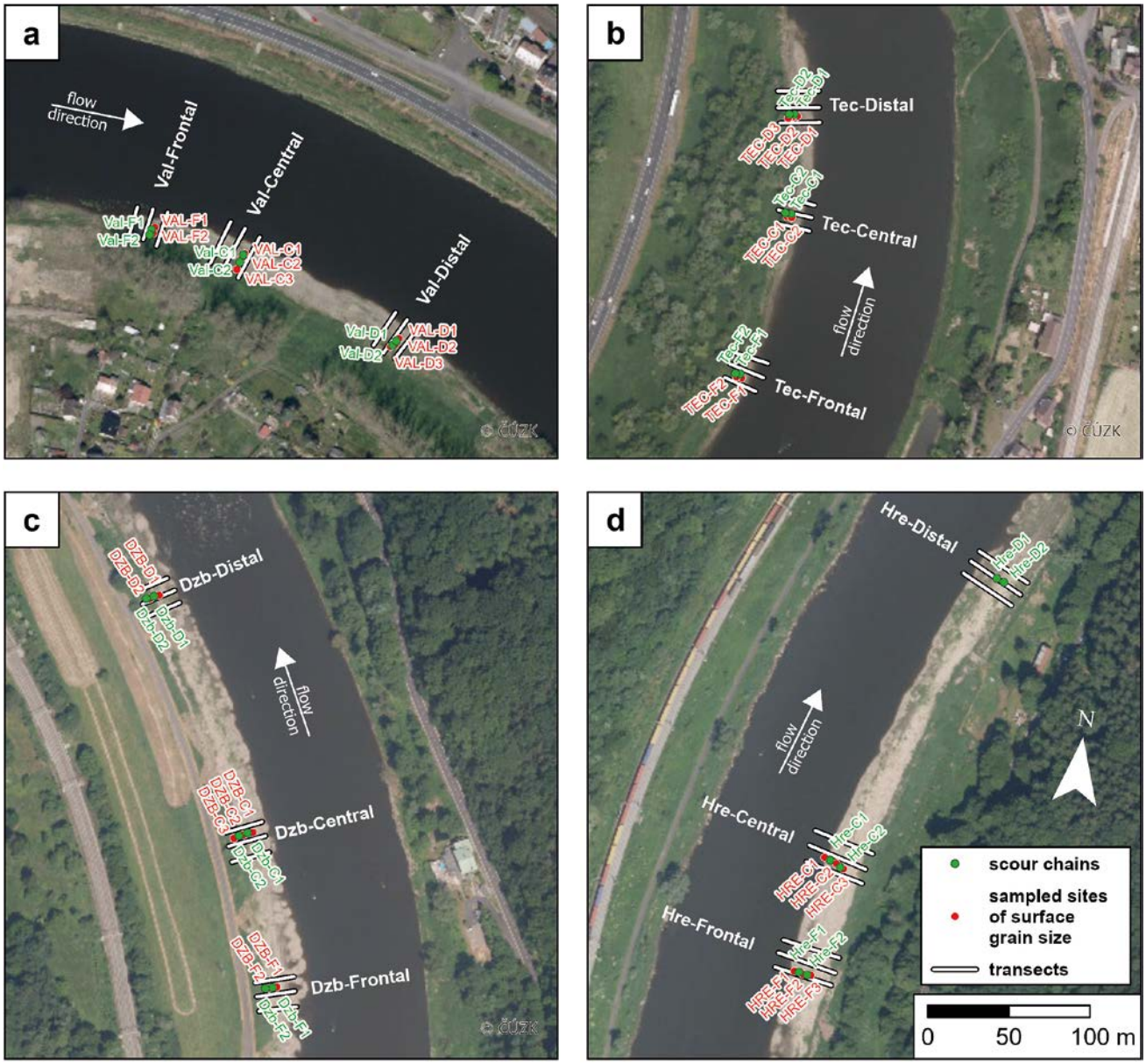

Fig. 1 Studied bars in the Elbe River: a – Val, b – Tec, c – Dzb, d – Hre; data source: Czech Office for Surveying, Mapping and Cadastre. The positions of the monitored cross-sectional transects, scour chains and surface grain-sizes are indicated.

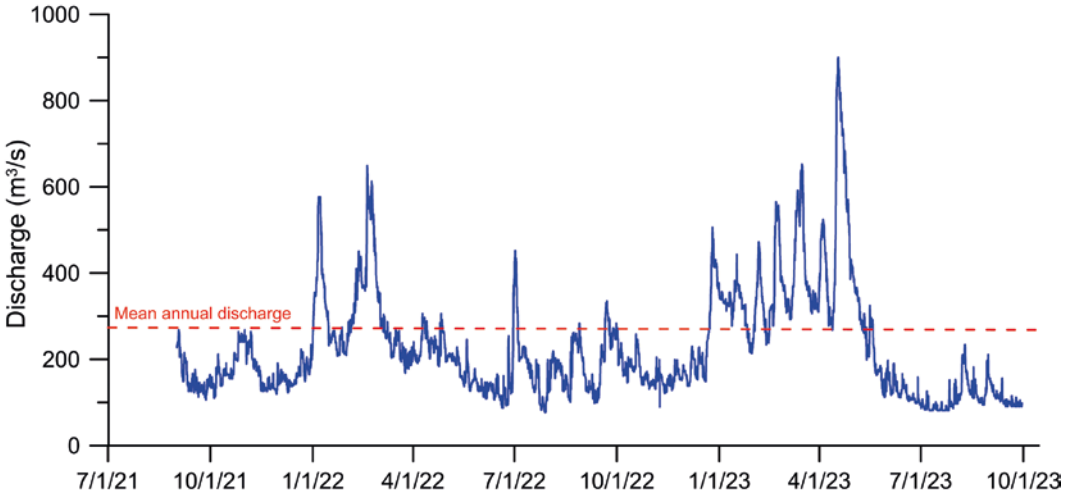

Fig. 2 Hydrograph of hourly discharges from Děčín gauging station for the studied period 9/2021–9/2023 (data source: Czech Hydrometeorological Institute).

Tab. 2 Flow characteristics of Děčín gauging station (data source: Czech Hydrometeorological Institute).

Flow recurrence interval	Discharge
Mean annual discharge	287 m^3/s
1-year	1300 m^3/s
2-year	1720 m^3/s
5-year	2300 m^3/s
20-year	3240 m^3/s
100-year	4290 m^3/s

recorded no significant flood events during this period. The highest discharge recorded was on April 17, 2023, at 900 m^3/s (Fig. 2). This high flow event did not even reach 1-year discharge (Tab. 2), indicating that the bars' morphology and sediment dynamics during the study period were not influenced by extreme flooding events.

2.2 Monitoring of cross-sectional transects

We monitored transects arranged perpendicularly to the flow direction across three sections (frontal, central, and distal) of each studied bar. In each section, we established three parallel transects, spaced 5 meters apart. These transects were geodetically surveyed using a total station, with measurements taken at 1-meter intervals along each transect in September 2021 and again in September 2023. We meticulously recorded the coordinates by GNSS station at both the start and end of each transect. Due to slight fluctuations in water levels between our two measurement periods, which affected the starting points of the transects in relation to the water surface, we standardized the length of the transects for direct comparisons between the years of survey.

Due to little variations in individual measurements of relative elevation at 1-m intervals – attributable to factors such as the presence of coarse material or the resolving power of the total station, which can introduce errors up to several centimeters – it was challenging to precisely compare potential morphological changes along a pair of transects. These changes could be of a similar scale as the potential measurement error. Consequently, we focused our comparisons on the differences in concavity across the frontal, central, and distal sections of the studied bars. The concavity parameter is defined by the elevation difference between two consecutive points along a transect (Laub et al. 2012):

$$Conc = \Sigma(|x_2 - x_1| + |x_3 - x_2| + \ldots + |x_{n-1} - x_n|) \quad (1)$$

By computing the average concavity *Conc* for each transect (that is, by averaging the relative elevation changes between points x_1, x_2, ... x_n, which are spaced 1 meter apart, from the water surface to the outer edge of the sampled transect), we obtained insights into potential variations in the surface heterogeneity of the bars. Specifically, lower concavity values imply a relatively flat and homogeneous surface between successive points along the transect, whereas higher concavity values point to a more irregular or heterogeneous surface. This implies that we did not assess absolute vertical changes across the transects; instead, we focused on examining the changes in morphological heterogeneity within the transects.

2.3 Monitoring of scour chains

In September 2021, we placed 24 scour chains across the monitored bars to observe the dynamics of the surface sediment layer. For each bar, we positioned two chains in the frontal, central, and distal sections, respectively, near the monitored cross-sectional transects. This setup necessitated excavating around 0.5 meters into the bar's surface, altering its sedimentary structure. The burial depth of the 1-meter-long scour chains was 50 cm, with the remaining

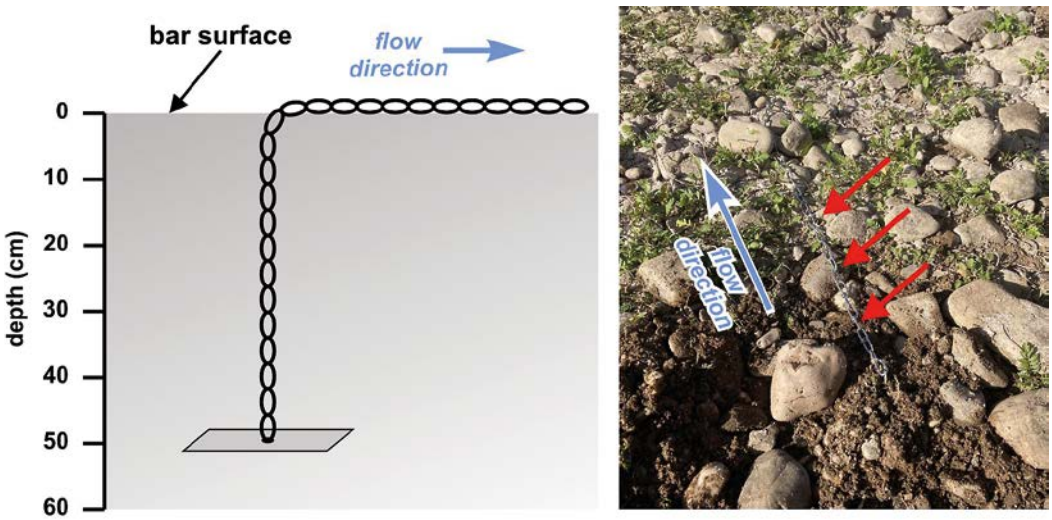

Fig. 3 Photograph and schematic illustration of scour chain installation in bar sediments.

protruding part oriented in alignment with the expected flow direction (Fig. 3). To assess changes in sediment dynamics – particularly regarding the burial or exposure of the chains – we conducted analyses over two distinct intervals: September 2021 to September 2022 and September 2022 to September 2023. We then disregarded data from the first period to reduce the influence of sediment settling on our findings related to chain burial or exposure. Therefore, our reported results reflect observations from only the latter one-year period, capturing data through the highest recorded discharge on April 17, 2023, which was 900 m^3/s.

2.4 Monitoring of bar sediments

In the frontal, central, and distal sections of each bar studied, we evaluated the surface grain size for particles equal to or larger than 8 mm. In September 2021, we set up 2–3 parallel rectangular areas (each measuring 1 m by 0.75 m) in each section, depending on the width of the bar (the minimal distance between the areas should be ca. 5 meters). These areas were meticulously cleared of litter and sparse vegetation, and their coordinates were recorded using a total station and GNSS. We captured orthogonal photographs of each area, which were later analyzed with the PebbleCounts software (Purinton and Bookhagen 2019). This software facilitates the automatic identification of individual grains. Following this preprocessing step, we selected accurately detected particles in each photograph. Utilizing the b-axis values generated by PebbleCounts, we randomly selected 150 values. Subsequently, we constructed a grain-size distribution curve and calculated the median grain-size value (D_{50}). In September 2023, we replicated the entire procedure in the same designated areas to assess temporal changes. To do this, we calculated the changes in median particle diameter by determining the ratio of median sizes obtained in 2021 to those in 2023.

2.5 Potential uncertainties in the used methods

Potential uncertainties related to geodetic measurements, such as the precision of geodetic total stations and the influence of pebbles on the bar surface, or issues with automated grain-size analysis (where incorrectly identified clasts were excluded from the final automated measurements), should be recognized. Additionally, the use of scour chains introduces certain uncertainties due to their susceptibility to errors in capturing multiple phases of erosion and deposition. Furthermore, the establishment of a small terrestrial vegetation patch near the scour chain burial site may influence the stability of the bar surface or the deposition of fine sediments, due to flow roughness induced by the vegetation. Nonetheless, it is unlikely that these factors significantly altered the general observed trend of changes between the 2021 and 2023 datasets.

3. Results

Despite the occurrence of relatively low flows that did not reach the level of a 1-year recurrence interval during the monitoring period – suggesting an expected low level of morphological activity on the studied bars – we observed measurable changes in both bar morphology and surface grain sizes. This indicates that even under conditions of low hydrological activity,

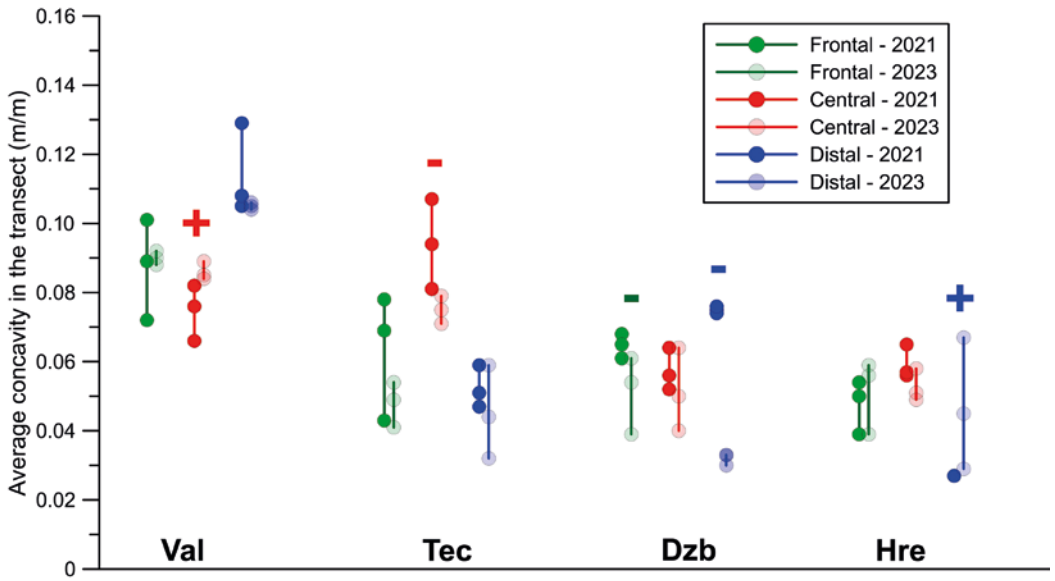

Fig. 4 Visualization of average concavities recorded along individual transects from field measurements in 2021 and 2023; the symbols "+" and "–" indicate significant changes, with all concavities in a section being higher or lower in 2023 compared to 2021, respectively.

Tab. 3 Changes in surface relative elevation (in cm) based on variations in scour chain length above the bar surface between September 2022 and September 2023. Positive values indicate erosion, negative values indicate deposition, an asterisk (*) denotes additional deposition on top of a scour chain lying on the surface, and NR signifies "not recovered", likely due to vandalism.

Bar	F1	F2	C1	C2	D1	D2
Val	−1*	−1	4*	−1	−1	−1
Tec	NR	1	NR	NR	1*	−1
Dzb	0	2*	−4	−15	NR	NR
Hre	0	1	0*	−1*	1*	2

significant alterations to the bars' physical characteristics can still occur.

3.1 Changes in cross-sectional transects

Overall, the average concavities (i.e., relative elevation changes per 1 m length) typically ranged between 3 to 10 cm, with the highest values observed for the Val bar, which exhibits a morphology closely resembling that of a point bar (Fig. 4). The different average concavity values observed between 2021 and 2023 indicated frequent alterations in the heterogeneity of the bar surfaces. However, these alterations did not follow a consistent pattern across the different bars or their respective sections, as illustrated in Fig. 4. Specifically, Val displayed an increase in average concavity, particularly in its central section, while Tec exhibited a decrease in concavity in the same section. Hre showed an increase in concavity in its distal section, whereas Dzb experienced a decrease in concavity in both its distal and frontal sections. These variations suggest that the responses of the bar surfaces to environmental factors are highly variable, influenced by the specific morphology of each bar, as well as potentially by local vegetation succession.

3.2 Recorded erosion/deposition by scour chains

Observations of scour chain burial dynamics across all monitored bars from 2022 to 2023 revealed variations, although several chains (three in Tec and two in Dzb) were not retrieved, likely due to vandalism (Tab. 3). Variations in the length of exposed chain were generally minor and within the anticipated margin of measurement error for most locations. It is important to note that some chains experienced additional sediment deposition, with exposed scour chains becoming slightly buried under sediment layers of 1–3 cm. This suggests multiple phases of sediment erosion and deposition during the 2022–2023 period, or more specifically, sediment deposition following an erosion event (i.e., erosion during the rise of high flow and deposition during its recession phase). Dzb demonstrated the most significant morphodynamics, with erosion of up to 15 cm observed in its middle section. Nonetheless, geodetically measured concavities exhibited minimal variance when compared to its distal or frontal sections (Fig. 4).

3.3 Changes in median grain-sizes

Firstly, none of the bars exhibited a coarser D_{50} grain size in their frontal sections, while the two upstream

Tab. 4 D_{50} surface grain-size percentiles displayed in mm and the 2023/2021 ratio of D_{50} values for sampled sites in 2021 and 2023 (colors indicate whether the ratio is positive or negative); F = frontal, C = central, and D = distal sections of the bar, with numbers denoting the position from the water surface to the outer edge of the bar; NS = not sampled.

Bar/year	F1	F2	F3	C1	C2	C3	D1	D2	D3
Val									
2021	40	36	NS	46	43	36	30	29	33
2023	32	35	NS	41	34	32	35	25	27
Change	0.80	0.97	NS	0.89	0.79	0.89	1.17	0.86	0.82
Tec									
2021	39	38	NS	46	38	NS	32	33	26
2023	34	34	NS	41	36	NS	35	30	25
Change	0.87	0.89	NS	0.89	0.95	NS	1.09	0.91	0.96
Dzb									
2021	33	35	NS	29	34	30	24	33	NS
2023	32	30	NS	33	36	39	36	27	NS
Change	0.97	0.86	NS	1.14	1.06	1.30	1.50	0.81	NS
Hre									
2021	33	24	23	25	24	27	NS	NS	NS
2023	29	23	21	38	30	23	NS	NS	NS
Change	0.88	0.96	0.91	1.52	1.25	0.85	NS	NS	NS

bars (Val and Tec) displayed noticeably larger D_{50} in their middle sections. However, finer D_{50} are typically observed in the distal sections of all the bars studied (Tab. 4 and Fig. 5). During the monitoring period, a significant number of grain-size samples exhibited substantial shifts in their median values, with 19 out of 28 samples showing an increase or decrease in D_{50} of more than 10%. We noted a somewhat contradictory trend between the upstream bars (Val and Tec) and the downstream bars (Dzb and Hre) regarding changes in median grain size on their surfaces. As indicated in Tab. 4, with the exception of a single measurement in the distal section, the upstream bars exhibited a degree of fining in their D_{50} values, most notably in the central section of Val, where the D_{50} 2021 to D_{50} 2023 ratio reached as high as 0.79. Conversely, the central sections of Dzb and Hre, in particular, showed signs of surface sediment coarsening, with the ratio climbing up to 1.52. This variation suggests differing responses of the bars over the two-year period, without a consistent trend in median grain size evolution. Additionally, we were unable to process any samples from the distal section of Hre during both 2021 and 2023 field campaigns, as the dominance of silt to sand-sized particles prevented their automated analysis by the PebbleCount software.

4. Discussion

All three geomorphic methods used in our study suggest that gravel bars with some content of finer grain-size fractions in a large regulated river are prone to changes in their morphological and sedimentological characteristics, such as variations in surface morphology or median grain sizes, even during periods of low flow that do not reach the level of a one-year recurrence interval. However, it is important to note that our observations are based on a two-year period only, and thus we cannot predict the future evolutionary trajectory of the investigated bars. Future changes over the coming decades will depend on ongoing climate changes and the approaches to local water management, including water abstraction or

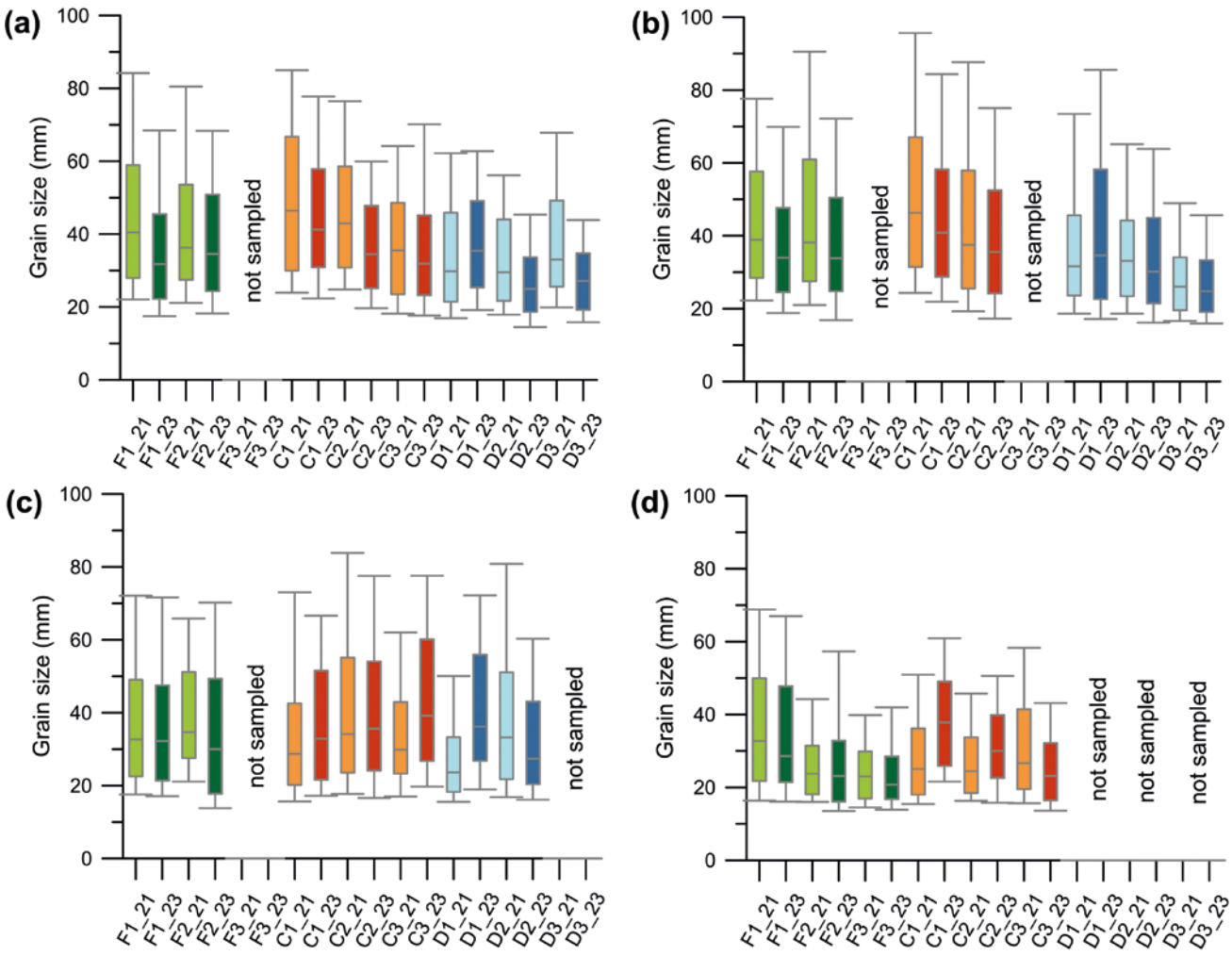

Fig. 5 Grain-size distribution of all sampled sites: (a) – Val, (b) – Tec, (c) – Dzb, (d) – Hre; whiskers show 10th and 90th grain-size percentile, F = frontal, C = central, and D = distal sections of the bar, with numbers denoting the position from the water surface to the outer edge of the bar (_21 and _23 represents the years of the sampling).

discharge regulation by dams in the upstream parts of the Elbe catchment. It should be noted that the potential impact of changing climate on the morphodynamic trajectories of rivers and their components, like gravel or sandy bars, is still largely unexplored (Redolfi et al. 2023).

During the two-year study period, we observed a variety of responses from the bars, which prevented us from identifying a consistent trend in bar evolution or morphodynamics in the studied reach of the Elbe River, subject to significant anthropogenic pressure. Despite their differences in morphology and size, the upstream bars (Val and Tec) exhibited larger median grain sizes in their central sections and showed some tendencies towards fining of the surface sediment layer between 2021 and 2023. Concurrently, their central sections exhibited contrasting morphodynamics, with an increase in concavity in Val and a decrease in Tec. A completely different scenario was observed in the downstream bars (Dzb and Hre), which tended towards sediment coarsening in their central sections. However, these bars also showed notable differences in concavity trends between 2021 and 2023. This clearly highlights the uniqueness of individual bars, despite their presence in a regulated river reach with a homogeneous planform. Our study is exploratory in nature, which necessitates caution when attributing specific factors to the observed variations within a single two-year period. For example, the coarsening observed in the central sections of bars located downstream of Děčín city (Dzb and Hre) may be due to the more confined nature of the local valley. This area lacks floodplain segments, potentially increasing transport capacity and sediment supply from adjacent steep catchments, even during low flows. However, to ascertain reliable factors, a longer monitoring period that includes high flow events is recommended.

In the context of short-term monitoring, our findings align intriguingly with those of (Kibler et al. 2011), who observed the evolution of median grain size (D_{50}) on gravel bars following dam removal. They noted a rapid increase in D_{50} size immediately downstream of the removed dam, underscoring the rapid response of sediment characteristics to such environmental changes. However, they also highlighted the variability of D_{50} and the challenges in ascribing significant meaning to downstream D_{50} changes. This perspective resonates with our observations, suggesting a parallel in the characterization of D_{50}. Furthermore, their work underscores the notable inter-annual variability in grain size, reinforcing the importance of linking grain size changes to flow magnitude. This connection becomes particularly relevant for bar surfaces prone to frequent flooding, where signs of morphological change are observable at flow events with one- to two-year recurrence intervals, as indicated by Haschenburger and Wilcock (2003). They documented the surface activity of grains across four monitoring phases, each associated with a distinct flow magnitude, affecting different active zones of the channel. Our data lead to a comparable insight, emphasizing that not just the flood magnitude and active grain size matter, but also the position within the channel, such as relative elevation or flow direction, plays a critical role in shaping sediment dynamics. In this context, based on our observations of scour chains, we anticipate not only suspended sediment transport but also a degree of bedload transport during periods of relatively low flow, as evidenced by the partial burial of some chains by fine gravels.

Short-term (year-to-year) detailed examinations of the grain size and morphological development of bars in large regulated "stable" rivers are almost absent in field research, especially when compared to studies on freely meandering or braided rivers. This scarcity of data makes it difficult to directly compare our results with those from other rivers affected by intensive human activities. Jaballah et al. (2015) observed swift alterations in bar dynamics – ranging from several months to a few years – due to engineering constructions and damming in a previously wandering Alpine gravel-bed channel. These interventions resulted in a decrease in the number of bars and an elongation of their lengths. However, details regarding variations in their grain sizes or surface heterogeneity were not disclosed. The recent disruption in the natural development of bars in the Elbe, relative to rivers in a more natural state, is highlighted by the absence of the coarsest sediment fractions in the frontal sections of the bars. Conversely, the finest median grain sizes were observed in the distal sections of the studied bars, aligning with the natural development processes of bars as documented by researchers like (Ashworth and Ferguson 1986; Smith 1974). Two of the bars examined in our study, Val and Tec, exhibited the highest D_{50} values in their central sections. This observation suggests a similarity with alternate sand-gravel bars in the middle Loire River, which has also been influenced by various river training works, such as embankments, groyne construction, and sediment extraction (Cordier et al. 2020). Some long-term (decadal-scale) studies have focused on the biogeomorphic interactions between bar morphodynamics and vegetation in channelized river reaches. Although our study did not explore the development or composition of vegetation, the influence of vegetation in trapping sediments or stabilizing bars is undeniable. Projected climate changes, which influence the timing and frequency of floods linked to the development of vegetation as demonstrated in numerical simulations of alpine channelized river reaches (Jaballah et al. 2015; Jourdain et al. 2020), suggest a potential future transformation of bars. Over the past decade, relatively low flows in the Elbe River have likely encouraged the establishment and spread of vegetation on exposed bar surfaces, a phenomenon recently also observed in another central-European river, the Odra, across both channelized and meandering sections

(Holušová et al. 2023). Conversely, the maintenance of the Elbe reach, associated with ship navigation and irregular dredging of sediments from the channel bottom to banks or bar surfaces, may somewhat replicate the disturbance effects typically caused by high flows.

Our methodology could serve as a template for cost-effective monitoring of the dynamics of bars in channelized river segments. Bars in such settings often manifest as extended strips along the inner parts of river bends and are generally accessible and temporally quite stable (e.g., Adami et al. 2016), in contrast to the more dynamically changing natural channels like wandering or braided rivers. The use of unmanned aerial vehicles (UAVs) and airborne LiDAR systems has the potential to accelerate data collection and facilitate the monitoring of more extensive areas of bar surfaces or a larger number of bars. Nonetheless, it is crucial to address and reduce the impact of vegetation on the generated digital elevation models (e.g., Caponi et al. 2019; Langhammer and Vacková 2018; Rusnák et al. 2018). Field data are essential for precisely characterizing the habitats of fauna and flora inhabiting these boundary zones between aquatic and terrestrial environments, and this information is crucial for improving their management in the context of sustainable river usage (Brierley and Fryirs 2016). Our study exemplifies the need for tailored management approaches for bars in large regulated rivers, as their characteristics and morphodynamic trajectories can differ markedly across individual locations. For instance, Hre bar exhibited a relatively flat and muddy distal section that precluded the processing of grain-size samples via photogrammetry, a situation not encountered in the other three bars studied.

5. Conclusions

Our study comprehensively examines the morphological and sedimentological dynamics of bars within a regulated reach of the Elbe River over a two-year period, highlighting the susceptibility of these geomorphic features to changes despite low flow conditions. The utilization of three classic geomorphic methods revealed significant variability in surface heterogeneity, median grain sizes, and morphodynamic trends among the studied bars, underscoring the complexity of bar evolution in regulated rivers. Particularly notable were the observed divergent trends in sediment coarsening and fining, as well as variations in concavity across different studied bars. This study also underscores the need for detailed, site-specific research to understand the impacts of regulation and climate change on river morphology. Moreover, our methodology offers a blueprint for cost-effective monitoring of morphodynamic changes in channelized river segments, providing essential data for the sustainable management of river habitats.

Acknowledgements

The authors thank to Lukáš Vaverka and Stanislav Ruman for their help during fieldworks. The authors would like to thank two anonymous reviewers whose comments significantly improved the initial manuscript. This research was funded by Technological Agency of Czech Republic, grant number SS03010279.

References

Abbe, T. B., Montgomery, D. R. (1996): Large woody debris jams, channel hydraulics and habitat formation in large rivers. Regulated Rivers: Research and Management 12(2–3), 201–221, https://doi.org/10.1002/(SICI)1099-1646(199603)12:2/3<201::AID-RRR390>3.0.CO;2-A.

Adami, L., Bertoldi, W., Zolezzi, G. (2016): Multidecadal dynamics of alternate bars in the Alpine Rhine River. Water Resources Research 52(11), 8938–8955, https://doi.org/10.1002/2015WR018228.

Arróspide, F., Mao, L., Escauriaza, C. (2018): Morphological evolution of the Maipo River in central Chile: Influence of instream gravel mining. Geomorphology 306, 182–197, https://doi.org/10.1016/j.geomorph.2018.01.019.

Ashworth, P. J., Ferguson, R. I. (1986): Interrelationships of Channel Processes, Changes and Sediments in a Proglacial Braided River. Geografiska Annaler: Series A, Physical Geography 68(4), 361–371, https://doi.org/10.1080/04353676.1986.11880186.

Balatka, B., Kalvoda. J. (1995): Development of the Labe valley in the Děčínská vrchovina Highland. Geografie – Sborník ČSG, 100, 3, 173–192. Bridge, J. S. (1993): The interaction between channel geometry, water flow, sediment transport and deposition in braided rivers. Geological Society, London, Special Publications 75, 13–71, https://doi.org/10.1144/GSL.SP.1993.075.01.02.

Brierley, G. J., Fryirs, K. A. (2016): The Use of Evolutionary Trajectories to Guide 'Moving Targets' in the Management of River Futures: Moving Targets for River Management. River Research and Applications 32(5), 823–835, https://doi.org/10.1002/rra.2930.

Caponi, F., Koch, A., Bertoldi, W., Vetsch, D.F., Siviglia, A. (2019): When Does Vegetation Establish on Gravel Bars? Observations and Modeling in the Alpine Rhine River. Frontiers in Environmental Sciences 7, 124, https://doi.org/10.3389/fenvs.2019.00124.

Claret, C., Marmonier, P., Boissier, J. M., Fontvieille, D., Blanc, P. (1997): Nutrient transfer between parafluvial interstitial water and river water: influence of gravel bar heterogeneity. Freshwater Biology 37(3), 657–670, https://doi.org/10.1046/j.1365-2427.1997.00193.x.

Cordier, F., Tassi, P., Claude, N., Crosato, A., Rodrigues, S., Pham Van Bang, D. (2020): Bar pattern and sediment sorting in a channel contraction/expansion area: Application to the Loire River at Bréhémont (France). Advances in Water Resources 140: 103580, https://doi.org/10.1016/j.advwatres.2020.103580.

Corenblit, D., Baas, A., Balke, T., Bouma, T., Fromard, F., Garófano-Gómez, V., González, E., Gurnell, A. M., Hortobágyi, B., Julien, F., Kim, D., Lambs, L., Stallins, J. A., Steiger, J., Tabacchi, E., Walcker, R. (2015): Engineer

pioneer plants respond to and affect geomorphic constraints similarly along water–terrestrial interfaces world-wide. Global Ecology and Biogeography 24(12), 1363–1376, https://doi.org/10.1111/geb.12373.
Crosato, A., Mosselman, E. (2020): An Integrated Review of River Bars for Engineering, Management and Transdisciplinary Research. Water 12(2): 596, https://doi.org/10.3390/w12020596.
Duró, G., Crosato, A., Tassi, P. (2016): Numerical study on river bar response to spatial variations of channel width. Advances in Water Resources, Numerical modelling of river morphodynamics 93, Part A, 21–38, https://doi.org/10.1016/j.advwatres.2015.10.003.
Edwards, P. J., Kollmann, J., Gurnell, A. M., Petts, G. E., Tockner, K., Ward, J. V. (1999): A conceptual model of vegetation dynamics on gravel bars of a large Alpine river. Wetlands Ecology and Management 7, 141–153, https://doi.org/10.1023/A:1008411311774.
Gilvear, D., Willby, N. (2006): Channel dynamics and geomorphic variability as controls on gravel bar vegetation; River Tummel, Scotland. River Research and Applications 22(4), 457–474, https://doi.org/10.1002/rra.917.
Haschenburger, J. K., Wilcock, P. R. (2003): Partial transport in a natural gravel bed channel. Water Resources Research 39(1), 1020, https://doi.org/10.1029/2002WR001532.
Hey, R. D., Bathurst, J. C., Thorne, C. R. (1982): Gravel-Bed Rivers: Fluvial Processes, Engineering and Management. Wiley.
Holušová, A., Galia, T. (2020): Downstream fining trends of gravel bar sediments: a case study of Czech Carpathian rivers. AUC Geographica 55(2), 229–242, https://doi.org/10.14712/23361980.2020.17.
Holušová, A., Poledniková, Z., Vaverka, L., Galia, T. (2023): Spatiotemporal dynamics and present perception of gravel bars in natural and regulated environments. Science of The Total Environment 892: 164711, https://doi.org/10.1016/j.scitotenv.2023.164711.
Hradecký, J., Čuda, J., Frouz, J., Hanel, M., Galia, T., Škarpich, V., Ruman, S., Vaverka, L., WIild, J., Hadincová, V., Petřík, P., Bureš, L., Heřminovský, M., Hummel, J., Prošek, J., Borovec, J., Breton, F., Goncharov, O., Kotilová, P., Tomková, I., Osafo, N. (2024): Optimalizace managementu dolního úseku Labe s ohledem na přítomnost biotopu 3270 a zlepšení hydromorfologického stavu na základě mezioborové studie 2021–2023 (research report, in Czech). University of Ostrava, Ostrava.
Jaballah, M., Camenen, B., Pénard, L., Paquier, A. (2015): Alternate bar development in an alpine river following engineering works. Advances in Water Resources, Fluvial Eco-Hydraulics and Morphodynamics 81, 103–113, https://doi.org/10.1016/j.advwatres.2015.03.003.
Jourdain, C., Claude, N., Tassi, P., Cordier, F., Antoine, G. (2020): Morphodynamics of alternate bars in the presence of riparian vegetation. Earth Surface Processes and Landforms 45(5), 1100–1122, https://doi.org/10.1002/esp.4776.
Kibler, K., Tullos, D., Kondolf, M. (2011): Evolving Expectations of Dam Removal Outcomes: Downstream Geomorphic Effects Following Removal of a Small, Gravel-Filled Dam1. JAWRA Journal of the American Water Resources Association 47(2), 408–423, https://doi.org/10.1111/j.1752-1688.2011.00523.x.
Kondolf, G. M. (1997): Hungry Water: Effects of Dams and Gravel Mining on River Channels. Environmental Management 21, 533–551, https://doi.org/10.1007/s002679900048.
Langhammer, J., Vacková, T. (2018): Detection and Mapping of the Geomorphic Effects of Flooding Using UAV Photogrammetry. Pure and Applied Geophysics 175, 3223–3245, https://doi.org/10.1007/s00024-018-1874-1.
Laub, B. G., Baker, D. W., Bledsoe, B. P., Palmer, M. A. (2012): Range of variability of channel complexity in urban, restored and forested reference streams: Channel complexity and stream restoration. Freshwater Biology, 5, 57, 1076–1095, https://doi.org/10.1111/j.1365-2427.2012.02763.x
Lewin, J. (1976): Initiation of bed forms and meanders in coarse-grained sediment. GSA Bulletin 87(2), 281–285, https://doi.org/10.1130/0016-7606(1976)87<281:IOBFAM>2.0.CO;2.
Li, Z., Wang, Z., Pan, B., Zhu, H., Li, W. (2014): The development mechanism of gravel bars in rivers. Quaternary International, Large Asian Rivers VII 336, 73–79, https://doi.org/10.1016/j.quaint.2013.12.039.
Ock, G., Gaeuman, D., McSloy, J., Kondolf, G.M. (2015): Ecological functions of restored gravel bars, the Trinity River, California. Ecological Engineering 83, 49–60, https://doi.org/10.1016/j.ecoleng.2015.06.005.
Parker, G., Andrews, E.D. (1985): Sorting of Bed Load Sediment by Flow in Meander Bends. Water Resources Research 21(9), 1361–1373, https://doi.org/10.1029/WR021i009p01361.
Purinton, B., Bookhagen, B. (2019): Introducing *PebbleCounts*: a grain-sizing tool for photo surveys of dynamic gravel-bed rivers. Earth Surface Dynamics 7(3), 859–877, https://doi.org/10.5194/esurf-7-859-2019.
Redolfi, M., Carlin, M., Tubino, M. (2023): The Impact of Climate Change on River Alternate Bars. Geophysical Research Letters 50(5): e2022GL102072, https://doi.org/10.1029/2022GL102072.
Redolfi, M., Welber, M., Carlin, M., Tubino, M., Bertoldi, W. (2020): Morphometric properties of alternate bars and water discharge: a laboratory investigation. Earth Surface Dynamics 8(3), 789–808, https://doi.org/10.5194/esurf-8-789-2020.
Rusnák, M., Sládek, J., Kidová, A., Lehotský, M. (2018): Template for high-resolution river landscape mapping using UAV technology. Measurement 115, 139–151, https://doi.org/10.1016/j.measurement.2017.10.023.
Škarpich, V., Galia, T., Ruman, S., Máčka, Z. (2019): Variations in bar material grain-size and hydraulic conditions of managed and re-naturalized reaches of the gravel-bed Bečva River (Czech Republic). Science of The Total Environment 649, 672–685, https://doi.org/10.1016/j.scitotenv.2018.08.329.
Smith, N. D. (1974): Sedimentology and Bar Formation in the Upper Kicking Horse River, a Braided Outwash Stream. The Journal of Geology 82(2), 205–223, https://doi.org/10.1086/627959.
Syvitski, J. P. M., Vörösmarty, C. J., Kettner, A. J., Green, P. (2005): Impact of Humans on the Flux of Terrestrial Sediment to the Global Coastal Ocean. Science

308(5720), 376–380, https://doi.org/10.1126/science.1109454.
Tubino, M., Repetto, R., Zolezzi, G. (1999): Free bars in rivers. Journal of Hydraulic Research 37(6), 759–775, https://doi.org/10.1080/00221689909498510.
Zawiejska, J., Wyżga, B., Radecki-Pawlik, A. (2015): Variation in surface bed material along a mountain river modified by gravel extraction and channelization, the Czarny Dunajec, Polish Carpathians. Geomorphology 231, 353–366, https://doi.org/10.1016/j.geomorph.2014.12.026.
Zeng, Q., Shi, L., Wen, L., Chen, J., Duo, H., Lei, G. (2015): Gravel Bars Can Be Critical for Biodiversity Conservation: A Case Study on Scaly-Sided Merganser in South China. PLoS ONE 10(5): e0127387, https://doi.org/10.1371/journal.pone.0127387.

Using eye tracking to study reading landscape: a systematic review

Tomáš Měkota*

Charles University, Faculty of Science, Department of Social Geography and Regional Development, Czechia
* Corresponding author: tomas.mekota@natur.cuni.cz

ABSTRACT
More studies have understood landscape as a perceived entity since the European Landscape Convention was approved in 2004. This article adopts a systematic review approach in line with the PRISMA statement to delineate the utilization of eye tracking in studying landscapes. A comprehensive analysis of 55 studies sourced from the Web of Science and Scopus databases was conducted. Various aspects were scrutinized, encompassing landscape attributes, media employed for landscape representation, eye tracking data visualizations, and eye tracking metrics. The prevalence of eye tracking usage in landscape studies has notably increased since 1998, with research conducted across all continents. The most studied aspects of the landscape are saliency and specifics of particular types of landscape. Amongst the varied media used to represent landscape, photographs reign supreme, while heatmaps prominently feature as a means to visualize eye tracking data. The spectrum of metrics applied is extensive, showcasing distinct suitability for specific landscape attributes. Drawing from this review, recommendations for prospective research directions are outlined. The insights garnered from this review stand to serve as a valuable overview for researchers delving into the realm of reading landscape.

KEYWORDS
landscape perception; reading landscape; eye tracking; systematic review

Received: 4 December 2023
Accepted: 5 June 2024
Published online: 24 June 2024

Měkota, T. (2024): Using eye tracking to study reading landscape: a systematic review. AUC Geographica 59(1), 120–136
https://doi.org/10.14712/23361980.2024.8

1. Introduction

Landscape can be perceived as a dynamic entity, a segment of the environment infused with natural and social elements, appearing distinct to various individuals. Different aspects of the landscape hold unique personal meanings for observers, with perception shaped by aesthetic values and prior experiences. This perspective gained traction following the publication of the European Landscape Convention in 2000, which defined landscape as "an area perceived by people, characterized by the interplay of natural and/or human factors" (Council of Europe 2000). Subsequently, an increasing number of studies have honed in on reading landscape (Khaledi et al. 2022).

Understanding reading landscape holds significant utility in establishing perceptual priorities based on what people perceive and discern in the landscape. It aids responsible engagement with the landscape and informs place-based education initiatives (Smith 2002). Moreover, it serves as a potent tool to comprehend and interpret the landscape.

Various methodologies have been devised to study reading landscape. One approach draws from Kevin Lynch's (1960) method of studying city perception, where individuals sketch the cityscape and articulate their thoughts about their drawings. Another approach involves the observation and assessment of photographs, employed to ascertain aspects such as landscape attractiveness or beauty (Kaplan et al. 1989). Technological advancements have expanded the array of methods available for studying reading landscape, potentially yielding more precise outcomes. Notably, eye tracking, a method that records an observer's eye movements, has gained increasing prominence. It allows for the precise tracking of an observer's gaze, facilitating detailed analysis of the areas being observed. Despite some publications delving into eye tracking research (Klein and Ettinger 2019) and exploring the relationship between eye movements and interpretation (Hu et al. 2022), these works have not been specifically focused on the landscape context (Scott et al. 2019; Hu et al. 2022). Shynu et al.'s (2021) systematic review on environmental perception encompasses a broader range of data collection methods. As the number of studies utilizing eye tracking to study reading landscape continues to grow, it becomes challenging to track the evolution of metrics, visualizations, and their appropriateness for studying reading landscape. Therefore, this review endeavors to aid researchers studying reading landscape with eye trackers by summarizing how previous studies have employed eye tracking methodology in reading landscape research.

2. Reading landscape

In the research on reading landscape, two notions are encountered whose meanings are not consistently clear: "reading landscape" and "landscape perception". While both terms broadly describe the same process, some authors interpret them more narrowly than others (see below). Bell (2001) conceptualized landscape perception as a three-step process involving the reception of visual stimuli, the intuitive recognition of aesthetic qualities, and the integration of sensory information with existing knowledge to form opinions. In contrast, Antrop and van Eetvelde (2017) delineated four primary layers of reading the landscape: scene, natural system, cultural system, and history. In this review, the term "reading landscape" is used interchangeably with "landscape perception".

The process of reading landscape can be understood through two distinct lenses: factual and aesthetic.

Factual reading landscape is grounded in observing what truly exists within it and understanding the intricate connections. This approach is heavily influenced by one's scientific perspective. Historians view the landscape as a palimpsest imbued with data from different historical eras (Cronon 2020). Geographers undertake the most comprehensive interpretation, considering the interplay between the natural and social elements of the landscape. Lewis (1979) emphasized the study of the cultural landscape, proposing seven axioms for its interpretation. These axioms encompass cultural, historical, ecological, and natural perspectives on the landscape, also integrating commonplace elements in landscape contemplation. Widgren (2004) contends that reading the landscape is an everyday human activity and forms the basis for geographical research. He also underscores the significance of human-made structures in the landscape, emphasizing the need to decipher cultural symbols and representations of cultural practices within it.

Aesthetic interpretation of a landscape is rooted in the impact of the landscape on the observer rather than the objective elements present in it. In most cases, studies utilizing this perspective aim to evaluate the visual quality of the landscape. Several models explore what renders a landscape beautiful (Tveit et al. 2006 who used the notion landscape perception) or elucidate the landscape qualities that account for inter-individual differences in its evaluation (Kaplan et al. 1989 who also used the notion landscape perception). Another concept within this perspective delves into the characteristics, knowledge, and experiences of the observer, implying that the meaning of the landscape can be interpreted differently by various observers (Duncan and Duncan 1988 who wrote about reading landscape). Despite having theoretical perspectives that explain processes linked to landscape reading, numerous questions remain unanswered. Eye tracking appears to be a highly effective tool for elucidating uncertainties in both theoretical approaches to this process. Consequently, studies based on both approaches were included in this systematic review.

3. Methods

This study conducted a review of research employing eye tracking to explore reading landscape. To make the search complete and systematic, the PRISMA statement procedure was chosen as methodological guideline, since it is recommended and accepted as a frame for writing systematic reviews (Page et al. 2021). The process commenced with the formulation of research questions stated as follows:

- Which aspects of the landscape have been studied?
- What medium is used to study reading landscape with eye tracking?
- Which visualizations of eye tracking data are used in reading landscape research?
- Which eye tracking metrics are used to study reading landscape?
- Which eye tracking metrics are used to study different aspects of landscape?
- What are the limitations of using eye tracking methodology to read landscape?

Addressing these research questions necessitated an extensive literature search. In the initial phase, titles, abstracts, and keywords of articles, reviews, and book chapters were scrutinized in two major electronic bibliographic databases: Web of Science and Scopus. The search employed the following keyword combination: ("landscape" or "urban environment" or "natural environment" or "scene perception") and ("eye tracking" or "eye tracker" or "eye movements" or "visual attention"). This choice was based on commonly used notions in the landscape reading process and eye tracking methodology, serving as criteria for article inclusion in the review. There were no restrictions on publication years or subject areas. The search encompassed articles available until December 20, 2020, and was limited to those written in English. A total of 427 records were identified in Scopus, 228 in the Web of Science database, with 161 records being duplicate for both databases. Consequently, the overall count of potentially relevant articles stood at 494 (Fig. 1).

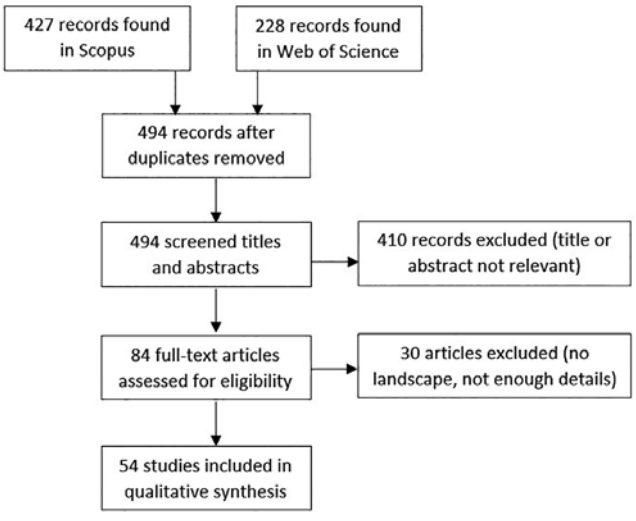

Fig. 1 Flow diagram of the literature selection process.

In the second stage, article titles were examined to evaluate their relevance. Articles completely unrelated to the topic were excluded from the analysis (e.g., neuroscience articles found in the databases that were not relevant to our objectives). A total of 273 articles were excluded based on title reading, leaving 220 abstracts for scanning in the third stage.

During the abstract analysis, it was essential to ascertain whether the study focused on reading the landscape, as defined in section 2, and if eye tracking was utilized as at least one of the methods. If this information was not evident in the abstract, the article was excluded. At this stage, 137 articles did not meet the criteria and were excluded, leaving 84 articles deemed relevant for our review. Subsequently, full-text articles were meticulously examined in the next stage.

Despite meeting our criteria, not all selected articles were utilized for the review. Some lacked pertinent information needed to address the research questions, while others were primarily oriented towards aspects like orientation, especially in flat terrain, rather than the landscape. Ultimately, 54 articles were included in the review, encompassing 56 studies (2 articles contained 2 studies).

Data from the selected studies were extracted in accordance with the research questions. The documented characteristics included the focus of the study, medium used to represent the landscape, number of participants, eye tracking metrics used and their significance, visualization of eye tracking data and its application, and results of the study. This information was recorded in a MS Excel table.

Initially, lists of topics, media, visualizations, and metrics used in the studies, along with accompanying notes, were generated. Using these lists, a summary was created. Due to the extensive variety of metrics, visualizations, and study topics, the data were coded using open coding based on grounded theory to form broader groups, aiding navigation in the lists based on identified similarities during the study readings.

Given the substantial variation in topics, an examination of the relationships between the topic and metrics employed to study it was conducted. These relationships were visualized using graph generated in SankeyMATIC application, and conclusions were drawn based on this graphical representation.

4. Results

4.1 Basic summary of the included studies

The years for potential study selection were not restricted; the earliest study included dates to 1998. Studies utilizing eye tracking methodology to

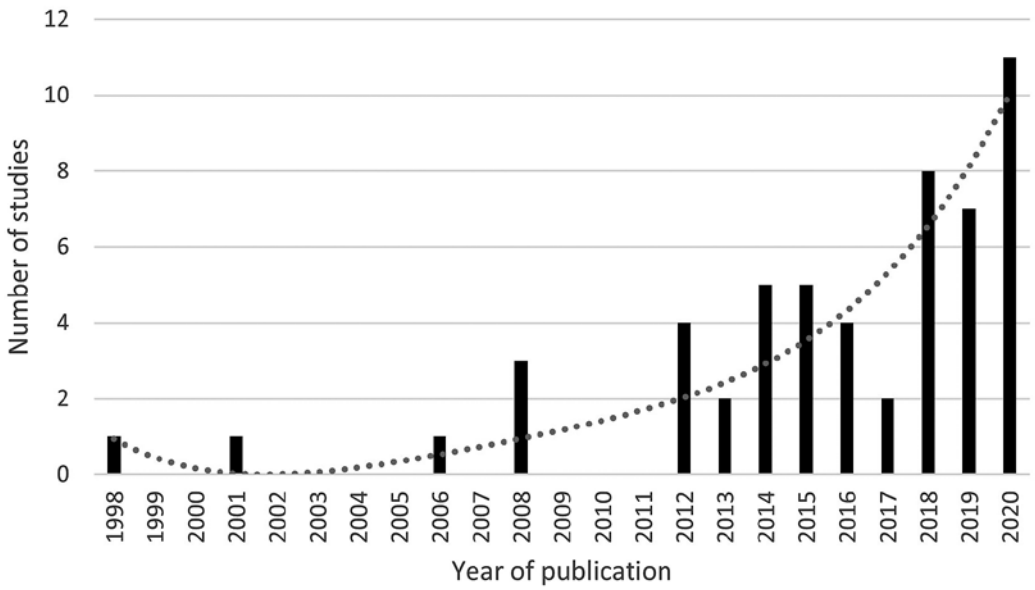

Fig. 2 Years of publication of the included studies. The trend line is a result of linear regression model and shows that number of research papers using eye tracking in landscape research has soared.

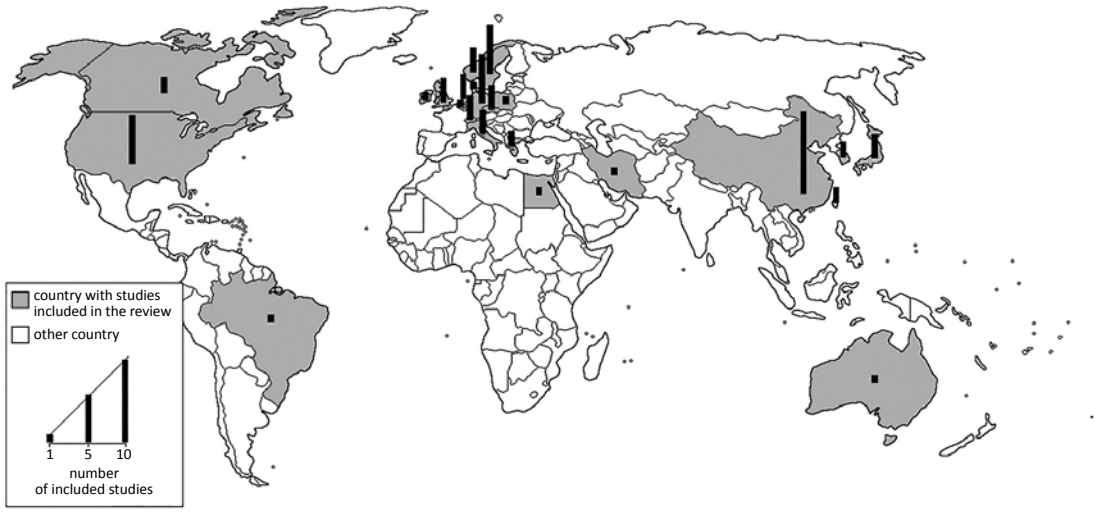

Fig. 3 The countries where studies were carried out.

investigate landscapes have been continuously conducted since 2012 (Fig. 2), demonstrating a growing trend in their number. The peak number of studies was recorded in 2020, reaching 11 studies.

Most of the studies were conducted in Europe, the second region is East Asia, with most studies conducted in China (10 studies), followed by North America. Additionally, one study each was conducted in Brazil and Australia, one study was conducted in cooperation with researchers from Egypt, and one from Iran (Fig. 3).

The number of participants in the studies varied significantly (Fig. 4). The mean number of participants was 40, with the most common range being between 26 and 50. Minimum was 3 (Nathanael et al. 2012), maximum 158 (Ren 2019).

4.2 Which aspects of the landscape are explored in the studies?

In the selected articles, a broad spectrum of study foci and aspects of landscape were observed. To address this diversity, topics and foci were coded and grouped into a more manageable set of categories. Ultimately, 8 categories were identified. It is important to note that some studies were included in multiple categories, as the categories were not initially designed to be mutually exclusive; the categorization of individual studies is shown in Tab. 1. The identified categories were as follows:

(i) **Saliency or attractiveness in the landscape** (15 studies) where parts of the landscape that attract the most attention from observers were studied.

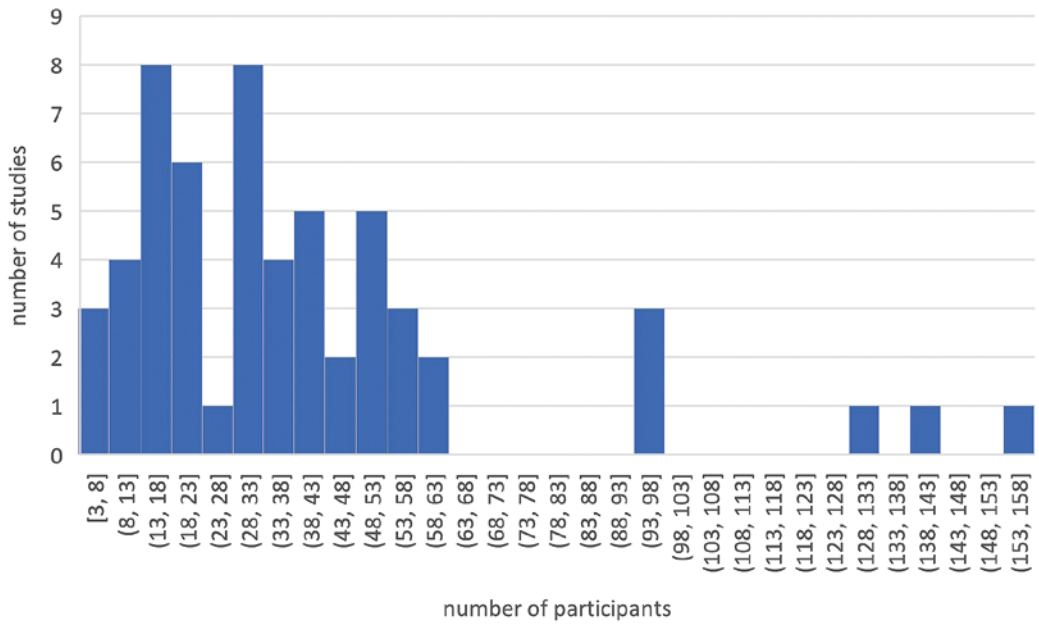

Fig. 4 Number of participants in reviewed studies.

Some also explored objects within the landscape that aid in memory recall.

(ii) **Particular type of landscape** (15 studies) focused on a specific type of landscape (e.g., pasture, forest, urban parks) and how people perceive this type of landscape. Some studies compared the perception of two different types of landscapes.

(iii) **Marketing** (8 studies) explored attractive objects/elements of landscapes to draw people's attention, often in the context of tourism (e.g., pictures in travel agency catalogs, hotel advertisements). One study focused on the effective localization and visual features of advertisements to attract the most attention.

(iv) **Restorativeness** (9 studies) investigated elements of the landscape perceived as restorative or stress-relieving, often providing recommendations for landscape designers.

(v) **Affective responses** (8 studies) focused on the positive or negative emotions and feelings people experience when observing the landscape, including differences between different types of landscapes and individual preferences for certain areas/objects within the landscape.

(vi) **Localization** (7 studies) examined map orientation and the ability of individuals to find their way or locate themselves based on a map.

(vii) **Traffic safety** (6 studies) explored the visual behavior of various traffic participants, with a primary focus on attention distribution. The studies often concluded with recommendations for urban planning and architecture.

(viii) **Other topics** (3 studies) encompassed a variety of diverse aims, including studies on the influence of sounds on reading landscape, differences in eye movements when observing static versus moving pictures, the role of text in reading landscape, and cross-cultural differences in reading landscape.

4.3 What medium is used to study reading landscape with eye tracking?

Eleven different types of media were identified in the selected studies. The most used media were various types of images, including photographs (31 studies), pictures (3), maps (1), street view (2), and aerial photographs (1). The second most frequently used medium was the real environment, where participants' eye movements were recorded in the actual landscape (15 studies). Other types of media were less commonly used and included audio-visual stimuli (2), animations (2), videos (2), a driving simulator (1), and virtual reality (1). Some studies utilized a combination of multiple media types: Kiefer et al. (2014a) used both the real environment and maps, Dong et al. (2020) combined the real environment with street view, and Hayata and Ino (1998) compared static pictures, videos, and animations.

Despite technological advancements, the presumption that static stimuli would be replaced by the natural environment, virtual reality, or videos is disproven according to our analysis. Photographs remain the most utilized medium for studying landscape reading with eye tracking. However, since 2014, when enough studies allowed for comparison, a broader range of media has been employed.

As technological advancements continue, especially with the development of mobile eye trackers, it could be anticipated that there might be a shift in the media used to study landscapes, transitioning from static pictures to dynamic media such as animations or videos, and from desktop settings to natural

Tab. 1 Classification of studies according to their topics.

Topic	Studies
Saliency or attractiveness in the landscape	Davies et al. (2006); Schumann et al. (2008); Credidio et al. (2012); Potocka (2013); Dupont et al. (2015); Pihel et al. (2015); Wang et al. (2020); Dupont and van Eetvelde (2014; 2 studies); Lin et al. (2014); Hayek et al. (2019); Spanjar and Suurenbroek (2020); Valsecchi et al. (2020); Franěk et al. (2018a); Petružálek et al. (2018); Backhaus et al. (2020)
Particular type of landscape	Nordh (2012); Potocka (2013); Nordh et al. (2013); Sang et al. (2014); Valtchanov, Ellard (2015); Cho (2016); Sang et al. (2016); Amati et al. (2018); Petružálek et al. (2018); Franěk et al. (2018a, b); Elsadek et al. (2019); Misthos et al. (2020); Zhu et al. (2020); Gao et al. (2020); Spanjar and Suurenbroek (2020)
Marketing	Takahashi et al. (2001); Potocka (2013); Li et al. (2016); Fedotov et al. (2018); Wang et al. (2018); Liu et al. (2019); Liu et al. (2020); Zhu et al. (2020)
Restorativeness	Nordh (2012); Nordh et al. (2013); Valtchanov and Ellard (2015); Amati et al. (2018); Franěk et al. (2018b); Elsadek et al. (2019); Kang and Kim (2019); Bianconi et al. (2019)
Affective responses	Liener et al. (2017); Cottet et al. (2018); Ren (2019); Stevenson et al. (2019); Gao et al. (2020); Khachatryan et al. (2020); Spanjar and Suurenbroek (2020)
Localization	Kiefer et al. (2014; 2 studies); Spiers and Maguire (2008); Emo (2012); Dong et al. (2020); Franke and Schweikart (2016); Sayegh et al. (2015)
Traffic safety	Nathanael et al. (2012); Antonson et al. (2014); Brazil et al. (2017); Stelling-Konczak et al. (2018); Dong et al. (2020); Cullen et al. (2020)
Other topics	Ren and Kang (2015; sounds); Liu et al. (2019; sounds); Hayata and Ino (1998; static vs. moving stimuli)

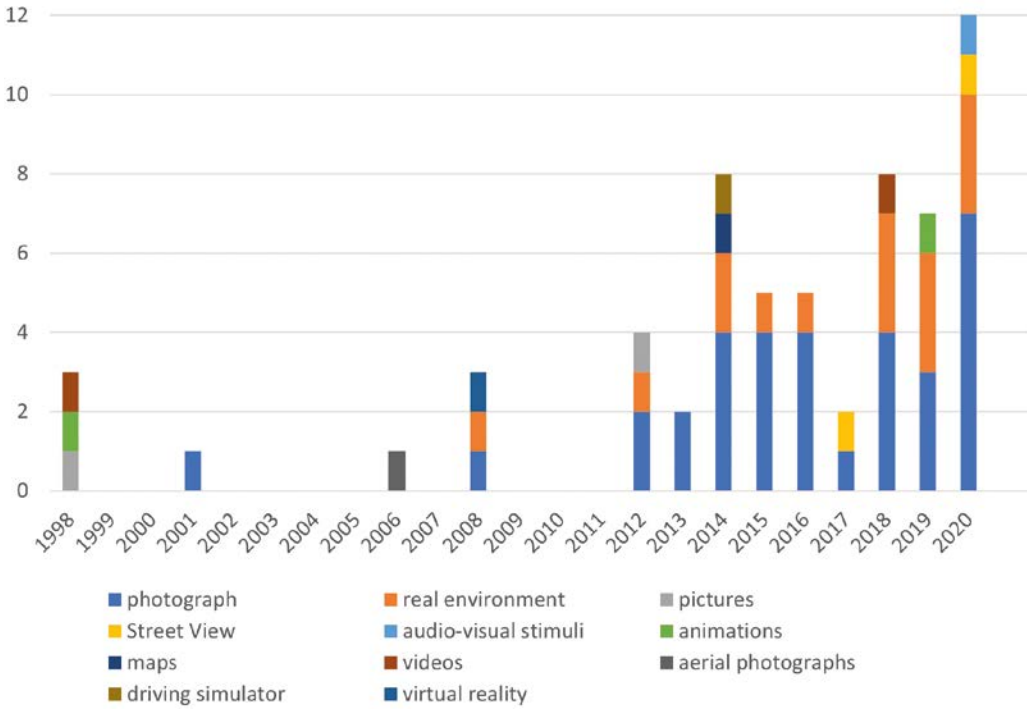

Fig. 5 Media used in the included studies according to the year of publication as they are called in the studies.

environments. Although a slight increase in the proportion of eye tracking landscape studies conducted in natural environments is observed (Fig. 5), photographs remain the most frequently used medium for this type of research, and static stimuli continue to feature prominently in most studies (Fig. 6).

4.4 Which visualizations of eye tracking data are used in landscape reading research?

In the selected studies, 14 methods of visualization of eye tracking data were identified. The most frequently used are shown in Fig. 7.

(i) **Heatmaps** (also called heat maps, attention heatmaps; 18 studies) represent the intensity of fixation in various parts of the stimulus. Heatmaps are valuable for identifying highly attended objects or symbolizing fixated areas. They are easily generated using eye tracking data processing software, and their clarity is advantageous for all readers. However, their difficult quantification is a commonly cited drawback. Heatmaps can also be employed to study different areas of the stimulus fixated by observers at various times during the observation, aiding in identifying reading strategies for the landscape (Spanjar and Suurenbroek 2020).

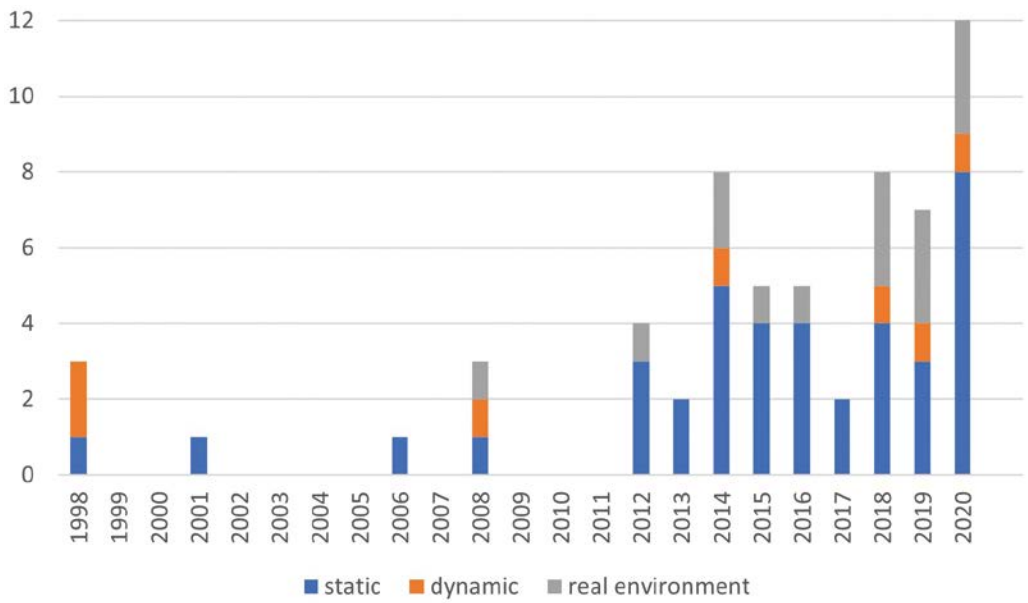

Fig. 6 Categories of media used in the included studies according to the year of publication.

(ii) **Scanpath** (also called trajectory map, gaze plot; 10 studies) is the direct visualization of eye movements. Scanpaths provide insights into the complexity and difficulty of reading the landscape.

(iii) **Luminance maps** (also called opacity maps; 4 studies) is a visualization method similar to heatmaps. Instead of color, luminance maps depict the most fixated areas of the stimulus based on opacity. Like heatmaps, luminance maps are not easily suited for quantitative research.

(iv) **Salience map** (3 studies) visualizes objects expected to naturally attract the most attention

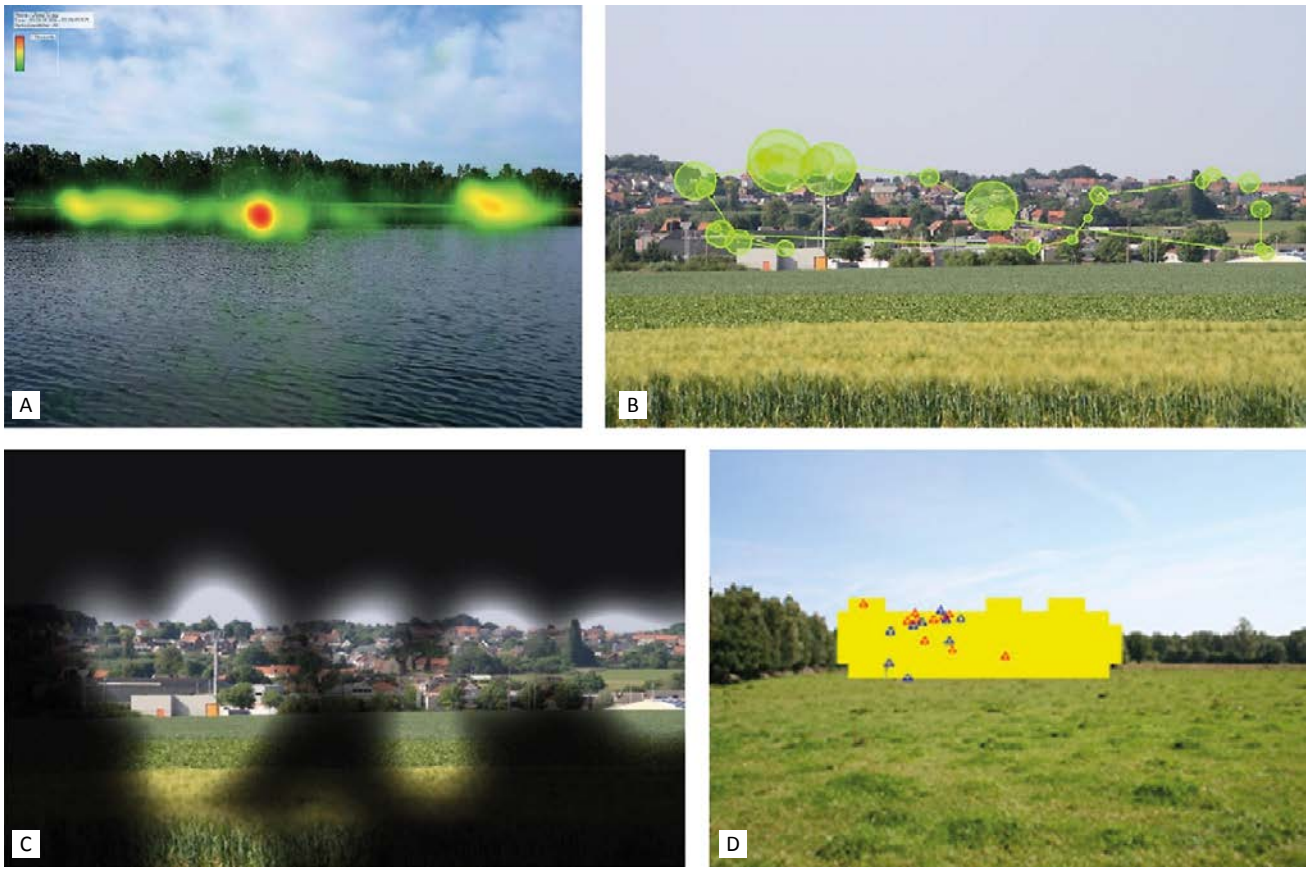

Fig. 7 The most frequently used visualizations of eye tracking/fixations data: a) heatmap (Potocka 2013), b) scanpath (Dupont and van Eetvelde 2015), c) luminance map (Dupont and van Eetvelde 2015), d) salience map (Sang et al. 2016).

Tab. 2 Overview of eye tracking metrics used to study reading landscape.

Fixations metrics	Saccades metrics	Metrics to study areas of interest	Eye characteristics	Stimulus observation characteristics
Number of fixations Fixation duration Fixation frequency Fixations per minute Fixations positions First fixation position First fixation time First fixation duration Timing of the last fixation Temporal evolution of mean fixation duration	Number of saccades Amplitude of saccades Saccades length Saccade frequency	Number of fixations in AOI Duration of fixations in AOI Number of visits in an AOI Time of the first visit in an AOI First saccade amplitude to interest area AOIs sequences	Pupil size Blink rate	Scanpath length Horizontal and vertical angle viewed Total gaze points Average nearest neighbor ratio Mean lateral visual span Mean portrait visual span Number of crossing the center line Time-course of fixations Entropy Predictability

during free viewing tasks. Identification is based on object color, intensity, and orientation. This visualization type is often used alongside heatmaps. Comparing salience maps and heatmaps can reveal the reading strategy: stimulus-driven if the maps correspond and task-driven if there are differences in visualizations. The differences can be identified by reviewing the visualizations or by examining specific objects, their salience, and fixation intensity.

(v) **Hits in cells** (1 study) is a method applicable to eye tracking without an eye tracker. The stimulus is divided into 25 cells, and after presentation, participants report the first number they see among the 25 presented (one in the center of each cell).

(vi) **Voronoi Cells** (1 study) serve to visualize the dispersion of fixations. A cell is a polygon containing all points with the lowest distance to the fixation location. Clustering of fixations results in smaller polygons.

(vii) **Boxplots** (1 study) were utilized for eye tracking analysis of video to compare the distribution of fixations between areas of interest in different landscapes. For each area of interest, boxplots were drawn and compared for both landscapes.

(viii) **Proportional graphs** (1 study) were employed to analyze the types of objects participants fixated on at different observation times. These graphs can be created for each participant to study interindividual differences or for all participants, aiding in qualitative comparison.

(ix) **Attention radius** (1 study) is the radius of the extended area resulting from the combination of all separate attention areas, which are areas with higher number of fixations in the heatmap.

(x) **Attention points** (1 study) are the numbers of separated attention areas in the heatmap.

(xi) **Total attention area** (1 study) is the area of higher attention areas in the heatmap, that are the areas for attention points.

(xii) **Fixation spatial distribution map** (1 study) is a graphical representation of fixations similar to a heatmap but also includes fixation duration. The XY axes represent coordinates from the stimulus, and the Z axis represents fixation duration. Longer fixations are represented by higher points.

(xiii) **Points in pictures** (1 study) is a method similar to the scanpath, but without the lines representing saccades; only fixations are depicted.

(xiv) **Emotions-colored cells** (1 study) is a method to visualize the emotions evoked by each object in the stimulus. The stimulus is divided into cells, each colored based on the emotion it evoked, as detected by EEG. The object's location is tracked using an eye tracker.

4.5 Which eye tracking metrics are used to study reading landscape?

There are 46 different eye tracking metrics used in 56 studies included in this review. The metrics are grouped according to the types of characteristics of eye movement into five groups: fixation metrics, saccades metrics, metrics to study areas of interest, eye characteristics metrics, and metrics of picture observation. An overview of the metrics is presented in Tab. 2.

4.5.1 Fixation metrics

Fixation metrics are crucial characteristics of eye movements extensively used to analyze reading landscapes. Fixations denote periods during which the eyes remain directed towards a single point. They are typically identified by a distance between gaze points smaller than a threshold value and a time where the participant gazes at a position for a duration exceeding the threshold. The threshold values for time varied across the included studies, ranging from 50 ms to 200 ms.

The identified metrics from the 55 studies are outlined below:

- *Number of fixations*, also known as fixation counts, number of gaze points, or total gaze points (22 studies). This metric involves counting the total number of fixations during stimulus observation and comparing them between images. A higher number of fixations might indicate less fascination with the stimulus or difficulty in observation (Berto et al. 2008; Nordh et al. 2013). Additionally, it can be interpreted in terms of stimulus

memory: more fixations may imply better recall of the stimulus.
- *Fixation duration*, also called fixation time (19 studies). Mean fixation duration was utilized in 8 other studies. It measures the length of fixations and can be compared between images, participants, or participant groups. Longer fixations are associated with experts (Sang et al. 2014) and may signify a more challenging task or greater interest in the stimulus (Liu et al. 2020). Conversely, shorter fixations a more restorative landscape (Valtchanov and Ellard 2015; Kang and Kim 2019).
- *Fixation frequency* (1 study) can be interpreted similarly to fixation duration. It represents the number of fixations per unit of time.
- *Fixations per minute* were used by Stevenson et al. (2019) to account for varying walking speeds among participants in a natural environment. They found that participants exhibited a higher number of fixations per minute in a natural environment, although the precise interpretation remains unclear within the study's context.
- *Fixations positions*, also referred to as fixation locations, were widely used in the 55 studies. They are commonly employed for data visualization. Ren (2019) utilized fixation coordinates to investigate differences in assessing the tranquility of various landscape types.
- *First fixation position*, *first fixation time*, and *first fixation duration* were used to examine the most salient objects in the stimuli. First fixation position was compared to salience maps to determine whether the viewing strategy is stimulus-driven or task-driven. Sang et al. (2016) discovered that evaluating stewardship and characterizing the pasture are both task-driven. Dupont et al. (2015) discovered that the length of first fixations is higher for landscape experts than for novices. Wang et al. (2020) used first fixations as a component of a method to preserve cultural heritage. They discovered that, combined with fixation counts and previous observation length, first fixations were efficient in identifying important objects.
- *Timing of the last fixation* was used to study runners' reading of sidewalks (Cullen et al. 2020). They identified situations where participants ran towards the sidewalk curb and measured the timing of the last fixation as a percentage of the trial in which it occurred.
- *Temporal evolution of mean fixation duration* is a metric used by Franěk et al. (2018b) to examine differences in fixation durations at various times during stimulus observation. Participants watched each stimulus for 15 seconds, which was divided into three 5-second intervals, and mean fixation duration was calculated for each part. The study revealed that longer stimuli presentations correlated with longer fixations.

4.5.2 Saccades metrics

The fast eye movements between fixations are called saccades. They are supposed to not provide information about the stimulus to the observer. However, they may provide meaningful information about the strategy and the process of reading landscape. The metrics related to saccades in included studies were:
- *Number of saccades*, also called *saccades count*, counts the saccades made by an observer while viewing a stimulus. A higher count of saccades suggests a broader observation of the stimulus, contributing to a broader perception and holistic understanding of the landscape (Dupont et al. 2015). Landscape experts did more saccadic movements than laymen while observing landscape photographs.
- *Amplitude of saccades*, also called *mean exploration* measures the length of a saccade in degrees of view angle, providing insights into the main observation pattern. Smaller amplitudes, as observed in experts by Dupont et al. (2015), may indicate a more holistic and systematic perception of the stimulus. Additionally, longer amplitudes are associated with photographs that require more effort to be read (Berto et al. 2008). The amplitude of saccades depends on the task. When the task is more holistic oriented, the amplitudes are longer than by analytic oriented tasks.
- *Saccades length* is a metric similar to the amplitude of the saccades, but it is measured in pixels. It reveals valuable information about the saccade lengths. Notably, participants' saccades tend to shrink with increasing task difficulty in search tasks (Credidio et al. 2012).
- *Saccade frequency* calculates the number of saccades per unit of time. A higher frequency may indicate that the stimulus is either too simple or too complex, making it challenging for the observer to find the area of interest. Saccades were found to be less frequent when pleasant sounds or music were playing while participants read the landscape (Liu et al. 2019).

4.5.3 Metrics to study areas of interest

The stimulus could be divided into parts to better understand the way that people read the landscape. These parts are usually called areas of interest. Lin et al. (2014) used the term interest areas, Dong et al. (2020) objects of interest. There are a lot of metrics used with areas of interest:
- *Number of fixations in AOI* represents the count of fixations that the participant made in an AOI. This metric gives a basic view on objects or the parts of the stimulus that attract the most attention. People, signs, or moving objects attract most attention. But the results are influenced by the size of the areas/objects in the stimulus, so that it should be normalized by the size (Dong et al. 2020). In

case of searching tasks, the AOI could be drawn around the object that should be found. The higher the number of fixations, the lower discrimination efficiency (Lin et al. 2014).
- *Duration of fixations in AOI*, also called dwell time in the AOI or time spent looking on particular object, expresses the time duration of fixations in an AOI. It is calculated as the sum of times of each fixation in the AOI. It also could be counted relatively, as a proportion of the total fixations time in the stimulus. This metric is connected to the attractivity of the parts of stimuli. In the case of search tasks, longer fixations in AOIs may signal difficulties to identify the target (Lin et al. 2014). Longer fixations in an AOI may also signalize more fascination with the AOI (Misthos et al. 2020). The experts have longer dwell times in AOIs than novices for tasks connected to biodiversity evaluation (Pihel et al. 2015). The landscape experts spend less time gazing on buildings than laymen in free viewing experiments (Dupont et al. 2015).
- *Number of visits in an AOI* is the number of fixations in the AOI that followed a fixation outside the AOI.
- *Time of the first visit in an AOI* is the time from the beginning of the experiment to the first fixation detected in the AOI. It provides information on the ability to attract attention of the AOI: Shorter times indicate higher attractiveness. The metric also depends on the position of the AOI in the stimulus: for the AOIs placed in the center or on the left side, the time is shorter than for the AOIs in the right part of the stimulus (Misthos et al. 2020). This also is valid for hazards identification by cyclists, as objects located in the center of their view attract their attention faster than the hazards on the sides, although these hazards are more dangerous (Brazil et al. 2017). An object is perceived as more disturbing, the time of the first fixation is shorter (Hayek et al. 2019).
- *First saccade amplitude to interest area* measures the amplitude of the saccade preceding the first fixation in the AOI, particularly useful in search tasks. A shorter saccade amplitude indicates increased difficulty in finding the target (Lin et al. 2014).
- *AOIs sequences* are the sequences of AOIs that were fixated in the time order in which they were fixated. They could be used to study a detailed self-localization strategy (Kiefer et al. 2014). An observer should be successful in the case he/she has the symbol/stimulus in his/her work memory, which means that the AOIs in map and in real environment should be close to each other to provide the effective information.

4.5.4 Eye characteristics

The characteristics of eyes are rarely used in the reading landscape research. There were two metrics in the studies included:
- *Pupil size*, also called *average pupil diameter*. It is related to the restorativeness of the landscape: the more restorative the landscape is, the smaller the pupil is (Nordh et al. 2013). When the stimulus is easy to perceive, the pupil is larger than in the case of difficult stimuli (Gao et al. 2020).
- *Blink rate*, which is counted as the number of blinks per minute, could be a sign of cognitive load: the number of blinks rises with cognitive load (Valtchanov, Ellard 2015). Urban scenes increased blink rates, which means they are more difficult to observe. The blink rate is also positively correlated with the number of fixations and negatively correlated with the fixation duration. The higher the blink rate, the more difficult it is to find the target.

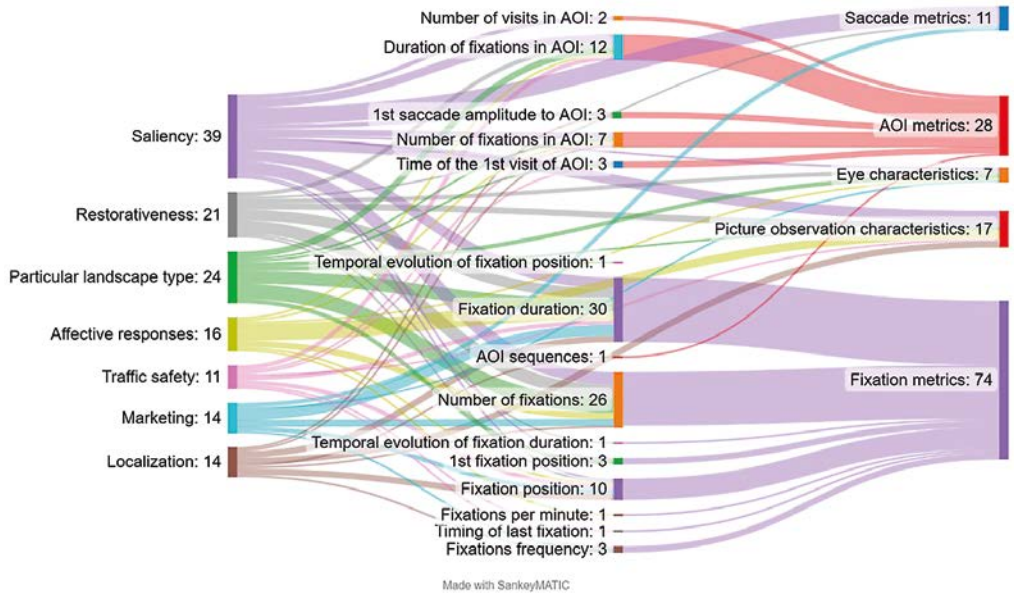

Fig. 8 Relationship of the topic of the study and metrics used.

4.5.5 Stimulus observation characteristics

There is also a wide range of metrics that provide a view on the observation of the stimulus. The metrics used in the included studies were the following:

- *Scanpath length*, also called *eye travel distance* or *former observation length* measures the length of eye movements as the gaze moves from one fixation point to another, typically measured in pixels (Kang and Kim 2019). A shorter scanpath length is associated with natural landscapes compared to built/urban landscapes, indicating a more restorative or coherent landscape (Franěk et al. 2018b). However, Valtchanov and Ellard (2015) found no significant differences in scanpath length between natural and urban landscapes, suggesting the importance of considering fixation counts alongside scanpath length. The metric could also give a rough idea about the proportion of the image that was explored when the longer scanpath corresponds with the larger proportion scanned. Landscape experts have longer scanpaths than laymen when observing landscape (Dupont et al. 2015).
- *Horizontal and vertical angle viewed* represents the range of horizontal and vertical eye movements in the stimulus.
- *Total gaze points*, also called *number of gaze points*, is the number of all points that the eye was caught during the observation. Ren and Kang (2015) and Ren (2019) used this metric, noting variations in gaze points with different landscape types and tasks. For instance, fewer gaze points were observed when assessing visual aesthetic quality compared to tranquility. However, the number of gaze points was not significantly influenced by the type of landscape (Ren 2019).
- *Average nearest neighbor ratio* is a GIS measure that quantifies the spatial distribution of points, where a lower value indicates more clustered points. Dong et al. (2020) utilized this to study stimulus exploration, finding fixations to be more clustered in a real environment compared to a desktop environment during a self-localization task.
- *Mean lateral visual span* represents the effective visual range horizontally and vertically, respectively, while participants gaze at a stimulus (Gao et al. 2020). The higher the satisfaction is, the smaller the mean lateral visual span.
- *Mean portrait visual span* is the effective visual range obtained by participants gazing vertically at a stimulus and the usage and the meaning are the same as the mean lateral visual span (Gao et al. 2020).
- *Number of crossing the center line* is useful when observers need to choose between two variants in the stimulus, such as selecting the left or right street at a crossroads (Emo 2012), indicating the difficulty of making choices.
- *Time-course of fixations* was utilized to study whether participants look at a selected road first, for longer durations, or repeatedly in tasks like choosing a route at crossroads (Emo 2012).
- *Entropy* could be used to characterize the degree of uniformity of a distribution of fixation locations (Backhaus et al. 2020). It varies with the task, being higher for guess tasks, indicating a more even distribution of fixations, and is influenced by what needs to be counted in the picture.
- *Predictability* is the function that can be used to investigate how well an empirically observed fixation density or the fixation density generated by a computational model predicts a set of fixation locations (Backhaus et al. 2020). It is also a task-dependent metric.

4.6 Which eye tracking metrics are used to study different aspects of landscape?

In the initial analysis, metric groups for different topics were examined. Fixation metrics, being the most universally used, were employed across all topic groups. Metrics related to picture observation characteristics and AOIs were utilized in all groups except for marketing studies. Interestingly, in saliency studies, AOIs and fixation metrics were nearly equally prevalent. Saccades metrics were utilized for only two topics: marketing and saliency (Fig. 8).

Among fixation metrics, fixation duration was the most frequently employed metric across all topics (Fig. 8). Except for studies focused on a particular type of landscape (where fixation position was not used) and studies centered on traffic safety (where fixation duration was not used), both fixation position and number of fixations were commonly used across almost all topics. For the traffic safety studies, there were notable differences in fixation metrics and their structure.

In the realm of AOIs metrics, the duration of fixations in AOIs emerged as the most commonly used metric across all but one topic (Fig. 8). The exception was marketing studies, for which no AOIs metrics were utilized. The number of fixations in AOIs was also frequently employed for five topics, excluding marketing and restorativeness. AOI metrics were predominantly employed for studying saliency and particular landscape types. In the case of saliency, there was a diverse range of metrics (five different types, most of them used more than once).

4.7 What are the limitations of using the eye tracking methodology to read landscape?

The eye tracking methodology has introduced new avenues for studying visual attention towards landscapes; however, it also harbors several limitations. Firstly, it is linked to the eye-mind hypothesis, assuming no delay between fixation and processing (Just and Carpenter 1980). The validity of the eye tracking methodology hinges on accepting this hypothesis.

Physiological measures are less sensitive than cognitive measures, posing challenges, especially in studying restorativeness (Nordh et al. 2013). Eye movement data can be affected by motion sickness and visual fatigue. Sang et al. (2014) highlighted that relying solely on heatmaps or first fixation measures is not precise enough for studying reading landscape. Liu et al. (2019) even emphasized the need for additional measures such as EEG or electrodermal activity for a more precise understanding of perception. Another potential issue stems from the risk of movements in infrared reflection lenses, which can disrupt calibration (Cullen et al. 2020). Eye trackers can pinpoint where attention is directed, but not explain the cognitive processes behind it (Lappi 2015). Moving objects often draw attention, irrespective of their other qualities, posing challenges for eye tracking data analyses (Dong et al. 2020).

Furthermore, there are limitations related to laboratory eye tracking experiments. Many authors have cited the restricted field of view (e.g., Schumann et al. 2008; Lappi 2015), which could mean a lack of peripheral object information (Stelling-Konczak et al. 2018) and most fixations being near the center of the picture (Brazil et al. 2017). Focusing solely on eye-in-head movements overlooks head movements. In numerous cases, head movements, a vital aspect of visual attention study, cannot be measured by an eye-tracker (Schumann et al. 2008), and the perception is a passive, not active process (Berto et al. 2008). Participants can't move in a typical laboratory setting, creating difficulties in generalizing research results to real environments where individuals change positions (Dong et al., 2020) or need to navigate around other people to prevent collisions (Franke and Schweikart 2016). The limitation also extends to the tasks given by instruction in a laboratory environment, which aren't naturalistic (Lappi 2015).

Other limitations are tied to using eye trackers in real environments. Real-life situations are exceedingly complex and continuously changing, making it challenging to compare different participants observing different landscapes (Spanjar and Suurenbroek 2020). The accuracy of mobile eye trackers is lower compared to laboratory eye trackers, partly due to infrared radiation from the Sun disrupting infrared eye trackers (Lappi 2015). Processing data from mobile eye trackers, particularly when participants move during the experiment, is time-consuming, leading to a smaller number of participants in studies (Cottet et al. 2018).

5. Discussion

The objective of this systematic review was to aid researchers studying reading landscape with eye trackers by summarizing how previous studies have employed eye tracking methodology in reading landscape research. The findings revealed a noticeable increase in the number of such studies since 2012, mirroring trends observed in research on other phenomena utilizing eye tracking methodology (Borozan et al. 2022 in a study of financial decision making; Blascheck et al. 2017). These studies have primarily been conducted in Europe, North America, and East Asia, with at least one study conducted on each continent, aligning with patterns observed in eye tracking studies on financial decision making (Borozan et al. 2022). The average number of research participants was 40, with a relatively large variance, consistent with eye tracking studies in various fields (Strzelecki 2020; Deng and Gao 2022).

Despite the rapid advancement of digital technology and mobile eye trackers, the most utilized medium continues to be the photograph, typically presented on a computer screen. This preference likely stems from the necessity to acquire high-quality data, as computer-connected eye trackers still offer greater accuracy than their mobile counterparts. However, in comparison to other research domains, real-world experiments are more prevalent in landscape reading studies (Blascheck et al. 2017; Shynu et al. 2021; Borozan et al. 2022; Ke et al. 2024).

The most commonly utilized visualizations of eye tracking data in landscape reading are heatmaps and scanpaths, although accurately evaluating and comparing them can be quite challenging. However, heatmaps are relatively straightforward to read and interpret. This trend is consistent with other topics investigated using eye tracking methodologies (Raptis et al. 2016; Scott et al. 2019; Strzelecki 2020). However, in the realm of landscape reading, there exists a greater diversity in visualization methods. Despite this, several potentially beneficial data visualization methods remain untapped in landscape reading research (Blascheck et al. 2017).

Within landscape reading studies, the metrics employed exhibit greater diversity compared to other areas of eye tracking research, but the most frequently utilized metrics remain consistent: primarily, these involve the number or duration of fixations, followed by saccade metrics (Raptis et al. 2016; Scott et al. 2019; Strzelecki 2020; Ke et al. 2024). Characteristics of eyes are less commonly employed. The use of AOIs, which is typical in landscape reading studies, is absent in research on certain other phenomena (Strzelecki 2020; Ke et al. 2024). While the interpretation of metrics generally aligns (such as cognitive demand for fixation duration or pupil size (Ke et al. 2024)), differing interpretations of some metrics are not uncommon (for instance, a higher number of fixations may indicate greater cognitive demand, but also higher salience of the region in the context of video-based learning studies (Deng and Gao 2022), and reduced engagement with the stimulus

in the case of landscape reading). Several metrics have rather specific interpretations in the context of landscape reading, particularly concerning restorativeness.

The studies included in this review agree that eye tracking has great potential in studying various aspects of landscape reading. It is the second most commonly used method in the study of environmental perception (after EEG, Shynu et al. 2021). The method also appears to be suitable for studying a number of other topics (e.g., Borozan et al. 2022).

5.1 Future directions

Based on the insights from the reviewed studies, several recommendations for future research can be proposed. Firstly, authors are encouraged to provide a more precise description of the eye tracking metrics utilized in their research – the definitions should be more comprehensive to enable readers understand, imagine, calculate and apply the metrics in future research. It should be clarified whether the metric is calculated individually for each participant or collectively for all participants. Authors should also specify whether they calculate the metric from all fixations coordinates or from a specific range within a heatmap. This will enhance reader comprehension and facilitate the assessment of study validity. Secondly, the selection process of participants and their backgrounds should be comprehensively described in each study, to enable readers to evaluate potential generalizability of research outcomes.

Thirdly, there is a need to develop a robust method for the precise analysis of heatmaps, given their frequent use for data visualization and interpretation. Current practices may not fully exploit their potential validity, and leveraging artificial intelligence could significantly enhance the accuracy of heatmap analysis.

Considering the limitations associated with laboratory eye tracking experiments and their potential lack of generalizability to real-life situations, a greater emphasis on conducting eye tracking experiments in real environments is advised. In these settings, a more realistic representation of visual attention may be provided. Progress has been made in analyzing mobile eye-tracker data, leading to increased efficiency, reduced time costs, and improved accuracy (Hooge et al. 2024), thereby enhancing the potential for conducting eye tracking research in real environments. Pervasive gaze sensing technology could potentially be utilized for research in real environments, as it can monitor people's gaze without their knowledge (Valsecchi and Codispoti 2022), thus mitigating the risk of Hawthorne effect potentially occurring during eye-tracking experiments (Worthy et al. 2024).

Another method to address the limitations of laboratory environments is the adoption of webcam-based eye tracking, which has shown increasing accuracy (Kaduk et al. 2023; Saxena et al. 2023). This approach may rely e.g. on computer vision and deep learning techniques (Saxena et al. 2023). With webcam-based eye tracking experiments, participants can remain at home, utilizing their own laptops. Research has demonstrated that employing this form of eye tracking, as opposed to infrared eye trackers, does not significantly affect the outcomes of certain psychological studies (Bogdan et al. 2024). Furthermore, many reviewed studies focused on participant observation without specific tasks, leading to stimulus-driven results. Exploring task-driven perception of landscapes and discerning the strategies employed by different groups of people for varied tasks in the landscape would be intriguing and enrich our understanding. It has been demonstrated that various tasks exert a significant influence on eye movements (Marconi et al. 2023).

Lastly, with the rapid advancements in artificial intelligence, novel methods emulating eye tracking have emerged (e.g., 3M VAS). Future research could delve into understanding how assumptions made by artificial models differ from the perception of diverse groups, such as novices and experts. Notably, significant differences in eye movements have been observed among these groups during landscape observation, warranting a deeper exploration of these disparities.

6. Conclusions

The number of studies focusing on landscape reading utilizing eye tracking methodology has been steadily increasing. Consequently, a systematic review summarizing the methodologies employed in this research was undertaken. The research was primarily conducted in three regions: Europe, North America, and East Asia. A diverse array of media was employed to visualize the landscape. Despite the growing accessibility of mobile eye trackers, photographs remain the predominant choice. Heatmaps and scanpaths emerged as the most frequently used methods for visualizing data, with fixation metrics being the predominant choice in landscape reading research. In the case of saliency studies, metrics of AOIs were utilized just as frequently as fixation metrics.

This review offers a comprehensive overview of the metrics and visualizations associated with eye tracking data in landscape reading research, accompanied by explanations and possible interpretations. As a result, this review stands to be invaluable for researchers in this field, providing reassurance and guidance for their ongoing or future research endeavors. Moreover, journal article reviewers will find this overview exhaustive and informative, aiding them in assessing the accuracy and benefits of new research.

References

Amati, M., Parmehr, E. G., McCarthy, C., Sita, J. (2018): How eye-catching are natural features when walking through a park? Eyetracking responses to videos of walks. Urban Forestry & Urban Greening 31, 67–78, https://doi.org/10.1016/j.ufug.2017.12.013.

Antrop, M., van Eetvelde, V. (2017): Landscape Perspectives. Springer, Dordrecht, https://doi.org/10.1007/978-94-024-1183-6.

Antonson, H., Ahlström, C., Märdh, S., Blomqvist, G., Wiklund, M. (2014): Landscape heritage objects' effect on driving: A combineddriving simulator and questionnaire study. Accident Analysis and Prevention 62, 168–177, https://doi.org/10.1016/j.aap.2013.09.021.

Backhaus, D., Engbert, R., Rothkegel, L. O. M., Trukenbrod, H. A. (2020): Task-dependence in scene perception: Head unrestrained viewing using mobile eye-tracking. Journal of Vision 20(5), 1–21, https://doi.org/10.1167/jov.20.5.3.

Bell, S. (2001): Landscape pattern, perception and visualisation in the visual management of forests. Landscape and Urban Planning 54(1–4), 201–211, https://doi.org/10.1016/S0169-2046(01)00136-0.

Bianconi, F., Filippucci, M., Seccaroni, M. (2019): Survey and Co-design the Urban Landscape. Innovative Digital Path for Perception Analysis and Data-driven Project. Int. Arch. Photogramm. Remote Sens. Spatial Inf. Sci., XLII-2/W15, 165–175, https://doi.org/10.5194/isprs-archives-XLII-2-W15-165-2019.

Blascheck, T., Kurzhals, K., Raschke, M., Burch, M., Weiskopf, D., Ertl, T. (2017): Visualization of Eye Tracking Data: A Taxonomy and Survey. Computer Graphics Forum 36(8), 260–284, https://doi.org/10.1111/cgf.13079.

Bogdan, P. C., Dolcos, S., Buetti, S., Lleras, A., Dolcos, F. (2024): Investigating the suitability of online eye tracking for psychological research: Evidence from comparisons with in-person data using emotion-attention interaction tasks. Behavioral Research Methods 56, 2213–2226, https://doi.org/10.3758/s13428-023-02143-z.

Borozan, M., Loreta, C., Riccardo, P. (2022): Eye-tracking for the study of financial decision-making: A systematic review of the literature. Journal of Behavioral and Experimental Finance 35: 100702, https://doi.org/10.1016/j.jbef.2022.100702.

Brazil, W., O'Dowd, A., Caulfield, B. (2017): Using eye-tracking technology and Google street view to understand cyclists' perceptions, 2017 IEEE 20th International Conference on Intelligent Transportation Systems (ITSC), Yokohama, Japan, 1-6, https://doi.org/10.1109/ITSC.2017.8317619.

Cho, H. (2016): A Study on the Comparison of the Visual Attention Characteristics on the Facade Image of a Detached House Due to the Features on Windows. Journal of Asian Architecture and Building Engineering 15(2), 209–214, https://doi.org/10.3130/jaabe.15.209.

Cottet, M., Vaudor, L., Tronchére, H., Roux-Michollet, D., Augendre, M., Brault, V. (2018): Using gaze behavior to gain insights into the impacts of naturalness on city dwellers' perceptions and valuation of a landscape. Journal of Environmental Psychology 60, 9–20, https://doi.org/10.1016/j.jenvp.2018.09.001.

Credidio, H. F., Teixeira, E. N., Reis, S. D. S., Moreira, A. A., Andrade, J. S. (2012): Statistical patterns of visual search for hidden objects. Scientific Reports 2: 920, 1–6, https://doi.org/10.1038/srep00920.

Cronon, W. (2020): The making of the American landscape. Retrieved from http://www.williamcronon.net/courses/469/ (accessed July 21, 2022).

Cullen, M. M., Schmitt, D., Granatosky, M. C., Wall, C. E., Platt, M., Larsen, R. (2020): Gaze-behaviors of runners in a natural, urban running environment. PLoS ONE 15(5): e0233158, https://doi.org/10.1371/journal.pone.0233158.

Davies, C., Tompkinskon, W., Donnelly, N., Gordon, L., Cave, K. (2006): Visual saliency as an aid to updating digital maps. Computers in Human Behavior 22(4), 672–684, https://doi.org/10.1016/j.chb.2005.12.014.

Deng, R., Gao, Y. (2023): A review of eye tracking research on video-based learning. Education and Information Technologies 28, 7671–7702, https://doi.org/10.1007/s10639-022-11486-7.

Dong, W., Liao, H., Liu, B., Zhan, Z., Liu, H., Meng, L., Liu, Y. (2020): Comparing pedestrians' gaze behavior in desktop and in real environments. Cartography and Geographic Information Science 47(5), 432–451, https://doi.org/10.1080/15230406.2020.1762513.

Dupont, L., Antrop, M., Van Eetvelde, V. (2015): Does landscape related expertise influence the visual perception of landscape photographs? Implications for participatory landscape planning and management. Landscape and Urban Planning 141, 68–77, https://doi.org/10.1016/j.landurbplan.2015.05.003.

Duncan J., Duncan N. (1988): (Re)reading the landscape. Environment and Planning D: Society and Space 6(2), 117–126, https://doi.org/10.1068/d060117.

Dupont, L., Van Eetvelde, V. (2014): The use of eye-tracking in landscape perception research. ETRA '14: Proceedings of the Symposium on Eye Tracking Research and Applications, 389–390, https://doi.org/10.1145/2578153.2583036.

Hu, T., Wang, X., Xu, H. (2022): Eye-Tracking in Interpreting Studies: A Review of Four Decades of Empirical Studies. Frontiers in Psychology 13, https://doi.org/10.3389/fpsyg.2022.872247.

Elsadek, M., Sun, M., Sugiyama, R., Fujii, E. (2019): Cross-cultural comparison of physiological and psychological responses to different garden styles. Urban Forestry & Urban Greening 38, 74–83, https://doi.org/10.1016/j.ufug.2018.11.007.

Emo, B. (2012): Wayfinding in Real Cities: Experiment at Street Corners. In: Stachniss, C., Schill, K., Uttal, D. (eds.) Spatial Cognition VIII. Spatial Cognition 2012. Lecture Notes in Computer Science 7463. Springer, Berlin, Heidelberg, https://doi.org/10.1007/978-3-642-32732-2_30.

Fedotov, D., Matsuda, Y., Takahashi, Y., Arakawa, Y., Yasumoto, K., Minker, W. (2018): Towards Estimating Emotions and Satisfaction Level of Tourist based on Eye Gaze and Head Movement. IEEE International Conference on Smart Computing. Taormina, Italy, 2018, 399–404, https://doi.org/10.1109/SMARTCOMP.2018.00036.

Franěk, M., Šefara, D., Petružálek, J., Cabal, J., Myška, K. (2018a): Differences in eye movements while viewing images with various levels of restorativeness. Journal of

Environmental Psychology 57, 10–16, https://doi.org/10.16910/jemr.11.2.8.
Franěk, M., Šefara, D., Mlejnek, R., Petružálek, J., van Noorden, L. (2018b). Eye movements in scene perception while listening to slow and fast music. Journal of Eye Movement Research 11(2): 8, https://doi.org/10.16910/10.16910/jemr.11.2.8.
Franke, C., Schweikart, J. (2016). Investigation of Landmark-Based Pedestrian Navigation Processes with a Mobile Eye Tracking System. In: Gartner, G., Huang, H. (eds.), Progress in Location-Based Services. Lecture Notes in Geoinformation and Cartography. Springer, Cham, https://doi.org/10.1007/978-3-319-47289-8_6.
Gao, Y., Zhang, T., Zhang, W., Meng, H., Zhang, Z. (2020): Research on visual behavior characteristics and cognitive evaluation of different types of forest landscape spaces. Urban Forestry & Urban Greening 54: 126788, https://doi.org/10.1016/j.ufug.2020.126788.
Hayata, N., Ino, S. (1998). The Differences in Eye Movements and Visual Impressions in Response to Static versus Motion Picture Imagery of Streetscapes. Journal for Geometry and Graphics 2(1), 85–91.
Hayek, U. W., Müller, K., Göbel, F., Kiefer, P., Spielhofer, R., Gret-Regamy, A. (2019): 3D Point Clouds and Eye Tracking for Investigating the Perception and Acceptance of Power Lines in Different Landscapes. Multimodal Technologies and Interaction 3(2): 40, https://doi.org/10.3390/mti3020040.
Hooge, I. T. C., Niehorster, D. C., Nyström, M., Hessels, R. S. (2024): Large eye-head gaze shifts measured with a wearable eye tracker and an industrial camera. Behavioral Research Methods, https://doi.org/10.3758/s13428-023-02316-w.
Just, M. A., Carpenter, P. A. (1980): A theory of reading: from eye fixation to comprehension. Psychological Review 87(4), 329–354, https://doi.org/10.1037/0033-295X.87.4.329.
Kaduk, T., Goeke, C., Finger, H., König, P. (2023): Webcam eye tracking close to laboratory standards: Comparing a new webcam-based system and the EyeLink 1000. Behavioral Research Methods, https://doi.org/10.3758/s13428-023-02237-8.
Kang, Y., Kim, E. J. (2019): Differences of Restorative Effects While Viewing Urban Landscapes and Green Landscapes. Sustainability 11(7): 2129, https://doi.org/10.3390/su11072129.
Kaplan, R. et al. (1989): Environmental Preference: A Comparison of Four Domains of Predictors. Environment and behavior 21(5), 509–530, https://doi.org/10.1177/0013916589215001.
Ke, F., Liu, R., Sokolikj, Z., Dahlstrom-Hakki, I., Israel, M. (2024): Using eye-tracking in education: review of empirical research and technology. Educational technology research and development, https://doi.org/10.1007/s11423-024-10342-4.
Khachatryan, H., Rihn, A., Hansen, G., Clem, T. (2020): Landscape Aesthetics and Maintenance Perceptions: Assessing the Relationship between Homeowners' Visual Attention and Landscape Care Knowledge. Land Use Policy 95: 104645, https://doi.org/10.1016/j.landusepol.2020.104645.
Khaledi, H. J., Khakzand, M., Faizi, M. (2022): Landscape and Perception: A systematic review. Landscape Online 97, 1098, https://doi.org/10.3097/LO.2022.1098.
Kiefer, P., Giannopoulos, I., Raubal, M. (2014): Where Am I? Investigating Map Matching During Self-Localization With Mobile Eye Tracking in an Urban Environment. Transactions in GIS 18(5), 660–686, https://doi.org/10.1111/tgis.12067.
Klein, C., Ettinger, U. (eds.) (2019): Eye Movement Research. Springer Cham, https://doi.org/10.1007/978-3-030-20085-5.
Lappi, O. (2015). Eye tracking in the Wild: the Good, the Bad and the Ugly. Journal of Eye Movement Research 8(5), 1–21, https://doi.org/10.16910/jemr.8.5.1.
Lewis, P. K. (1979): Axioms for Reading the Landscape. In: Meinig, D. W., The Interpretation of Ordinary Landscape: Geographical Essays (pp. 1–12). Oxford University Press, Oxford.
Li, Q., Huang, Z., Christianson, K. (2016): Visual attention toward tourism photographs with text: An eye-tracking study. Tourism Management 54, 243–258. http://dx.doi.org/10.1016/j.tourman.2015.11.017.
Liener, P., Sütterlin, B., Siegrist, M. (2017): The influence of high-voltage power lines on the feelings evoked by different Swiss surroundings. Energy Research & Social Science 23, 46–59, https://doi.org/10.1016/j.erss.2016.11.010.
Lin, C. J., Chang, C.-C., Lee, Y. H. (2014): Evaluating camouflage design using eye movement data. Applied Ergonomics 45(3), 714–723, https://doi.org/10.1016/j.apergo.2013.09.012.
Liu, Y., Hu, M., Zhao, B. (2019): Audio-visual interactive evaluation of the forest landscape based on eye-tracking experiments. Urban Forestry & Urban Greening, 46: 126476, https://doi.org/10.1016/j.ufug.2019.126476.
Liu, Y., Hu, M., Zhao, B. (2020): Interactions between forest landscape elements and eye movement behavior under audio-visual integrated conditions. Journal of Forest Research 25(1), 21–30, https://doi.org/10.1080/13416979.2019.1707341.
Lynch, K. (1960): The Image of the City. M. I. T., Cambridge and London.
Marconi, M., Do Carmo Blanco, N., Zimmer, C., Guyon, A. (2023): Eye movements in response to different cognitive activities measured by eyetracking: a prospective study on some of the neurolinguistics programming theories. Journal of Eye Movement Research 16(2), https://doi.org/10.16910/jemr.16.2.2.
Misthos, L-M., Pavlidis, A., Karabassakis, E., Menegaki, M., Krassanakis, V., Nakos, B. (2020): Exploring the visual impact from open pit mines applying eye movement analyses on mining landscape photographs. International Journal of Mining, Reclamation and Environment 34(9), 609–624, https://doi.org/10.1080/17480930.2019.1576582.
Nathanael, D., Portouli, E., Gkikas, K., Papakostopoulos, V. (2012): What does a motorcyclist look at while driving at urban arterials? Work 41(Supplement 1), 4900–4906, https://doi.org/10.3233/WOR-2012-0783-4900.
Nordh, H. (2012): Quantitative methods of measuring restorative components in urban public parks. Journal of Landscape Architecture 7(1), 46–53, https://doi.org/10.1080/18626033.2012.693780.
Nordh, H., Hagerhall, C. M., Holmqvist, K. (2013): Tracking Restorative Components: Patterns in Eye Movements as a Consequence of a Restorative Rating Task. Landscape

Research 38(1), 101–116, https://doi.org/10.1080/01426397.2012.691468.
Page, M. J., et al. (2021). The PRISMA 2020 statement: an updated guideline for reporting systematic reviews. BMJ 372: n71, https://doi.org/10.1136/bmj.n71.
Petružálek, J., Šefara, D., Franěk, M., Kabeláč, M. (2018): Scene perception while listening to music: an eye-tracking study. In ACM Symposium on Eye Tracking Research & Applications, Warsaw, Poland, June 14-17, 2018, https://doi.org/10.1145/3204493.3204582.
Pihel, J., Sang, Å. O., Hagerhall, C., Nyström, M. (2015): Expert and novice group differences in eye movements when assessing biodiversity of harvested forests. Forest Policy and Economics 56, 20–26, https://dx.doi.org/10.1016/j.forpol.2015.04.004.
Potocka, I. (2013): The Lakescape in the Eyes of a Tourist. Quaestiones Geographicae 32(3), 85–97, https://doi.org/10.2478/quageo-2013-0018.
Raptis, G. E., Fidas, C. A., Avouris, N. M. (2016): Using Eye Tracking to Identify Cognitive Differences: A Brief Literature Review. PCI '16: Proceedings of the 20th Pan-Hellenic Conference on Informatics, no. 21, 1–6, https://doi.org/10.1145/3003733.3003762.
Ren, X. (2019): Consensus in factors affecting landscape preference: A case study based on a cross-cultural comparison. Journal of Environmental Management 252: 109622, https://doi.org/10.1016/j.jenvman.2019.109622.
Ren, X., Kang, J. (2015): Interactions between landscape elements and tranquility evaluation based on eye tracking experiments. The Journal of the Acoustical Society of America 138(5), 3019–3022, http://doi.org/10.1121/1.4934955.
Sang, Å. O., Hagerhall, C., Pihel, J., Holmqvist, K. (2014): Swedish Pasture—An Exploration of Perceptual Attributes and Categorisation. Landscape Research 39(4), 402–416, https://doi.org/10.1080/01426397.2013.793763.
Sang, Å. O., Tveit, M. S., Pihel, J., Hägerhäll, C. M. (2016): Identifying cues for monitoring stewardship in Swedish pasture landscapes. Land Use Policy 53, 20–26, https://doi.org/10.1016/j.landusepol.2015.09.020
Sayegh, A., Rudin, J., Andreani, S., Yan, X., Li, L. (2015): A New Method for Urban Spatial Analysis: Measuring Gaze, Attention, and Memory in the Built Environment UrbanGIS'15: Proceedings of the 1st International ACM SIGSPATIAL Workshop on Smart Cities and Urban Analytics. Bellevue, WA, USA, https://doi.org/10.1145/2835022.2835030.
Saxena, S., Fink, L. K., Lange, E. B. (2023): Deep learning models for webcam eye tracking in online experiments. Behavioral Research Methods 56, 3487–3503, https://doi.org/10.3758/s13428-023-02190-6.
Schumann, F., Einhäuser-Treyer, W., Vockeroth, J., Bartl, K., Schneider, E., König, P. (2008): Salient features in gaze-aligned recordings ofhuman visual input during free exploration of natural environments. Journal of Vision 8(14), 1–17, https://doi.org/10.1167/8.14.12.
Scott, N., Zhang, R., Le, D., Moyle, B. (2019): A review of eye-tracking research in tourism. Current Issues in Tourism 22(10), 1244–1261, https://doi.org/10.1080/13683500.2017.1367367.
Shynu, R. V., Santhosh Kumar, K. G., Sambath, R. D. (2022): Factors influencing environmental perception: A Systematic Review. Journal of Physics: Conference Series 1950: 012040, https://doi.org/10.1088/1742-6596/1950/1/012040.
Smith, G. A. (2002): Place-based education: Learning to be where we are. Phi Delta Kappan 83(8), 584–594, https://doi.org/10.1177/003172170208300806.
Spanjar, G., Suurenbroek, F. (2020): Eye-Tracking the City: Matching the Design of Streetscapes in High-Rise Environments with Users' Visual Experiences. Journal of Digital Landscape Architecture 5, 374–385, https://doi.org/10.14627/537690038.
Spiers, H. J., Maguire, E. A. (2008): The dynamic nature of cognition during wayfinding. Journal of Environmental Psychology 28(3), 232–249, https://doi.org/10.1016/j.jenvp.2008.02.006.
Stelling-Konczak, A., Vlakveld, W. P., van Gent, P., Commandeur, J. J. F., van Wee, B., Hagenzieker, M. (2018): A study in real traffic examining glance behaviour of teenage cyclists when listening to music: Results and ethical considerations. Transportation Research Part F: Traffic Psychology and Behaviour 55, 47–57, https://doi.org/10.1016/j.trf.2018.02.031.
Stevenson, M. P., Dewhurst, R., Schilhab, T., Bentsen, P. (2019): Cognitive Restoration in Children Following Exposure to Nature: Evidence from the Attention Network Task and Mobile Eye Tracking. Frontiers in Psychology 10: 4,. https://doi.org/10.3389/fpsyg.2019.00042.
Strzelecki, A. (2020): Eye-Tracking Studies of Web Search Engines: A Systematic Literature Review. Information 11(6): 300, https://doi.org/10.3390/info11060300.
Takahashi, M., Fujibayashi, K., Shimonaka, T., Sato, M., Sawa, K. (2001): Analysis of colors used on outdoor advertising in urban landscape: a case study in Osaka city. Proc. SPIE 4421, 9th Congress of the International Colour Association, 6 June 2002, https://doi.org/10.1117/12.464635.
Tveit, M. et al. (2006). Key concepts in a framework for analysing visual landscape character. Landscape Research 31(3), 229–255, https://doi.org/10.1080/01426390600783269.
Valsecchi, M., Akbarinia, A., Gil-Rodriguez, R., Gegenfurtner, K. R. (2020): Pedestrians Egocentric Vision: Individual and Collective Analysis. ETRA '20 Short Papers: ACM Symposium on Eye Tracking Research and Applications, Stuttgart, Germany, https://doi.org/10.1145/3379156.3391378.
Valsecchi, M., Codispoti, M. (2022): Eye tracking applied to tobacco smoking: current directions and future perspectives. Journal of Eye Movement Research 15(1), https://doi.org/10.16910/jemr.15.1.2.
Valtchanov, D., Ellard, C. (2015): Cognitive and affective responses to natural scenes: Effects of low level visual properties on preference, cognitive load and eye-movements. Journal of Environmental Psychology 43, 184–195, https://dx.doi.org/10.1016/j.jenvp.2015.07.001.
Wang, M., Zhao, M., Lin, M., Cao, W., Zhu, H., An, N. (2020): Seeking lost memories: application of a new visual methodology for heritage protection. Geographical Review 110(4), 556–574, https://doi.org/10.1080/00167428.2020.1715800.
Wang, T. C., Tsai, C. L., Tang, T. W. (2018): Exploring Advertising Effectiveness of Tourist Hotels' Marketing

Images Containing Nature and Performing Arts: An Eye-Tracking Analysis. Sustainability 10(9), 3038, https://doi.org/10.3390/su10093038.
Widgren, M. (2004): Can Landscape Be Read? In: Palang, H., Sooväli, H., Antrop, M., Setten, G. (ed.), European Rural Landscape: Persistence and Change in a Globalising Environment. Springer, Dordrecht, https://doi.org/10.1007/978-0-306-48512-1_28.
Worthy, D. A., Lahey, J. N., Priestley, S. L., Palma, M. A. (2024): An examination of the effects of eye-tracking on behavior in psychology experiments. Behavior Research Methods, https://doi.org/10.3758/s13428-024-02393-5.
Zhu, X., Zhang, Y., Zhao, W. (2020): Differences in Environmental Information Acquisition from Urban Green – A Case Study of Qunli National Wetland Park in Harbin, China. Sustainability 12(19): 8128, https://doi.org/10.3390/su12198128.

The analysis of premature mortality in selected Central and East European countries

Irina Pahomii[1,2,*]

[1] Charles University, Faculty of science, Department of Demography and Geodemography, Czechia
[2] Center for Demographic Research, NIER, AESM, Moldova
[*] Corresponding author: irina.pahomii@natur.cuni.cz

ABSTRACT

Despite mortality improvements across Europe, premature mortality notably persists in Central and East European countries. This study is aimed to assess premature mortality variations across Central and East European countries from 1970 to 2019, employing both classical premature mortality indicators and the more nuanced lifespan disparity indicators. Specifically, the analysis utilised the proportion of deaths up to the age of 65, lifespan disparity, and an age threshold derived from lifespan disparity to explore mortality trends. The findings reveal a stable reduction in premature mortality within Central European and Baltic countries, contrasting with the pronounced fluctuations experienced by East European countries. Remarkably, Czechia, Slovakia, and Estonia demonstrating the most significant progress in mitigating premature deaths. The trajectory of premature mortality in Central and Eastern European nations underscores the influence of socioeconomic crises and distinct alcohol consumption patterns on mortality trends. The study highlights the limitations of employing a static age threshold of 65 years in analysis of premature mortality, which fails to capture the full scope of premature mortality realities, particularly among females. However, the traditional metric of deaths before age 65 provides a broadly understandable measure, the nuanced insights offered by lifespan disparity and its derived age threshold enhance our understanding of premature mortality dynamics. Recognising the strengths and limitations of each indicator is essential for advancing our grasp of premature mortality and for refining the development and execution of targeted public health interventions throughout Europe.

KEYWORDS

premature mortality; lifespan disparity; age threshold; proportion of deaths

Received: 15 February 2024
Accepted: 12 June 2024
Published online: 25 June 2024

Pahomii, I. (2024): The analysis of premature mortality in selected Central and East European countries. AUC Geographica 59(1), 137–148
https://doi.org/10.142/23361980.2024.9

1. Introduction

Over the past five decades, life expectancy at birth has shown a consistent upward trend across all European countries, albeit following different paths and trajectories. Certain countries, particularly those in Western Europe, have achieved remarkable success, witnessing substantial increases in life expectancy. Conversely, East European countries have experienced more modest gains in reducing mortality levels. Furthermore, the mortality process in European countries has undergone significant transformations, evident in changes in overall mortality levels and intensities and in shifting societal attitudes and perspectives towards mortality. Significantly, considerable variation exists in the age structure of mortality among European countries, reflecting diverse societal, cultural, and healthcare contexts. Against this backdrop, premature mortality emerges as a subject of profound interest and concern.

This study aims to assess the variations in premature mortality across selected Central and East European countries – Belarus, Bulgaria, Czechia, Estonia, Hungary, Latvia, Lithuania, Moldova, Poland, Russia, Slovakia and Ukraine – from 1970 to 2019.

One of the central objectives of this study is to employ two distinct methodological frameworks – traditional and alternative – to capture the evolution of premature mortality. The traditional framework implies an indicator based on a pre-defined age to highlight premature deaths. This approach could induce some distortions when the analysis is conducted on a set of countries or for some extended period of time. At the same time, the alternative framework will imply the lifespan disparity indicator. Lifespan disparity is a measure of the variation in age at death among individuals within a population. This metric complements traditional mortality measures by providing insight into the distribution of deaths across different ages, thus reflecting on the equity of health outcomes across a population. Also, the lifespan disparity is particularly sensitive to deaths occurring at younger ages, making it a valuable tool for assessing the impact of policies or interventions aimed at reducing premature mortality.

2. Literature review

In scholarly discourse, premature mortality garners substantial attention, yet a consensus on its precise definition remains elusive (Committee on Population National Research Council 2015; Sørheim et al. 2024). Conceptually, premature mortality encompasses deaths occurring before their anticipated time, posing a challenge in delineating a threshold that distinguishes premature from "late" mortality (Lapostolle et al. 2008). In the field literature could be distinguished various approaches corresponding to different conceptions of premature mortality (Sørheim et al. 2024). One and more common approach used a pre-defined, absolute age threshold. Based on this conception, all deaths which occurred under the pre-defined age threshold are considered premature ones. Various age thresholds, including 65 (Eames et al. 1993; Eurostat 2002; French National Institute for Statistic and Economic Studies 2023), 70 (OECD 2011) and 75 years (Wong et al. 2002) have been proposed, yet a universally accepted mechanism for their determination remains absent. The researcher's scientific interest predominantly influences this selection process (Wise et al. 1988; Mingot et al. 1991).

Another approach, which involves the existence of an age threshold but offers a more dynamic perspective linked to mortality dynamics and temporal fluctuations, is based on lifespan variation. According to this framework, the deaths are categorised as premature when their incidence contributes to an increase in the lifespan disparity (Sørheim et al. 2024). Based on this approach, premature mortality is evaluated through the lifespan disparity indicator, which indicates an average number of years lost. In typical scenarios, this measure of disparity suggests a threshold value ($a^{\dagger}$) for a population. Preventing deaths below this threshold decreases the disparity measure, while preventing deaths above it increases disparity (Zhang and Vaupel 2009; Zhang and Li 2020). Therefore, this disparity point shifts over time in response to changes in a population's longevity.

Despite the methodological issues, premature mortality is subject to intensive investigation and is recognised as a significant concern in Eastern Europe (Németh et al. 2023). The collapse of the Soviet Union significantly influenced the trajectory of premature mortality in countries from region. Following this event, Bobadilla and colleagues conducted a comprehensive analysis, assessing the level of premature mortality and identifying key contributing factors (Bobadilla et al. 1997). They underscored the role of risk behaviours in shaping premature mortality trends. Moreover, the impact of risk behaviours, notably alcohol consumption, was highlighted in Central European countries such as Czechia, Hungary and Poland, compared to other European countries such as France, Sweden and the United Kingdom (Rehm et al. 2007). Another noteworthy aspect of premature mortality in East European countries is the pronounced gender disparity (Murphy 2011), exceeding that observed in Central or West European counterparts (McKee and Shkolnikov 2001). However, Central European countries exhibit an intermediate pattern of premature mortality evolution between East and West European countries (Megyesiova and Lieskovska 2019; Németh et al. 2023).

3. Background

This study delves into the period between 1970 and 2019. This period is characterised by distinctive socioeconomic and political evolution in Eastern and Central Europe. These changes have had far-reaching impacts, notably on the demographic trends within the region, especially on the evolution of mortality.

In the socialist period in the countries from the region, the Semashko centralised model for healthcare was implemented. While effective in some respects, such as in controlling communicable diseases and achieving high vaccination coverage rates, the model's downfall began with the Soviet Union's economic challenges in the 1980s, leading to a decline in healthcare quality (Glushkova et al. 2023). After the dissolution of the Soviet Union and the gaining of independence, the Baltic and Central European countries developed distinct healthcare models compared to East European countries, mainly based on the Semashko model.

It is important to note that the period of pre- and post-dissolution of the Soviet Union brought a high divergence in aspects of the region's socioeconomic development. Most East European countries needed a more extended period to recover after the unstable

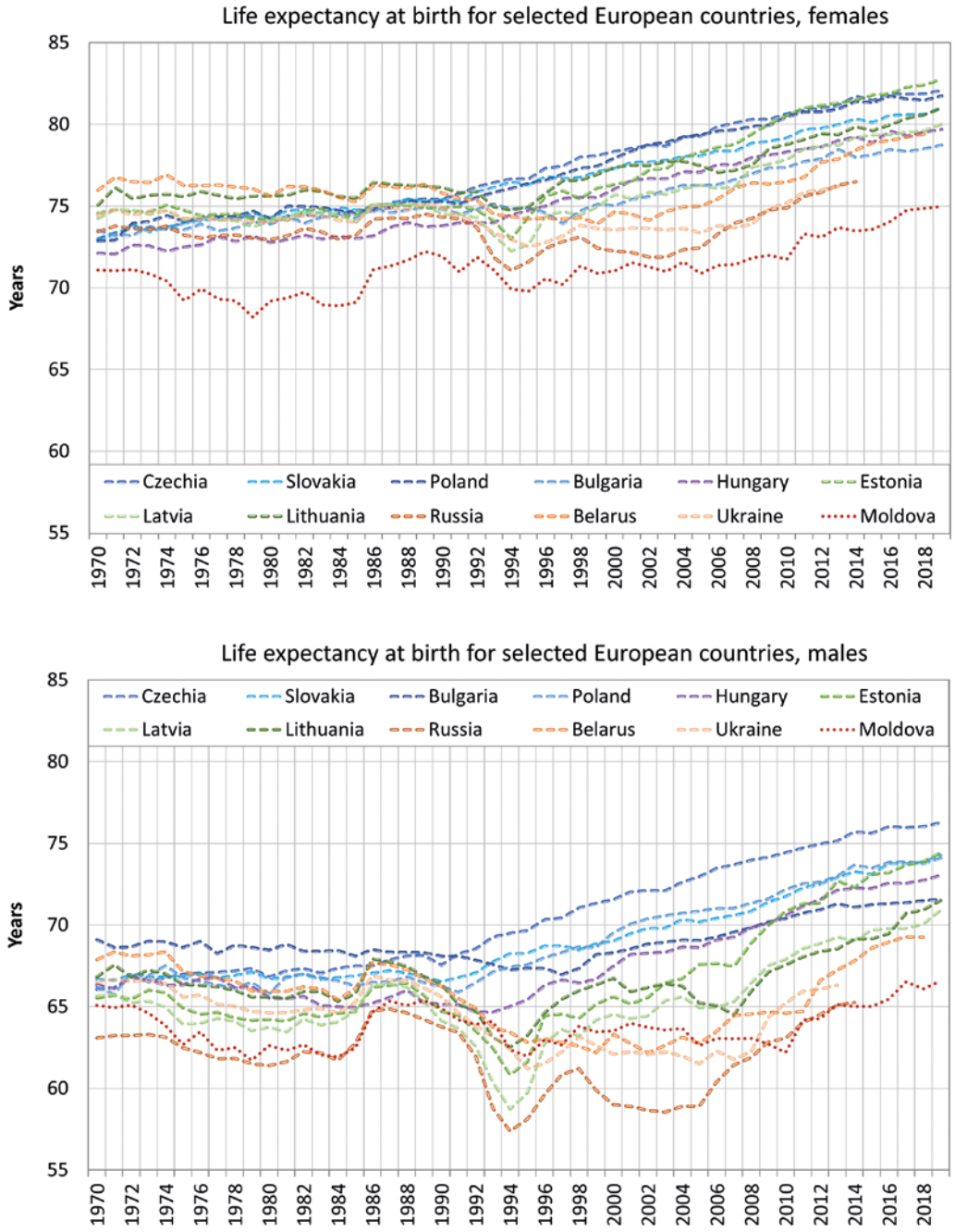

Fig. 1 Life expectancy at birth dynamic in selected European countries, both sexes.
Source: Based on HMD data for all countries except Moldova.

period of the '90s, followed by several regional financial crises. Towards the late 20th century, socioeconomic and political upheavals substantially reduced life expectancy at birth, especially among males, dropping below levels seen between 1965–1970. A resurgence in life expectancy was only evident in the early 21st century, eventually matching the 1970 levels. That highlights the substantial impact that socio-political fluctuations have on public health indicators.

Despite all the changes and transformations observed in the analysed period, overall mortality declines in all analysed countries, with significant variation by region and sex. Central European countries have shown remarkable progress, particularly among females (Fig. 1). Czech females, in particular, exhibited an impressive growth of 9.1 years in life expectancy at birth, while their male counterparts experienced a notable increase of 10.2 years. Similarly, females in Poland, Slovakia, and Hungary demonstrated commendable progress, with respective gains of 8.9, 8.1, and 7.6 years. Although the corresponding male populations were experiencing slightly smaller increments, they still showcased significant improvements at 7.9, 7.6, and 6.7 years. Comparatively, Bulgaria recorded more modest advancements for both genders in Central European countries. Females in Bulgaria experienced an increase of 5.2 years in life expectancy at birth, while males saw a twice smaller growth of 2.5 years. Notably, Baltic countries displayed more favourable indicators when contrasted with their East European counterparts. Estonia witnessed a robust growth in life expectancy at birth, mirroring other Central European countries, with increases of 8.2 years for females and 8.9 years for males. Meanwhile, Latvia and Lithuania demonstrated gains of 5.8 and 6 years in females and 5.3 and 4.7 years in males. Conversely, East European countries exhibited the most minor progress in life expectancy at birth during the abovementioned period. In Moldova, females gained 3.9 years to life expectancy at birth values; in Belarus, 3.4 years for 1970–2018; and in Russia and Ukraine, 3 and 1.8 years for 1970–2014 and 1970–2013, respectively. In males, the gains were much more modest – 1.5, 1.4, 2.2 and –0.2 years.

Even though life expectancy at birth is growing in almost all countries, the age pattern of mortality varies greatly (Meslé 2004). The countries achieving the most significant gains in life expectancy at birth have successfully postponed deaths to the oldest ages and reduced premature mortality – a trend not as prevalent in East European countries.

4. Data and methods

This study focuses on an analysis across selected European countries, specifically East European countries (Belarus, Russia, Ukraine, Moldova), Baltic (Estonia, Latvia, Lithuania), and Central European countries (Bulgaria, Czechia, Hungary, Poland, Slovakia). The research encompasses the period from 1970 to 2019.

The choice of the initial year for analysis, 1970, is dictated by the earliest available data for Moldova, while the terminal year, 2019, marks the last year before the onset of the global pandemic. The exclusion of the pandemic period from this study is deliberate, aiming to scrutinise the trends in premature mortality during a phase of normal mortality evolution devoid of extraordinary circumstances. Furthermore, it is essential to note the variability in the data endpoints for Belarus, Russia, and Ukraine. Specifically, the dataset extends to 2018 for Belarus, 2014 for Russia, and 2013 for Ukraine. Despite the temporal discrepancies in the datasets for these countries, their inclusion in the analytical model is justified by their critical significance in understanding the mortality dynamics in East European contexts. These nations serve as pivotal models for the analysis of East European countries.

Mortality data for all examined countries, except Moldova, were sourced from the Human Mortality Database (HMD). Owing to challenges associated with accurately accounting for migration, data for Moldova were obtained from two distinct sources. The initial dataset, covering the period from 1970 to 2013, incorporates information on the population exposed to risk and the number of deaths by age and sex. This dataset was derived from an alternative source, specifically the retrieved population data published by Olga Penina et al. (2015). From 2014 to 2019, data concerning the exposed population and mortality by age and sex were procured from the National Bureau of Statistics Database (NBS). This latter dataset has been adjusted to exclude long-term migrants and residents living abroad, ensuring its compatibility with the alternative data provided by Penina and colleagues.

For the countries subject to analysis, excluding Moldova, complete life tables were obtained directly from the HMD. For Moldova, the author calculated the complete life table, employing methodologies compatible with the HMD to mitigate any substantial discrepancies. Even data for Moldova supposed the engagement data from diverse sources was very important to include Moldova in this analysis, because this enabled the generation of a more thorough depiction of the situation in the East European region. In the base of the life tables data was computed lifespan disparity. The lifespan disparity ($e^{\dagger}$ – e-dagger) is the average remaining life expectancy when death occurs or life years lost due to death (Shkolnikov et al. 2011). It weights the average remaining life expectancy at age x by the number of life table deaths at age x (Kibele 2012).

The used formula is expressed as follows:

$$e^{\dagger} = \sum_{\alpha=0}^{\omega-1} d_{\alpha} \bar{e}_{\alpha} \quad (1)$$

Where,
ω – is the highest age group;
$\bar{e}_{\alpha}$ – is the average remaining life expectancy at age α;
d_{α}– is the number of life table deaths at age α;
α – age.

The age threshold, which divided "early/premature" by "late" deaths, was highlighted based on lifespan disparity. The age threshold derived from the lifespan disparity indicator represents, in essence, the age at which many deaths and a high remaining life expectancy are observed (Vaupel et al. 2011; Kibele, 2012). According to Zhang and Vaupel (Zhang and Vaupel 2009), this age threshold can be identified based on the following relationship:

$$e^{\dagger} = e(a)(1 - H(a)) \quad (2)$$

Where,
$H(a)$ – cumulative hazard to the age a;
$e(a)$ – life expectancy at age a.

Thus, according to the method presented by Zhang and Vaupel, $a^{\dagger}$ is the age at which the relationship shown in equation 2 is true. To identify this age, the direct interpolation method was applied.

To evaluate premature mortality based on a "traditional" age pre-defined approach, the proportion of deaths occurring before the age of 65 was calculated. This age threshold, 65 years, was selected to avoid underestimating premature mortality in East European countries, where male mortality rates are particularly high. The calculation of the proportion of premature deaths was refined using life table deaths, allowing for an assessment that mitigates the impact of population number and structure variances, thus providing a more precise measure of premature mortality in the region.

5. Main results

The period under analysis can be delineated into two different phases, corresponding to the socioeconomic and political development of countries involved in the analysis. The initial phase encompasses the era up to the dissolution of the USSR, while the subsequent phase commences in 1992, following the dissolution. The proportion of premature deaths, defined here as deaths occurring before the age of 65 years, exhibits divergent trends across the analysed countries (Fig. 2) during these two phases. The first stage, between 1970–1991, is characterised by a higher convergence than the period from 1992. The data variance in males from 1992 to 2019 is 5 times higher than for the previous period, while it was just two times higher for females. Females are characterised by higher convergence in terms of trends of premature mortality compared to males in both periods before and after the dissolution of URSS.

Females exhibit a lower proportion of premature deaths before the age of 65 in comparison to males. During the timeframe spanning 1970 to 1991, gender-based discrepancies in the proportion of premature deaths before the age of 65 varied from 1.5 to 2.2, indicating that the proportion of premature deaths before the age of 65 among males was between 1.5 and 2.2 times greater than that observed in females. The most minimal discrepancies were observed in Moldova, attributable to the relatively higher proportion of premature deaths recorded among females in this region. After the dissolution of the USSR, the gender gap in terms of the proportion of premature mortality before the age of 65 widened further, with the rate among males rising to between 1.9 and 2.5 times the rate seen in females.

Between 1970 and 1991, most countries engaged in this study exhibited remarkably parallel trends regarding the evolution of premature mortality levels (Fig. 2). Initially, in 1970, these countries commenced with notably similar levels of premature mortality, with the exceptions being Bulgaria and Russia for males and Moldova for females. Moldova, in particular, documented the highest proportion of premature deaths up to the age of 65 among females relative to other countries in the analysis. Among males, Bulgaria recorded a lower proportion of premature deaths up to 65 years, whereas Russia reported the highest when compared to all other countries under examination. Starting from 1992, a significant divergence among the countries can be observed, with distinct patterns of premature mortality rate evolution emerging for both females and males. Central European countries followed a steady and practically linear course in reducing the rate of premature deaths, whereas significant fluctuations characterised countries from the East European and Baltic countries. These fluctuations disrupted the overall trend of reduction, highlighting a contrast in the progression of premature mortality rates between the two groups of countries.

The period between 1970 and 1991, in the evolution of the proportion of premature deaths among females, can be characterised more by stagnation and insignificant fluctuations. An exception in this regard is presented by Moldova, where fluctuations were more intense than in other countries, yet the general trend of stagnation in the overall level of premature mortality was still maintained. The highest reduction in this phase, 1970–1991, was registered in Czechia – 3.9 p.p. After 1992, the proportion of premature deaths among females in Central European countries, particularly in the Czechia, Slovakia, and Poland, followed a very steady and linear decreasing trend. The reductions were less significant but similarly characterised by a marked linearity for Bulgaria and Hungary. Countries from the East region and

Baltic zone experienced pronounced fluctuations immediately after the dissolution of the USSR, reaching a peak in 1994–1995. After the mid-90s, the Baltic countries (Estonia, Latvia, and Lithuania) joined the firm trend of reduction observed in the Central European countries. Due to these fluctuations, females from East European countries remained at a relatively high level of premature mortality compared with other countries. The highest reduction in the East European and Baltic countries from 1992 was registered for Estonia – 10.5 p.p.

For males, the situation is quite different. Even from 1970 through 1991, different trajectories could be observed in the evolution of the proportion of premature deaths among males. Hungary represented an intermediate model of evolution. In all countries except Czechia, during this period, an increase in the proportion of premature deaths was noted. A slight decrease of 2.6 percentage points in Czechia was recorded – from 38.5% to 35.9%. In the other countries, the increase varied from 1.1 percentage points in Russia – from 46% to 47.1% – to 9.7 percentage points – from 35.6% to 45.2% in Hungary. One of the noteworthy moments during this period was the reduction in premature mortality between 1986 and 1988 in the East European and Baltic countries.

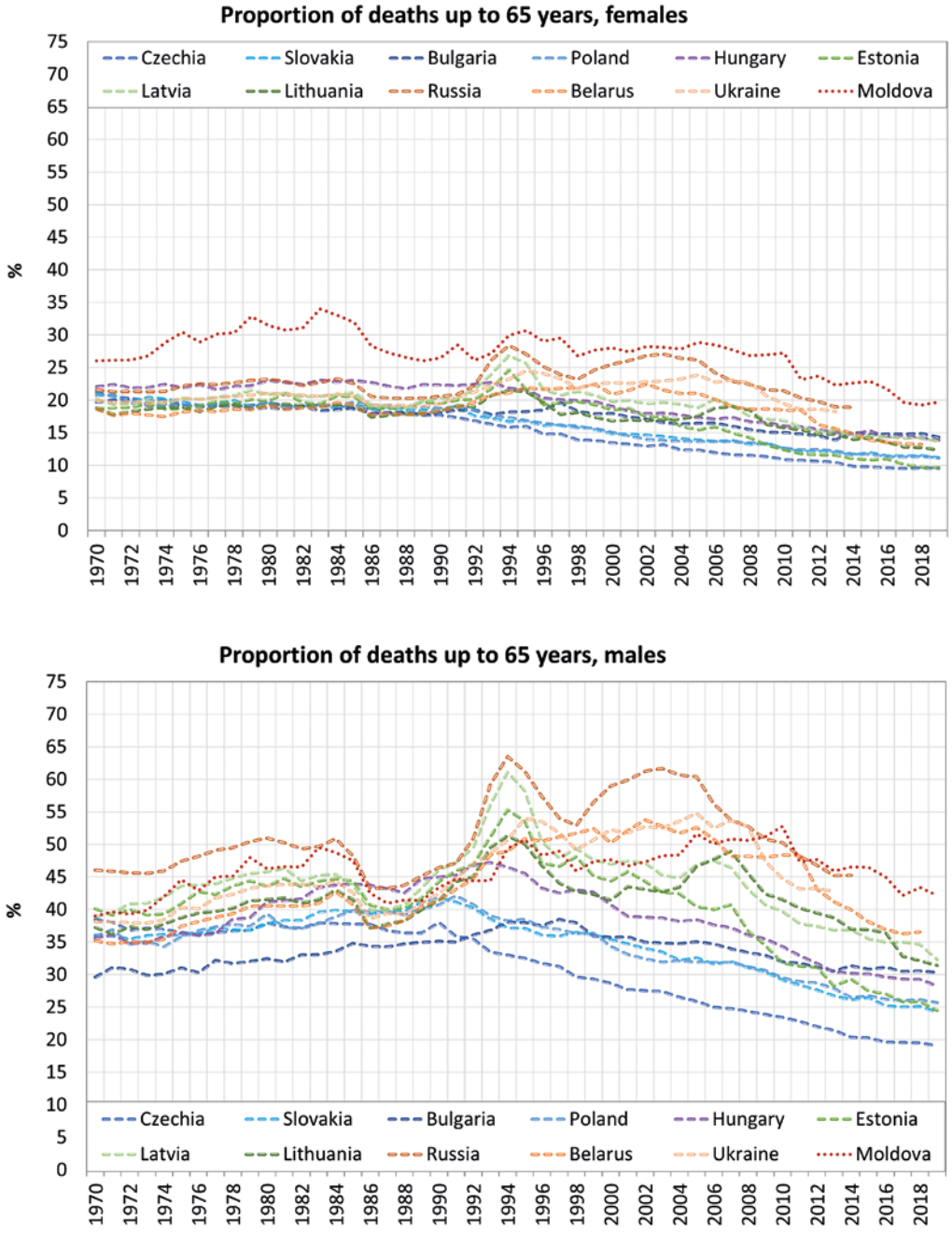

Fig. 2 Proportion of premature deaths up to 65 years in selected European countries, both sexes.
Source: Author calculations based on HMD data for all countries except Moldova.

This reduction, which is very evident among males, represents the effect of the anti-alcohol campaign promoted by Gorbachev. The proportion of premature deaths was reduced by 3 to 5 percentage points in the countries within the bloc. The collapse of the USSR and the subsequent socioeconomic crisis led to a significant increase in premature mortality among males. The dissolution of the USSR resulted in a dramatic and sudden transition to a market economy for the East European and Baltic countries, as well as for the Central European countries. The most affected were the post-socialist countries, especially those in Eastern Europe. In Belarus, Moldova, Russia, and Ukraine, an increase in the proportion of premature deaths was observed over a more extended period; disregarding some fluctuations, this lasted until the beginning of the new millennium. The prolonged increase was determined by perpetuating the trend observed immediately after dissolution. In the years immediately after the collapse of the USSR, males from Belarus noted an increase in the proportion of premature deaths from 44.7% in 1992 to 50.8% in 1995; in Moldovan males, it increased from 44.4% to 50.7% in the same period. In Russia, the proportion of premature deaths among males increased by approximately 13 percentage points in the next two years after the collapse of the USSR; in Ukraine, the rise constituted 7 percentage points in the period 1992–1995. The Baltic countries, despite a considerable increase in the proportion of premature deaths in the years following the collapse – 9 percentage points noted in Estonia from 1992 to 1994 years, 11 percentage points for Latvia and 6 percentage points for Lithuania for the same period; managed to recover at a much faster pace. Among the Central European countries, only Bulgaria and Hungary were observed to have a similar trend but at a significantly lower level than that observed in Baltic countries. At the same time, in Czechia, Slovakia, and Poland, the beginning of a stable period of reduction in the proportion of premature deaths was noted. Cumulatively, for the entry analysed period, 1970–2019, the highest reduction was observed in Czech males – 19.4 p.p. while in the East European countries was observed the worst situation – the proportion of premature deaths at the end of the analysed period was even higher than values from the beginning. The Baltic countries registered an intermediary position between the Central and East European countries. Estonia obtained a reduction in the proportion of premature deaths up to 65 years in males by 15.6 p.p., and Latvia and Lithuania gained more moderate reductions by 6.6 and 5.8 p.p., respectively. The evolution of the proportion of premature mortality up to 65 years is very fragmentary in males from East European countries. The proportion of premature deaths up to 65 years in Ukrainian males in 2013 was approximately 5 p.p. higher than in 1970, while in Russian males, just 0.8 p.p. lower. This is mainly determined by the deterioration of the mortality structure that expanded in the early and mid-1990s.

Throughout the analysis period, a consistent trend toward diminishing disparities in lifespan was noted across all examined countries and both sexes (Fig. 3). However, this trend exhibited a more uniform progression in Central European countries, particularly in Czechia and Slovakia, contrasting with a more segmented pattern observed within the East European and Baltic countries. Notably, the divergence in lifespan disparity's evolution across historical epochs – namely the socialist and post-socialist periods – was predominantly evident within the East European and Baltic countries, where Central European countries displayed a relative insensitivity to the socio-political shifts of that era.

In 1970, the disparity in lost life years among females ranged from 14.1 years in Moldova to 11.3 years in Czechia. Moldova presents a distinct and notably specific scenario compared to the mortality structure and patterns observed in other countries included in this study. The lowest level of lifespan disparity and a linear trend toward reduction were notably observed in Czechia and Slovakia. Females from East European and Baltic countries recorded reductions towards the late '80s, aligning with a previously identified gradual decline modestly accentuated by the anti-alcohol campaign. The subsequent crisis following the USSR's dissolution profoundly impacted the trend of lifespan disparity in post-Soviet states. A marked increase in lost life years was observed in Russia, Estonia, and Latvia during 1994–1995. The Baltic countries rapidly ameliorated this surge, achieving significantly lower values by 2019, with Estonia particularly noteworthy. Russia's experience, however, was characterised more by a stagnation in lifespan disparity until a consistent, albeit modest, reduction trend emerged post-2005. The most substantial decreases were seen in Moldova and Belarus, where lifespan disparity values decreased by 28.4% and 23.6%, respectively. These significant reductions were mainly attributable to the exceedingly high initial values recorded at the study's onset. Despite lesser reductions – 17.5% and 15.6% – Czechia and Estonia reported the lowest disparity values at the study's end, mainly due to the lower initial values observed in 1970. Ukraine and Russia experienced the most minor reduction, at 9.5% and 8.7%, respectively. However, it is critical to acknowledge that both countries had already demonstrated a clear downward trend, which likely would have persisted.

Regarding males, a less pronounced reduction in lifespan disparity was observed compared to females. Notably, Estonia and Latvia presented exceptions where the decline was more significant in males than in females, with Estonia witnessing a 16.2% reduction in males compared to 15.6% in females. While not substantial, these discrepancies indicate a divergent trend from other countries under analysis.

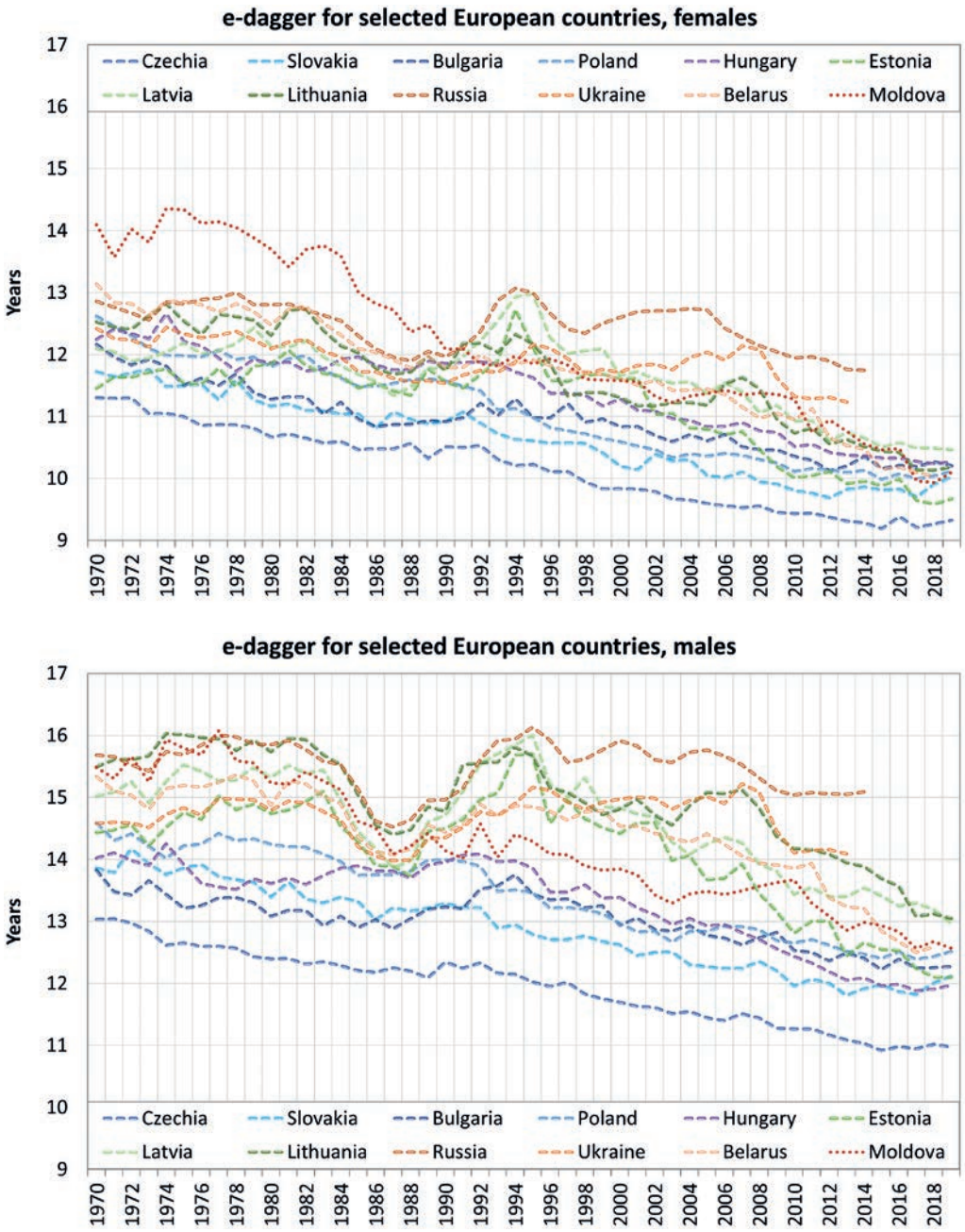

Fig. 3 Lifespan disparity in selected European countries, both sexes.
Source: Author calculations based on HMD data for all countries except Moldova.

Czechia and Slovakia represent distinctive models in the evolution of lifespan disparity among males, exhibiting a steadfast and stable reduction pathway. Czechia, in particular, reported the lowest life years lost towards the study's end. East European and Baltic countires, having been more exposed to the tumultuous events in the former USSR, noted a significant reduction in lost years due to lifespan disparities in the late '80s – attributed to the anti-alcohol campaign – and a profound deterioration in the mid-90s, following the USSR's dissolution and the ensuing socioeconomic crisis. It is paramount to highlight that the deterioration was significantly more severe for Russia and the Baltic States.

Males in Moldova and Belarus saw a more considerable reduction in lifespan disparity throughout the study period, 18.8% and 17.9%, respectively. Estonia, Czechia, and Lithuania also successfully reduced lifespan disparity among males, with reductions approximating 16%. The remaining Central European and Baltic countries obtained reductions between 11 and 15%, with Russia and Ukraine showing minimal progress, at 3.8% and 3.4%, respectively.

Utilising lifespan disparity as a foundational metric, an age threshold delineating premature mortality from deaths occurring at more advanced ages was established. Patterns in age threshold ($a^{\dagger}$) evolution reveal distinct trajectories for males and

females within the analysed European countries (Fig. 4). Among females, a pronounced convergence was observable until the early 1990s, succeeded by a phase of emerging and intensifying divergences. In contrast, male populations consistently diverged across countries from 1970 to 2019. This divergence became particularly pronounced in the early 1990s and the mid-first decade of the 21st century.

For males, divergences showed a clear upward trend from the onset of the period under review, peaking in 2005, followed by a subsequent decline phase. The gap in age thresholds among males widened from 7.3 years in 1970 to 22.2 years in 2005 before narrowing to 9.3 years by 2019. Russia exhibited the lowest age thresholds throughout this period, a distinction that shifted to Belarus and Latvia by 2019. Moldova and Bulgaria displayed the highest thresholds until 1993, after which Czechia consistently showed the highest values for the next 26 years.

In East European countries and Hungary, the male age threshold exhibited significant volatility, contrasting with the more stable trends observed in Czechia, Slovakia, Poland, and Bulgaria. Notably, the latter group experienced a slight decrease in the early 1990s, followed by an increasing trend. Despite

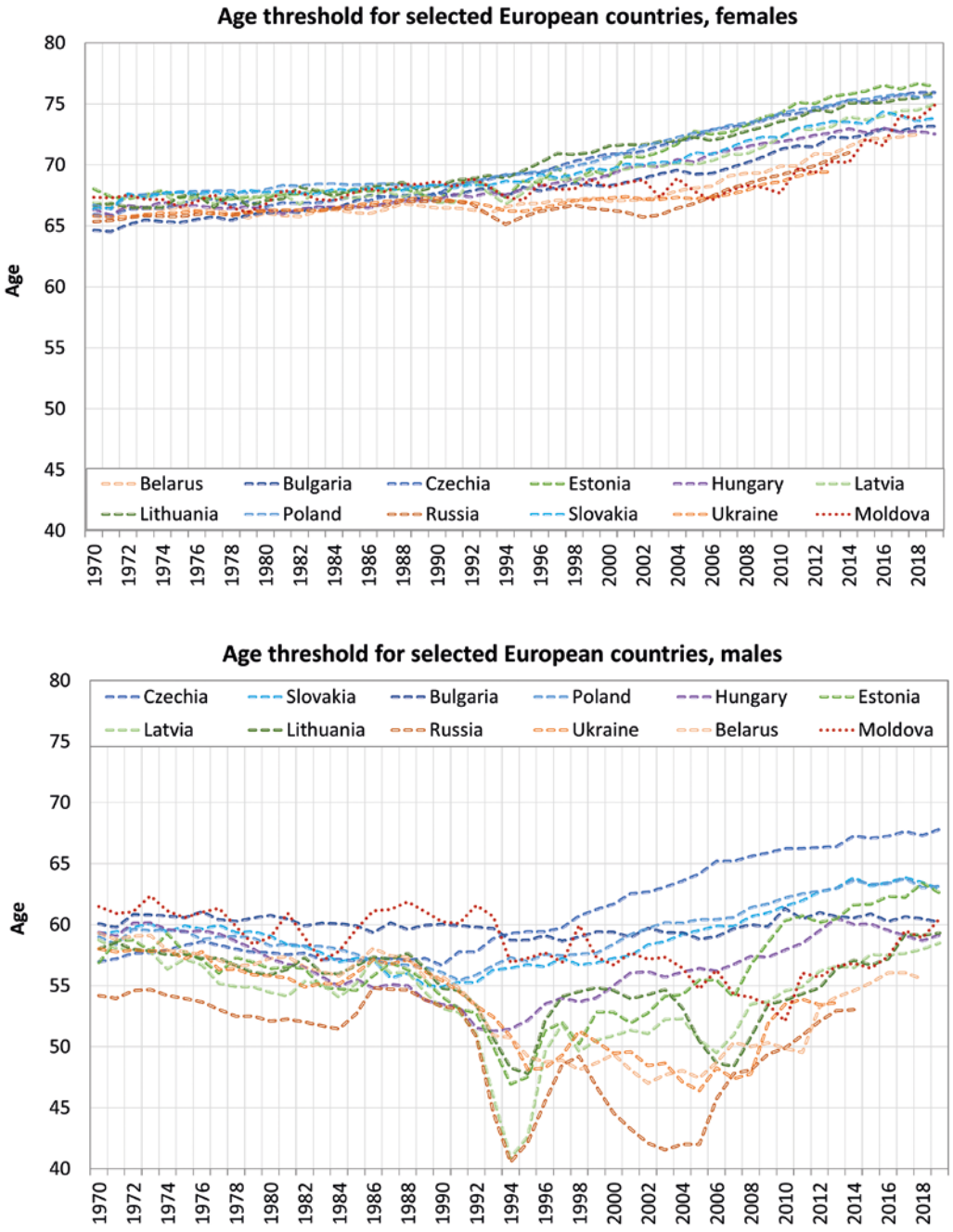

Fig. 4 Age threshold based on lifespan disparity in selected European countries, both sexes.
Source: Author calculations based on HMD data for all countries except Moldova.

starting with one of the highest thresholds in 1970, Bulgaria's trajectory is marked by stagnation, with the age threshold mainly maintaining similar values throughout the period under examination.

6. Discussion

This discussion draws upon comparative studies within the field to further elucidate the complex interplay between healthcare systems, socioeconomic development, and behavioural factors in shaping premature mortality. For instance, Nolte and McKee (2004) and subsequent analyses (Nolte et al. 2004) offer foundational insights into how the efficacy of healthcare systems critically influences levels of premature mortality. Our findings resonate with these insights, highlighting the nuanced roles of healthcare accessibility and quality in East and Central European countries. Acknowledging that the Semashko model implemented in analysed countries played an essential role in reducing premature mortality by promoting universal access to healthcare services is crucial. However, the gains achievable through these measures eventually reached their limits, necessitating systemic modifications to sustain the positive trend in reducing premature mortality. The importance of system transformations, along with the introduction of innovations, is clearly defined in Czech scholarly research, albeit focusing on increasing life expectancy (Lukášová 2018).

Moreover, by integrating the socioeconomic dimensions explored by different researchers (Kontopantelis et al. 2015; Plümper et al. 2018) and the behavioural dimensions of premature mortality, as explored by Leon et al. (2007) and Mackenbach et al. (2015), this study offers a comprehensive analysis that aligns with broader research trends. It is crucial to highlight that these socioeconomic and behavioural factors constitute the primary distinctions between East European and Baltic countries and their Central European counterparts, with alcohol consumption patterns particularly noteworthy. The impact of alcohol consumption was predominantly evident in the improvements noted as a result of the anti-alcohol campaign promoted by Gorbachev. Indeed, during the anti-alcohol campaign, the level of premature mortality observed in East European and Baltic countries was similar to that observed in Central European countries.

The significant disparities in premature mortality outcomes across different socio-political contexts underscore the multifactorial nature of this issue, reinforcing the need for a multidimensional approach to tackling premature deaths. The observed fluctuations in premature mortality, especially during the socioeconomic upheavals after the dissolution of the Soviet Union, provide a case study of the critical importance of resilient and adaptable healthcare systems in mitigating the adverse effects of such transitions on population health.

7. Conclusion

This study thoroughly examines premature mortality trends across European nations, leveraging both traditional and alternative indicators to shed light on the intricate dynamics of early mortality. Traditional indicators, such as the proportion of premature deaths before age 65, benefit from a direct calculation method and straightforward interpretation, facilitating widespread comprehension and application in public health evaluations. However, introducing lifespan disparity as an alternative indicator offers a more nuanced perspective on mortality patterns. By aligning closely with age-specific mortality trends, lifespan disparity adds significant analytical depth and introduces complexity in its calculation and interpretation.

The research underscores the utility of the age threshold derived from lifespan disparity, particularly when juxtaposed with static and absolute age thresholds. This comparison highlights the shifts in general mortality trends and the shortcomings of applying a uniform age threshold over time. Moreover, the derived age threshold from lifespan disparity possesses practical relevance for formulating targeted health strategies and policies. Identifying age groups where reductions in mortality would most effectively diminish lifespan disparity provides critical insights for interventions aimed at curtailing premature mortality. Using lifespan disparity and its associated age threshold allows us to devise nuanced and effective public health strategies tailored to the unique mortality challenges of diverse populations.

Nonetheless, these indicators are not devoid of limitations. The traditional method, while user-friendly, risks simplifying the complexities of premature mortality and might miss significant variations in mortality patterns across different demographics and temporal scales. Conversely, despite offering rich insights, the complexity inherent in the lifespan disparity indicator demands substantial data and analytical expertise, which could hinder its immediate utility in some contexts.

The empirical analysis reveals a consistent trend towards reducing premature mortality across all studied countries, albeit at disparate rates. Central European and Baltic countries display more consistent trends in reducing premature mortality, in contrast to the significant fluctuations observed in East European countries. Notably, Czechia, Slovakia, and Estonia are identified as frontrunners in advancing efforts to reduce premature mortality, evidencing the effectiveness of their public health policies and healthcare systems.

Additionally, the study points to persistent disparities between males and females in premature mortality level, with males disproportionately affected compared to females. This trend remained relatively unchanged throughout the study period, indicating a persistent challenge beyond healthcare access and improvements.

The analysis further critiques the adequacy of the conventional 65-year age threshold in accurately reflecting the nuances of premature mortality, particularly among females, in the examined countries. This observation advocates for a dynamic and context-sensitive approach to defining and assessing premature mortality, capable of accurately capturing mortality pattern shifts and the efficacy of mortality-reduction interventions.

Highlighting the divergent paths of premature mortality reduction in Central European versus East European and Baltic countries the study illustrates the intricate influence of socioeconomic development, healthcare system efficiency, and behavioural factors on health outcomes. The turbulent experience of the East European and Baltic countries emphasises the significant impact of socio-political changes on public health, necessitating ongoing research and targeted interventions.

In conclusion, this research charts the trajectory of premature mortality over a crucial period of European history and establishes a foundation for subsequent research. It advocates for an in-depth understanding of the drivers behind premature mortality and the creation of focused, evidence-based interventions. The findings stress the importance of dynamic, adaptable public health policies capable of effectively addressing the evolving challenges of premature mortality, thus fostering healthier and more resilient societies across Europe. Additionally, the study highlights the imperative of choosing mortality indicators congruent with public health research's specific aims and limitations. While the traditional metric of deaths before age 65 provides a broadly understandable measure, the nuanced insights offered by lifespan disparity and its derived age threshold enhance our understanding of premature mortality dynamics. Recognising the strengths and limitations of each indicator is essential for advancing our grasp of premature mortality and refining the development and execution of targeted public health interventions throughout Europe.

References

Bobadilla, J., Costello, C., Mitchell, F. (1997): Premature death in the new independent states. Washington DC: National Academies Press, https://doi.org/10.17226/5530.

Committee on Population National Research Council (2015): Data Sources and Methodology in the Study of Premature Mortality. Measuring the Risks and Causes of Premature Death: Summary of Workshops (pp. 7–26). Washington: National Academies Press.

Eames, M., Ben-shlomo, Y., Marmot, M. (1993): Social deprivation and premature mortality: regional comparison across England. British Medical Journal 307(6912), 1097–1102, https://doi.org/10.1136/bmj.307.6912.1097.

Eurostat (2002): Chapter 4: Premature mortality. In Eurostat, Atlas on mortality in the European Union, 23–25. Luxembourg: European Communities. Retrieved from https://ec.europa.eu/eurostat/web/products-statistical-books/-/ks-08-02-004.

French National Institute for Statistic and Economic Studies (2023): Definition, methods and quality. Definition. Retrieved from French National Institute for Statistic and Economic studies: https://www.insee.fr/en/metadonnees/definition/c2232.

Glushkova, N., Semenova, Y., Sarria-Santamera, A. (2023): Public health challenges in post-Soviet countries during and beyond COVID-19. Frontiers in Public Health 11: 1290910, https://doi.org/10.3389/fpubh.2023.1290910.

Kibele, E. (2012): Mortality Differentials Across Germany's Federal States. In E. Kibele, Regional Mortality Differences in Germany. Springer Science and Business Media Dordrecht, https://doi.org/10.1007/978-94-007-4432-5.

Kontopantelis, E., Springate, D., Ashworth, M., Webb, R., Buchan, I., Doran, T. (2015): Investigating the relationship between quality of primary care and premature mortality in England: a spatial whole-population study. BMJ 350:h904, https://doi.org/10.1136/bmj.h904.

Lapostolle, A., Lefranc, A., Gremy, I., Spira, A. (2008): La mesure de la mortalité prématurée: comparaison des décès avant 65 ans et des années espérées de vie perdues [Measure of premature mortality: comparison of deaths before age 65 and expected years of life lost]. Revue d'Épidémiologie et de Santé Publique 56(4), 245–252, https://doi.org/10.1016/j.respe.2008.05.025.

Leon, D. A., Saburova, L., Tomkins, S., Andreev, E., Kiryanov, N., McKee, M., Shkolnikov, V. M. (2007): Hazardous alcohol drinking and premature mortality in Russia: a population based case-control study. The Lancet 369(9578), 2001–2009, https://doi.org/10.1016/S0140-6736(07)60941-6.

Lukášová, T. (2018): Semashko health financing model–economic and health consequences in Czechia. Ecoforum 7(1), 7. Retrieved from https://www.ceeol.com/search/article-detail?id=1048055.

Mackenbach, J. P., Kulhánová, I., Menvielle, G., Bopp, M., Borrell, C., Costa, G., Deboosere, P., Esnaola, S., Kalediene, R., Kovacs, K., Leinsalu, M., Martikainen, P., Regidor, E., Rodriguez-Sanz, M., Strand, B.H., Hoffmann, R., Eikemo, T.A., Östergren, O., Lundberg, O. (2015): Trends in inequalities in premature mortality: a study of 3.2 million deaths in 13 European countries. J Epidemiol Community Health 69(3), 2007–2017, https://doi.org/10.1136/jech-2014-204319.

McKee, M., Shkolnikov, V. (2001): Understanding the toll of premature death among men in eastern Europe. BMJ 323:1051, https://doi.org/10.1136/bmj.323.7320.1051.

Megyesiova, S., Lieskovska, V. (2019): Premature Mortality for Chronic Diseases in the EU Member States. International Journal of Environmental Research and Public Health 16(20): 4021, https://doi.org/10.3390/ijerph16204021.

Meslé, F. (2004): Mortality in Central and Eastern Europe: long-term trends and recent upturns. Demographic research 2, 45-70, https://doi.org/10.4054/DemRes.2004.S2.3.

Mingot, M., Rué, M., Borrell, C. (1991): Years of potential life lost: Comparison of 3 calculation methods. Gaceta Sanitaria 5(22), 21–28, https://doi.org/10.1016/S0213-9111(91)71045-5.

Murphy, M. (2011): Adult Mortality in the Former Soviet Union. In R. Rogers, E. Crimmins, International Handbook of Adult Mortality. International Handbooks of Population, vol 2. Springer. Dordrecht, https://doi.org/10.1007/978-90-481-9996-9_4.

Németh, N., Boncz, I., Pakai, A., Elmer, D., Horváth, L., Pónusz, R., Csákvári, T., Kívés, Z., Horváth, I.G., Endrei, D. (2023): Inequalities in premature mortality from ischaemic heart disease in the WHO European region. Central European Journal of Public Health 31(2), 120–126, https://doi.org/10.21101/cejph.a7287.

Nolte, E., McKee, M. (2004): Does health care save lives? Avoidable mortality revisited. London: The Nuffield Trust.

Nolte, E., Scholz, R. D., McKee, M. (2004): Progress in health care, progress in health?: Patterns of amenable mortality in Central and Eastern Europe before and after political transition. Demographic research 2, 139–162, https://doi.org/10.4054/DemRes.2004.S2.6.

OECD (2011): Premature mortality. In Health at a Glance 2011: OECD Indicators (p. 204). Paris: OECD Publishing, https://doi.org/10.1787/health_glance-2011-en.

Penina, O., Jdanov, D., Grigoriev, P. (2015): Producing reliable mortality estimates in the context of distorted population statistics: the case of Moldova, https://doi.org/10.4054/MPIDR-WP-2015-011.

Plümper, T., Laroze, D., Neumayer, E. (2018): Regional inequalities in premature mortality in Great Britain. PLoS One 13(2): e0193488, https://doi.org/10.1371/journal.pone.0193488.

Rehm, J., Sulkowska, U., Mańczuk, M., Boffetta, P., Powles, J., Popova, S., Zatoński, W. (2007): Alcohol accounts for a high proportion of premature mortality in central and eastern Europe. International Journal of Epidemiology 36(2), 458–467, https://doi.org/10.1093/ije/dyl294.

Shkolnikov, V., Andreev, E., Zhang, Z., Oeppen, J., Vaupel, J. (2011): Losses of expected lifetime in the United States and other developed countries: methods and empirical analyses. Demography 48(1), 211–239, https://doi.org/10.1007/s13524-011-0015-6.

Sørheim, P., Barra, M., Norheim, O. F., Gamlund, E., Solberg, C. T. (2024): Premature Death as a Normative Concept. Health Care Analysis 32, 88–105, https://doi.org/10.1007/s10728-023-00471-x.

Vaupel, J., Zhang, Z., van Raalte, A. (2011): Life expectancy and disparity: an international comparison of life table data. BMJ open 1(1): e000128, https://doi.org/10.1136/bmjopen-2011-000128.

Wise, R. P., Livengood, J. R., Berkelman, R. L., Goodman, R. A. (1988): Methodological alternatives for measuring premature mortality. American Journal of Preventive Medicine 4(5), 268–273.

Wong, M., Shapiro, M., Boscardin, W., Ettner, S. (2002): Contribution of major diseases to disparities in mortality. New England Journal of Medicine 347(20), 1585–1592, https://doi.org/10.1056/NEJMsa012979.

Zhang, Z., Li, Q. (2020): The ratio of expansion to compression: A new measure of lifespan disparity. PLoS ONE 15(12): e0243482, https://doi.org/10.1371/journal.pone.0243482.

Zhang, Z., Vaupel, J. (2009): The age separating early deaths from late deaths. Demographic Research 20, 721–730, https://doi.org/10.4054/DemRes.2009.20.29.

The COVID-19 pandemic as the next divergent phase of the East-West mortality gap in Europe

Adéla Pola*, Klára Hulíková Tesárková

Charles University, Faculty of science, Department of Demography and Geodemography, Czechia
* Corresponding author: adela.pola@natur.cuni.cz

ABSTRACT
This paper analyses the variability of life expectancy at birth in Europe after 1950. It aims to assess the development of the East-West mortality gap and to identify the sub-regions or countries that most influenced mortality divergent and convergent trends in Europe. To achieve the goals, European countries are divided into Western and Eastern according to their political history, and the squared coefficient of variation is used for analysis of variability. This measure is further decomposed into between- and within-group components. The results of the study show that there were 4 divergent periods during the study period associated with the delayed cardiovascular revolution and mortality crisis in Eastern Europe and the COVID-19 pandemic. Variability of mortality in Europe during the pandemic was the highest in comparison to all previous divergent periods. Throughout the studied period, the between-group variability was influenced by both the continual progress of Western Europe and the lagging of Eastern Europe, with both regions contributing more or less similarly. However, since the 1990s, in case of within-group variability, a strong dominance of Eastern Europe can be observed, and therefore post-socialist countries deserve special attention. The results also suggest that some longer-term trends in behavior and attitudes towards health may persist in society, and that in the case of an unexpected crisis, there is a greater risk of mortality divergence reappearing.

KEYWORDS
East-West mortality gap; life expectancy at birth; decomposition; post-socialist countries; COVID-19

Received: 26 April 2024
Accepted: 19 June 2024
Published online: 28 June 2024

Pola, A., Hulíková Tesárková, K. (2024): The COVID-19 pandemic as the next divergent phase of the East-West mortality gap in Europe. AUC Geographica 59(1), 149–158
https://doi.org/10.14712/23361980.2024.10

1. Introduction

Mortality in Europe has experienced a turbulent development in recent years in the context of the COVID-19 pandemic, with a disruption of the convergence in mortality between Western and Eastern Europe observed since roughly the beginning of the 21st century. The pandemic is therefore an example of how progress in medicine and relative economic and social stability clearly do not ensure positive mortality trends. On the contrary, the pandemic has reminded us that mortality trends are not linear, as it can be seen as another divergent phase of long-term divergent-convergent mortality sequences. Among other things, it highlighted the weaknesses of the health systems of some European countries, as different countries in Western and Eastern Europe were able to cope with the pandemic in different ways. The effect of the COVID-19 pandemic on the East-West gap needs to be evaluated in the long term and compared with past milestones of divergent-convergent mortality trends in Europe, which is what this article presents.

The rapid decline in mortality in Europe since the beginning of the 20th century can be measured, among other things, by an increase in life expectancy. However, it cannot be said that the development in this indicator of mortality has been constant and consistent in all European countries. On the contrary, since the Second World War, Central, and Eastern Europe has experienced a rapid increase in life expectancy, stagnation, a significant decline, and a renewed increase in the indicator (Aburto and Raalte 2018), while Western Europe has more or less experienced an improvement in mortality rates all along, although the tempo has changed as well. After the period of mortality homogeneity in the 1960s, the divergence between Western and Eastern Europe has been more evident in the male population, especially since the 1970s, when the cardiovascular revolution took place in Western Europe, while the post-socialist countries have not been successful in suppressing cardiovascular diseases. The gap between the two parts of Europe continued to widen, culminating in the 1990s, when mortality rates continued to improve in the West, while some Eastern European countries faced a mortality crisis (Meslé 2004). High mortality rates in Central and especially Eastern Europe have been associated with excess alcohol consumption, violence (Bye 2008; Leon et al. 1997), or high mortality rates among young men (McKee and Shkolnikov 2001).

Since the mid-1980s, it has been possible to observe divergence not only between Western and Eastern Europe but also within the Eastern region. In 1985 Grobachev introduced an anti-alcohol campaign, which had a short-term positive effect across all post-soviet countries. After 1987, however, mortality rates in the Eastern Region diverged (Aburto and Raalte 2018), as mortality trends began to reverse in Central Europe and one country after another restored health progress. In contrast, countries of the former Soviet Union have experienced a renewed decline in life expectancy. In the first half of the 1990s, the economic crisis associated with the transition to a market economy added to the unfavorable demographic trends, which together resulted in a mortality crisis (Meslé 2004).

Since the second half of the 1990s, life expectancy has been increasing all over Eastern Europe, and after the turn of the millennium, it began to converge towards Western Europe. In recent years, however, convergence has started to slow down and there has even been discussion of parallel development between European regions (Leon 2011).

A new perspective on the development of the East-West gap has been brought about by the COVID-19 pandemic when mortality rates worsened across all of Europe, but the course and impact varied between regions. In 2020, mortality rates increased across the whole of Europe, but Western European countries coped better with the pandemic and were able to restore progress in life expectancy in 2021. In contrast, post-socialist countries have been more affected by the pandemic, and life expectancy gains have not yet been restored in many of them. Thus, the COVID-19 pandemic has again widened the gap between Western and Eastern Europe (Shkolnikov et al. 2023).

The mortality burden of the pandemic can also be seen, for example, in the excess mortality, whose level and geographical distribution changed during the pandemic (Hajdu et al. 2024). According to their analysis, the increase in inequality was mainly due to much higher-than-average excess mortality in countries with low pre-pandemic life expectancy at birth as the bottom fifth of analyzed European countries have seen the largest reductions in life expectancy. The increase in variability was greatest in 2021, as confirmed by the largest difference between observed and expected life expectancy. They also pointed out that regional differences in life expectancy would have remained at roughly pre-pandemic levels if COVID-19 had not broken out. In 2022, the variance returned to pre-pandemic levels, although life expectancy was lower than would have been expected in the absence of the pandemic.

The post-war development of mortality in Europe is well known and widely described (e.g. Leon 2011; Meslé 2004; Meslé and Vallin 2002), but less attention has been paid to the variability of life expectancy, which offers a different perspective to assess convergent and divergent mortality trends. This paper fills this gap and presents an analysis of the variability of life expectancy at birth in Europe after 1950. Since mortality trends during the period under review differed not only between Western and Eastern Europe but also within regions, the analysis includes a decomposition of the overall variability into between- and within-group components. Thus, the aim of the

paper is not only to assess how mortality variability has changed in Europe after the Second World War but also to identify the turning points where the long-term trend in variability has been disrupted and the countries that caused the divergence. Finally, the paper aims to determine whether the increase in overall variability was driven more by differences between Western and Eastern Europe or by variability within these regions.

2. Data and methods

We analyzed the variability of life expectancy at birth in Europe between 1950 and 2022 using data from World Population Prospects (United Nations 2022). Most European countries were involved in the analysis, excluding those with less than 1 million inhabitants, and Bosnia and Herzegovina because of the war between 1992 and 1995, which could be expected to have a major impact on the results. As the aim of this paper is to examine trends, the fluctuation due to war is not desirable. For the purpose of the analysis, European countries were divided based on a political history and literature review into Western (Region 1) and Eastern (Region 2). Region 1 consists of 17 countries from Northern, Western, and Southern Europe, and Slovenia, which is included in the Western region for geographical reasons and also due to the development of mortality rates since the end of the 20th century, since when it has been remarkably converging towards Western European mortality trends. Region 2 includes 17 post-socialist countries from Central, South-Eastern, and Eastern Europe, the Baltic States and Albania, Northern Macedonia, and Serbia. A list of all countries analyzed, together with their affiliation to the Western or Eastern region, is provided in the Tab. 1.

Tab. 1 Analyzed European countries and their regional affiliation.

Region 1 = Western Europe	Region 2 = Eastern Europe
Austria	Albania
Belgium	Belarus
Denmark	Bulgaria
Finland	Croatia
France	Czechia
Germany	Estonia
Greece	Hungary
Ireland	Latvia
Italy	Lithuania
Netherlands	North Macedonia
Norway	Poland
Portugal	Republic of Moldova
Slovenia	Romania
Spain	Russian Federation
Sweden	Serbia
Switzerland	Slovakia
United Kingdom	Ukraine

The first step of the analysis was to assess convergence trends between Western and Eastern Europe. As a basic measure of variability, we used the coefficient of variation squared (as defined e. g. by Chameni Nembua 2006):

$$CV^2 = \frac{Var}{\mu^2} = \frac{\frac{1}{n}\sum_{i=1}^{n} x_i^2 - \mu^2}{\mu^2} = \frac{1}{2n\mu^2}\sum_{i=1}^{n} x_i^2 + \frac{1}{2n\mu^2}\sum_{j=1}^{n} x_j^2 - \frac{1}{\mu^2}\left(\frac{1}{n}\sum_{i=1}^{n} x_i\right)\left(\frac{1}{n}\sum_{j=1}^{n} x_j\right) =$$
$$= \frac{1}{2n^2\mu^2}\sum_{i=1}^{n}\sum_{j=1}^{n} x_i^2 + \frac{1}{2n^2\mu^2}\sum_{i=1}^{n}\sum_{j=1}^{n} x_j^2 - \frac{2}{2n^2\mu^2}\sum_{i=1}^{n}\sum_{j=1}^{n} x_i x_j =$$
$$= \frac{1}{2n^2\mu^2}\sum_{i=1}^{n}\sum_{j=1}^{n}\left(x_i^2 + x_j^2 - 2x_i x_j\right) = \frac{1}{2n^2\mu^2}\sum_{i=1}^{n}\sum_{j=1}^{n}\left(x_i - x_j\right)^2$$

where CV^2 stands for the square of the coefficient of variation, Var for the variance, and μ for the mean of population P with n units. The parameter x indicates country-specific (1, 2, … i and j represent particular countries) values of the evaluated variable (life expectancy at birth). Since the average value of the indicator, i.e. the life expectancy, enters the calculation, the result is the relative variability of the indicator around the average.

In the analysis, the overall observed changes in variability of the mortality trends were decomposed into two components – the within-group (WG) variability and the between-group (BG) variability. The first component represents the increase or decrease of variability within the groups of countries, while the other identifies the increase or decrease in differences between European regions.

In decomposition, the between-group component (CV_B^2) was estimated using the formula (Chameni Nembua 2006):

$$CV_B^2(P_h) = \frac{n_h}{n}\left(1 - \frac{\mu_h}{\mu}\right)^2 + s_h(1 - f_h)CV_h^2$$

$$f_h = \frac{n_h}{n} \; and \; s_h = \frac{n_h}{n}\left(\frac{\mu_h}{\mu}\right)^2$$

where P_h stands for a particular sub-population (one of the compared groups of countries in our case) and n_h for the number of countries in this group. Parameter μ_h represents the means of the evaluated variable in particular regions. Symbols without the lower index are related to the whole analyzed set of countries. The within-group component was estimated only as a difference between the total variability and the between-group part of it.

3. Results

Between 1950 and 2022, there was an overall decline in the variability of life expectancy at birth, with the squared coefficient of variation and both components of total variability reaching higher values for men

(Fig. 1). This downward trend was disrupted by four divergent periods which are defined on the basis of local minimum and maximum values of variability of life expectancy at birth (1973–1984, 1986–1994, 1998–2005, 2017–2022). The increases in variability are more pronounced in males, and therefore only results for men are presented in detail in this paper. The results for women are about the same, but less significant.

The first divergent period started in 1973 and it was the longest period of increasing variability in life expectancy at birth since the mid-20th century, peaking in 1984. The second divergent period began in 1986 and the variability increased until 1994. The largest absolute increase in variability occurred during this interval, with the squared coefficient of variation rising by 0.0034 years squared. Given the turbulent political, economic, and social changes in Eastern Europe at the turn of the 1980s and 1990s, it can be assumed that the considerable increase in variability in the second divergent period is precisely related to the heterogeneous development of mortality in post-socialist countries. The third divergent period started in 1998, reached its maximum in 2005, and can be characterized by the smallest increase in variability when the square of the coefficient of variation increased by 0.0007 years squared. The fourth divergent period started in 2017 and continued until the last year analyzed. The largest annual increments of the square of the coefficient of variation indicate a sharp increase in variability during that interval mainly after 2019 when the COVID-19 pandemic started. The importance of the last divergent period is demonstrated by the fact that the variability achieved due to different mortality trends during the pandemic overcame the turbulent and heterogeneous development in Europe during the transition years of the 1990s (Fig. 1).

Fig. 1 shows, among other things, that throughout the period under study, differences between groups, i.e. between Western and Eastern Europe, contributed more to the overall variability. The share of between-group variability in total variability peaked at 90% in 1990 and has remained above 80% since then. Until the late 1960s, differences between regions were more influenced by Eastern European countries, with a peak of about 65% in 1960. Since then, the contribution of the two regions to between-group variability has been more or less equal (Fig. 2). This means that during all four divergent periods, both the more rapid rise of Western European countries and the lagging behind of post-socialist countries have contributed equally to the growing gap between Western and Eastern Europe.

The development of within-group variability was more dynamic during the period under review. This component of the total variability was more pronounced almost throughout the entire period in Region 2, with the contributions of Eastern European countries starting to increase significantly in the 1990s. Since then, Region 2 has completely dominated the within-group variability, reaching a maximum contribution of over about 92% in 2014 (Fig. 2). This reflects the very different development of Western and Eastern Europe since the late 1980s and early 1990s, when Western European countries remained

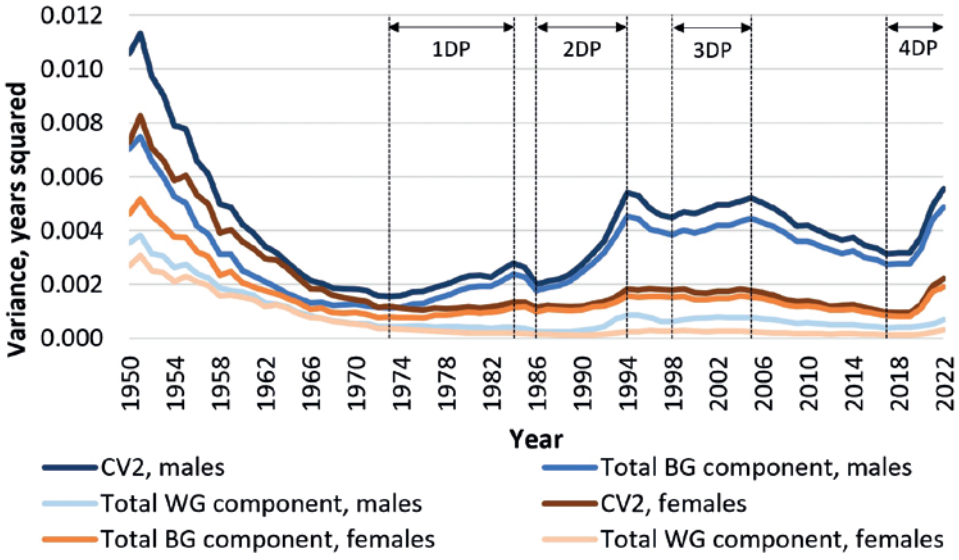

Fig. 1 Variability of life expectancy at birth expressed by square of the coefficient of variation and its components between- and within-group variability, men and women, European countries, 1950–2022.
Notes: The dashed vertical lines delineate the four divergent periods.
CV2 = square of the coefficient of variation; BG = between-group component of the total variability; WG = within-group component of the total variability; DP = divergent period
Data: United Nations

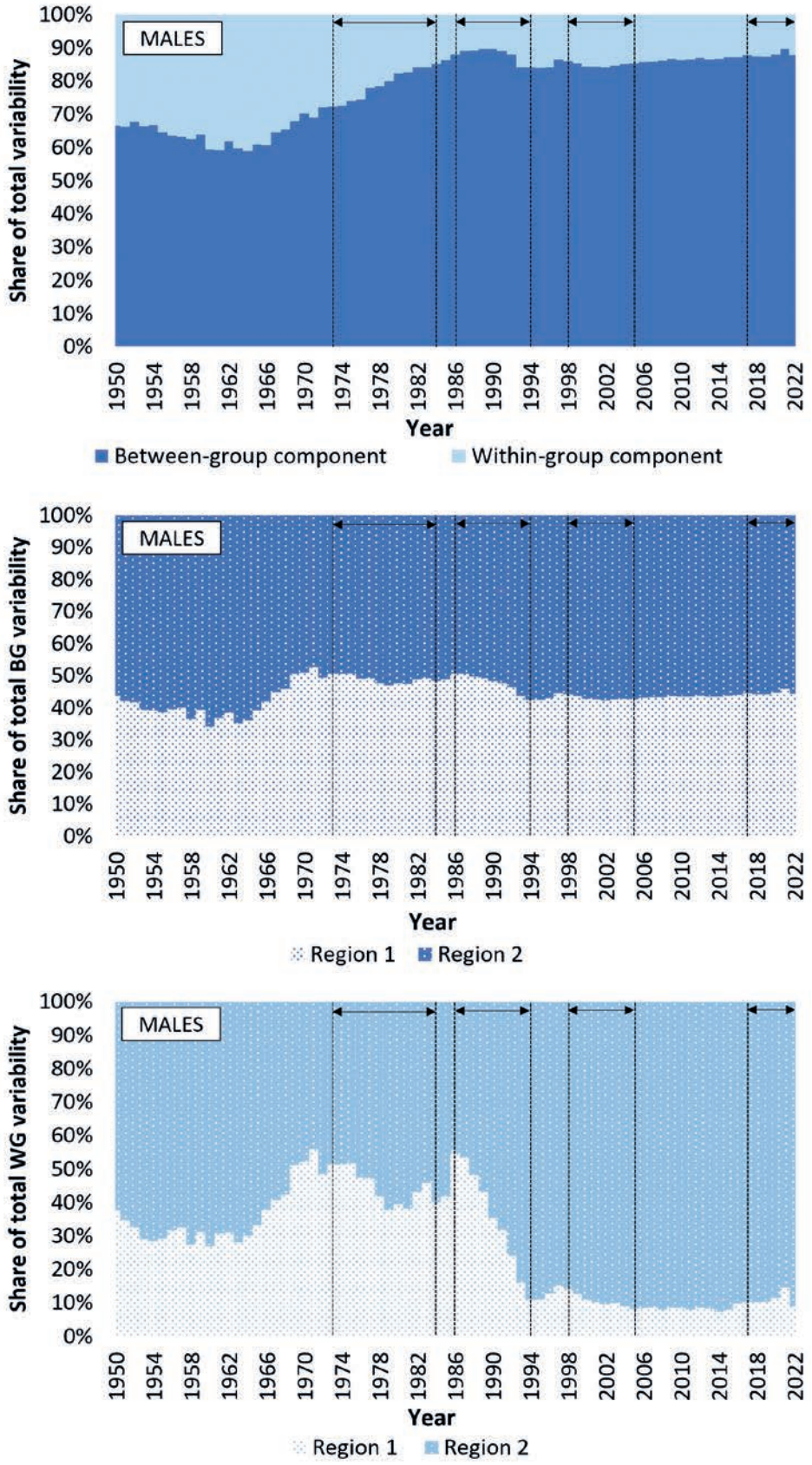

Fig. 2 Contributions of between- and within-group components to the total variability (upper panel) and contributions of Regions to the between- (middle panel) and within-group (bottom panel) components of the total variability, men and women, European countries, 1950–2022.

Notes: The dashed vertical lines delineate the four divergent periods.

BG = between-group component of the total variability; WG = within-group component of the total variability; Region 1 = Western Europe; Region 2 = Eastern Europe

Data: United Nations

homogeneous, while mortality trends among post-socialist countries differed greatly in the context of the transition and subsequent mortality crisis.

For a better understanding of the development of the variability and its components, the following Fig. 3, 4, 5, and 6 show the development of life expectancy at birth during the four divergent periods. The graphs always compare life expectancy in two years – the year before the divergent phase began, i.e. the year with the local minimum value of the squared coefficient of variation, and the year when variability peaked in a given divergent period (1973–1984, 1986–1994, 1998–2005 and 2017–2022). These divergent periods are analyzed in more detail to identify the countries that are most responsible for the increase in mortality variability.

During the first divergent period (1973–1984), all Western European and some Eastern European countries experienced an increase in life expectancy at birth. In Region 2, however, the level of the indicator stagnated or even declined in several cases. The largest increases between 3 and 4 years occurred in Albania and Macedonia, and in Region 1 in Portugal, Finland, Italy, and Spain. Belarus experienced the greatest loss of life expectancy at birth by almost 3 years, but due to its relatively good starting position in 1973, it was not among the countries with the lowest level of the indicator at the end of the first divergent period. This position was held by Russia and the Republic of Moldova at both the beginning and the end of this period, despite different trends, with life expectancy in Russia declining by about one and a half years between 1973 and 1984, while in Moldova the indicator increased by about one and a half years (Fig. 3). Thus, regarding the first divergent period, we can conclude that there were changes in both Regions, which corresponds to the results above that the share of Western and Eastern European countries in between-group variability was comparable during this period. However, the variability was higher in Region 2, and therefore the contribution of Eastern Europe to within-group variability increased at the expense of Western Europe (Fig. 2).

Even in the second divergent period (1986–1994), all Western European countries experienced an increase in life expectancy at birth. In the case of Eastern Europe, some countries showed increasing trends (mainly Central European countries), but most faced a deterioration in mortality rates. The largest declines in life expectancy (by more than 3 years) occurred in Ukraine, the Baltic States, Belarus, and especially in Russia, where the level of the indicator fell by almost 7 years. Moreover, Russia had the worst starting position in 1986, so that, combined with the largest drop in life expectancy at birth, it lagged behind not only Western Europe but also other Eastern European countries at the end of the second divergent period. In contrast, the largest gains in life expectancy at birth in Region 2 can be observed in Slovenia, which was more in line with Eastern Europe during the second divergent period of life expectancy levels, but its convergent tendency towards Western Europe is evident

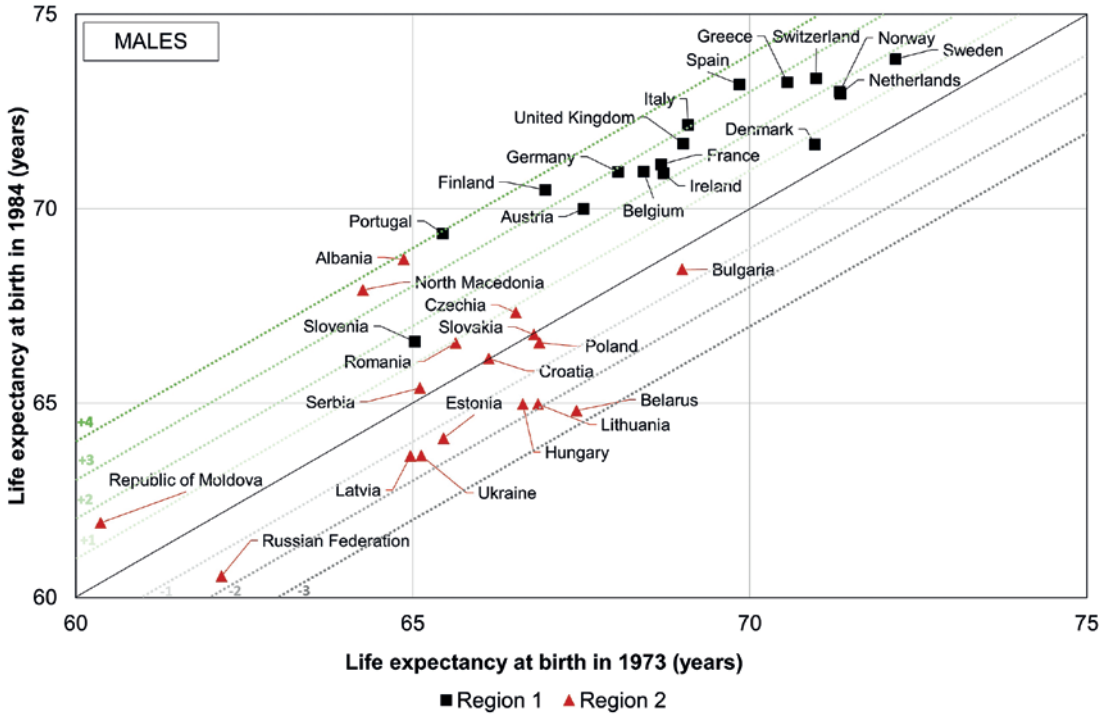

Fig. 3 Changes in life expectancy at birth between 1973 and 1984, men, European countries.
Notes: Region 1 = Western Europe; Region 2 = Eastern Europe
Data: United Nations

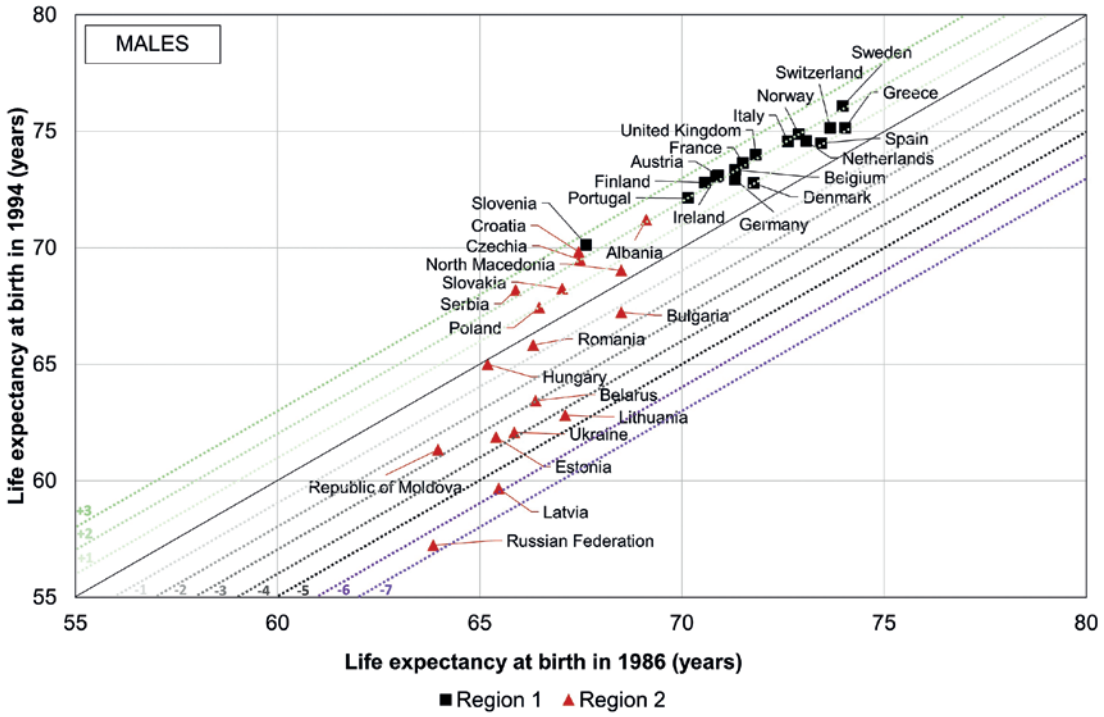

Fig. 4 Changes in life expectancy at birth between 1986 and 1994, men, European countries.
Notes: Region 1 = Western Europe; Region 2 = Eastern Europe
Data: United Nations

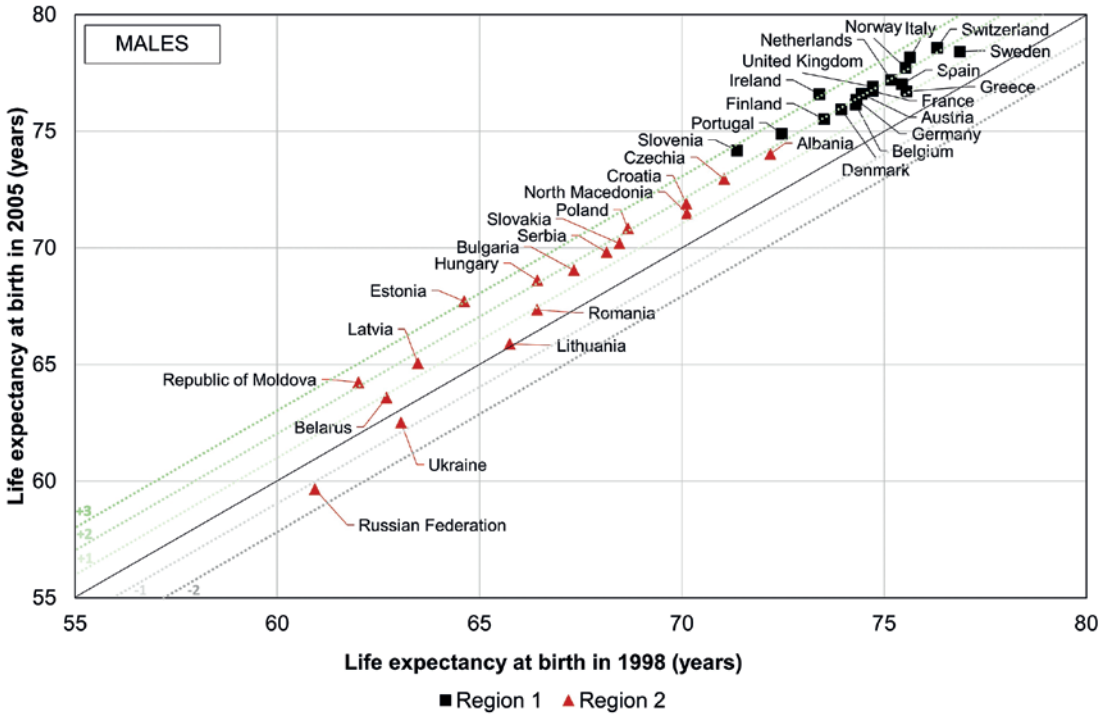

Fig. 5 Changes in life expectancy at birth between 1998 and 2005, men, European countries.
Notes: Region 1 = Western Europe; Region 2 = Eastern Europe
Data: United Nations

(Fig. 4). The increase in between-group variability during this period was influenced by both regions, as Western Europe experienced a substantial increase in life expectancy, while Eastern Europe showed a slower increase and in some cases a substantial decrease. The large increase in the share of Region 2 in within-group variability (Fig. 2) corresponds with the large differences between Eastern European countries, while Western European countries held much more together.

Overall, the third divergent period (1998–2005) can be characterized by the lowest mortality levels, as an increase in life expectancy at birth occurred in all Western and Eastern European countries except Ukraine and Russia. At first glance, it is clear that Region 1 is much more homogeneous, while the variability within Region 2 is large, which corresponds to the dominant share of Eastern European countries in the overall within-group variability (Fig. 2). It can even be observed that Region 2 has split into more subgroups during this divergent period. Best mortality rates are shown by Central European countries, Albania, Croatia or Northern Macedonia. The Baltic States are a special group, which is moving away from the other post-Soviet countries, with Estonia showing an increase in life expectancy of about 3 years, one of the largest gains in this period. The situation is most severe again in Russia and Moldova, but also in Ukraine and Belarus (Fig. 5). This heterogeneous development of the Region 2 countries, and in particular the convergent tendencies of some post-socialist countries towards Western Europe and the separation of some post-Soviet countries, shows that the different countries have managed to cope with the consequences of the transition and the mortality crisis at different paces.

For the fourth divergent period (2017–2022), it can no longer be said that all Western European countries experienced an increase in life expectancy at birth, as the value of the indicator fell slightly in Germany and Greece. However, the loss was marginal compared to Eastern Europe. In Region 2, by contrast, mortality rates deteriorated in all countries except Croatia, Estonia, and Latvia. At first glance, it is clear that Western Europe was much more homogeneous than Eastern Europe during the fourth divergence period, where even Moldova, Ukraine, and Russia were separated. These three countries had the worst starting positions in 2017 and also experienced a decline in life expectancy. The largest drop of about 6 years in the indicator occurred in Ukraine. It is also worth noting the evolution of Slovenia, which completed its convergence towards Western Europe (Fig. 6). Even during the fourth divergence period, the two regions affected between-group variability in very similar ways, as Western Europe saw further progress in life expectancy at birth, while Eastern Europe experienced an increase in mortality. The greater divergence within Eastern European countries then corresponds with the continued dominance of Region 2 in total within-group variability over that period (Fig. 2).

4. Discussion

The results of this study show that since the second half of the 20th century, mortality rates in Europe have not only improved, but that there were also periods or regions affected by more or less temporary mortality worsening, despite general progress in health care, standards of living, or social and economic development. This heterogeneous development

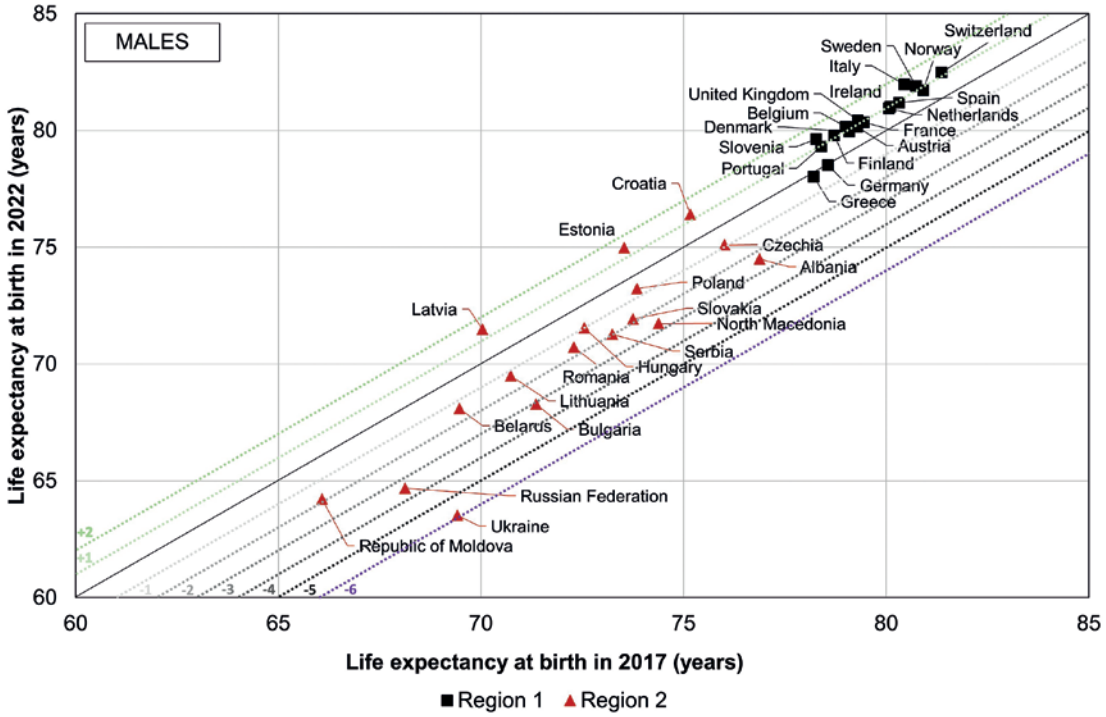

Fig. 6 Changes in life expectancy at birth between 2017 and 2022, men, European countries.
Notes: Region 1 = Western Europe; Region 2 = Eastern Europe
Data: United Nations

was reflected in the variability of mortality rates, which experienced four divergent periods during the period under review.

The increase in variability since the mid-1970s has been associated with the cardiovascular revolution. In the late 1960s, life expectancy at birth began to increase in Western European countries, due to the successful control of cardiovascular diseases. However, this significant progress did not take place in Eastern Europe, which instead entered a long period of stagnation or even an increase in mortality, especially in the case of men (Vallin and Meslé 2004). The decline in variability in the second half of the 1980s was related to the introduction of an anti-alcohol campaign in the countries of the former Soviet Union between 1985 and 1987, but the effect was short-lived due to lack of policy follow-up (Caselli et al. 2002).

This was followed by a widening of the gap between Western and Eastern Europe, which reached a peak around the mid-1990s. However, the mortality crisis did not affect all Eastern European countries equally. In fact, since the mid-1980s, it has been possible to distinguish the former Soviet republics from the countries of Central Europe, where advances in health care were made earlier and, after the collapse of the Soviet Union, one country after another began to reverse the adverse mortality trends (Meslé 2004). The countries of the former Soviet Union did not see a reduction in mortality rates until about the mid-1990s, as by then they faced not only a mortality crisis but also an economic crisis associated with the transition to a market economy (Shkolnikov et al. 1998; Gavrilova et al. 2001). Moreover, the improvement was first seen in the Baltic States. The different mortality trends in Central Europe and the Baltic States compared to other Eastern European countries are explained by many factors, including changes in nutrition, progress in medicine, and the countries' entrance into the European Union. Although they did not officially join the EU until 2004, already in the 1990s the governments of the accession countries had to take measures in areas ranging from housing to workplace safety that could have had a positive impact on health (Leon 2011). It was not until around the turn of the millennium that mortality rates began to decline in the remaining post-Soviet countries, and since then it has been possible to speak again of a convergence of mortality rates in Europe.

This positive trend was disrupted at the end of the second decade of the 21st century when variability increased sharply. The observed trends in variability among the European countries are a natural consequence of the pandemic period (COVID-19). As was already shown (Schöley et al. 2022; Shkolnikov et al. 2023), the first pandemic year (2020) brought a mortality worsening to almost all European countries, regardless of the region of the country. On the other hand, the second pandemic year (2021) was the source of increasing mortality variability in Europe. In 2021, many of the Western European countries returned to the pre-pandemic mortality levels, however, most of the Eastern European countries suffered even deeper mortality worsening. Thus, we can conclude that the impact of the pandemic was more severe in countries with worse pre-pandemic mortality rates and the COVID-19 pandemic deepened significantly the European mortality differences.

Frequently mentioned factors influencing the impact of a pandemic include, for example, the resilience of countries to external influences and their ability to adapt to circumstances (Haldane et al. 2021; Berawi 2020), or the degree of involvement in international trade and tourism (Ascani et al. 2020; Bontempi and Coccia 2021). For this reason, Western European countries in many cases experienced higher excess mortality at the beginning of the pandemic because of more intense trade links, whereas the epidemic did not spread as rapidly to Central and Eastern European countries at the very beginning. However, by the second pandemic year, Western European countries were already showing better adaptation and response, whereas Eastern Europe was more affected by the pandemic, again confirming the link between the impact of the pandemic and pre-pandemic levels of life expectancy. In other words, lifestyle, nutrition, health care or infrastructure can be said to influence life expectancy levels perhaps even more during pandemics than outside of them. This is important for policy makers and the future development of the risk countries, which are less resilient to epidemics and need more external support.

5. Conclusion

The divergent-convergent development of mortality in Europe in the second half of the 20th century is evident in the results of this study. We can observe a steady increase in life expectancy at birth in all Western European countries in the first (1973–1984), second (1986–1994), and third (1998–2005) divergent periods, while Eastern European countries have in most cases experienced stagnation or decline in the indicator. Related to this is the increase in the influence of the between-group component on overall variability since the 1960s, with Western and Eastern Europe contributing almost equally to the between-group differences since the 1970s. The increase in variability was rapid in the second divergent period when the between-group component of variability was at its highest and the difference between Western and Eastern Europe was therefore the largest. At that time, life expectancy continued to rise in Western European countries, while some countries in Eastern Europe faced a mortality crisis, especially Russia, the Baltic States, Ukraine, and Belarus. This is related to the significant increase in contributions of Region 2 to the total within-group component of variability after

1985. Divergence within the Eastern European region also played a role in the increase in variability in the late 1990s when first the Central European countries and then the Baltic states separated from the rest of the post-socialist countries.

During the most recent divergent period associated with the COVID-19 pandemic, there was a larger increase in variability than in all the other divergent periods. The between-group component of total variability was again influenced by both Regions, i.e., progress in Western Europe (especially in Switzerland, Norway, Sweden, and Italy) and deterioration in mortality in Eastern Europe (especially in Russia, Ukraine, and Moldova). Within-group variability continued to be more affected by Region 2, although the contribution of Region 1 increased slightly.

The four divergent periods show that the increase in mortality variability can be due to many factors, whether it is the gradual manifestation of progress in health care, political and economic changes, or epidemics. It is, therefore, necessary to assume that further divergent-convergent mortality sequences will occur in the future, and it is extremely important to learn how to respond to mortality crises so that future ones have as little impact as possible, not only on European societies.

References

Aburto, J. M., van Raalte, A. (2018): Lifespan dispersion in times of life expectancy fluctuation: the case of Central and Eastern Europe. Demography 55(6), 2071–2096, https://doi.org/10.1007/s13524-018-0729-9.

Ascani, A., Faggian, A., Montresor, S. (2021): The geography of COVID-19 and the structure of local economies: The case of Italy. Journal of Regional Science 61(2), 407–441, https://doi.org/10.1111/jors.12510.

Berawi, M. A. (2020): Empowering healthcare, economic, and social resilience during global pandemic Covid-19. International Journal of Technology 11(3), 436–439, https://doi.org/10.14716/ijtech.v11i3.4200.

Bontempi, E., Coccia, M. (2021): International trade as critical parameter of COVID-19 spread that outclasses demographic, economic, environmental, and pollution factors. Environmental Research 201:111514, https://doi.org/10.1016/j.envres.2021.111514.

Bye, E. K. (2008): Alcohol and homicide in Eastern Europe: A time series analysis of six countries. Homicide Studies 12(1), 7–27, https://doi.org/10.1177/1088767907310851.

Caselli, G., Meslé, F., Vallin, J. (2002): Epidemiologic transition theory exceptions. Genus 58(1), 9–51, https://www.jstor.org/stable/29788712.

Chameni Nembua, C. (2006): A note on the decomposition of the coefficient of variation squared: comparing entropy and Dagum's methods. Economics Bulletin 4(8), 1–8, https://www.researchgate.net/publication/4829489_A_Note_on_the_Decomposition_of_the_Coefficient_of_Variation_Squared_Comparing_Entropy_and_Dagum's_methods.

Gavrilova, N. S., Evdokushkina, G. N., Semyonova, V. G., Gavrilov, L. A. (2001): Economic crises, stress and mortality in Russia. The Population Association of America 2001 Annual Meeting, Washington. Available online: http://longevity-science.org/Gavrilova-PAA-2001.pdf (accessed on 20. 2. 2024).

Hajdu, T., Krekó, J., Tóth, C. G. (2024): Inequalities in regional excess mortality and life expectancy during the COVID-19 pandemic in Europe. Scientific Reports 14: 3835, https://doi.org/10.1038/s41598-024-54366-5.

Haldane, V. et al. (2021): Health systems resilience in managing the COVID-19 pandemic: lessons from 28 countries. Nature Medicine 27(6), 964–980, https://doi.org/10.1038/s41591-021-01381-y.

Leon, D. A. (2011): Trends in European life expectancy: a salutary view. International Journal of Epidemiology 40(2), 271–277, https://doi.org/10.1093/ije/dyr061.

Leon, D. A., Chenet, L., Shkolnikov, V. M., Zakharov, S., Shapiro, J., Rakhmanova, G., Vasin, S., McKee, M. (1997): Huge variation in Russian mortality rates 1984–94: Artefact, alcohol, or what? Lancet 350(9075), 383–388, https://doi.org/10.1016/S0140-6736(97)03360-6.

McKee, M., Shkolnikov, V. (2001): Understanding the toll of premature death among men in Eastern Europe. BMJ 323: 1417, https://doi.org/10.1136/bmj.323.7326.1417a.

Meslé, F. (2004): Mortality in Central and Eastern Europe: long-term trends and recent upturns. Demographic Research Special Collection 2(3), 45–70, https://doi.org/10.4054/DemRes.2004.S2.3.

Meslé, F., Vallin, J. (2002): Mortality in Europe: the Divergence Between East and West. Population 57(1), 157–197, https://doi.org/10.3917/popu.201.0171.

Schöley, J., Aburto, J. M., Kashnitsky, I., Kniffka, M. S., Zhang, L., Jaadla, H., Dowd, J. B., Kashyap, R. (2022): Life expectancy changes since COVID-19. Nature Human Behaviour 6, 1649–1659, https://doi.org/10.1038/s41562-022-01450-3.

Shkolnikov, V. M., Cornia, G. A., Leon, D. A., Meslé, F. (1998): Causes of the Russian mortality crisis: evidence and interpretations. World Development 26(11), 1995–2011, https://doi.org/10.1016/S0305-750X(98)00102-8.

Shkolnikov, V. M., Timonin, S., Jdanov, D., Islam, N., Leon, D. A. (2023): East-West mortality disparities during the COVID-19 pandemic widen the historical longevity divide in Europe. medRxiv (preprint), https://doi.org/10.1101/2023.11.08.23298275.

United Nations (2022): World Population Prospects 2022. Department of Economic and Social Affairs, Population Division. Available online: https://population.un.org/wpp/Download/Standard/Mortality/ (accessed on 25. 11. 2023).

Vallin, J., Meslé, F. (2004): Convergences and divergences in mortality: a new approach of health transition. Demographic Research Special Collection 2(2), 11–44, https://doi.org/10.4054/DemRes.2004.S2.2.